Author:
Pesik, Lisa Josephine

Title:
Practical investigation of Butler matrix application for beamforming with circular antenna arrays

Practical Investigation of Butler Matrix Application for Beamforming with Circular Antenna Arrays

Lisa Josephine Pesik

January 2007

A thesis submitted to the University of Bristol in accordance with the requirements for the degree of Doctor of Philosophy in the Faculty of Engineering, Department of Electrical and Electronic Engineering.

Abstract

As today's generation sees wireless communications as a daily essential, the available spectrum and system efficiency becomes a greater issue day by day. The merits of antenna arrays over single antennas have long been realised as a powerful instrument for capacity enhancement. Application of Uniform Linear Arrays (ULAs) has been extensively researched and the technology is widely used in wireless applications. One of the well-known ULA excitation techniques is the Butler matrix, which produces orthogonal beams through performing Fast Fourier transform of the incoming signals. Incorporating hybrid couplers and phase shifters, the matrix is particularly attractive for its low cost. The use of ULAs, however, limits the look direction to a sector of the azimuth plane. Uniform Circular Arrays (UCAs) present a desirable advantage due to their ability to cover the entire 360^o of the azimuth plane. Research suggests that with an appropriate excitation function, a Butler matrix network used to feed a UCA provides a virtual transformation from UCA to ULA in such a way that ULA pattern synthesis techniques can be applied to a UCA. However, very limited detailed investigation in terms of accuracy of an implemented system is available.

In this thesis, the author presents practical investigations of UCA-Butler matrix systems through the use of measured, FDTD generated and ideal data. In these cases, ideal scenarios are based on the assumption that there are no errors caused by manufacturing tolerance and mutual coupling. Theories regarding UCA radius, number and type of elements are evaluated. Results reveal that embedded pattern compensation is essential in order to obtain desirable results. When an $N \times N$ correction matrix is employed, up to ≈ -30dB SLL is achievable. Data collected from FDTD modeling is utilised in order to simplify the correction matrix, leading to derivation of practical values for $(2M+1)\times(2M+1)$ *diagonal* matrix for embedded pattern compensation. Error analysis is performed in order to obtain the manufacturing tolerance for the compensation as well as the UCA itself.

To My Mother And Father

Acknowledgements

I would like to begin by expressing my sincere appreciation and heartfelt thanks to my supervisor, Professor Mark Beach for guiding and encouraging me meticulously throughout the course of my PhD and for giving me the confidence and support to perform this research. I like to thank Dr. Geoff Hilton, whose continuous guidance, practical advice and expertise on antennas I could not have done without. I am truly indebted to him for without his guidance, I would not have come this far. I also like to gratefully acknowledge Toshiba Research Laboratories (TRL) for the financial contribution.

My sincere gratitude is offered to Dr. Dominique Paul, Professor Chris Railton and Dr. Ian Craddock for sharing their valuable knowledge and guidance on the FDTD tools and techniques. My special thanks to my former coleague Dr. Phill Urwin-Wright for his interest, discussions and advice throughout this work. This accelerated my understanding and knowledge of antenna measurements.

My deepest appreciation goes to my family back home in Indonesia for supporting me financially and emotionally throughout my studies in the UK. My sincere appreciation for my parents who have supported me financially and emotionally throughout my studies in the UK.

The past five years have been filled with times of trial and happiness and during the course of writing up this thesis, my closest friends, Dr. Arun Arumugam, Li-Wei Lee and Rachel Poole, have been a great source of endless encouragement and inspiration to me.

On a final note, I would like to extend my most sincere thanks to my beloved husband Darren, for providing me with support in a multitude of ways in the past year. This thesis would never have finished without his belief in my ability and the support and encouragement that he always gives. For not letting me quit, for wiping away my tears, for standing by me, thank you.

Author's Declaration

Unless otherwise acknowledged, the content of this thesis is the original and sole work of the author. No portion of the work in this thesis has been submitted by the author in support of an application for any other degree or qualification, at this or any other university or institute of learning. The views expressed in this thesis are those of the author, and not necessarily those of the University of Bristol.

Lisa Josephine Pesik Date: 30 January 2007

Copyright

Attention is drawn to the fact that the copyright of this thesis rests with the author. This copy of the thesis has been supplied on condition that anyone who consults it is understood to recognised that its copyright rests with the author and that no quotation from the thesis and no information derived from it may be published without the prior written consent of the author. This thesis may be made available for consultation within the University Library and may be photocopied or lent to other libraries for the purpose of consultation.

Contents

List of Publications

[1] L.J. Pesik, M.A. Beach, B.H. Allen, "Performance analysis of switched-sector antennas for indoor wireless LANs", *IEEE 54th VTS Vehicular Technology Conference*, Vol. 1, pp.385-362, 2001.

[2] L.J. Pesik, M.A. Beach, B.H. Allen, "Performance analysis of switched-sector antennas for indoor wireless LANs", *6th IEEE High Frequency Postgraduate Student Colloquium*, pp.30-34, September 2001.

[3] L.J. Pesik, M.A. Beach, D.P. McNamara, P.N. Fletcher, "Performance analysis of smart antenna systems for indoor wireless LANs", *Third International Conference on 3G Mobile Communication Technologies*, No. 489, pp.418-422, May 2002.

[4] C.M. Tan, M. Landmann, A. Richter, L.J. Pesik, M.A. Beach, Ch. Schneider, R.S. Thoma, A.R. Nix, "On the application of circular arrays in direction finding Part II: Experimental evaluation on SAGE with different circular arrays", COST 273, May 2002.

List of Tables

List of Figures

List of Abbreviations

A/D	Analogue to Digital
AUT	Antenna Under Test
AMSAR	Airbourne Multifunction Solid-state active Array Radar
AP	Access Point
BER	Bit Error Rate
BS	Base Station
CCK	Complementary Code Keying
CDMA	Code Division Multiple Access
DFT	Discrete Fourier Transform
DSSS	Direct Sequence Spread Spectrum
DoA	Direction of Arrival
ESPRIT	Estimation of Signal Parameters via Rotational Invariance Techniques
ETSI	European Telecommunications Standards Institute
FCA	Filled Circular Array
FDD	Frequency Division Duplex
FDMA	Frequency Division Multiple Access
FDTD	Finite Difference Time Domain
GMSK	Gaussian Minimum Shift Keying
GSM	Global System for Mobile Communications (Group Special Mobile)
HIPERLAN	High Performance Local Area Network
IEEE	Institute of Electrical and Eletronic Engineers
IFFT	Inverse Fast Fourier Transform
IF	Intermediate Frequency
LAN	Local Area Network
LSE	Least Square Error
MAN	Metropolitan Area Network
MIMO	Multiple Input Multiple Output
MMSE	Minimum Mean Square Error

MoM	Method of Moment
MT	Mobile Terminal
MUSIC	Multiple Signal Correlation Algorithm
OFDM	Orthogonal Frequency Division Multiplexing
PAN	Personal Area Network
PBCC	Packet Binary Convolution Code
PPA	Projected Planar Array
RAM	Radar-Absorbing Material
RF	Radio Frequency
RX	Receiver
SAGE	Space Alternating Generalised Expectation
SDMA	Space Division Multiple Access
SLL	Side Lobe Level
SNR	Signal to Noise Ratio
TD-SCDMA	Time Division Synchronous Code Division Multiple Access
TDD	Time Division Duplex
TDMA	Time Division Multiple Access
TX	Transmitter
UCA	Uniform Circular Array
ULA	Uniform Linear Array
UMTS	Universal Mobile Telecommunication Systems
WAN	Wide Area Network
Wi-Fi	Wireless Fidelity
WLAN	Wireless Local Area Network
WMAN	Wireless Metropolitan Area Network
WPAN	Wireless Personal Area Network
WWAN	Wireless Wide Area Network

Chapter 1

Introduction

The wireless telephony technology has evolved tremendously in the past century [1]. The technology that was once considered impossible is now regarded as common everyday use. For example, extensive research and development of wireless technology has extended the use of conventional telephones to mobile phones, which are now widely used around the world. This explosive growth of the wireless industry, coupled by the boom in internet usage in the recent years, has led to the development of wireless data access.

Wireless network technology provides the freedom of mobility to its users. Instead of being tied down to their desks or the vicinity of a network socket, users are now able to use their laptops anywhere within the service area. Such superior technology undoubtedly will prove to be much in demand. However, as wireless services become more and more widely used, radio resources in turn become more and more scarce [2]. Limited bandwidth availability at the frequency of interest becomes a barrier for wireless networks in providing the low cost and very high data rates similar to that of wired networks. This chapter presents an overview of the growth of wireless communication over the years, its future and how the limited capacity and bandwidth could be extended through the use of antenna arrays. The issue of the need for low cost solution is also discussed, before proceeding with an overview of the thesis.

1.1 Overview of Wireless Communications

Up until recently, multimedia and networking services have been limited to wired networks. Although wireless technology has been around for decades, one recent boom of handheld and mobile devices has spurred the demand necessary to create robust networks. New advances in the wireless industry has brought wireless connectivity that was once considered impossible into reality. Today, plenty of wireless-based consumer electronic devices are available off the shelf. Many daily applications have evolved from wired to wireless. Extensive research in the consumer electronics area has also brought about lower costs and component size reduction. Wireless services available today include cellular mobile radio systems, cordless telephones, high-speed WLANs and satellite-based mobile systems such as global positioning systems.

The wireless network hierarchy, as shown in Figure 1.1, is very much like its wired counterpart. Seamless connectivity is achieved through a combination of four types of wireless networks, each with different coverage range. The various networks, briefly described in [3], are as follows:

- **Wireless Personal Area Network (WPAN)** or IEEE 802.15 [4]- [5] provides low-power, short-range connectivity between devices such as PDA, laptop, and mobile phone around a user's workspace. With operating frequency of 2.4GHz and a typical range of approximately 10m, WPAN uses Bluetooth or ETSI HiperPAN standards and provides seamless connection between the user's devices.

- **Wireless Local Area Network (WLAN)** is often termed *Wi-Fi* [6]- [8] and uses IEEE 802.11 or ETSI HiperLAN standards. With an approximate range of 300 yards, WLAN is widely used in home and office environments. WLAN networks will be discussed further in the following section.

- **Wireless Metropolitan Area Network (WMAN)** or WiMAX [9]- [11] concentrates on connectivity between different cities in the country, based on the IEEE 802.16 or ETSI HiperMAN and HiperACCESS standards. WMAN provides the possibility of extending the Wi-Fi range and supporting both fixed and mobile devices, including voice and multimedia applications.

- **Wireless Wide Area Network (WWAN)** provides global connectivity and therefore the greatest range, allowing interconnectivity between branch-offices around the world. WWAN standards include the IEEE 802.20, 3GPP and EDGE. Its evolution has brought it through generations of networks such as the 2G GSM, as well as CDMA and

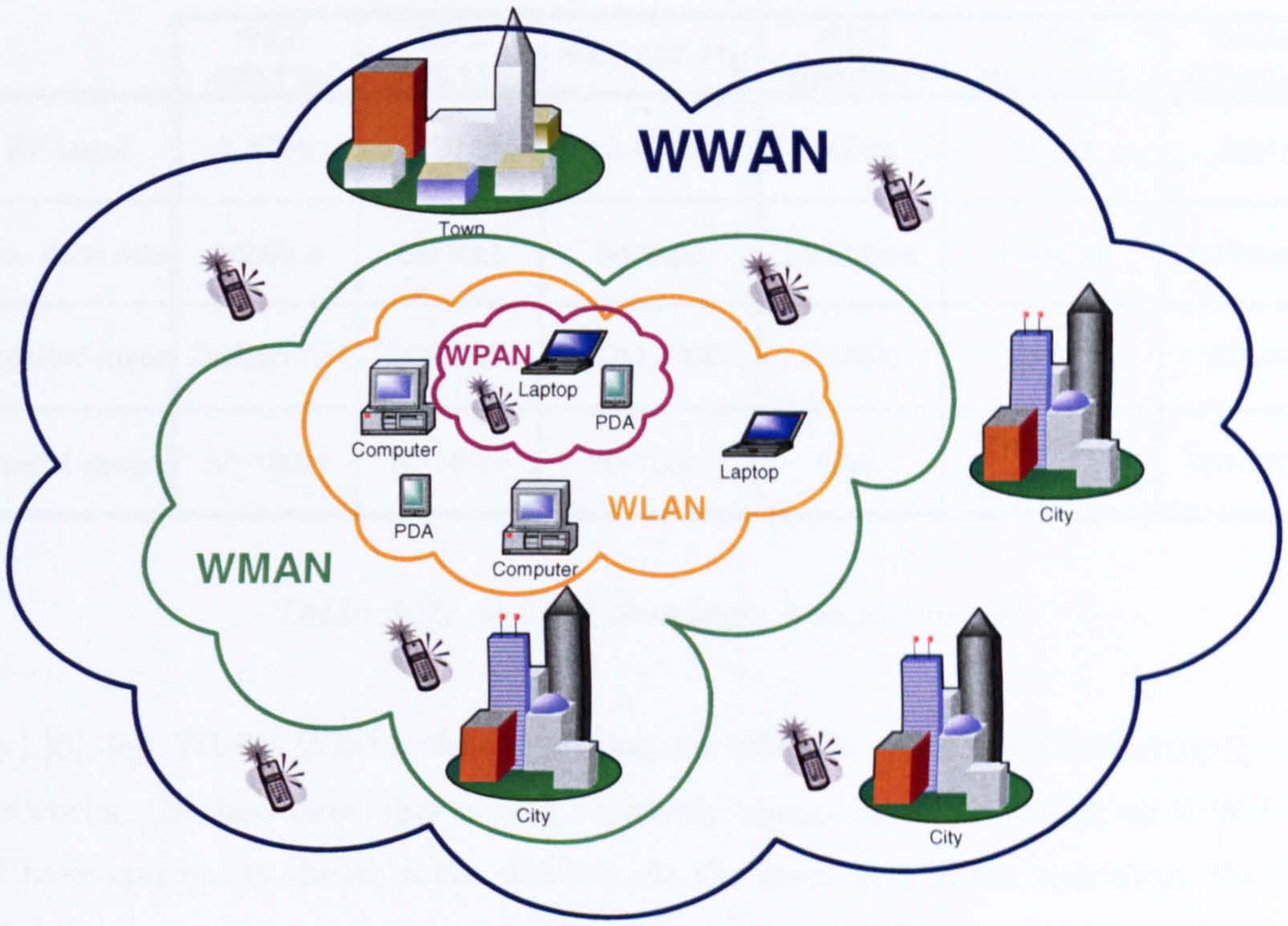

Figure 1.1: *Wireless Network Hierarchy*

TDMA, the 2.5G Richochet and GPRS, to today's 3G 144Kbps - 2Mbps CDMA2000 and WCDMA [12]- [13].

At present, communication within WWAN and WMAN is mostly established through the second generation (2G) cellular systems. Mobile devices interface with radio towers, which carry the signal to a mobile switching center. The signal is then passed on to the intended public or private network, i.e. the Internet or and organisation's existing network [14]. The authors of [15] also discuss *vertical handoff* which provides seamless handoff between WWAN and WLAN in their paper.

1.2 Wi-Fi and WiMAX: The Future of Wireless Networking

Over the recent years, the IEEE 802 committee has developed various standards for WPAN, WLAN, WMAN and WWAN. These include the 802.3 standards for Ethernet (wired) networks, the 802.15 standards for WPANs, the 802.11 standards for WLANs, and the 802.16 standards for WMANs [3].

The area of particular interest in the work presented in this thesis is the smaller scale wireless (IEEE 802.11) standard, which is more commonly known among its users as *Wi-Fi* (Wireless

	IEEE 802.11b	IEEE 802.11a	IEEE 802.11g	ETSI Hiperlan/1	ETSI Hiperlan/2	MMAC HiSWANa
RF band	2.4GHz	6GHz	2.4GHz	5GHz	5GHz	5GHz
Max. data rate	11Mbps	54Mbps	54Mbps	23.5Mbps	54Mbps	27Mbps
Physical layer	DSSS/CCK	OFDM	OFDM, PBCC	GMSK	OFDM	OFDM
Typical range	50-100m	50-100m	50-100m	50m	50m indoor, 300m outdoor	100-150m

Table 1.1: WLAN Standards comparison [5]

Fidelity) [6], [8]. Whilst WiFi technology does not offer the same degree of ubiquity as wide area networks, the fast data speeds and relatively cheap costs of setting up a WiFi-based WLAN have spurred it ahead in the market. At the lower end of the spectrum, the 802.11b is a WLAN standard operating at 2.4GHz with data rates of up to 11Mbps. At the 5GHz frequency range is the 802.11a with data rates of up to 54Mbps. 802.11g was for WLANs operating in the 2.4 GHz frequency band but with a maximum data rate of 54 Mbps. 802.11g is currently used in most laptop computers. It offers data speeds up to 54Mbps while operating in the 2.4GHz and 5GHz bands, making it backward compatible with 802.11b.

Parallel to the IEEE 802.11, the European Telecommunications Standards Institute (ETSI) establised the High Performance LAN (HIPERLAN) standards. Like the IEEE 802.11a, HIPERLAN/2, first published in the year 2000, employs Orthogonal Frequency Division Multiplexing (OFDM) and operates in the 5GHz frequency band with data rates of up to 54Mbps. However, dynamic frequency selection (DFS) in HIPERLAN/2 reduces interference as well as increase spectrum utilisation [7]. Similarly, Multimedia Mobile Access Communication-High Speed Wireless Access Network (MMAC-HiSWAN) was developed in Japan. Similar to the 802.11a and Europe's HIPERLAN/2, HiSWANa utilises the 5GHz spectrum and uses OFDM. The standaed provides speeds of up to 27Mbps [7]. A summary of the WLAN standards is presented in Table 1.1.

In addition to IEEE 802.11a/b/g, the IEEE 802.11 Working Group is actively developing IEEE 802.11n, which specifies higher throughput as well as speed enhancement. The 802.11n is capable of producing a maximum throughput of at $\geq$ 100Mb/s. Further, 802.11n is designed to be compatible with MIMO technology, which provides capacity improvements through TX and RX diversity [16]- [18].

With data rates of up to 54Mb/s, all IP-based services will be available through wireless connections. Laptop computers can now be used anywhere within the building with high-speed connection to the fixed network. Although the use of wireless devices will mainly be stationary, users will benefit through the ease at which they can move around from one location to another, instead of having to find a spot where a network socket is present. In a meeting or lecture, documents can easily be distributed among participants through their laptops. Video conferencing are no longer bound to a specific conference room where a fixed network is present. The presence of Wi-Fi in several university buildings mean that students can access their emails and lecture materials on their laptops anywhere within the building, instead of having to go to a computer room. Wi-Fi networks are rapidly becoming a common feature of many busy public places such as coffee shops, hotels, airport lounges and other locations where people gather. More and more travelers and mobile professionals clamor for fast and secure internet access wherever they are.

Adaptability is another great advantage of WLANs. Altering and extending a fixed network is difficult and costly. Digging a ditch for fiber typically costs £180 to £730 per meter. A wireless link providing 100 Mbps over 100m can cost less than £1,300 [19][1]. In certain environments such as historic buildings, galleries, factories and warehouses, too much drilling and wiring are often impractical and undesirable. Wireless networks are advantageus in buildings where the floor planning changes frequently, such as shopping centres and exhibition halls. Alteration and maintenance would be easier and cheaper in comparison to wired networks. Adding another wireless node to an existing Wi-Fi network only involves plugging in a card or USB connection. A business that needs to move from one location to another no longer needs to abandon its investment in network infrastructure or pay for rewiring at the new location. The Wi-Fi system can be operational within minutes, avoiding network downtime.

Owing to the fact that WLAN networks use unlicensed frequency bands, wireless suppliers are much less restricted in the type of services they can provide compared to those that utilise licensed spectrum. Thus, wireless technologies in the unlicensed spectrum has evolved tremendously in the past 10 years [19]. Research presented by InStat [20] predicts a growth of 73.5% in business Wi-Fi equipment and 117% in consumer Wi-Fi equipment in the Asia Pacific region within the next 10 years. A survey by InStat also suggests that the number of mobile workers in the US alone will reach 103 million by 2008. Research carried out in the US [21] shows that over 64% office workers carry at least two wireless devices every day.

[1] feet and $ converted into meter and £

WiMAX [9]- [11] is based on the IEEE 802.16 and ETSI HiperMAN standards. The standard is designed and optimised for Metropolitan Area Networks (MANs). It is intended as a complement to Wi-Fi as it extends the range, providing a "Wi-Fi like" coverage and user experience on a larger scale, instead of a replacement for Wi-Fi. Latest versions of WiMAX are the IEEE 802.16-2004 and 802.16e, with the latter also providing support for Multiple Input Multiple Output (MIMO) and adaptive antenna systems. WiMAX is designed to support a wide range of frequencies (up to 62GHz) and bandwidth (1.25 - 20MHz). Both 802.16-2004 and 802.16e have maximum throughput of 15Mbps for a 5MHz channel, or 35Mbps for a 10MHz channel. It is estimated that within the 2006-2008 timeframe, both 802.11 and 802.16 will be available to end users of devices such as laptops and PDAs. Wireless connectivity will then be available for the end users at home, in the office and on the move. In the future, Wi-Fi networks may be found in urban areas providing coverage throughout the central city, or even lining major highways.

The rapid increase in the demand for wireless services as well as the requirement for future wireless communication systems to support a wide range of services including video, data and voice has led to the necessity for higher capacity for wireless systems. Limited bandwidth availability at the frequency of interest becomes a barrier for wireless networks in providing the low cost and very high data rates similar to that of wired networks.

1.3 Antenna Arrays for Wireless Communications

It has long been realised that arrays of two or more antenna elements are useful tools for capacity improvements in wireless systems. The variety of array types, coupled with the increasing knowledge of array theory and associated processing technologies, has brought about tremendous opportunities to those involved in this field. A range of different antenna array geometries is described in Chapter 2. The most commonly used array geometry is the Uniform Linear Array (ULA) [22], although the studies presented in this thesis is mainly focused on Uniform Circular Arrays (UCAs) [23]. This is due to their ability to serve the full 360^o of the azimuth plane without any significant pattern degradation across the azimuth angles, unlike the case for their linear counterpart. This property of UCAs is attractive, particularly in Wi-Fi applications where it is desirable that the Access Point (AP) is mounted centrally. Further, the author feels that capabilities of UCAs haven't been fully exploited as the added complexities brought about by their geometry has somewhat hindered extensive

research in the area.

With beamforming, the array radiation pattern often consists of a main beam and several smaller sidelobes on either side of the main beam. This main beam can be conveniently steered electronically, thus removing the need of cumbersome mechanical scanning of a single antenna. Printed antenna technology has also brought about a significant advantage to the application of antenna arrays. This technology has enabled antenna arrays to be mounted discretely on many surfaces, in other words in the form of a conformal array.

With the massive growth of wireless communication systems [24] - [25], the available bandwidth is rapidly becoming a scarce resource and interference mitigation a necessity. Using spatial domain processing, a main beam can now be steered towards the direction of the transmit antenna, giving a higher gain in this direction and significantly lower gain, i.e. suppression, in other directions. This is the basic principle of spatial domain separation, commonly refered to as *spatial filtering*. Using an antenna array, the spatial domain may be divided into several different spatial channels, thus also increasing the system capacity [26] - [28] as well as suppressing co-channel and inter-channel interference. This is illustrated in Figure 1.2.

Figure 1.2 illustrates three users A, B and C operating in the same frequency and located in the same cell, served by access point (AP) X. An antenna array at X can be configured to form a radiation pattern with a main lobe pointing in the direction of A, therefore enhancing the signal received from A and suppressing those received from B and C. With several beams pointing in different directions the spatial domain can now be separated into several different channels, all in the same frequency of operation. A main beam in the direction of wanted signal can also suppress those unwanted reflected signals. This concept may also be used in Direction of Arrival (DoA) estimation. Similarly, a transmit antenna array can be configured to form a beam in the direction of the desired receiving user, thus enhancing the gain in this direction and limiting the transmit power in all other directions. It can be concluded that power is more efficiently utilised by using antenna array compared to a single monopole, since transmitted and received power is concentrated in the desired direction, thus avoiding transmission to the direction where a receiver is not present. The use of spatial domain separation as a multiple access scheme is often termed Space-Division Multiple Access (SDMA). A further advantage of using SDMA is that it can be used alongside other multiple access schemes such as FDMA and CDMA, further increasing the system capacity.

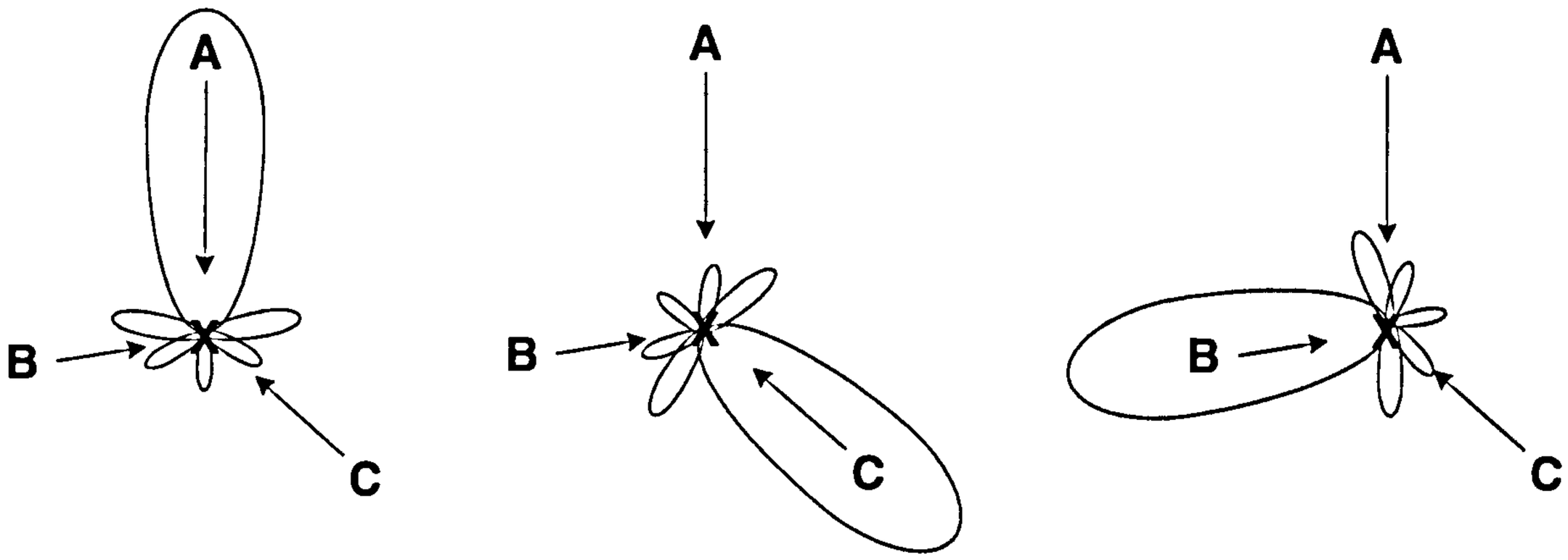

Figure 1.2: Spatial separation between users A, B and C

1.4 Benefits of Antenna Arrays in WLAN Applications

The beamforming and spatial separation capabilities of antenna arrays present a range of benefits in their Wi-Fi application, such as:

- **Range extension**

  In large open spaces such as a shopping complex, coverage extension is often more desirable as oppose to capacity improvement. In such areas, gain provided by smart antenna systems over an omni directional antenna can extend a cell coverage to a larger area compared to omni directional antennas. As illustrated in Figure 1.3, only Mobile Terminal (MT) 1 lies within the coverage range of the omni directional antenna. With smart antenna at the Access Point (AP), the increased gain extends the coverage and cell size to cover MTs 1-4.

Assuming an ideal environment, where no interference are present, the coverage area of an omni directional antenna, A_c, is given by

$$A_c = \pi R^2 \tag{1.1}$$

where R is the transmitter-receiver range. The received power, P_r, is described by

$$P_r = P_t G_t G_r L(d_0) \left(\frac{R}{d_0}\right)^{-\gamma} \tag{1.2}$$

where P_t is the transmit power, G_t and G_r represents the transmit and receive antenna gains, $L(d_0)$ is the free space path loss at a reference distance d_0 from the transmitter, and γ is the path loss exponent. Assuming $R \geq d_0$, this becomes

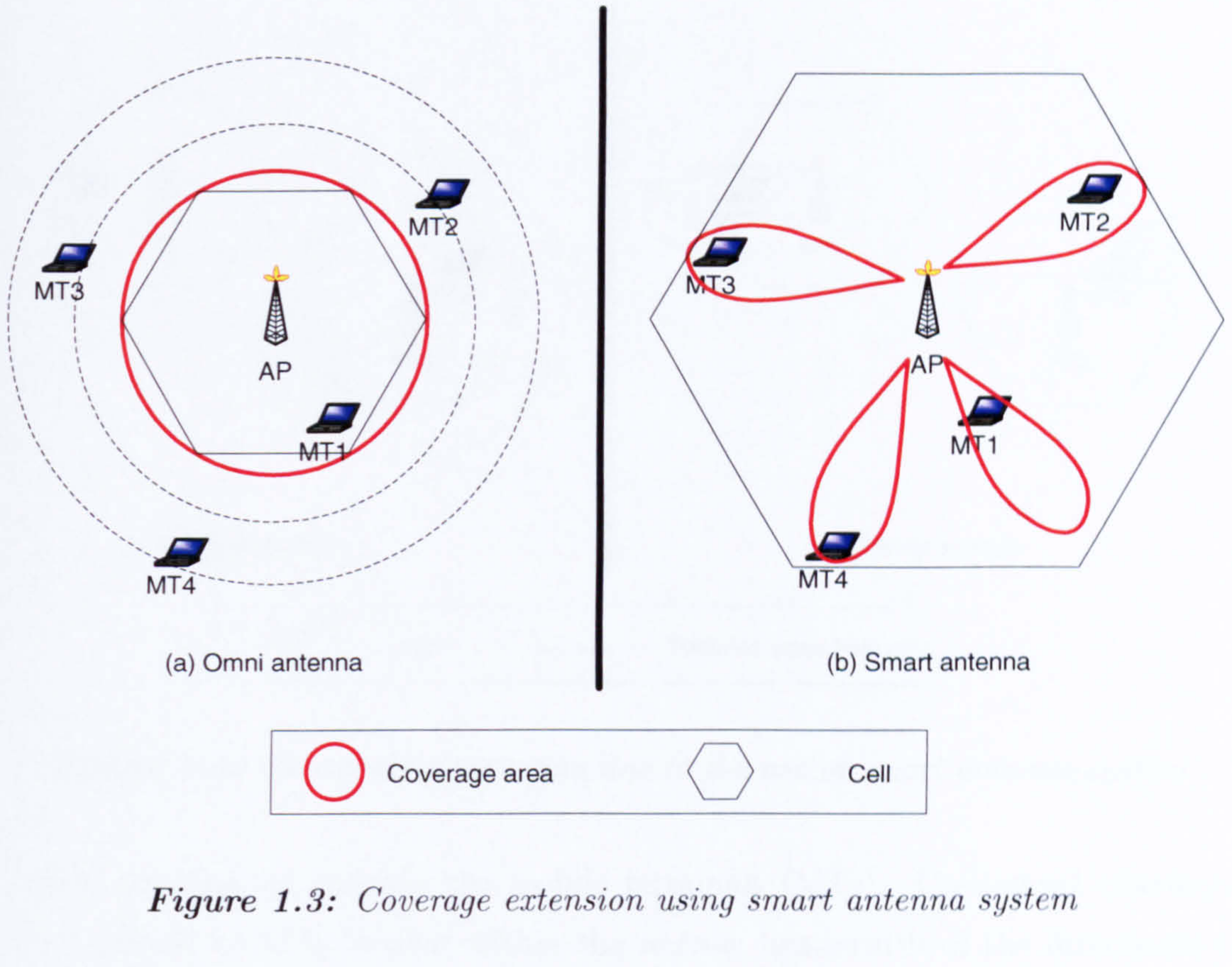

Figure 1.3: *Coverage extension using smart antenna system*

$$R = d_0 \left(\frac{P_t G_t G_r L(d_0)}{P_r} \right)^{1/\gamma} \tag{1.3}$$

and the relationship between coverage area and the antenna gain is

$$A_c \propto G^{2/\gamma} \tag{1.4}$$

where G is either the transmit or receive antenna gain, while the gain of the other is held constant.

In areas with high user density, coverage extension alone may not be sufficient as it may result in dropped or blocked connections due to insufficient capacity. In such a case, range extension is only practical when coupled with one of the following approaches.

- **Interference reduction and rejection**

  Two ways of increasing the capacity of a wireless system are interference reduction on the downlink and interference rejection on the uplink. Figure 1.4(a) shows signals from an omnidirectional AP1 arriving at an adjacent cell and acting as an interference. Using smart antennas (Figure 1.4(b)), directional beams are are formed by the access

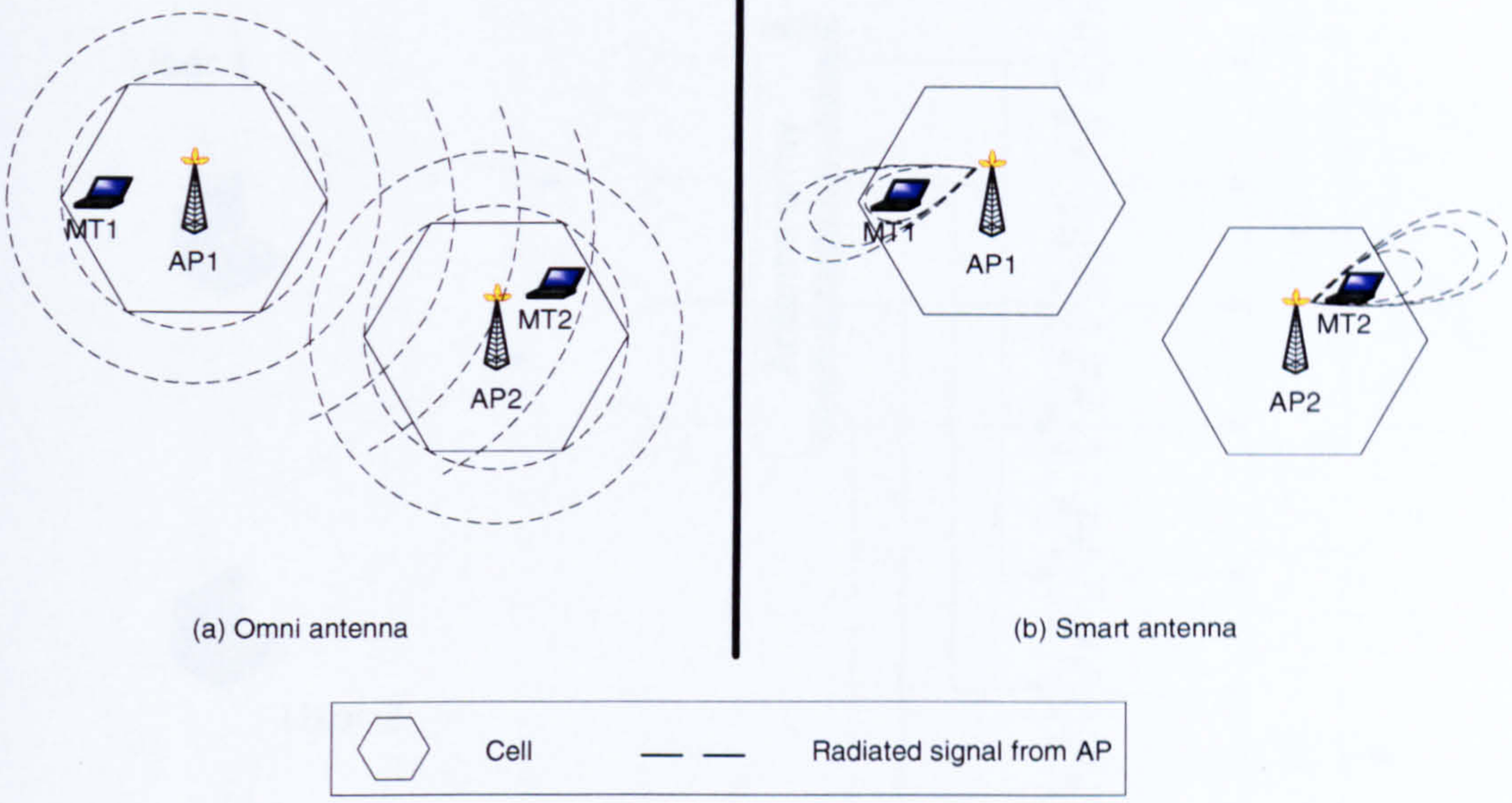

Figure 1.4: *Interference reduction due to the use of smart antenna system*

points and steered towards the mobile terminals (MTs). Co-channel interference is then limited to MTs located within the narrow beamwidth of the directional beam. By reducing coverage to the confined area of the beamwidth, probability of co-channel interference is reduced compared with a system with omnidirectional AP antennas. Similarly, the receiver pattern can be adjusted to form a directional beam towards the wanted MT and nulls towards co-channel users in order to reject interference caused by co-channel users [29] - [32]. These in turn affect the system capacity. The use of directional beams also reduces adjacent channel interference.

- **Space Division Multiple Access**

  Among the most sophisticated methods of adaptive beamforming is Space Division Multiple Access (SDMA). SDMA systems use N-element arrays in order to simultaneously form beams in several directions in the spatial domain, thus dividing the space into several spatial domains. This is shown in Figure 1.5 [33]. Each set of weights is chosen to retain the signal from one user and eliminate the signals from other users. Thus the system is able to communicate with X different users in the same cell on the same frequency, time or code channel. In order for this scheme to work, angular separation between users is necessary. However, scattering due to the propagation channel may cause the received signals from the mobile terminal to be broadened in terms of their angle of arrival, thus overlapping signals from different users despite their angular separation [34]- [35]. It follows that SDMA systems greatly relies on the capabilities of

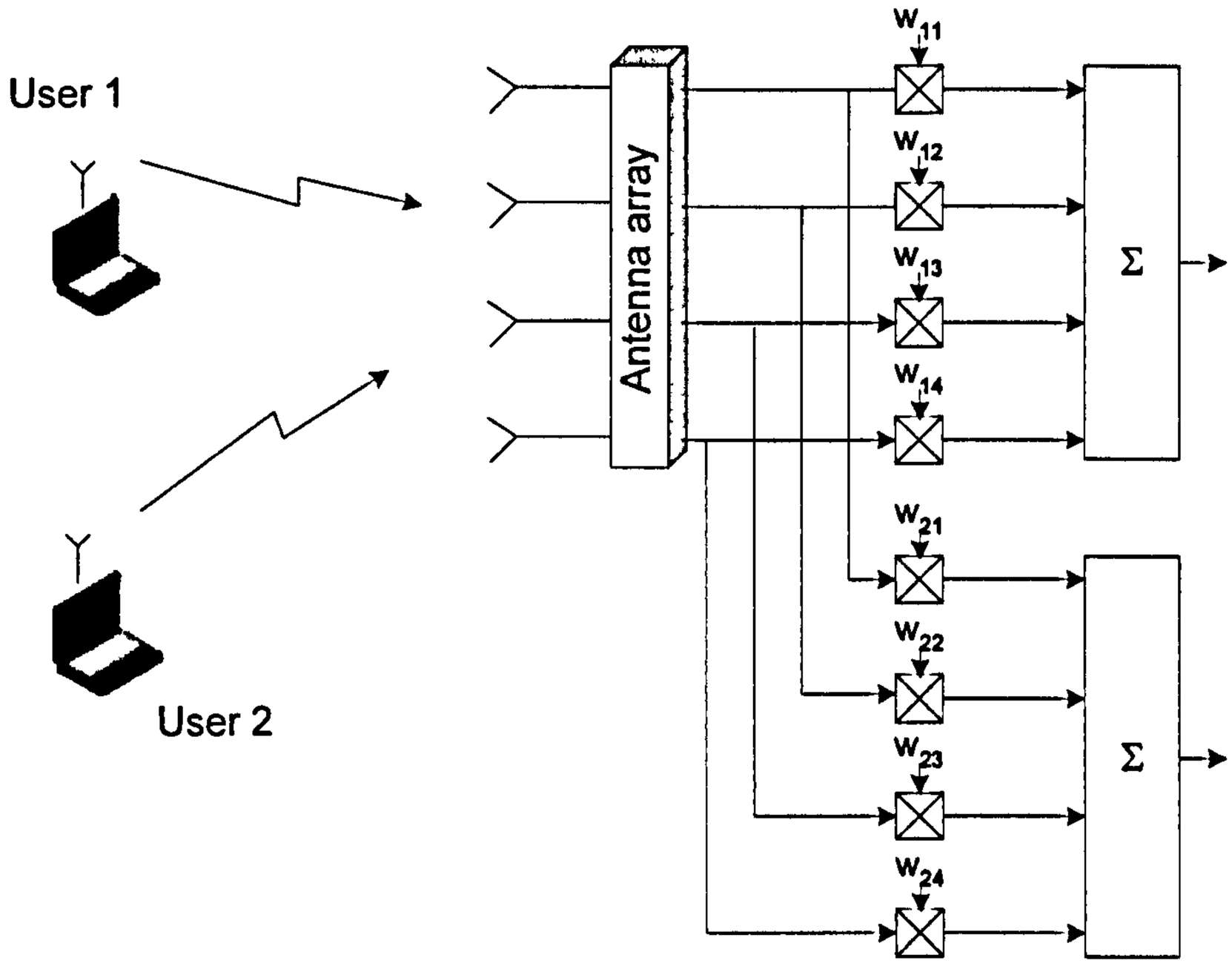

Figure 1.5: *Two-channel SDMA system*

the adaptive array used as well as the propagation channel characteristics. On top of the obvious spatial separation advantage, the use of antenna arrays with SDMA systems also provides uplink (UL) and downlink (DL) power saving capabilities as signals are transmitted solely towards the intended destination. This in turn extends the battery life of mobile terminals as well as providing the possibility of increasing cell radius, thereby reducing the number of required base stations. The probability of co-channel interference is also reduced.

[36] suggests that *spatial signature*, described as the received signal as a function of azimuth angle at the receiver, of a base station transmitter is stable for a period of minutes provided a line of sight is present. The spatial signature varies when propagation solely consists of reflected signals. At slow (i.e. walking) speed, spatial signature shows significant variation in 10s, although not much variation occurs within 1s when a direct path between BS and MT exists. It is shown that there can be significant difference in spatial signatures even for closely spaced transmitters, thus spatial diversity may be available despite small separation distance between two or more MTs. The benefit of the use of SDMA with indoor WLANs is confirmed through link-level simulations using measured indoor channel data, as discussed in [37].

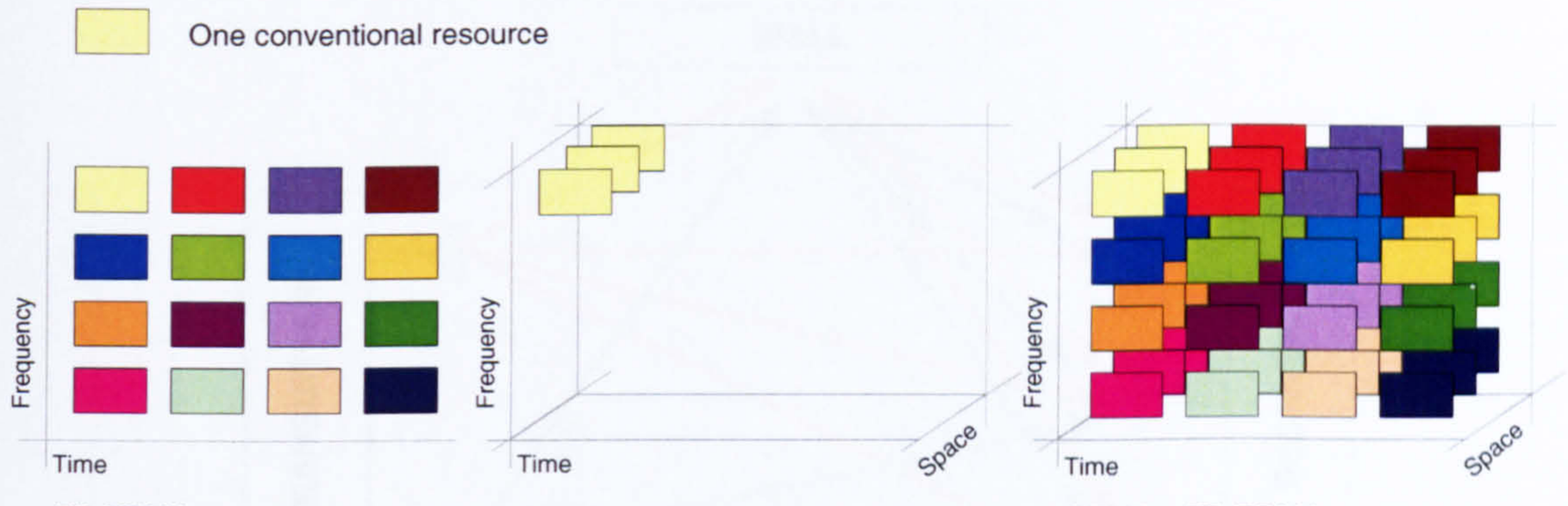

Figure 1.6: *SDMA combined with a TDMA system [34].*

Several communication systems exploit combinations of two multiple access sytems in order to further increase user capacity. The IS-95 cellular system uses combines CDMA and FDMA, using spread spectrum over 1.25MHz channels. [38] and [39] discuss systems that combines CDMA with TDMA in order to increase capacity and reduce interference. Similarly, an SDMA system can conveniently be used on top of another multiple access scheme. Figure 1.6 illustrates an SDMA system applied as a complement to an TDMA system. It can be seen that this increases the capacity of the overall system by up to S times, where S is the number of spatial channels available. [40] presents a combined CDMA/SDMA technique for cellular systems using space-time block code. The bit error rate (BER) performance of this arcitechture reveals that this arcitechture works well with the UMTS UTRA TDD and Time Division Synchronous Code Division Multiple Access (TD-SCDMA). A similar system can also be adapted to TDMA/SDMA systems. Liberti and Rappaport [41] presents a pseudo-SDMA approach with a combination of smart antennas and CDMA, which proves to increase capacity. The authors derived theoretical expressions for total interference power as well as BER. Computer simulations for the forward and reverse links are performed. In the reverse link, simulations shows a reduction of 1-3 orders of magnitude in BER compared to an omnidirectional antenna system, and the number of supportable users is increased by up to a factor of 4.

Some research is focused on the development of SDMA algorithms using full blind channel estimation [42], [43]. These algorithms rely heavily on linear algebra techniques and involve complex matrix decompositions, hence there is a strong need for computationally efficient algorithms. Several novel adaptive subspace based signal processing algorithms have been developed [44]- [46], leading to solutions which are mostly con-

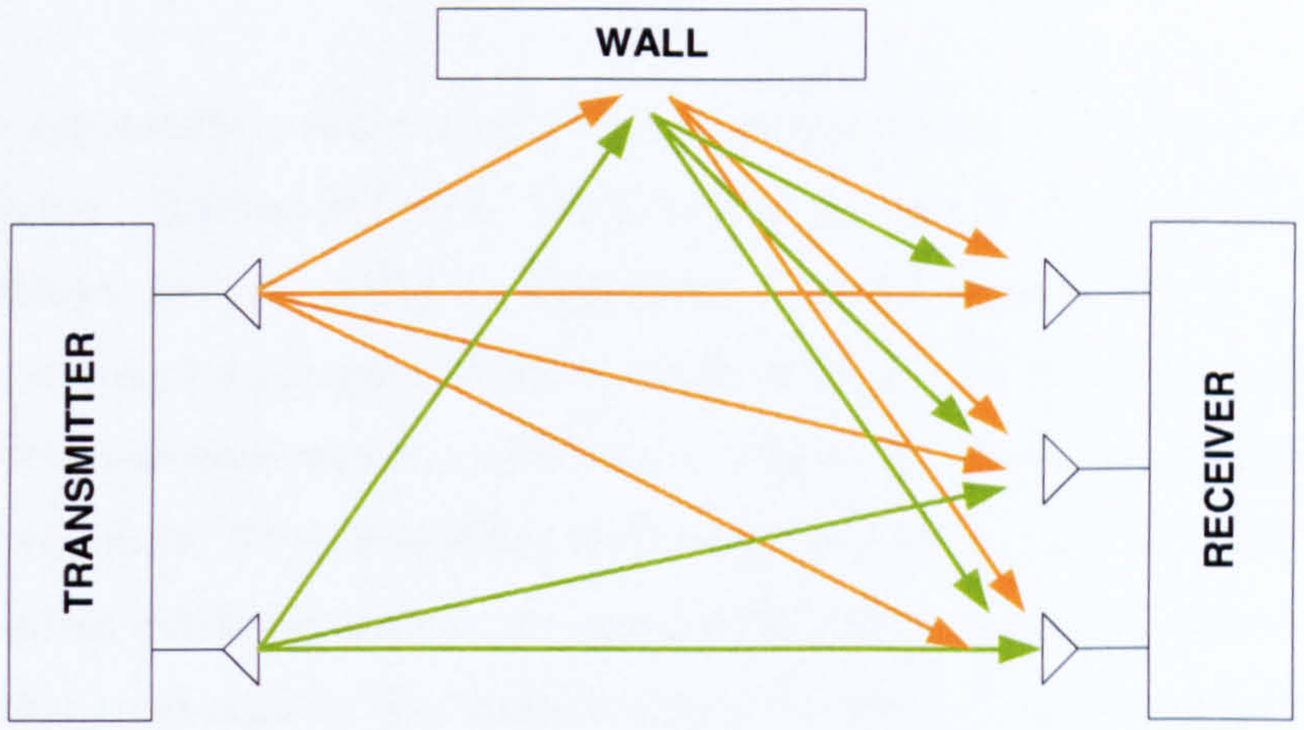

Figure 1.7: *Multiple paths MIMO system*

siderably more efficient than any other solution previously available in the literature.

- **Multiple Input Multiple Output (MIMO)**

  Multiple-Input Multiple-Output (MIMO) wireless systems [16]- [18] include the use of antenna arrays at both the transmitter and receiver ends. MIMO represents an economical way to increase user capacity in a variety of environments. MIMO algorithms send information out through an antenna array at the transmitter, and the information is received via multiple antennas as well. MIMO systems use the additional pathways to transmit more information and then recombines the signal on the receiving end (Figure 1.7). This allows multiplicative increase in capacity and spectral efficiency. Diversity created by the multiple antenna systems allow for dramatic fading reductions. Furthermore, MIMO systems provides improved resistance to interference. In short, MIMO systems provide a significant capacity gain over conventional single antenna systems, along with more reliable communication.

1.5 The Need for a Low Cost Solution for Wi-Fi APs

Many Wireless APs currently available in the market consist of a single antenna. A few employ two antenna elements for diversity. However, these are unsuitable for beamforming purposes. Examples of WLAN antennas currently available can be found in [47]. Smart antennas are becoming increasingly popular applications in the wireless world due to their abilities to enhance capacity. Nevertheless, array beamforming techniques vary widely in complexity and cost. A trade-off is required that provides a balance between cost, complexity and performance according to the intended application.

Researchers are constantly seeking novel solutions to the highly demanding and rapidly growing wireless market. Ruckus Wireless [48]produces its Smart Antenna technology, BeamFlex [49], for Wi-Fi devices, which is adaptable to any standard 802.11 a/b/g/n chipset. The technology employs a compact antenna array of high-gain directional antenna elements along with system software which continuously selects the optimum radiation pattern for each device in real time. This BeamFlex technology is said to offer over 300% performance improvement and an 800% expanded coverage for 802.11g/a networks. The system has been developed in order to maximise the Multiple Input-Multiple Output (MIMO) diversity, and can be implemented either at the Access Point (AP) or the Mobile Terminal (MT) or both.

Ofcom [50] is currently funding research under the spectrum efficiency scheme. A technology called *Semi-Smart Antennas* [51] which is based on providing sectored coverage as oppose to a narrow steerable beam is being developed, which relies on shaping the coverage according to the traffic needs [52]. The radiation pattern in a heavily loaded cell is contracted, and those of the adjacent cells are expanded in order to compensate for the coverage loss, as shown in Figure 1.8. This technique promises much lower complexity compared to a conventional smart antenna system. In addition, Ofcom has also developed a prototype of the IEEE 802.11a in order to gain a better understanding of the benefits of an adaptive antenna system.

ERA [53] is in the process of developing a Smart Antenna concept for WLAN applications, particularly the IEEE 802.11g [54]. The potential technology only requires a single driven element, surrounded by a set of parasitically excited radiators. Research is being carried out in order to identify the optimum antenna characteristics required as well as quantifying the performance benefits gained through the use of the Smart Antenna concept for the 802.11g.

When deployment is aimed towards the wireless applications such as Wi-Fi and WiMax, it is essential to realise that a low-complexity, hence a low-cost solution, is needed. Wi-Fi technology is quickly becoming extensively used in homes, offices, airports, university buildings and many other indoor environments. More than one AP may be needed to serve a given indoor wireless environment, hence it is paramount that these APs are affordable for the aimed market. On the other hand, it is also essential to bear in mind that the right balance is needed between the low cost and the beamforming capabilities of the system. While a low cost system is desirable, it should be noted that unless a sufficient increase in capacity and/or sufficient decrease in interference can be achieved, it may not be worth the extra cost of multiple antenna APs.

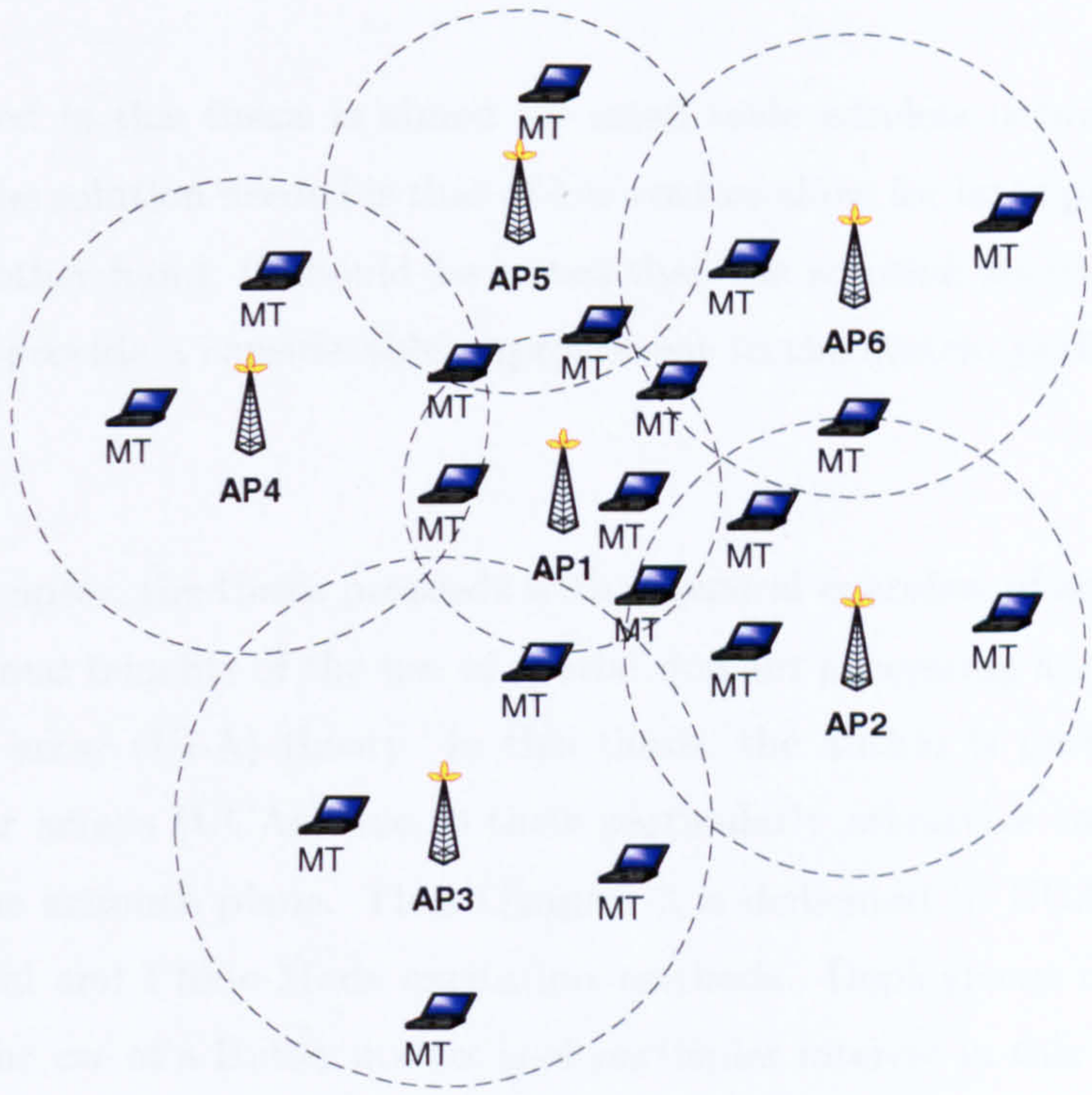

Figure 1.8: *Semi-smart antenna base stations co-operatively adjusting coverage to cope with traffic demand [51].*

1.6 Discussion and Thesis Overview

An overview of how wireless systems are rapidly evolving and the role of the antenna facet have been introduced in this chapter. The future of wireless networking in the form of Wi-Fi and WiMAX is discussed. The limited bandwidth availability in an ever-growing popularity of wireless solutions has lead to the use of smart antennas in an attempt to increase channel capacity as well as reduce interference. The chapter thus continued with a brief look of the advantages of using smart antennas in wireless communication systems. A range of different complexity solutions are discussed. There is often a trade-off between the quality of the received signals and the complexity of the solution. While simple beamforming methods are capable of producing some of the advantages a smart antenna could produce, the quality of the results, in terms of beamwidth, sidelobe level (SLL) and steerability of the beams, may be limited. On the other hand, an increased complexity in the form of adaptive beamforming presents improvements in signal quality. However, increased complexity typically involves increased costs, therefore an optimum solution which balances these aspects should be formulated for each application.

The work presented in this thesis is aimed for small scale wireless networking applications such as WLAN. The solution needed is that of low-cost to allow for large production volumes. However, on the other hand, it should be noted that the solution should be cost-effective. That is, it should provide a considerable improvement to the system performance as well as low-cost.

In the following chapter, the thesis proceeds with a general overview of array signal processing. Applications and benefits of the use of spatial domain processing are outlined, followed by uniform linear array (ULA) theory. In this thesis, the author is particularly interested in uniform circular arrays (UCAs) due to their particularly attractive capability of serving the full 360^o of the azimuth plane. Thus Chapter 3 is dedicated to UCA theory, including the Beam Cophasal and Phase-Mode excitation methods. Deployment of the Phase-Mode method through the use of a Butler matrix is of particular interest in this chapter due to the matrix' capability to transform UCA patterns in such a way that ULA weights can be applied to them. Several key issues in determining the circular array geometry are also discussed. Studies throughout this thesis are based on a working frequency of 5.2GHz for compatibility with IEEE 802.11a, however results and parameters can be easily scaled for other frequencies, such as 2.4GHz.

In Chapter 4, the pattern synthesis and array excitation techniques described in the preceding chapter are put to the test when applied to various practical arrays. Practical UCAs as well as a Finite Difference Time Domain (FDTD) model are constructed in order to aid the analysis, and results are compared to those of the ideal scenario. It is shown that in the real scenario where mutual coupling, manufacturing and measurement errors are unavoidable, employing these synthesis techniques on their own without accounting for the array imperfections produce results that are far less attractive than it appears to be under the ideal case.

In Chapter 5, the effects of mutual coupling and other array imperfections are introduced to the ideal model. A series of mutual coupling compensation methods are described. A method of tackling mutual coupling as well as array imperfections together, through the use of a Butler matrix, is presented. The method is applied to the ideal as well as real arrays for comparison purposes. Experimental results show that the errors introduced by a real scenario introduces further complications to the parameters used in this technique. Finite Difference Time Domain (FDTD) modeling is used in order to provide a more thorough understanding of the array behaviour. Through this model, the correcting parameter is simplified and error

analysis is presented in order to prescribe the optimum solution for cost-effective circular array beamforming.

Chapter 6 concludes the thesis, with a brief discussion on the findings presented in the preceeding chapters. Finally, suggestions for future work concludes the thesis.

1.7 Original Contributions to the Body of Knowledge

The Uniform Circular Array (UCA) has been used in several applications [55]- [69], however these are primarily high-level applications which involve complex hardware and direction finding algorithms. Furthermore, UCA beamforming solutions with the combined use of UCA and Butler matrix that are currently available in literature, such as [66], are often based on theoretical assumptions of ideal amplitude and phase responses. That is, amplitude and phase responses of the elements are perfectly symmetrical around the array circumference. However, this is not the case in practical environments where manufacturing tolerances as well as inter-element interactions result in asymmetrical element patterns and hence the resulting beam patterns, as shown in Chapter 4. The proposed solution presented in this thesis involves measured element patterns which include amplitude and phase variations.

Unlike other UCA applications that are currently available in literature, the work presented in this thesis is focused on low-complexity UCA Butler matrix for indoor wireless network Access Point (AP) applications, where minimum manufacturing cost is paramount for mass production purposes. The proposed capacity enhancement solution involves a set of simple phase and amplitude weights, avoiding the more complex algorithms [67] and digital signal processing [68]- [69]. The entire feeding network can be deployed as a microstrip network of couplers and splitters. While the proposed solution is not as *intelligent* as the more complex beamforming solutions, the author feels that its advantage in low manufacturing costs outweighs the performance advances of its counterparts.

Research presented in this thesis explores key issues regarding the use of UCAs. Results obtained from these studies and analysis form a set of contributions towards the constantly increasing knowledge of antenna array technology. This section presents a summary of these contributions.

- *A proposal has been made for the geometry of a UCA suitable for low-cost beamforming applications. Through the application of switched-beam and phase-mode excitation*

methods on ideal UCA radiation patterns, the UCA behaviour is analysed and the optimum configuration is proposed in terms of radius, number of antenna elements, and type of antenna elements used for the UCA.

- *Experimental evaluation of UCA switched-beam and phase-mode excitation methods through the use of measured data taken from practical UCAs. Practical performance of the UCA is presented in terms of the actual achieved beamwidth and sidelobe level. Results reveal that some form of pattern compensation is needed in order to improve the performance of the beamforming system which is limited by element interactions and array imperfections.*

- *A design for low-complexity UCA beamforming is proposed which includes practical values for embedded pattern compensation in order to improve UCA pattern synthesis performance, through the aid of FDTD modeling. The compensation involves a set of simple amplitude and phase weights which improves the achievable sidelobe level by at least 10dB.*

- *Error analysis is presented, through the use of measured data as well as additional FDTD modeling, in order to define the manufacturing tolerance of the UCA as well as the proposed pattern compensation.*

References

[1] J.S. Belrose, "Reginald Aubrey Fessenden and the Birth of Wireless Telephony", *IEEE Antennas and Propagation Magazine*, Vol.44, No.2, pp38-47, April 2002.

[2] J.M. Pereira, "Fourth generation: now, it is personal!", *IEEE International Symposium on Personal, Indoor and Mobile Radio Communications*, Vol. 2, pp.1009-1016, September 2000.

[3] R.B. Marks, I.C. Gifford, B. O'Hara, "Standards in IEEE 802 unleash the wireless Internet", *IEEE Microwave Magazine*, Vol. 2, Issue 2, pp.46-56.

[4] A. Chaturvedi, M.B.R. Murthy, "WPAN scheme for Bluetooth devices: a review", *4th National Conference on Telecommunications Technology Proceedings*, pp.5-7, January 2003.

[5] M.A. Marsan, C.F. Chiasserini, A. Nucci, G. Carello, L. De Giovanni, "Optimizing the topology of Bluetooth wireless personal area networks", *IEEE Computer and Communications Societies Proceedings*, INFOCOM, Vol. 2, pp.572-579, June 2002.

[6] Wi-Fi Alliance Website, *http://www.wi-fi.org/OpenSection/index.asp*, referenced in January 2006.

[7] J-H. Yeh, J-C. Chen, C-C. Lee, "WLAN standards", *IEEE Potentials*, Vol. 22, Issue 4, pp.16-22, October-November 2003.

[8] "Wi-Fi hotspot networks sprout like mushrooms", *IEEE Spectrum*, Vol. 39, Issue 9, pp.18-20, September 2002.

[9] WiMAX Forum Website, *http://www.wimaxforum.org*, referenced in January 2006.

[10] S.J. Vaughan-Nichols, "Achieving wireless broadband with WiMax", *Computer*, Vol. 37, Issue 6, pp.10-13, June 2004.

[11] A. Ghosh, D.R. Wolter, J.G. Andrews, R. Chen, "Broadband wireless access with WiMax/802.16: current performance benchmarks and future potential", *IEEE Communications Magazine*, Vol. 43, Issue 2, pp.129-136, February 2005.

[12] M. Suryanegara, E.R. Hutabarat, D. Gunawan, "The Interference on WCDMA System in 3G Coexistence Network", *IEEE Internal Symposium of Personal, Indoor and Mobile Radio Communications*, pp.1-5, September 2006.

[13] H. Honkasalo, K. Pehkonen, M.T. Niemi, A.T. Leino, "WCDMA and WLAN for 3G and beyond", *IEEE Wireless Communications*, Vol. 9, Issue 2, pp.14-18, April 2002.

[14] J. Fisher, R. Wang, "Wireless Wide Area Networks (WWANs)", *http://www.pdamd.com/vertical/features/wireless_4.xml*, referenced in October 2005.

[15] Chuanxiong Guo, Zihua Guo, Qian Zhang, Wenwu Zhu, "A seamless and proactive end-to-end mobility solution for roaming across heterogeneous wireless networks", *IEEE Journal on Selected Areas in Communications*, Vol. 22, Issue 5, pp.834-848, June 2004.

[16] J.M. Gilbert, Won-Joon Choi, Qinfang Sun, "MIMO technology for advanced wireless local area networks", *42nd Design Automation Conference Proceedings*, pp.413-415, June 2005.

[17] H. Boelcskei, "Fundamental tradeoffs in MIMO wireless systems", *Proceedings of the IEEE 6th Circuits and Systems Symposium on Emerging Technologies: Frontiers of Mobile and Wireless Communication*, Vol. 1, pp. 1-10, 2004.

[18] D. Gesbert, M. Shafi, S. Da-shan, P.J. Smith, A. Naguib, "From theory to practice: an overview of MIMO space-time coded wireless systems", *IEEE Journal on Selected Areas in Communications*, Vol. 21, Issue 3, pp.281-302, April 2003.

[19] M.W. Ritter, "The future of WLAN", *http://delivery.acm.org/10.1145/850000/846059/futurewlan.html?key1=846059&key2=8156537311&coll=GUIDE&dl=GUIDE&CFID=62499025&CFTOKEN=57429806*, referenced in December 2005.

[20] A. Scottsdale, "Wi-Fi services in Asia to reach nearly $1.3 billion in 2010", *In-Stat Press Release*, 4 January 2006, *http://www.instat.com/press.asp?ID=1529&sku=IN0502397ANT*, referenced in January 2006.

[21] Geoffrey Baird, "Avaya 2005 global research report: Working to bommunicate better in business", *http://www1.avaya.com/pc/GlobalMobilitySIPResearchReportFINAL2.pdf*, referenced in January 2006.

[22] R.C. Hansen, *Linear Arrays*, in Rudge et all. [70]

[23] R.C. Hansen, *Circular Arrays*, in Rudge et all. [70]

[24] *http://www.bbwexchange.com/news/archive/analysys112601.htm*, referenced in January 2006.

[25] "WiMAX and broadband wireless (Sub-11GHz) worldwide market analysis & trends 2005-2010", *http://www.wimax.com/commerce/catalog/2005wimaxmarket*, referenced in January 2006.

[26] M.A. Beach, R.L. Davies, P. Guemas, H. Xue, J.P. McGeehan, "Capacity and service extension for future wireless networks using adaptive antennas", *Ninth International Conference on Antennas and Propagation* (Conf. Publ. No. 407), ICAP '95, Vol. 1, pp.125-129, April 1995.

[27] S.C. Swales, M.A. Beach, D.J. Edwards, J.P. McGeehan, "The performance enhancement of multibeam adaptive base-station antennas for cellular land mobile radio systems", *IEEE Transactions on Vehicular Technology*, Vol. 39, Issue 1, pp.56-67, February 1990.

[28] L.J. Pesik, M.A. Beach, D.P. McNamara, P.N. Fletcher, "Performance analysis of smart antenna systems for indoor wireless LANs", *Third International Conference on 3G Mobile Communication Technologies* (Conf. Publ. No. 489), pp.418-422, May 2002.

[29] J.H. Winters, J. Salz, R.D. Gitlin, "Adaptive antennas for digital mobile radio", *Proc. IEEE Long Island Section Adaptive Antenna Systems Symposiom*, pp81-86, Long Island, Ny, November 1992.

[30] J. Kennedy, M.C. Sullivan, "Direction finding and smart antennas using software radio architectures", *IEEE Communications Magazine*, pp62-68, May 1995.

[31] R. Kohno, H. Imai, M. Hatori, S. Pasupathy, "Combination of an adaptive array antenna and a canceller of interference for direct-sequence spread-spectrum multiple access system", *IEEE JSAC*, Vol. 8, No. 4, pp675-682, May 1990.

[32] S. Anderson, M. Millnert, M. Viberg, B. Wahlberg, "An adaptive array for mobile communication systems", *IEEE Transactions on Vehicular Technology*, Vol. 40, No. 1, pp230-236, February 1991.

[33] S.R. Saunders, "Antennas and propagation for wireless communication systems", John Wiley & Sons, 1999.

[34] A.S.Y. Poon, D.N.C. Tse, R.W. Brodersen, "Impact of scattering on the capacity, diversity, and propagation range of multiple-antenna channels", *IEEE Transactions on Information Theory*, Vol. 52, Issue 3, pp.1087-1100, March 2006.

[35] J. Medbo, J.-E. Berg, "Spatio-temporal channel characteristics at 5 GHz in a typical office environment", *IEEE 54th Vehicular Technology Conference*, Vol. 3, pp1256-1260, October 2001.

[36] G. Xu, H. Liu, W.J. Vogel, H.P. Lin, S.S. Jeng, G.W. Torrence, "Experimental studies of space division multiple access schemes for spectral efficient wireless communications", *IEEE International Communications Conference*, Vol. 2, pp800-804, 1994.

[37] A.T. Alastalo, M. Kahola, "Smart-antenna operation for indoor wireless local-area networks using OFDM", *IEEE Transactions on Wireless Communications*, Vol. 2, Issue 2, pp.392-399, March 2003.

[38] K. Hamidian, J. Payne, "Combined CDMA with TDMA increases the capacity of a cellular communication system", *IEEE Pacific Rim Conference on Communications, Computers and Signal Processing*, Vol. 2, pp.769-773, May 1993.

[39] F. Hendessi, A.U.H. Sheikh, T.A. Gulliver, "A TDMA-CDMA cellular system", *IEEE Vehicular Technology Conference*, Vol. 1, pp.373-376, May 1997.

[40] W. Li, T.A. Gulliver, M. Esmaeili, "A new CDMA/SDMA structure with transmit diversity", ***http://www.ece.uvic.ca/~agullive/j1e.pdf***, referenced in January 2006.

[41] J.C. Liberti, Jr, T.S. Rappaport, "Analytical results for capacity improvements in CDMA, *IEEE Transactions on Vehicular Technology*, Vol. 43, No. 3, pp680-690, August 1994.

[42] H. Liu, M. D. Zoltowski, "Blind Equalization in Antenna Array CDMA Systems", *IEEE Transactions on Signal Processing*, Vol. 45, No. 1, January 1997, pp. 161-172.

[43] P. Vandenameele, L. Van der Perre, M. Engels, H. De Man, "Blind vs. trained channel estimation for an SDMA WLAN", *URSI International Symposium on Signals, Systems, and Electronics*, pp.465-470, September-October 1998.

[44] Jingmin Xin, A. Sano, "Efficient subspace-based algorithm for adaptive bearing estimation and tracking", *IEEE Transactions on Signal Processing*, Vol. 53, Issue 12, pp.4485-4505, December 2005.

[45] P. Strobach, "Fast recursive subspace adaptive ESPRIT algorithms", *IEEE Transactions on Signal Processing*, Vol. 46, Issue 9, pp.2413-2430, September 1998.

[46] J.W. Kim, C.K. Un, "A robust adaptive array based on signal subspace approach", *IEEE Transactions on Signal Processing*, Vol. 41, Issue 11, pp.3166-3171, November 1993.

[47] Wireless Network Products, *http://www.wirelessnetworkproducts.com*, referenced in January 2006.

[48] Ruckus Wireless Website, *http://www.ruckuswireless.com*, referenced in January 2006.

[49] "Beamflex", *http://www.ruckuswireless.com/technology/beamflex.php*, Ruckus Wireless Website [37], referenced in January 2006.

[50] Ofcom Website, *http://www.ofcom.org.uk*, referenced in January 2006.

[51] P. Nahi, C.G. Parini, S. Papadopoulos, L. Du, J. Bigham, L. Cuthbert, "A semi-smart antenna concept using real-time synthesis for use in a distributed load balancing scheme for cellular networks", *Twelfth International Conference on Antennas and Propagation* (ICAP), No. 491, Vol. 1, pp.168-171, March-April 2003.

[52] "Understanding and furthering emerging technologies: SMART Antennas", *http://www.ofcom.org.uk/research/technology/overview/emer_tech/smart/*, Ofcom Website [43], referenced in January 2006.

[53] ERA Website, *http://www.era.co.uk*, referenced in January 2006.

[54] "Increasing the capacity of wireless network using affordable SMART antennas", *Solutions ERA Technology* (*http://www.era.co.uk/news/pr0522.asp*), November 2005.

[55] D.E.N. Davies, M.S.A.S. Rizk, "Electronic steering of multiple-nulls for circular arrays", *Electronic Letters*, Vol. 13, pp669-670, October 1977.

[56] J.C. Lim, "Introduction of a sharp steerable null response in an otherwise omnidirectional pattern using a circular array", *Radio Electronic Engineering*, Vol.47, pp30-32, January/February 1977.

[57] D.E.N . Davies, J.R.F. Guy, "A UHF communication antenna employing open-loop control null steering", *Antennas and Propagation Society International Symposium*, Vol.19, pp276-279, June 1981.

[58] H.D. Griffiths, R. Eiges, "Sectoral phase modes from circular antenna arrays", *Electronic Letters*, Vol. 28, Issue 17, pp1581-1582, August 1992.

[59] H.D. Griffiths, "The use of circular arrays for direction finding applications", *IEE Colloquium on Passive Direction Finding*, pp7/1-7/4, January 1989.

[60] C.P. Mathews, M.D. Zoltowski, "Direction finding with circular arrays via phase mode excitation and Root-MUSIC", *Antennas and Propagation Society International Symposium*, Vol.2, pp1019-1022, July 1992.

[61] M. Zeytinoglu, J. Litva, J. Qian, "High-resolution direction finding using circular arrays", *International Conference on Acoustics, Speech, and Signal Processing*, Vol.5, pp3341-3344, April 1991.

[62] M. Cvetkovic, "A four element circular array direction finding and null steering system", *Sixth International Conference of Antennas and Propagation*, Vol.1, pp168-172, April 1989.

[63] J. Ramos, C.P. Mathews, M.D. Zoltowski, "FCA-ESPRIT: a closed-form 2-D angle estimation algorithm for filled circular arrays with arbitrary sampling lattices", *IEEE Transactions on Signal Processing*, Vol. 47, Issue 1, pp213-217, January 1999.

[64] G. Skahill, W. White, "A new technique for feeding a cylindrical array", *IEEE Transactions on Antennas and Propagation*, Vol.23, Issue 2, pp253-256, March 1975.

[65] J. Boyns, C. Gorham, A. Munger, J. Provencher, J. Reindel, B. Small, "Step-scanned circular-array antenna", *IEEE Transactions on Antennas and Propagation*, Vol. 18, Issue 5, pp590-595, September 1970.

[66] B. Sheleg, "A matrix fed circular array for continuous scanning", *IEEE Proceedings*, Issue 56, pp2016-2027, November 1968.

[67] A. Grau, J. Romey, L. Jofre, F. De Flaviis, "On the MIMO capacity using a Butler matrix with circular arrays in fading indoor environments", *IEEE Antennas and Propagation Society International Symposium*, Vol. 2A, pp.297-300, July 2005.

[68] S.C. Chan, H.H. Chen, K.L. Ho, "Adaptive beamforming using uniform concentric circular arrays with frequency invariant characteristics", *IEEE International Symposium on Circuits and Systems*, Vol. 5, pp.4321-4324, May 2005.

[69] G. Lehmann, C. Gessner, M. Haardt, "Evaluation of link-level performance improvements by using smart antennas for the TD-CDMA based UTRA TDD mobile radio

system", *52nd IEEE Vehicular Technology Conference*, Vol. 3, pp.1328-1332, September 2000.

[70] A.W. Rudge, K. Milne, A.D. Olver, P. Knight, Eds., *The Handbook of Antenna Design*, Vol. 1 and 2, Peter Peregrinus Ltd, London, UK, 1986.

Chapter 2

Array Signal Processing

The quality of service from a wireless communication network greatly relies on the efficiency of transmission and reception of electromagnetic energy. In some cases it is sufficient to do this using a single antenna element, which can be of various types depending on the frequency range, type of environment, and costs among many other factors. However, when the application demands higher directional gain, dynamic directivity, diversity and steerability, an array of two or more antenna elements may be used.

The advantages of antenna arrays over other single antennas have long been realised. Antenna arrays are now widely used in a variety of applications including medical, radar, cellular applications. Today, the types of antenna array used range from linear arrays, circular arrays and planar arrays to conformal arrays, although linear arrays are more commonly found. The variety of antenna elements used in these arrays includes half-wave dipoles, monopoles and patch antennas. The use of an antenna array coupled with array signal processing presents the ability to mould the radiation pattern into a desired shape. Over the years a vast amount of different array signal processing techniques have been developed. These range from the simple switched-beamforming methods [1]- [6] to the more complex adaptive processing where the array can be designed to adapt to changes in the environment in real time [7]- [9], as well as the more recent multiple-input multiple-output (MIMO) algorithms [10]- [13].

This chapter presents an overview of the benefits of spatial domain processing followed by a brief discussion on Uniform Linear Array (ULA) theory and the potential advantages of using Uniform Circular Arrays (UCAs). The chapter also illustrates the benefits of Butler Matrices and the underlying theory in array signal processing as well as some pattern control problems.

2.1 Directivity, Beamwidth, and Sidelobe Level

This sub-section outlines some of the useful measures often used in defining or comparing radiation pattern performance of arrays of different sizes, geometry or excitations.

An isotropic antenna is an antenna which radiates uniformly in all directions. In actual fact, all real antennas have some degree of non-uniformity in their three-dimensional radiation patterns. A perfectly uniform radiation pattern is impossible to achieve. *Directive gain* is defined as the ratio of radiated power in a particular direction, and at a particular distance, to the power density radiated by an isotropic antenna at the same distance. *Directivity* is the term used for the maximum directive gain. Therefore directivity D is also defined as:

$$D = \frac{4\pi \left|E(\theta_0, \phi_0)\right|^2}{\int_0^{2\pi} \int_0^{\pi} \left|E(\theta_0, \phi_0)\right|^2 \ sin\theta \ d\theta \ d\phi} \tag{2.1}$$

where $E(\theta_0, \phi_0)$ denotes the element far-field radiation in the direction (θ_0, ϕ_0). θ and ϕ are the elevation and azimuth angles surrounding the element.

In general, most array pattern manipulations aim to sculpt the radiation pattern so that it is concentrated into a single dominating "lobe". The width of this main lobe or beam is called *beamwidth*. The term is a measure of the angular width of the main beam, usually measured at the half-power point, i.e., the angular value between two points on either side of the main beam, which are 3dB below the peak of the main beam. In a receiver array, a narrow beamwidth could be useful in determining the direction from which a signal is arriving from. Pointing a narrow receiving beam towards the direction of the transmitter also results in an increased gain for the desired signal, and a reduced gain for the undesired signal. Similarly, in a transmitter array a narrow beam is used to transmit signals towards a particular desired direction. The narrower the beam, the more accurate these operations would be.

Sidelobe level is usually defined as the difference between the maximum sidelobe of the radiation pattern, to that of the main beam. In most cases, it is ideal to have low or no sidelobe levels as this suppresses the signals arriving from undesired directions.

2.2 Array Beamforming Methods

Generally, antenna array beamforming methods are divided into four different categories which are listed in the following subsections. These methods vary in complexity, cost and beamforming capabilities. The appropriate method of beamforming should be selected and

optimised according to the intended application.

2.2.1 Switched-sector

The simplest form of array processing is the *switched − sector* [14]- [18] method, where a switching network is employed together with an array of directional elements. Figure 2.1(a) illustrates an eight-element Uniform Circular Array (UCA) incorporating directional patch elements, each forming a beam which covers a sector of the array plane. The switching network, as shown in Figure 2.1(b), identifies the element with the highest level of received power and appoints this element as the active element until another element receives a higher received power. This is a very simple method of spatial isolation between beams as it does not involve any array radiation pattern beamforming, although evidently the degree of separation is limited to the shape of the directional elements.

2.2.2 Fixed beamforming network

Fixed beamforming system consists of a beamforming matrix which forms a set of $\leq N$ overlapping beams that, when combined together, result in continuous coverage of an area larger than the beamwidth. An example of this is shown in Figure 2.2. An advantage of these beamforming matrices is that they are bi-directional, i.e. transmission through a receiving port corresponding to a particular beam pattern produces a transmit beam of the same shape.

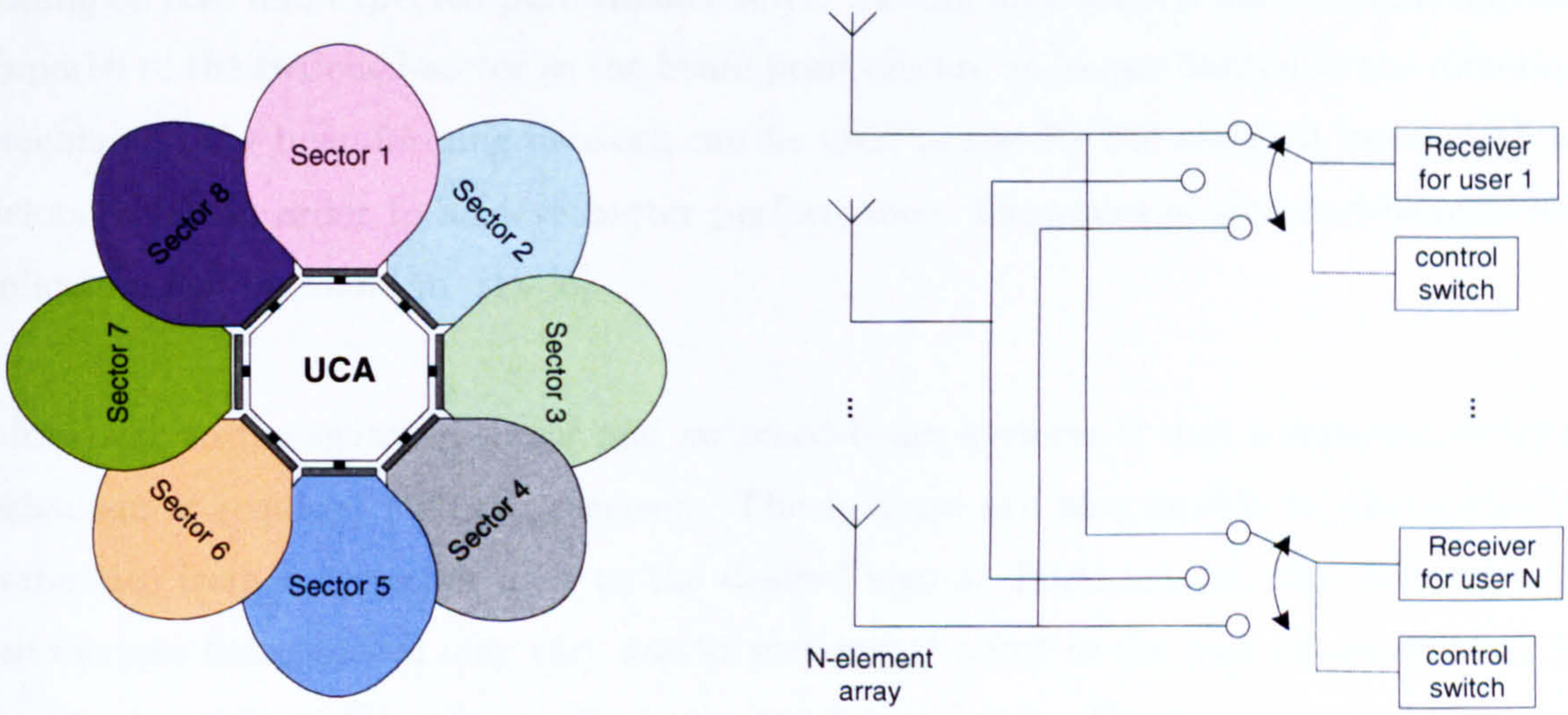

Figure 2.1: *(a)Eight-element UCA switched sector; (b)Switching mechanism for switched sector network*

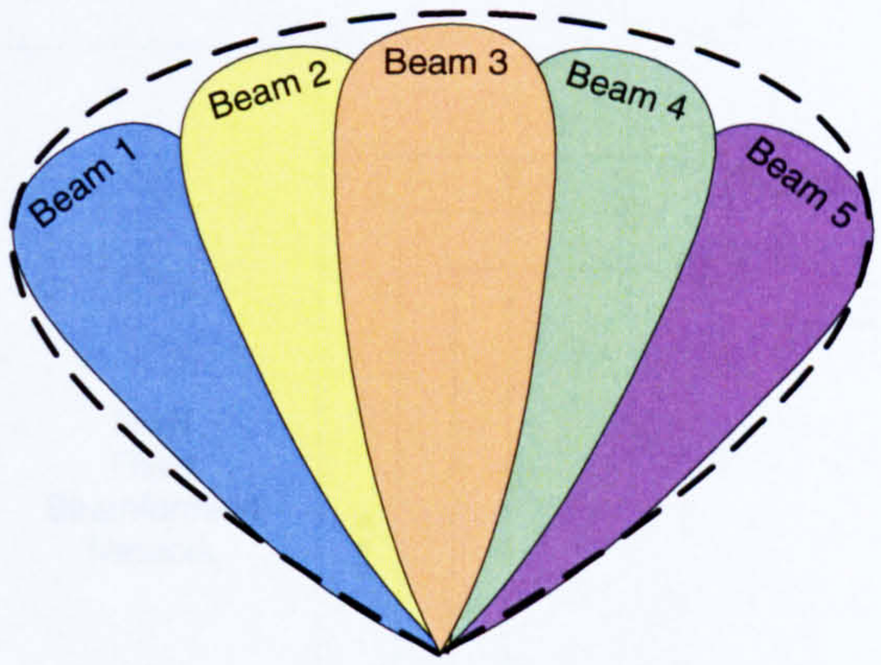

Figure 2.2: *Overlapping beams*

When the matrix consists of $N \times N$ orthogonal columns, the network produces N orthogonal beams. The peak of each of these beam patterns correspond to a null in the other beam patterns. An example of a commonly used beamforming matrix is the *Butler matrix* [1]- [2], [19]- [21] which is discussed in more detail in the next chapter.

When implemented on its own, a fixed beamforming system includes a *switching mechanism* that consists of an RF switch and control logic, in order to select the best beam with which to receive or transmit. This system is also often called a *switched beamforming system* [22] as shown in Figure 2.3. Switched-beam systems offer range extension as well as interference suppression in the directions away from the active beam. The beamforming network used in switched-beam systems may range from a simple algorithm to a more sophisticated one, depending on cost and expected performance level. The method gives a more flexible approach compared to the switched-sector as the beam positions are no longer limited to the directional elements and the beamforming network can be used to specify the required beamwidth and sidelobe levels in order to achieve better performance. Examples of switched-beamforming application can be found in [1]- [6].

A drawback to the switched-sector and switched-beam systems is that a separate switching mechanism is required for each receiver. The systems are also unable to distinguish any interference from a direction near to the desired signal. Furthermore, the received power from the user being served may vary due to *scalloping*[1] effect as the user moves around. The amount of variation depends on the beam cross-over levels. However, it should be noted that despite these disadvantages, a switched beam system and, to a lesser extent, a switched

[1] *Scalloping* is the rolling-off effect of the antenna pattern as a function of angle relative to a beam pattern at boresight [22].

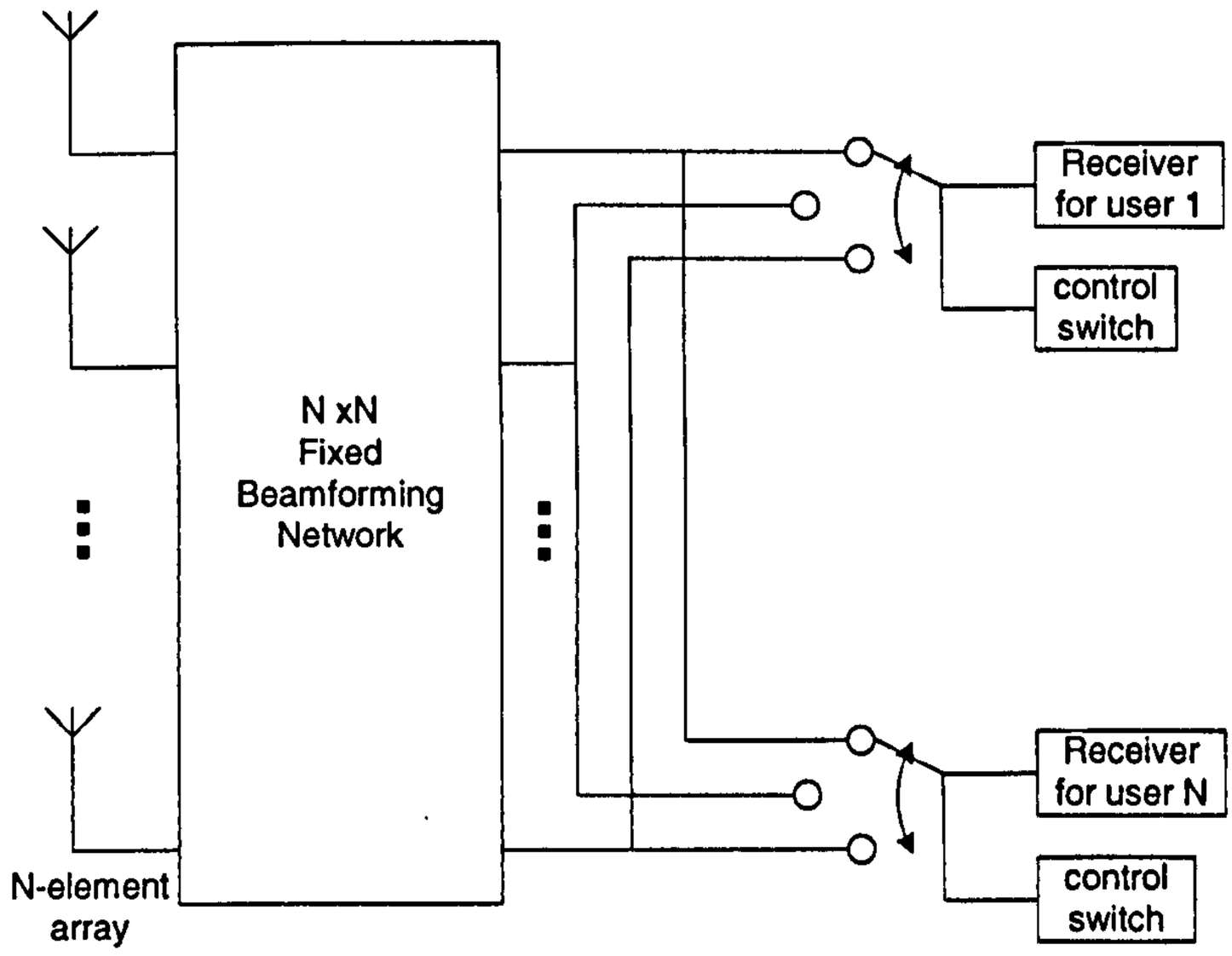

Figure 2.3: *Switched beamforming network [22]*

sector system, still bear the advantages of using an antenna array at the receiver/transmitter, including range extension and some interference rejection. It should also be noted that these systems are robust and low in complexity compared to the adaptive option.

An orthogonal beamforming matrix may also be used in conjunction with an adaptive array processor in order to improve the performance of the adaptive system. In this case, the fixed beamforming network provides an additional *filtering mechanism* which reduces interference from directions away from the desired signal. By doing this, dynamic range requirements on the down conversions are relaxed [22], thus reducing the complexity and cost of an adaptive array system.

2.2.3 Phased Array

In addition to switched beam and adaptive antenna arrays, another array technology which is widely used is the *phased array* technique [23]- [28]. This technique uses only phase weights, β_n, that are adjusted to allow beam steering, while amplitude weights, α_n, are kept constant. This technique bears the advantage of the ability for continuous beam scanning at a complexity that is similar to a switched beam system. Furthermore, the phase weighting system can easily be deployed through the use of readily available RF hardware. The drawback to this system is the fact that there is no mechanism for coherent combining of multipath signals.

2.2.4 Adaptive beamforming

An adaptive beamforming system (Figure 2.4) provides a slightly more complex yet more powerful method of array processing, compared to the techniques that have been discussed so far. It uses an iterative algorithm that adjusts the weight vector, $w_{k,i}$ for the $(k-1)^{th}$ signal with each iteration process, i, in order to maximise the output signal performance. When a desired signal impinges on the array at an angle θ_d and an undesired signal arrives at an angle θ_u, an adaptive array would steer the main beam towards θ_d and a null towards θ_u. [29] presents an introduction to the adaptive array theory. Several adaptive algorithms [30] - [37] have been developed in the past years. Applications of adaptive arrays are described in [7] - [9].

Two of the most popular adaptive beamforming techniques are the *Minimum Mean Square Error* (MMSE) [35]- [37] and *Least Squares* (LS) methods [38]- [40]. These two techniques minimise the square of the difference between the array output, $E(t) = \mathbf{w}_k^H \mathbf{u}(t)$, and the locally generated desired signal $\mathbf{d}_k(t)$ for each of the k^{th} users being served by the array. A *training sequence* is used in order to estimate the channel behaviour. This information, which is usually transmitted as preamble symbols preceding the data symbols, is available to both the transmitter and the receiver [41].

Decision-directed adaptation provides an alternative to the use of training sequences. The technique reconstructs the estimates of the desired signal samples, $\mathbf{d}_{k,i}$, based on the array and signal demodulator output. The technique requires no prior knowledge of the transmitted data, thus no training sequence is needed. However, depending on the Signal to Noise and Interference Ratio (SNIR), errors at the demodulator may distort the reconstructed estimate, thus a poor weight solution may be reached. An adaptive system may use both training sequence and decision-directed adaptation in order to reach a better solution.

The behaviour of adaptive antenna systems depends on the presence of coherent and incoherent multipath signals. When multipath components are coherent, the system is able to combine these components, taking advantage of path diversity. On the other hand, incoherent multipath components are treated as separate signals. The system chooses the component with highest power and form nulls in the direction of the other components.

Several other techniques have been developed that do not require any training sequence. These are referred to as *blind adaptive algorithms*, and is desirable since the use of a training

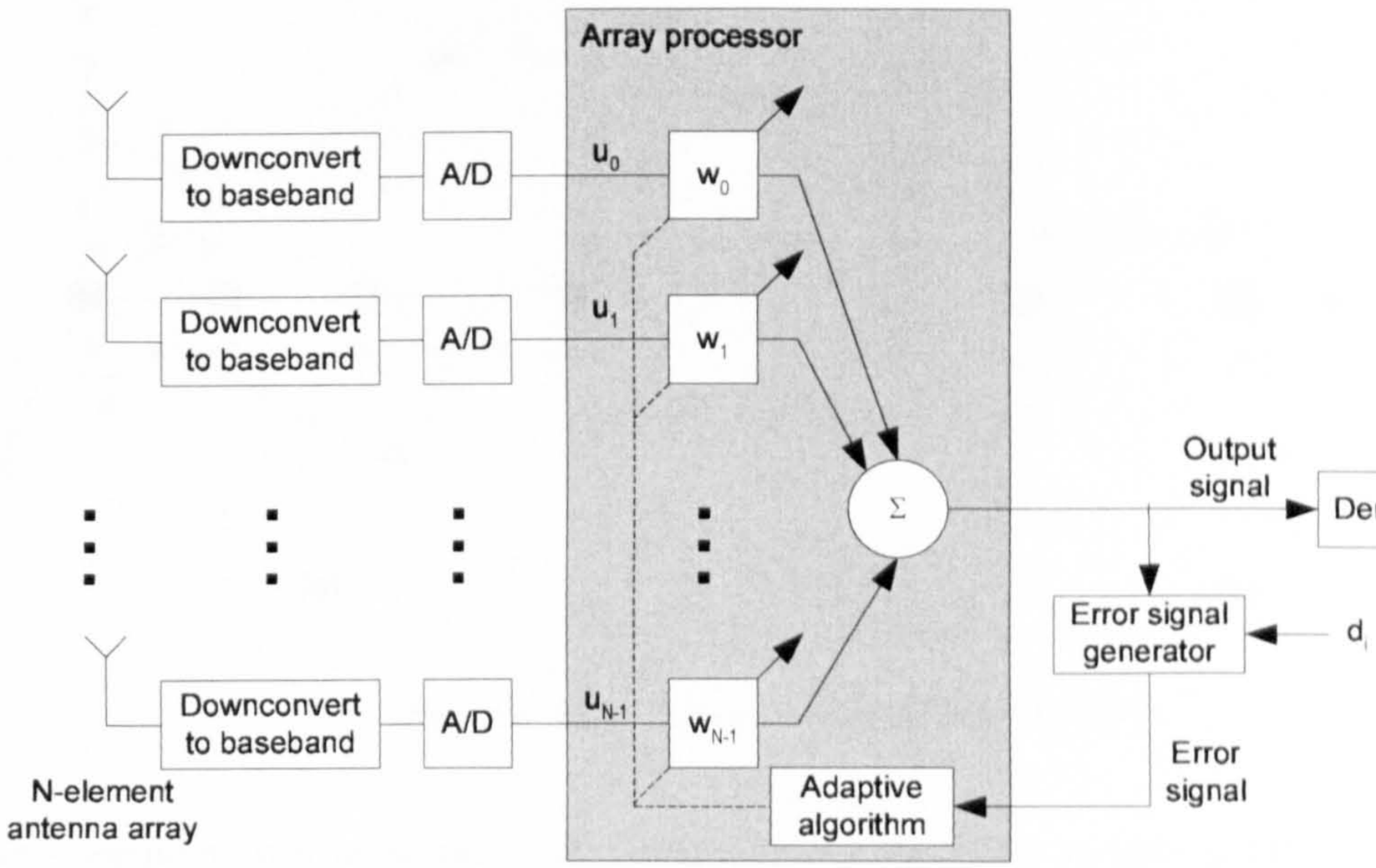

Figure 2.4: *Adaptive beamforming network*

sequence reduces the number of bits available for transmitting information. Examples of these algorithms are the *Bussgang technique* [42] and the *Least Squares Constant Modulus Algorithm* [43].

Perhaps the more sophisticated of adaptive antennas is in the field of Direction of Arrival (DoA) estimation [44]- [47], which provides the possibility of locating the position of the mobile user. Over the recent years a variety of DoA algorithms have been developed including *MUSIC* and *ESPRIT* [48]- [52]. These techniques vary in complexity, ranging from the conventional method that is based on classic beamforming theories discussed earlier in this section to more complex methods that exploit the eigen structure of the input signals.

2.3 Uniform Linear Array Theory

When radiating elements are combined together to form an array, the sum of all fields radiated by each individual element make up the array radiation pattern. These elements can be configured in different ways in order to make up different topologies. The linear array is the simplest and most well-researched form of array. Figure 2.5(a) shows a typical linear array configuration with N equally-spaced elements placed along the y-axis.

For simplicity, the analysis presented in this chapter will be based on the assumption that the

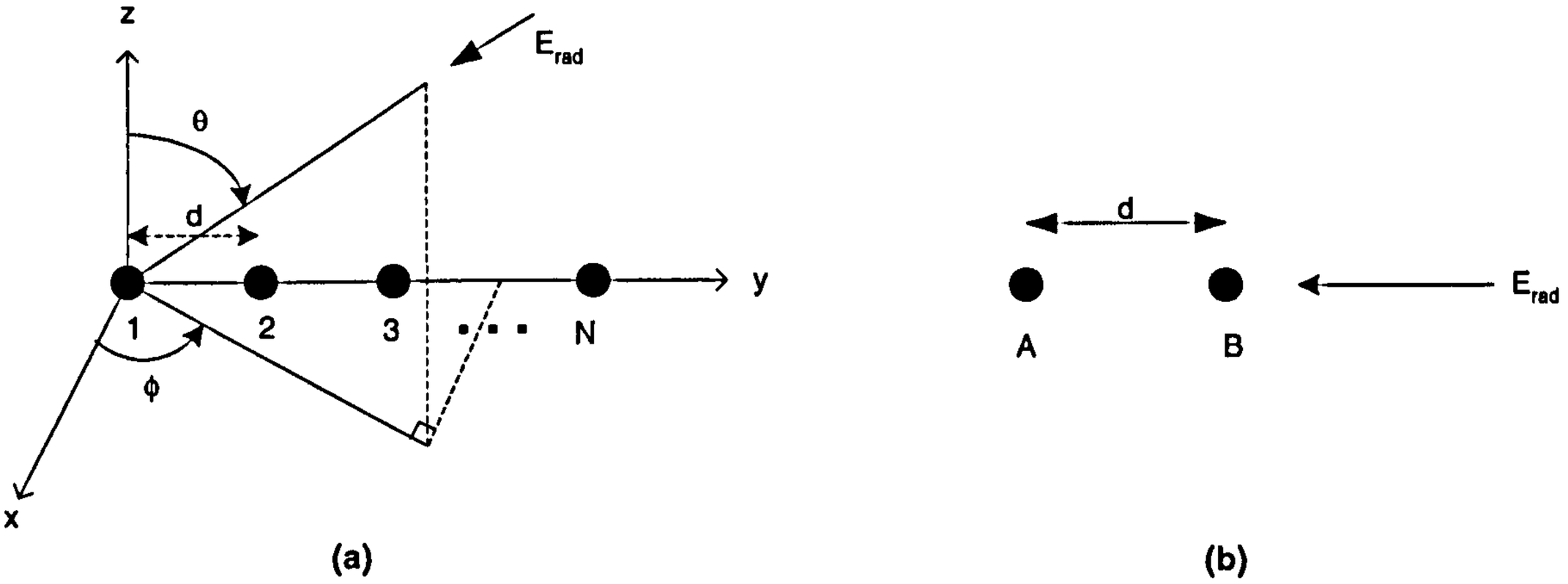

Figure 2.5: Linear array configuration

antenna elements are ideal isotropic elements with identical radiation patterns, $E_{elec}(\theta,\phi)$. In this case the elements do not couple with each other. Wave theory suggests that when a signal, E_{rad}, impinges on points A and B as shown in Figure 2.5(b), there is a phase difference $\Delta\Phi$ of:

$$\Delta\Phi = \frac{2d\pi}{\lambda_o} = kd \tag{2.2}$$

where λ_o is the free-space wavelength, d is the inter-element spacing and k is the free-space wave number of the centre frequency. It therefore follows that the phase difference between adjacent elements of the array in Figure 2.5(a) is:

$$\Delta\Phi = k\ d\ sin\theta\ sin\phi \tag{2.3}$$

The total received signal is therefore:

$$E(\theta,\phi) = \sum_{n=0}^{N-1} E_{elec}(\theta,\phi)\ e^{jkdn\ sin\theta\ sin\phi} = E_{elec}(\theta,\phi) \sum_{n=0}^{N-1} e^{jkdn\ sin\theta\ sin\phi} \tag{2.4}$$

The second part of equation (1.3) is called the array factor which contains details of the element location and excitation. Ideal array pattern synthesis is achieved by altering this array pattern.

Since in this case the amplitudes of the fields from the elements are assumed to be identical, it is taken as unity. Linear array beamforming is limited to the plane of elements, i.e. $\phi = 90^o$ in Figure 2.5. Consequently, the ϕ dependence on equation (1.3) may be omitted. By substitution and moving the phase reference point (currently at element 1) to the centre of the array, the array factor, E_{array}, can be written as:

$$E_{array}(\theta) \approx \frac{sin(\frac{Nkdsin\theta}{2})}{Nsin(\frac{kdsin\theta}{2})} \tag{2.5}$$

It can be seen that that the function of E_{array} is similar to that of a *sinc* function. Figure 2.6 shows the shape of far-field[2] radiation pattern of a 16-element uniformly-weighted linear array generated in MATLAB, with element separation $d = \lambda/2$.

2.3.1 Choice of Element Separation

The choice of inter-element separation is key to the design of a linear array. An increased element separation creates multiple lobes in the array radiation pattern E_{array} [53]. The far-field radiation pattern is a Fourier transform of the antenna aperture excitation. In the case of a discrete array, the array pattern is a Discrete Fourier Transform of the excitation of the array. When the element separation is too large the aperture becomes under-sampled, therefore creating grating lobes. Grating lobes occur when both the *sin* term in equation 2.5 equal to zero. In this case, the element separation becomes too large and the aperture becomes under-sampled. It follows that the element separation is required to be $d \leq \frac{\lambda}{2}$ in order to produce only one beam in the 'visible' space, defined by $-90^o \leq \theta \leq 90^o$.

The inter-element spacing may be used as another perturbating variable in the array pattern synthesis in order to achieve the required beamwidth and sidelobe levels. In the case of applications of antenna arrays in Radio-astronomy, large spacings are used in order to obtain many grating lobes with narrow beamwidths [53]. Element separation also affects the directivity of the array pattern. At larger spacings, directivity increases until $d \approx 2\lambda$. Beyond this point, directivity drops and second-order grating lobes appear. When $d < \frac{\lambda}{2}$, *superdirectivity* [53] may occur.

2.3.2 Pattern Synthesis

Linear array pattern synthesis has attracted much attention over the past years. As a result to this, a wide range of ideal array[3] pattern synthesis techniques are now available with plenty more being researched. This section provides a brief overview of some of the more common pattern synthesis techniques.

[2]The *far-field* region is discussed in Appendix A.

[3]*Ideal array* is defined as an array consisting of ideal elements as described in section 2.3.

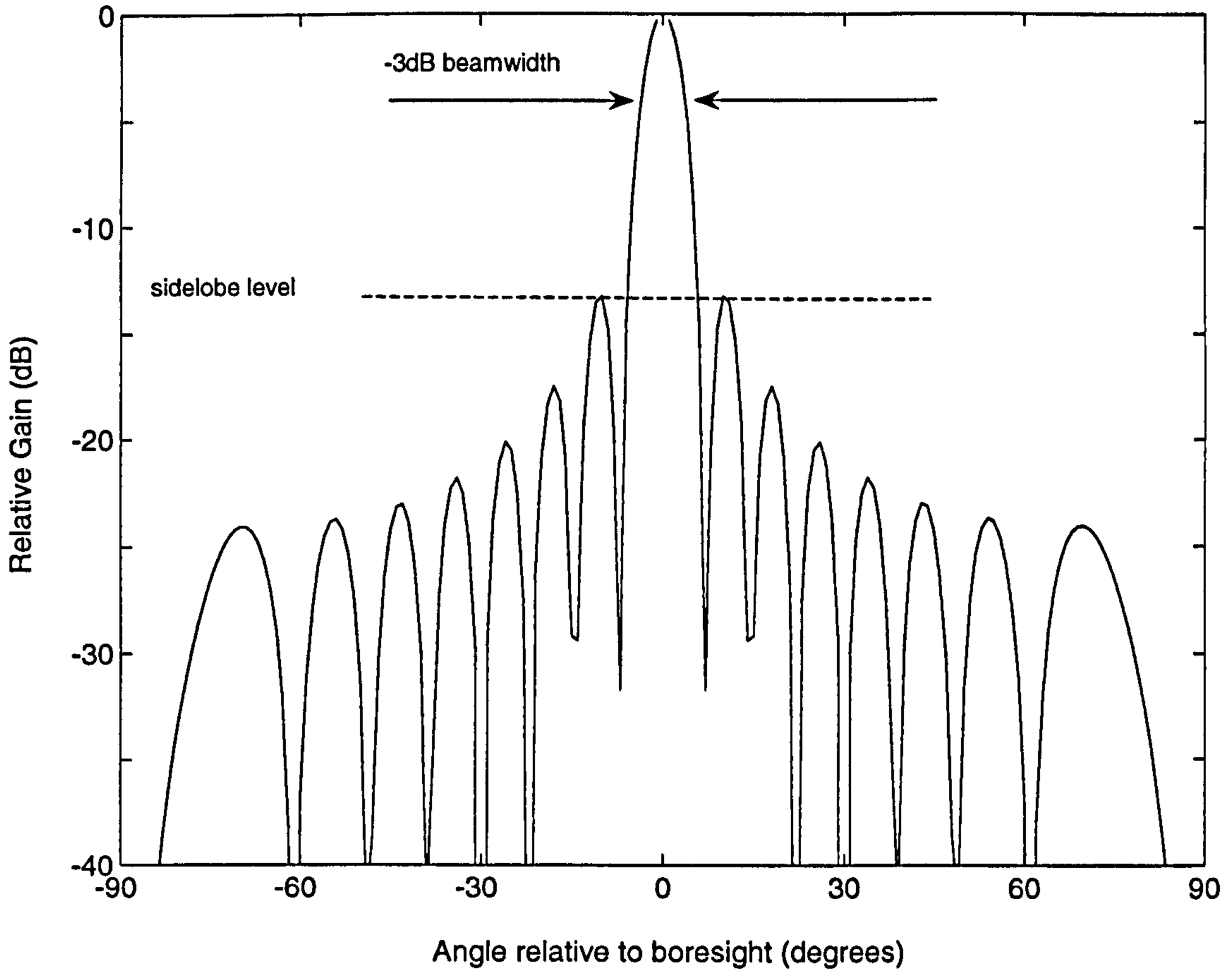

Figure 2.6: Linear array far-field radiation pattern

Array beamforming is achieved by applying different amplitude and phase weightings to individual array elements before they are summed together to produce the array radiation pattern. This is shown in Figure 2.7. Amplitude weights, α_n, are used to alter the shape of the beam pattern while phase weights β_n are used to alter the direction of the main beam. The art of beam shaping is essentially choosing the right weights in order to achieve the desired array radiation pattern. The simplest pattern synthesis method in order to form a main beam in the θ_0 direction is by applying a progressive phase shift of

$$\beta_n = -k\ d\ sin\theta_0 \tag{2.6}$$

thus aligning the phases of all the individual elements in the direction of θ_0.

Schelkunoff [54] defines the array factor of an equispaced linear array as a product of its roots:

$$E(\theta,\phi) = \sum_{n=0}^{N-1} e^{jkdnu} = \sum_{n=0}^{N-1} a^n = \prod_{n=1}^{N-1} (a - a_n) \tag{2.7}$$

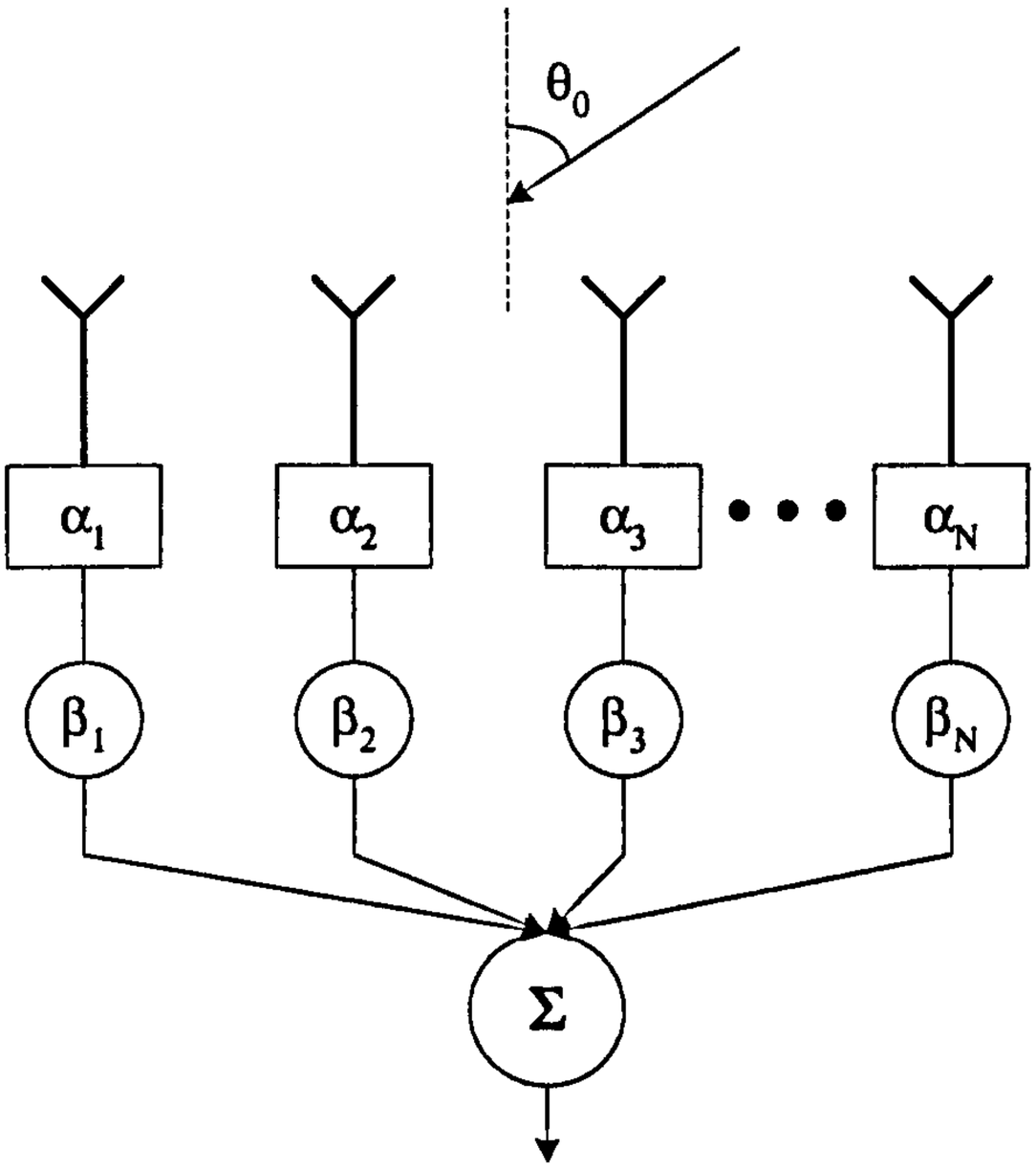

Figure 2.7: *Amplitude and phase weightings*

where $u = sin\theta$ and $a = e^{jkdu}$ and a_n are the array factor roots. The choice of element weights is equivalent to placement of the roots of this polynomial. These roots correspond to the nulls in the radiation pattern when they appear on the unit circle.

Dolph [55] developed the Dolph-Chebyshev synthesis technique which uses Chebyshev polynomials and yields a radiation pattern with sidelobe levels of equal amplitudes, as shown in Figure 2.8. The synthesised array has optimum characteristics in that the sidelobe level is the lowest for a specified main beamwidth, or the main beamwidth is the narrowest for a specified sidelobe level. However, as pointed out by Riblet [56], this is only true when $d \geq \frac{\lambda}{2}$ for $\theta_0 = \frac{\pi}{2}$ and $d \geq \frac{\lambda}{4}$ for $\theta_0 = 0$. However, aperture distribution in this technique may exhibit large peaks at its ends in attempt to obtain sidelobes that are the same level. Thus, the required element excitations may be difficult to achieve in practice.

Pattern synthesis of continuous linear sources has been presented by Taylor [57], which is a modified version of Dolph's synthesis with a modified requirement on the sidelobe level. This technique has been more widely used in comparison to the Dolph synthesis due to the fact that it is more physically deployable. However, this synthesis only holds the inner-most sidelobe level at the defined level while the others decay in a $\frac{1}{u}$ envelope where $u = sin\theta$. Further, the technique also has slightly higher sidelobe levels and wider main beamwidth. Every suppressed sidelobe incurs a cost to the main beamwidth, even though in some cases

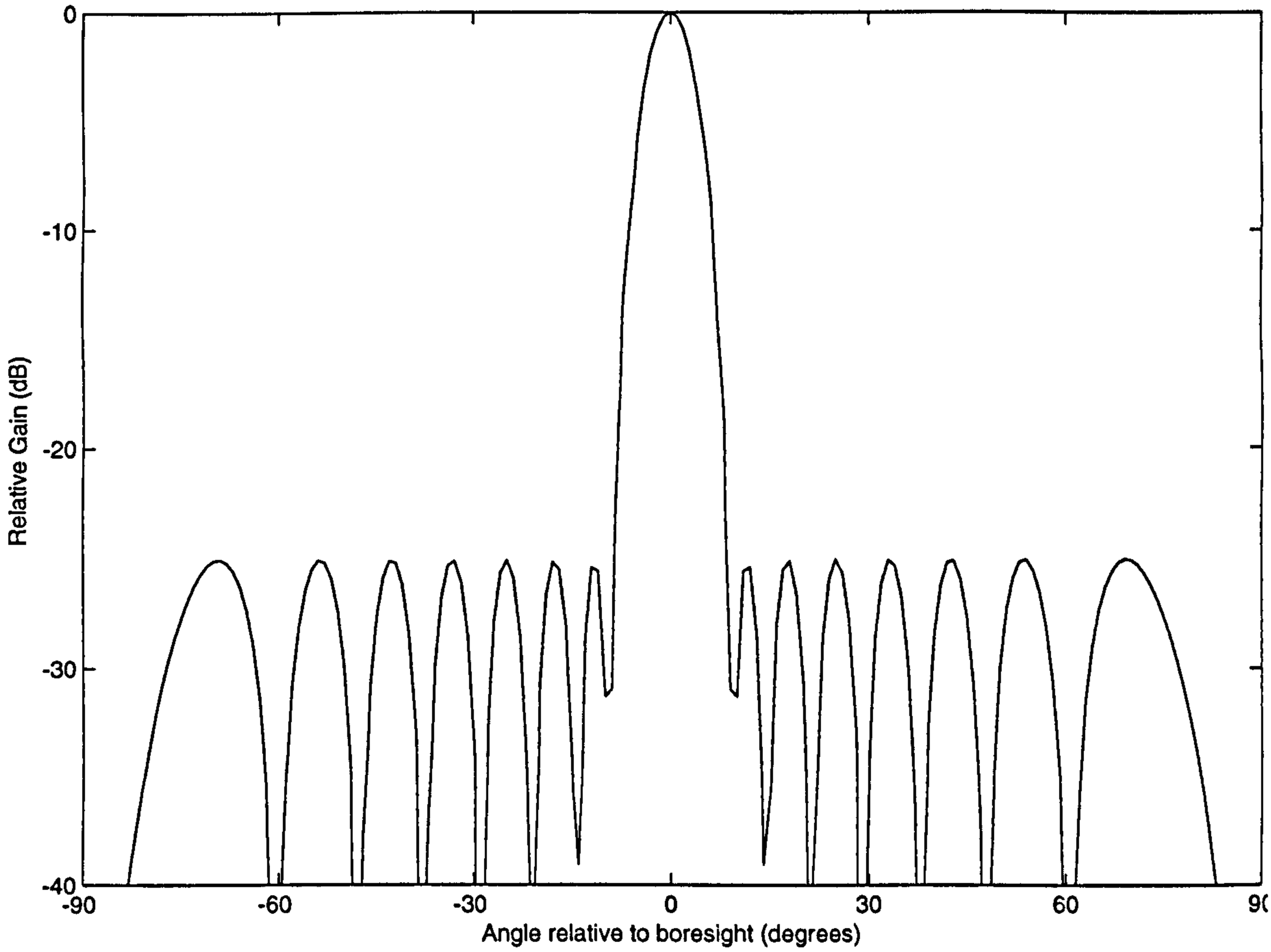

Figure 2.8: 16 element array with 25dB Dolph Chebyshev radiation pattern

some cases some directions in space may not be as important as others. In order to address this, Taylor patterns can be modified so that sidelobes may individually have different arbitrary heights. [58] - [60] present more detailed discussions on Dolph and Taylor techniques, together with several numerical and graphical examples.

The Bayliss theorem [61] provides a similar approach to the Taylor pattern except that it produces a symmetric difference pattern with twin main beams surrounded by sidelobes that diminish as $|u|^{-1}$ as oppose to sum patterns in the Taylor approach. Similarly, the continuous aperture may be root matched according to Schelkunoff unit circle to produce discrete element weights and arbitrary sidelobe topography may be deployed when necessary.

In some cases such as the airport beacon antenna, it is necessary to produce a radiation pattern without nulls in order to be able to maintain communication in all directions. In such cases, the Woodward-Lawson [62]- [63] method may be used. The technique utilises a sum of N orthogonal *sinc*-like patterns, each adjusted in phase and amplitude in order to produce a main beam peak in the direction where all the other patterns have zeros. The

outcome of the sum pattern is a single (omni-directional) main beam and no sidelobes.

Constrained synthesis adopts certain constraints as described in [53]. These constraints may be in terms of sidelobe levels, null placements or null broadening. More importantly, this technique is available for phase- or amplitude-only pattern synthesis. This is particularly useful for corporate feed structures where available element weights that can be applied are restricted. Adaptive array theory has vastly developed over the years and are increasingly widely used in wireless communication. Adaptive arrays [64]- [69] can place a beam in the direction of arriving signal and a null in the direction of high interference, and the pattern can automatically adapt to changes in the signal environment. There are also a large variety of optimisation techniques devised for linear array pattern synthesis [70]- [75], including the use of genetic algorithms [76]- [78]. These methods are evidently more costly compared to the non-adaptive methods. As the work presented in this thesis is mainly concentrated upon finding a low-complexity method to indoor wireless communications, adaptive techniques are not greatly considered.

2.3.3 Butler Matrix for Uniform Linear Array

Various array feeding methods such as the Butler [79]- [80] matrix and the Blass [81] matrix have been developed to generate several simultaneous beams directed at different angles. This is performed through the use of a matrix network. With these methods, each port feeding the matrix is connected to a receiver or transmitter depending on whether the antenna array is used for receiving or transmitting. Each receiver will then only receive signals from only one beam and each transmitter will generate one beam through that port. Alternatively, all the beams will be illuminated simultaneously when a transmitter power is distributed equally and in-phase among all the ports. This results in a radiation pattern which is a phasor addition of all the individual beam patterns. When the transmitter power is divided unevenly across the port, the overall far-field pattern will be adjusted accordingly.

The most well-known matrix feeding system used in array beamforming is the Butler matrix. This matrix may be applied to any number of elements, N, that equals to 2^x, where x is any positive integer. The matrix, with m ports, performs a Fourier transform on the signals and produces m orthogonal beams, where $m \leq 2^n$. Figure 2.9 illustrates the semantic diagram of a Butler matrix applied to an 8-element array. It contains hybrid couplers and fixed phase shifters, denoted by circles and squares respectively. The phase shifters are illustrated as

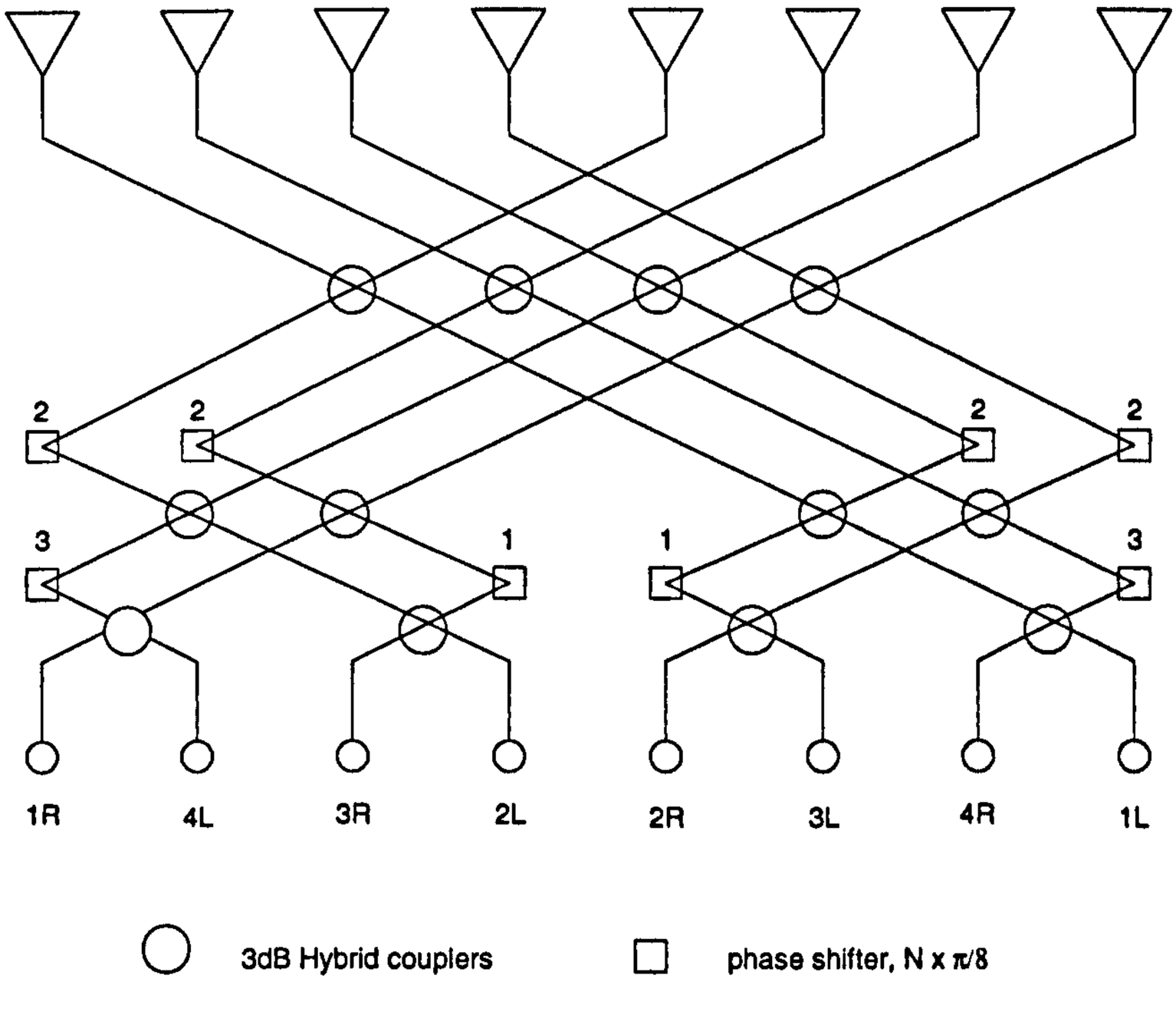

Figure 2.9: *8 x 8 Butler matrix*

multiples of $\pi/8$ radians, the multiplying factors denoted in the diagram by the numbers above the phase shifters. The labels on the output ports correspond to the beams generated by illuminating these ports, as illustrated in Figure 2.10. L and R stands for left and right respectively.

The ability of the Butler matrix to form orthogonal beams makes it a desirable technique for multiple beamforming. The peak of each beam points in the direction where all the other beams are at a null. Shelton [82] shows simple transposition on the elements of a linear array fed by a Butler matrix in order to improve the sidelobe level without significant degradation of the other array characteristics. A Butler matrix can easily be manufactured as simple transmission lines on a printed circuit board and therefore the cost of production is low and the dimensions limited, depending on the size of the matrix. Reference [83] presents the design and realization of a double four-port Butler matrix etched on both sides of the suspended stripline substrate in order to reduce the size and the losses of the network. The complexity of Butler matrix, however, greatly depends on the size of the antenna array.

2.4 Planar Arrays

In principle, planar arrays [84] allow control of the far-field radiation pattern in all directions, which may be required in certain applications such as military and radar purposes.

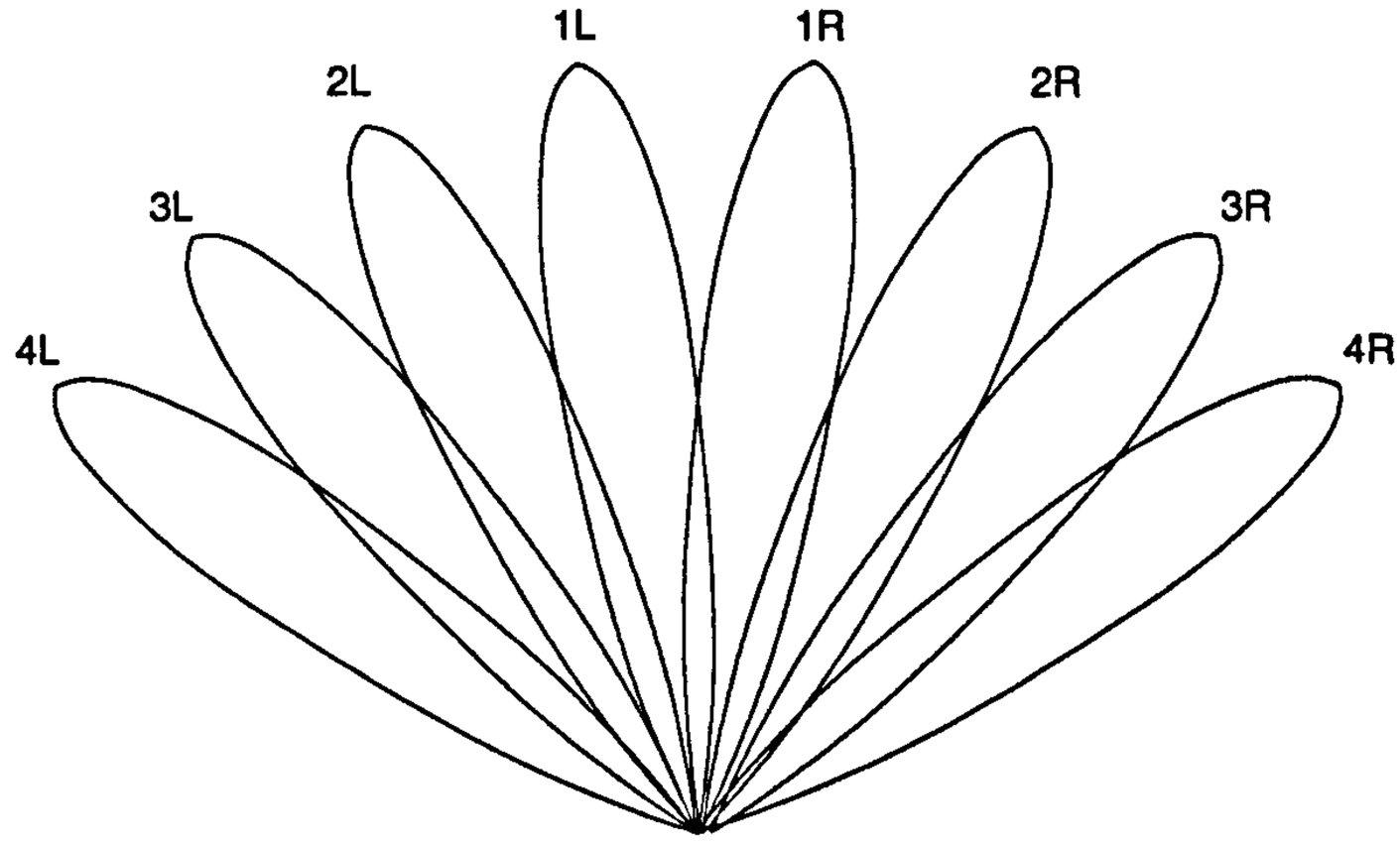

Figure 2.10: *Beam pattern from 8-element Butler matrix array*

The elements in a planar array may be arranged in a variety of ways. The simplest is shown in Figure 2.11 where N = M and element separations are identical along the respective axis. Array elements are placed on a regular grid in the x-y plane and the z plane is used to represent the array boresight. The inter-element separations are described by d_x and d_y. The configuration shown in the diagram is often called a *square lattice* array. Other types of configurations include *rectangular lattice*, *hexagonal lattice* and *triangular lattice*. The planar array theory is generally derived from the linear array concept, thus much of the linear array concept can be readily applied to this type of array.

The array factor for a square lattice array may be written in the form:

$$E(\theta,\phi) = \sum_{m=0}^{M-1}\sum_{n=0}^{N-1} \alpha_{n,m} e^{j\beta_{n,m}} e^{jk(nd_x u + md_y v)} \tag{2.8}$$

where

$$u = cos\ \gamma_x = sin\ \theta\ cos\ \phi \tag{2.9}$$

$$v = cos\ \gamma_y = sin\ \theta\ sin\ \phi \tag{2.10}$$

and $\alpha_{n,m}$ and $\beta_{n,m}$ are the amplitude and phase weightings respectively.

When $\alpha_{n,m} = \alpha_n \alpha_m$ and $\beta_{n,m} = n\beta_x + m\beta y$ where β_x and β_y are progressive phase shifts between elements in the respective directions, the array factor becomes the product of two linear arrays. Assigning $\alpha_{n,m} = 1$, and assuming ideal elements where amplitude and phase responses are identical, this becomes:

$$E(\theta,\phi) = \left(\frac{sin(\frac{N}{2}(kd_x u + \beta_x))}{N\ sin(\frac{1}{2}(kd_x u = \beta_x))}\right)\ \left(\frac{sin(\frac{M}{2}(kd_y u + \beta_y))}{M\ sin(\frac{1}{2}(kd_y u = \beta_y))}\right) \tag{2.11}$$

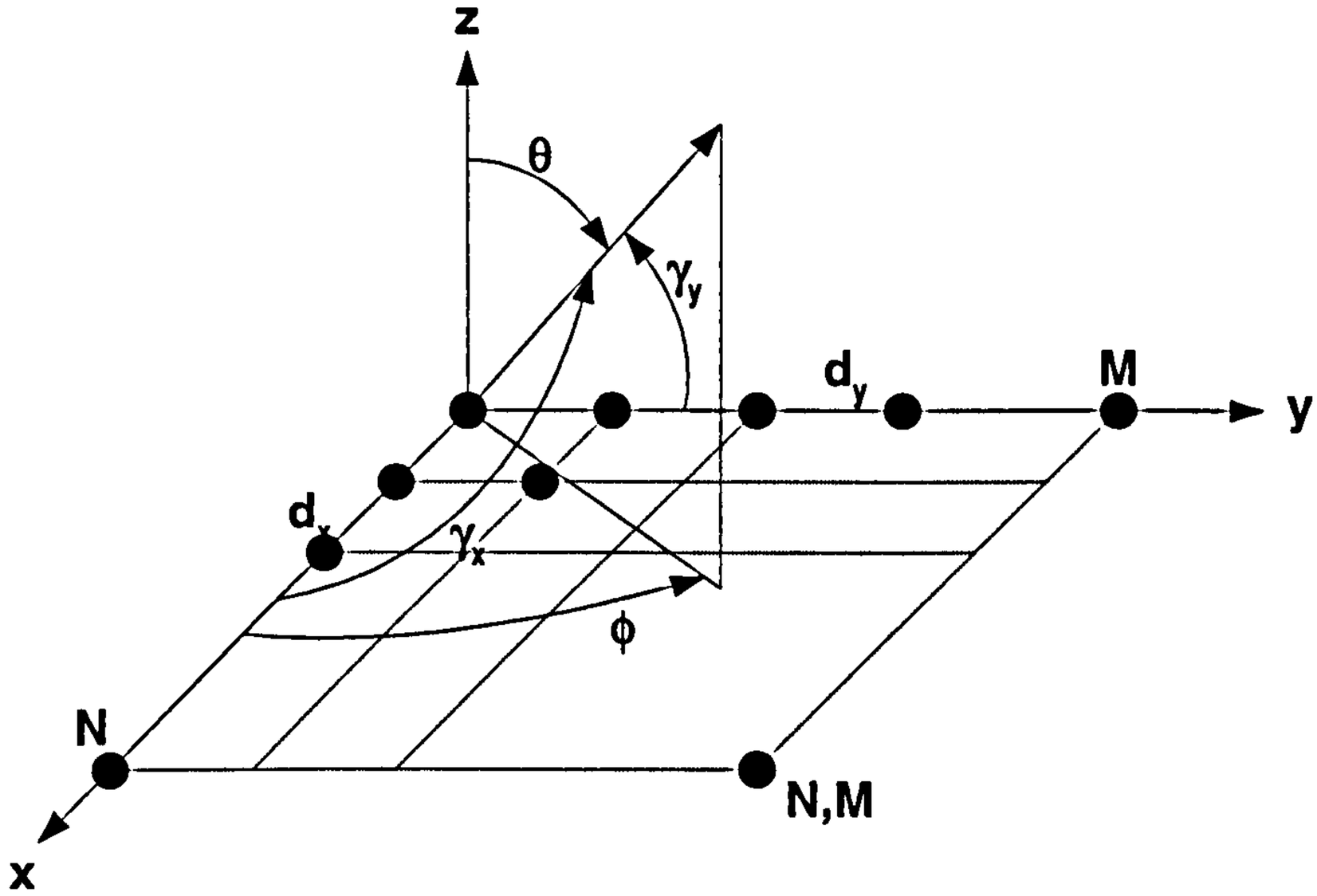

Figure 2.11: *Geometry of a rectangular lattice array*

The progressive phase shifts, β_x and β_y, required to steer the main beam to the direction of (θ_0, ϕ_0) can thus be found by

$$\beta_x = -kd_x \; sin\; \theta_0 \; cos\; \phi_0 \tag{2.12}$$

$$\beta_y = -kd_y \; sin\; \theta_0 \; sin\; \phi_0 \tag{2.13}$$

Element separation is an important factor in the design of planar arrays. A rectangular lattice behaves similarly to a linear array [84]. An element separation that is too large produces additional grating lobes in the radiation pattern. A method for analysing the grating lobe behaviour of a planar array has been developed by Von Aulock [24].

2.5 Ideal Conformal Array

In some cases the planar array structure may not be practical in terms of its mounting purposes and application. Furthermore, the maximum scan angle of a planar array is limited to maximum 60^o from boresight [85]. As a result, arrays which are non-planar but are conformal are desirable in several applications.

A conformal array is often defined as an array whose elements are flush mounted on a non-planar surface [85]. Due to their geometry, conformal arrays generally require more complex analysis compared to their planar and linear counterparts. Due to revolutionary new designs,

antenna engineers are now able to install conformal arrays which are up to a few inches thick, directly on the skin of an aircraft. The most advanced conformal arrays are load-bearing arrays, with elements embedded flush with the aircraft skin. These can be designed to bear high dynamic mechanical loads while radiating or receiving electromagnetic energy. Flush-mounted arrays are also attractive to many airbourne applications as they eliminate the disadvantage of additional additional drag otherwise introduced by planar arrays.

Figure 2.12 shows the geometry of an arbitrary array. The far-field radiation pattern of arbitrarily-positioned array elements may be represented by

$$E(\theta,\phi) = \sum_n w_n E^n_{elec}(\theta,\phi) e^{jk\hat{\mathbf{r}}\cdot\mathbf{r}_n} \tag{2.14}$$

where $E^n_{elec}(\theta,\phi)$ is the individual element pattern, w_n denotes the complex weighting function, and

$$\hat{\mathbf{r}} = \hat{\mathbf{x}}u + \hat{\mathbf{y}}v + \hat{\mathbf{z}}cos\ \theta \tag{2.15}$$

$$\mathbf{r}_n = \hat{\mathbf{x}}x_n + \hat{\mathbf{y}}y_n + \hat{\mathbf{z}}z_n \tag{2.16}$$

$\mathbf{r}_n$ represents the position vector of the n^{th} element from the origin O and () represents a unit vector. In general, each element in a conformal array configuration faces a different direction. As a result, the element pattern has to be included in the array pattern, as shown in Equation 2.14.

2.5.1 Pattern synthesis for conformal array

Pattern synthesis for conformal array is generally more complex than its linear and planar counterparts due to the non-identical shape of the individual element patterns. The simplest way of conformal array pattern synthesis is *co-phasal* excitation, which is also applicable to any other array geometry. The method utilises simple phasing of the array elements in order to produce maximum radiation in the direction of (θ_0,ϕ_0). The weighting function is given by

$$w_n = e^{-jk\hat{\mathbf{r}}\cdot\mathbf{r}_n} \tag{2.17}$$

The weighting function can also be designed to include the amplitude variations in the individual element patterns, thus

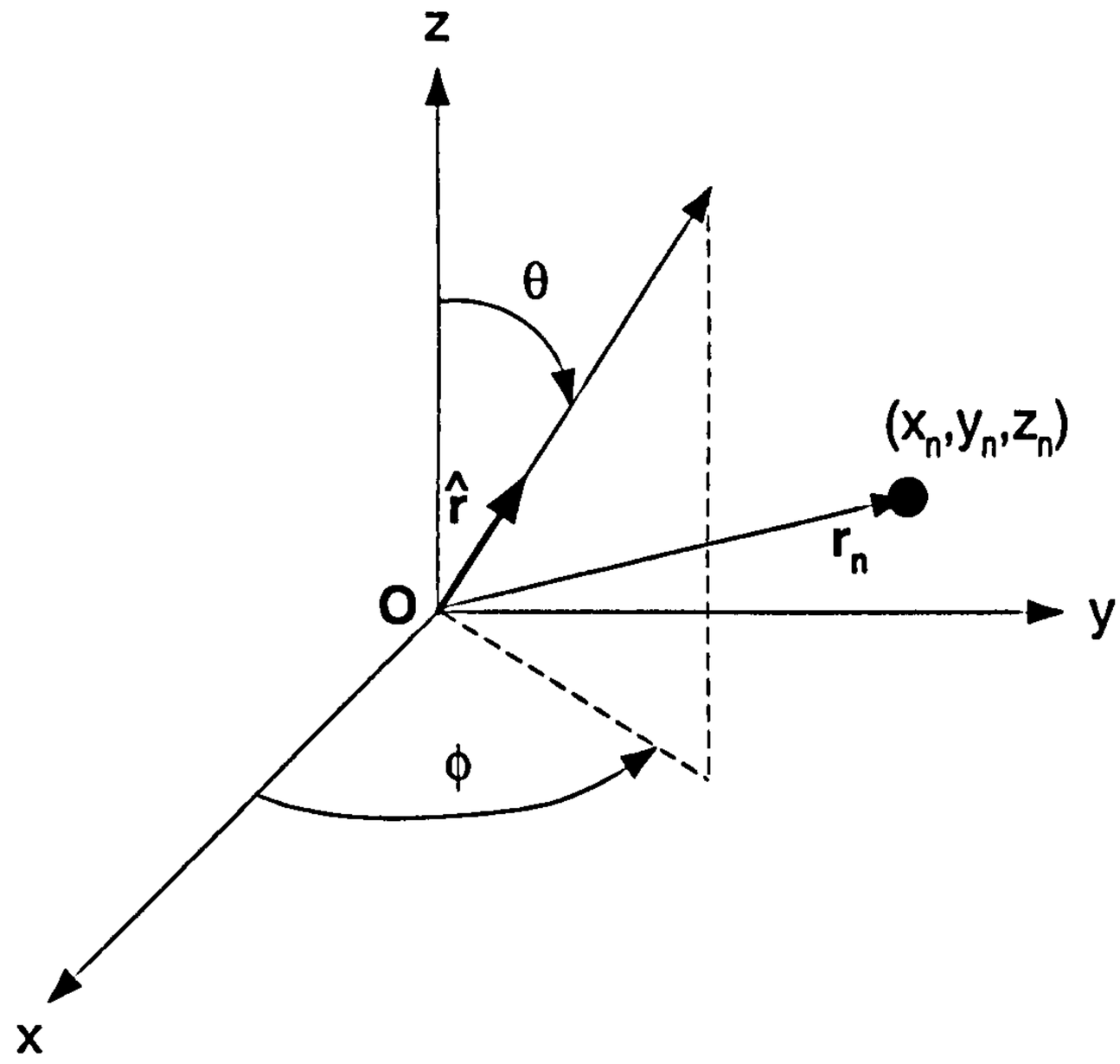

Figure 2.12: *Arbitrary array geometry*

$$w_n = (E^n_{elec}(\theta_0, \phi_0))^* \; e^{-jk\hat{\mathbf{r}}\cdot\mathbf{r}_n} \tag{2.18}$$

where (*) denotes the complex conjugate.

A technique called the *projected planar array* (PPA) [86] has also been developed for simple pattern synthesis. It involves the projection of conformal array elements onto a plane normal to the array boresight. Traditional planar array pattern synthesis can then be performed onto the projected conformal array and element weightings applied. However, this technique may present significant inaccuracies with array of large curvatures. Sullivan [87] also reveals that the sidelobe levels obtained by this technique is also lower than sidelobes from the original conformal array. Other methods [88]- [91] have also been developed for low sidelobe pattern synthesis of arbitrary conformal arrays.

2.5.2 Uniform circular array

The most significant form of conformal array is the uniform circular array (UCA). Although most of the research relating to array theory have been applied to communications systems since the late 1930s, circular arrays have received far less attention compared to the linear and planar counterparts. It is only in recent years that there has been a significant increase

in research for the application of circular arrays in direction finding systems. The circular array has been of particular interest to the author mainly because of its ability to cover the entire 360^o of the azimuth angle as oppose to linear arrays, whose patterns are very limited in the $\pm 90^o$ regions.

Aside to the great advantage of 360^o coverage, assuming good manufacturing tolerance, the symmetrical property of circular arrays also allows them to compensate for mutual coupling, whereas linear arrays require additional processing for this purpose. The array excitation can also be broken down to a series of symmetrical excitations around the array. However, the nature of the array geometry presents a complication in itself in that each individual element faces different directions. Davies [92] discusses the use of phase-mode excitation for circular array and outlines that through the use of a simple matrix network coupled with a set of compensating weights a circular array can be manipulated to behave like a linear array. Any linear array pattern synthesis method can then be applied to the system. A further advantage of this theory is that the main beam can be electronically steered towards any direction in the 360^0 array plane merely by adjusting the progressive phase shift around the array. This presents the possibility to design a cost-effective solution for wireless communication systems. More detailed discussion on uniform circular array theory is presented in the next chapter.

2.5.3 Other conformal array types

As well as UCAs, the semi-circular arc array is also a common type of conformal array. Pattern synthesis of a small-radius semi-circular arc array is similar to that of circular array, however in this case edge elements introduce additional mutual coupling which alters each element's radiation pattern. On the other hand, a large-radius curvature arc arrays are often treated similarly to linear arrays.

Another type of conformal array is the cylindrical array, an example application of which can be found in [93]. In this example, a 24-element cylindrical array is applied in the medical field as a method called *3D Hyperthermia*, which is a tumor control therapy. The method is especially designed for treating tumor in hard-to-reach areas. In this application, 24 dipole antennas are mounted in three sets of 8-element circular arrays. Driven by a 12-channel generator, the array provides unique pattern-shaping capabilities through amplitude and phase weight adjustments in each channel. This allows electromagnetic waves to be focused

3-dimensionally onto the tumor area.

2.6 Practical Applications of Spatial Domain Processing

A typical application of antenna arrays is ground-based radar arrays [94], which has employed antenna array technology over a number of years. Other deployments of spatial domain processing includes medical, seismic as well as sonar applications. Today, antenna arrays are also widely used in many wireless communication systems. ArrayComm's [95] licensed antenna technology for PHS which provides 9x greater capacity compared to the standard PHS network, has been in use since 1995 in the Asian market, where 250,000 base stations have been deployed. Similarly, their European GSM base stations incorporating smart antenna techniques also provides up to 400% capacity increase compared to standard GSM networks. The company's IntelliCell technology also claims up to 6x increase in capacity in its Wideband CDMA (WCDMA) application. Roy [96], [97] describes how ArrayComm's *Intelicell* smart antenna technology can increase spectrum efficiency.

Among the recent developments, the WiMAX Forum Mobile Task Group [98] have adopted both MIMO and adaptive antenna modes in the requirements for the IEEE 802.16e. Wireless LAN access point devices are now also starting to deploy antenna array technology. Ruckus Wireless' Smart Antenna technology for Wi-Fi devices, BeamFlex [99], is adaptable to any standard 802.11 a/b/g/n chipset and is said to offer over 3x performance improvement and an 8x expanded coverage for 802.11g/a networks. The ever-growing Direction of Arrival (DoA) estimation techniques, with algorithms such as MUSIC [48]- [49], SAGE [100]- [101] and ESPRIT [50]- [52], are also used in cellular communications as well as radar, seismic and military applications.

2.7 Discussion

A brief look of different types of antenna arrays has been presented in this chapter, including some of the existing radiation pattern synthesis methods. It is apparent that the pattern synthesis of linear arrays are more widely reported and by far the simplest among its counterparts. However, linear array technology is limited by the fact that it is only capable of serving a fraction of the azimuth plane at a time, thus limiting coverage area and possibly increasing costs due to the need for larger number of base stations to achieve total coverage

of a given area.

The following chapter takes a closer look at circular arrays and their pattern synthesis. Evidently, this is a less-researched area of array pattern synthesis as there is very limited knowledge on this type of array. However, the author feels that the promise of 360^o coverage of the azimuth plane earns circular array the rights for a closer evaluation.

References

[1] T.A. Denidni, T.E. Libar, "Wide band four-port butler matrix for switched multibeam antenna arrays", *IEEE Proceedings on Personal, Indoor and Mobile Radio Communications*, Vol. 3, pp.2461-2464, September 2003.

[2] M. Koubeissi, C. Decroze, T. Monediere, B. Jecko, "Switched-beam antenna based on novel design of Butler matrices with broadside beam", *Electronics Letters*, Vol. 41, Issue 20, pp.1097-1098, September 2005.

[3] Siou Teck Chew, T. Itoh, "A 22 beam-switching active antenna array", *IEEE MTT-S International Microwave Symposium Digest*, Vol. 2, pp.925-928, May 1995.

[4] M.E. Bialkowski, N.C. Karmakar, "A beamforming network for a compact circular switched-beam array antenna", *Asia Pacific Microwave Conference*, Vol. 3, pp.869-872, November-December 1999.

[5] L.J. Pesik, M.A. Beach, D.P. McNamara, P.N. Fletcher, "Performance analysis of smart antenna systems for indoor wireless LANs", *Third International Conference on 3G Mobile Communication Technologies*, No. 489, pp.418-422, May 2002.

[6] B. Allen, M. Beach, "On the analysis of switched-beam antennas for the W-CDMA downlink", *IEEE Transactions on Vehicular Technology*, Vol. 53, Issue 3, pp.569-578, May 2004.

[7] S. Werner, T. Laakso, J. Lilleberg, "Adaptive multiple-antenna receiver for CDMA mobile reception", *IEEE International Conference on Communications*, Vol. , pp1053 - 1057, June 1998.

[8] A.P. Ansbro, M. Crozzoli, L. Destro, D. Forigo, R. Vinassa, R.; "A dual-linear polarised microstrip array for fully-adaptive GSM antenna systems", *IEEE Antennas and Propagation Society International Symposium*, Vol. 2 , pp932 - 935, July 2000.

[9] P. Petrus, R.B. Ertel, J.H. Reed, "Capacity enhancement using adaptive arrays in an AMPS system", *IEEE Transactions on Vehicular Technology*, Vol. 47 , Issue 3 , pp717 - 727, Aug. 1998.

[10] C.Y. Chi, C.H. Chen, "Cumulant-based inverse filter criteria for MIMO blind deconvolution: properties, algorithms, and application to DS/CDMA systems in multipath", *IEEE Transactions on Signal Processing*, Vol. 49 , Issue 7 , pp1282 - 1299, July 2001.

[11] H.M. Chen, Q.Y. Xu, Z.X. Wang, "Transmit and receive weights optimization algorithm in MIMO-SDMA system", *14th IEEE Proceedings on Personal, Indoor and Mobile Radio Communications*, Vol. 3 , pp2868 - 2871, Sept 2003.

[12] E. Jorswieck, V. Jungnickel, T. Haustein, V. Pohl, C. von Helmolt, "On the performance of signal detection algorithms in flat-fading and frequency-selective MIMO channels", *IEEE 55th Vehicular Technology Conference*, Vol. 1 , pp40 - 44, May 2002.

[13] Jiun Siew; J. Coon, R.J. Piechocki, A. Dowler, A. Nix, M. Beach, S. Armour, J. McGeehan, "A channel estimation algorithm for MIMO-SCFDE", *IEEE Communications Letters*, Vol. 8 , Issue 9 , pp555 - 557, Sept. 2004.

[14] M. Cooper, M. Goldburg, "Intelligent antennas: spatial division multiple access", ArrayComm white paper on SDMA, *http://www.arraycomm.com/docs/spatial_division.pdf*

[15] Ning Li, Wenhua Chen, Zhenghe Feng, "A switched sector beam planar antenna", *IEEE Antennas and Propagation Society International Symposium*, Vol. 1A, pp.230-233, July 2005.

[16] L.J. Pesik, M.A. Beach, B.H. Allen, "Performance analysis of switched-sector antennas for indoor wireless LANs", *IEEE 54th VTS Vehicular Technology Conference*, Vol. 1, pp.385-362, 2001.

[17] A. Kalis, M.J. Carras, "A Sectored Phased Array for DBF Applications", *IEEE Transactions on Vehicular Technology*, Vol. 54, Issue 6, pp.1932-1936, November 2005.

[18] Hsueh-Jyh Li, Chen-Wei Huang, "Design of switched-sector planar antenna for wireless LAN", *IEEE Antennas and Propagation Society International Symposium*, Vol. 3, pp.662-665, June 2003.

[19] J. Butler, R. Lowe, "Beam-Forming matrix simplifies design of electronically scanned antennas", *Electronic Design*, pp.170-173, April 1961.

[20] M. Kiss, "Effects of random errors on the performance of a linear butler array", *IEEE Transactions on Antennas and Propagation*, Vol. 10, Issue 6, pp.708-714, November 1962.

[21] M. Bona, L. Manholm, J.P. Starski, B. Svensson, "Low-loss compact Butler matrix for a microstrip antenna", *IEEE Transactions on Microwave Theory and Techniques*, Vol. 50, Issue 9, pp.2069-2075, September 2002.

[22] J.C. Liberti Jr, T.S. Rappaport, "Smart antennas for wireless communications: IS-95 and third generation CDMA applications", Prentice Hall Communications Engineering and Emerging Technologies Series, 1999.

[23] N.C. Karmakar, M.E. Bialkowski, "A beam-forming network for a circular switched-beam phased array antenna", *IEEE Microwave and Wireless Components Letters*, Vol. 11, Issue 1, pp.7-9, January 2001.

[24] B. Palumbo, "Some examples of systems developments in Italy based on phased array technology", *IEEE International Symposium on Phased Array systems and Technology*, pp.444-449, October 1996.

[25] E. Rai, S. Nishimoto, T. Katada, H. Watanabe, "Historical overview of phased array antennas for defense application in Japan", *IEEE International Symposium on Phased Array Systems and Technology*, pp.217-221, October 1996.

[26] S. Samejima, "Phased array antenna systems for commercial applications in Japan", *IEEE International Symposium on Phased Array Systems and Technology*, pp.237-242, October 1996.

[27] T.A. Denidni, G.Y. Delisle, "A nonlinear algorithm for output power maximization of an indoor adaptive phased array", *IEEE Transactions on Electromagnetic Compatibility*, Vol. 37, Issue 2, pp.201-209, May 1995.

[28] W.H. Von Aulock, "Properties of phased arrays", *Proceedings of the IRE*, Vol. 48, pp1715-1727, 1960.

[29] S.P. Applebaum, "Adaptive arrays"', *IEEE Transactions on Antennas and Propagation*, Vol. 24, No. 5, pp585-598, Sept 1976.

[30] M. Martone, "Towards the Knowledge Millennium", *IEEE International Conference on Communications*, Vol. 3 , pp1356 - 1360, June 1997.

[31] S. Prasad, "Linear antenna arrays with broad nulls with applications to adaptive arrays", *IEEE Transactions on Antennas and Propagation*, Vol. 27 , Issue 2 , pp185 - 190, March 1979.

[32] P. Darwood, P.N. Fletcher, G.S. Hilton, "Pattern synthesis in small phased arrays using adaptive array theory", *Electronics Letters* , Vol. 33 , Issue 4 , pp254 - 255, Feb 1997.

[33] You Chung Chung, R.L. Haupt, "Optimum amplitude and phase control for an adaptive linear array using a genetic algorithm", *IEEE Antennas and Propagation Society International Symposium*, Vol. 2 , pp1424 - 1427, July 1999.

[34] P.N. Fletcher, M. Dean, "Low-cost digital adaptive antenna architecture combined with low-sidelobe beam synthesis", *IEE Proceedings on Radar, Sonar and Navigation*, Vol. 149 , Issue 6 , pp265 - 270, December 2002.

[35] Ye Li, N.R. Sollenberger, "Adaptive antenna arrays for OFDM systems with cochannel interference", *IEEE Transactions on Communications*, Vol. 47, Issue 2, pp.217-229, February 1999.

[36] K.M. Nasr, F. Costen, S.K. Barton, "An OFDM-MMSE smart antenna for an infrastructure WLAN in an indoor environment", *IEEE 59th Vehicular Technology Conference*, Vol. 1, pp.1-5, Maly 2004.

[37] Le Minh Tuan, Pham Van Su, Jewoo Kim, Giwan Yoon, "An MMSE-based beamforming algorithm for smart antenna applied to an MC-CDMA system with co-channel interference", *The 8th International Conference on Communication Systems*, Vol. 2, pp.1252-1256, November 2002.

[38] Xinyu Ma, Byong Kun Chang, "Least square method for optimum thinned antenna arrays", *IEEE Antennas and Propagation Society International Symposium Digest*, Vol. 4, pp.2232-2235, July 1997.

[39] H.M. Elkamchouchi, M.A.E.M. Adam, "A multitarget adaptive array algorithms for wireless CDMA systems", *IEEE Antennas and Propagation Society International Symposium*, Vol. 1, pp.427-430, June 2004.

[40] W.G. Najm, "Constrained least squares in adaptive, imperfect arrays", *IEEE Transactions on Antennas and Propagation*, Vol. 38, Issue 11, pp.1874-1878, November 1990.

[41] Q.T. Tran, S. Hara, Y. Nakaya, I. Ida, Y. Oishi, "An adaptive beamforming method for phased array antenna with MEMS phase shifters", *IEICE Transactions on Communications*, Vol 89B, No. 9, pp.2503-2513, September 2006.

[42] J.B.D. Filho, G. Favier, J.M.T. Romano, "New Bussgang methods for blind equalization", *IEEE International Conference on Acoustics, Speech, and Signal Processing*, Vol 3, pp.2269-2272, April 1997.

[43] R. Mendoza, J.H. Reed, T.C. Hsia, B.G. Agee, "Interference rejection using the time-dependent constant modulus algorithm (CMA) and the hybrid CMA/spectral correlation discriminator", *IEEE Transactions on Signal Processing*, Vol. 39, Issue 9, pp.2108-2111, September 1991.

[44] N. Yuen, B. Friedlander, "DOA estimation in multipath: an approach using fourth-order cumulants", *IEEE Transactions on Signal Processing*, Vol. 45 , Issue 5 , Pp1253 - 1263, May 1997.

[45] H. Weiguang, H.M. Kwon, "Effect of mixer phase distortions on the DOA tracking algorithm for an adaptive antenna array", *IEEE VTS 53rd Vehicular Technology Conference*, Vol. 1 , pp248 - 252, May 2001.

[46] F. Li, H. Liu, R.J. Vaccaro, "Performance analysis for DOA estimation algorithms: unification, simplification, and observations", *IEEE Transactions on Aerospace and Electronic Systems*, Vol.29 , Issue 4 , pp1170 - 1184, Oct. 1993.

[47] Y. Jia, H. Wu, Z. Bao, "A novel DOA estimation algorithm with uncalibrated array", *3rd International Conference on Signal Processing*, Vol.1 , pp465 - 468, Oct. 1996.

[48] N. Odachi, H. Shoki, Y. Suzuki, "High-speed DOA estimation using beamspace MUSIC", *IEEE Vehicular Technology Conference Proceedings*, Vol. 2, pp.1050-1054, May 2000.

[49] Y. Yang, C. Wan, C. Sun, Q. Wang, "DOA estimation for coherent sources in beamspace using spatial smoothing", *Proceedings of the 2003 Joint Conference of the Fourth International Conference on Information, Communications and Signal Processing*, Vol. 2, pp.1028-1032, December 2003.

[50] K. Almidfa, G.V. Tsoulos, "Performance analysis of ESPRIT, TLS-ESPRIT and Unitary-ESPRIT algorithms for DOA estimation in a W-CDMA mobile system", *IEE First International Conference on 3G Mobile Communication Technologies*, No. 471, pp.200-203, March 2000.

[51] F. Gao, A.B. Gershman, "A generalized ESPRIT approach to direction-of-arrival estimation", *IEEE Signal Processing Letters*, Vol. 12, Issue 3, pp.254-257, March 2005.

[52] Lei Huang, Shunjun Wu, Linrang Zhang, "Low-complexity ESPRIT method for direction finding", *IEEE International Conference on Accoustics, Speech and Signal Processing (ICASSP)*, Vol. 4, pp.iv/929-iv/932, March 2005.

[53] R.C. Hansen, *Linear Arrays*, in Rudge et all. [77]

[54] S.A. Schelkunoff, H.T. Friis, *Antenna Theory and Practice*, J. Wiley & Sons, New York, USA, 1952.

[55] C.L. Dolph, "A current distribution for broadside arrays which optimizes the relationship between beamwidth and side-lobe level", *Proceedings of the IRE*, Vol.34, pp335-348, 1946.

[56] H.J. Riblet, "Discussion of Dolph's paper", *Proceedings of the IRE*, Vol.35, No.5, pp489-492, 1947.

[57] T.T. Taylor, "Design of line-source antennas for narrow beamwidth and low sidelobes", *IRE Transactions on Antennas and Propagation*, Vol. 3, pp16-28, 1955.

[58] L.V. Blake, *Antennas*, Artech House, 1984.

[59] M.T. Ma, *Theory and Applications of Antenna Arrays*, Wiley-Interscience, c1974.

[60] J.D. Kraus, *Antennas*, 2nd edition, McGraw-Hill, ISBN 0071004823, 1988.

[61] E.T. Bayliss, "Design of monopulse antenna difference patterns with low sidelobes", *Bell System Technical Journal*, Vol. 47, pp623-640, 1968.

[62] P.M. Woodward, "A method of calculating the field over a plane aperture required to produce a given polar diagram", *IEE Proceedings*, vol. 32, No. 10, pp1129-1133, October 1984.

[63] P.M. Woodward, J.D. Lawson, "The theoretical precision with which an arbitrary radiation pattern may be obtained from a source of finite size", *IEE Proceedings*, vol. 95, Pt. III, pp. 363-371, 1948.

[64] E.C. Dufort, "Pattern synthesis based upon adaptive array theory", *IEEE Transactions on Antennas and Propagation*, Vol.37, No, 8, pp1011-1018, August 1989.

[65] A.J. Fenn, "Evaluation of adaptive phased array antenna, far-field nulling performance in the near-field region", *IEEE Transactions on Antennas and Propagation*, Vol. 38 , Issue 2 , pp173 - 185, Feb. 1990.

[66] Yiping Wang, J.R. Cruz, "Adaptive antenna arrays for cellular CDMA communication systems", *International Conference on Acoustics, Speech, and Signal Processing*, Vol. 3 , pp1725 - 1728, May 1995.

[67] R.T. Al-Mushcab, M.M. Dawoud, H.A. Ragheb, "Null steering in adaptive arrays by controlling the elevations of the antenna array elements", *Antennas and Propagation Society International Symposium Digest*, Vol. 2 , pp1244 - 1247, June 1994.

[68] L.C. Godara, "Improved LMS algorithm for adaptive beamforming", *IEEE Transactions on Antennas and Propagation*, Vol. 38 , Issue 10 , pp1631 - 1635, Oct. 1990.

[69] A. Malecot, D. Grenier, "Adaptive synthesis of a radiation pattern of an array antenna", *Canadian Electrical and Computer Engineering Conference Proceedings*, Vol. 2, pp477 - 480, Sept. 1994.

[70] D.J. Shpak, "A method for the optimal pattern synthesis of linear arrays with prescribed nulls", *IEEE Transactions on Antennas and Propagation*, Vol. 44 , Issue 3 , pp286 - 294, March 1996.

[71] J.B. Wang, M. Zhao, S.D. Zhou, Y. Yao, "Optimal sequences combined with antenna arrays to suppress the multiuser interference", *IEEE Wireless Communications and Networking Conference*, Vol. 2 , pp855 - 859, Sept. 2000.

[72] B.D.Carlson, D. Willner, "Antenna pattern synthesis using weighted least squares", *IEE Proceedings*, Vol. 139, Pt. J, No. 1, pp11-16, Feb 1992.

[73] T.S. Angell, A. Kirsch, R.E. Kleinman, "Antenna control and optimisation", *Proceedings of the IEEE*, Vol. 79, No. 10, pp1559-1568, October 1991.

[74] L. Wu, A. Zeilinkski, "An iterative method for array pattern synthesis", *IEEE Journal of Oceanic Engineering*, Col. 18, No. 3, pp280-286, July 1993.

[75] Y.C. Chung; R.L. Haupt, "Adaptive nulling with spherical arrays using a genetic algorithm", *IEEE Antennas and Propagation Society International Symposium*, Vol. 3 , pp2000 - 2003, July 1999.

[76] M.J. Buckley, "Linear array synthesis using a hybrid genetic algorithm", *Antennas and Propagation Society International Symposium Digest*, Vol. 1 , pp584 - 587, July 1996.

[77] R.L. Haupt, "Phase-only adaptive nulling with a genetic algorithm", *IEEE Transactions on Antennas and Propagation*, Vol. 45 , Issue 6 , pp1009 - 1015, June 1997.

[78] K.K. Yan, Y. Lu, "Sidelobe reduction in array-pattern synthesis using genetic algorithm", *IEEE Transactions on Antennas and Propagation*, Vol. 45, No. 7, pp1117-1121, July 1997.

[79] J.L. Butler, "Digital Matrix and Intermediate Frequency Scanning", *Microwave Scanning Antennas*, Vol. III, R.C. Hansen, ed., ch. 3, Academic Press, New York, 1966.

[80] J. Butler, R. Lowe, "Beam-Forming matrix simplifies design of electronically scanned antennas", *Electronic Design*, pp.170-173, April 1961.

[81] J. Blass, "The multidirectional antenna: A new approach to stacked beams", *IRE National Convention Rec.*, pp.48-50, 1960.

[82] J. Shelton, "Reduced sidelobes for Butler-matrix-fed linear arrays", *IEEE Transactions on Antennas and Propagation*, Vol. 17, Issue 5, pp645 - 647, Sep 1969.

[83] M. Bona, L. Manholm, J.P. Starski, B. Svensson,"Low-loss compact Butler matrix for a microstrip antenna", *IEEE Transactions on Microwave Theory and Techniques*, Vol. 50 , Issue 9 , pp2069 - 2075, September 2002.

[84] R.C. Hansen, "Planar Arrays", in Rudge et all. [91]

[85] G.V. Borgiotti, "Conformal Arrays", in Rudge et all. [91]

[86] W.H. Kummer, "Basic array theory", *Proceedings of the IEEE*, Vol. 80, Issue 1, pp.127-139, January 1992.

[87] E.J. Sullivan, 22Sidelobe behaviour of conformal arrays", *The Journal of the Acoustical Society of America*, Vol. 71, No. 2, pp.402-404, February 1982.

[88] L.I. Vaskelainen, "Iterative least-squares synthesis methods for conformal array antennas with optimised polarization and frequency properties", *IEEE Transactions on Antennas and Propagation*, Vol. 45, Issue 7, pp.1179-1185.

[89] A. Tennant, "Numerical pattern synthesis of difference beams in conformal arrays", *IEE Electronics Letters*, Vol. 31, Issue 12, pp.938-939, June 1995.

[90] O.M. Bucci, G.D'Elia, G. Romito, "Power synthesis of conformal arrays by generalised projection method", *IEEE Transactions on Antennas and Propagation*, Vol. 142, No. 6, pp.467-471, December 1995.

[91] Y.C. Jiao, W.Y. Wei, L.W. Huang, H.S. Wu, "A new low sidelobe pattern synthesis technique for conformal arrays", *IEEE Transactions on Antennas and Propagation*, Vol. 41, No. 6, pp.824-831, June 1993.

[92] D.E.N. Davies, "Circular Arrays", in Rudge et all. [102]

[93] *http://www.bsdmc.com/bsd2000-3d.html*, BSD Medical Corporation website.

[94] U. Nickel, "Comparison of a non-adaptive low-sidelobe array antenna with an adaptive phased array antenna", *Record of the IEEE 1990 International Radar Conference*, pp.486-490, May 1990.

[95] "Smart Antenna Solutions", *http://www.arraycomm.com/serve.php?page=IntelliCell*, ArrayComm Website [103], referenced in January 2006.

[96] R.H. Roy, "An overview of smart antenna technology: the next wave in wireless communications", *IEEE Aerospace Conference Proceedings*, Vol. 3, pp.339-345, March 1998.

[97] R.H. Roy, "Adaptive antennas for wireless information networks", *Northcon Conference Proceedings*, pp.60-65, October 1998.

[98] WiMAX Forum Website, *http://www.wimaxforum.org*

[99] "Beamflex", *http://www.ruckuswireless.com/technology/beamflex.php*, Ruckus Wireless Website [104], referenced in January 2006.

[100] Xuefeng Yin, B.H. Fleury, "Nominal direction and direction spread estimation for slightly distributed scatterers using the SAGE algorithm", *IEEE Vehicular Technology Conference*, Vol. 1, pp.25-29, May-June 2005.

[101] A. Logothetis, C. Carlemalm, "SAGE algorithms for multipath detection and parameter estimation in asynchronous CDMA systems", *IEEE Transactions on Signal Processing*, Vol. 48, Issue 11, pp.3162-3174, November 2000.

[102] A.W. Rudge, K. Milne, A.D. Olver, P. Knight, Eds., *The Handbook of Antenna Design*, Vol. 1 and 2, Peter Peregrinus Ltd, London, UK, 1986.

[103] ArrayComm Website, *http://www.arraycomm.com*

[104] Ruckus Wireless Website, *http://www.ruckuswireless.com*

Chapter 3

Uniform Circular Array

Circular arrays have received far less attention from the wireless industry in comparison to that of linear arrays, hence there is currently very limited understanding of the circular array properties and behaviour. However, circular arrays have a tremendous advantage over their linear counterparts as their symmetry allows beam steering across the 360^o azimuth angle without any significant degradation to the beam patterns. On the contrary beam patterns of linear arrays deteriorates as the main beam is steered away from broadside. The symmetrical property of circular arrays, in theory, also allows them to inherently compensate for mutual coupling without the need of further calibration. The array excitation can also be broken down into a series of symmetrical excitations around the array. In general, the task of pattern synthesis in circular arrays is not as simple as it is for linear or planar arrays due to the complexities presented by their geometry, explaining the lack of development in this area. The research presented in this thesis is driven by the fact that a vast amount of potential applications of such arrays exist due to its 360^o coverage capability outweigh the complexities.

This chapter addresses the uniform circular array (UCA) theory, including its geometry and pattern synthesis. Ideal arrays are used in order to simplify and better understand the circular array analysis. In this case each element is assumed to have identical radiation patterns, $E_{elec}(\theta,\phi)$, unless otherwise stated. Ideal arrays have a uniform inter-element spacing, d or, in the case of circular arrays, radius R. Further, it is assumed that there is no mutual coupling or any other interactions between the array elements. The analysis commences with the application of beam co-phasal and phase-mode UCA beamforming methods onto ideal arrays. The UCA geometry such as radius, R, number of elements, N, and the type of antenna elements used in the array are analysed in order to gain a better understanding of the UCA behaviour. An optimum geometry is then formulated for low-cost applications. The application of the Dolph-Chebyshev excitation method [9] for UCA beamforming and the

use of a Butler matrix [1] for UCA phase mode excitation is presented, including a method for modifying the matrix to suit its purpose in this case. The chapter concludes with a description of various UCA applications.

3.1 Circular Array Theory

The geometry of a circular array is shown in Figure 3.1. The circular array elements are uniformly distributed around the array circumference. For monopole elements, a flat circular ground plane is often used[1], whereas a cylindrical ground plane is often used for mounting patch antenna elements[2]. The physical dimensions of these patches in turn sets a limit to the minimum array radius that can be achieved, however the presence of a cylindrical ground plane isolates the element radiation patterns so that very little signal is radiated in the direction beyond $-90^o \leq \varphi \leq 90^o$. Back-to-back elements are then prevented from interfering with each other. The array radiation characteristics are dependent upon the array radius, element type, number of elements and the ground plane geometry. In this section the individual element patterns are assumed to be ideal directional patterns of with amplitudes

$$E_{elec}(\varphi) = \left\{ \begin{array}{ll} cos\varphi & -90^o \leq \varphi \leq 90^o \\ 0 & otherwise \end{array} \right\} \tag{3.1}$$

where φ is the angle relative to the arbitrary reference, i.e. $(\phi - \varphi_n)$.

Based on the same principal outlined in Chapter 2, the radiation pattern of a circular array can be described as:

$$E(\theta, \phi) = \sum^{n} \omega_n \left| A_n(\theta, \phi - \varphi_n) \right| \; e^{jkR\, cos(\phi - \varphi_n)\, sin\theta} \tag{3.2}$$

A_n is the n^{th} element pattern, φ_n is the position of the n^{th} antenna element with respect to the arbitrary reference point usually taken in the center of the circle, k is the wave number $k = \frac{2\pi}{\lambda}$, and R is the circular array radius. ω_n represents the weighting function applied to the n^{th} element of the array. Research presented in this thesis is based on 2D azimuth pattern synthesis (i.e. $\theta = 90^o$, therefore the $sin(\theta)$ term in equation 3.2 is eliminated from further equations.

[1] See Figure 4.2
[2] See Figure 4.7

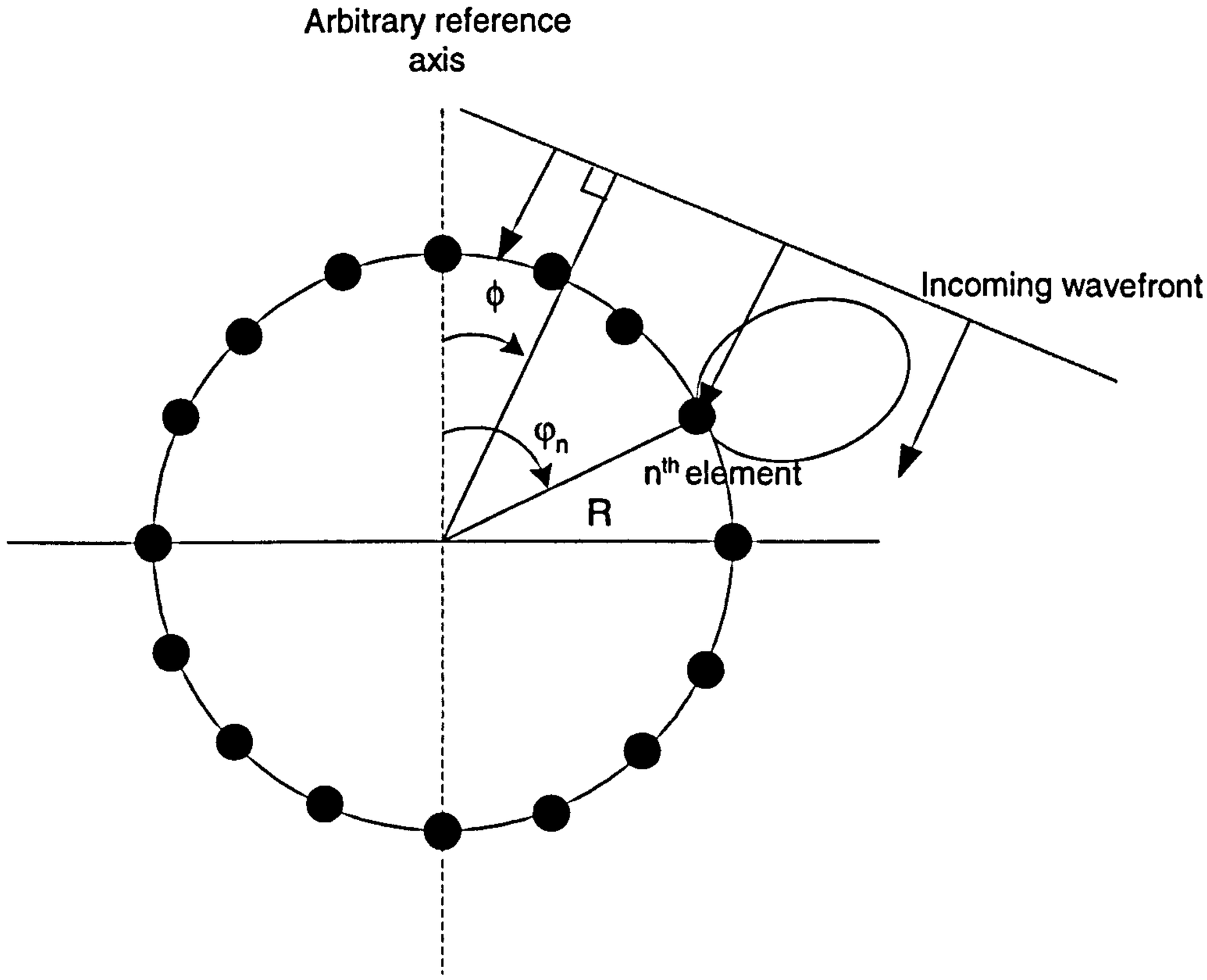

Figure 3.1: *Circular array geometry*

3.1.1 Beam Co-phasal Excitation

Beam co-phasal excitation is the simplest method of circular array excitation. In this method, each antenna elements' phase is altered to produce a radiation pattern with a main beam directed towards ϕ_0. This method does not allow sidelobe levels or array beamwidths to be specified. Davies [2] pointed out that for UCAs consisting of very large number of omni directional elements, the co-phasal excitation should be

$$\omega(\varphi) = e^{-jkR\ cos\phi} \tag{3.3}$$

and the resultant directional pattern can be expressed as

$$E(\varphi) = J_0\left(2kR\ sin\frac{\varphi}{2}\right). \tag{3.4}$$

Davies also suggested that an inter element spacing d of $< \lambda/2$ is employed. This corresponds to $R = \frac{N\lambda}{4\pi}$. However, Davies' theory is limited in that the UCA is required to have very large number of elements. For discrete UCAs, the co-phasal weight ω_n for the individual elements is given by

$$\omega_n = e^{-jkR\ cos(\phi_0 - \varphi_n)} \tag{3.5}$$

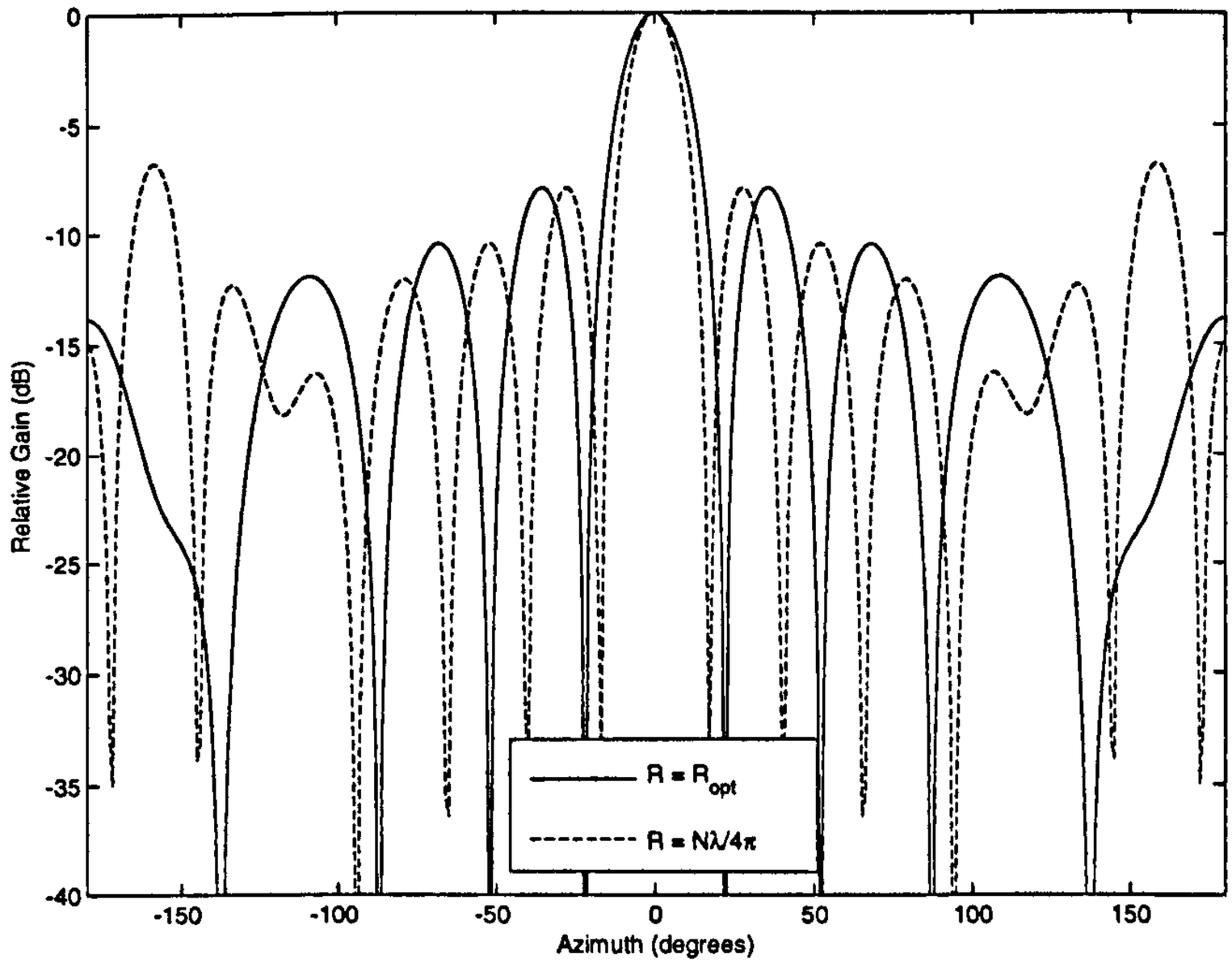

Figure 3.2: *Cophasal Excitation for 16-element omnidirectional UCA with* $R = \frac{N\lambda}{4\pi}$ *and* $R = R_{opt}$

Furthermore, it is found through rigorous simulations involving a range of values of R, that for discrete UCAs, a maximum radius of

$$R = R_{opt} = \frac{N\lambda}{16} \tag{3.6}$$

should be used in arrays with Beam Co-phasal excitation in order to obtain an array pattern with tapered sidelobe patterns similar to the $J_o(x)$ distribution where the highest sidelobe levels occur at the first pair of sidelobes, and the distribution decreases in a monotonic behaviour away from the main beam. Figure 3.2 illustrates a 16-element omni-directional UCA with $R = R_{opt}$ and $R = \frac{N\lambda}{4\pi}$. It can be seen that although the two radii yield first SLLs of the same level at -8dB, the beam pattern obtained with $R = R_{opt}$ shows a decaying pattern as described above, whereas the pattern obtained with $R = \frac{N\lambda}{4\pi}$ produces two sidelobes, each of -8dB height, in the directions $\phi = \pm 160^o$.

In practical applications, omni-directional UCAs suffer considerably from mutual coupling effects as the elements are *exposed* to each other. These effects, the extents of which are also dependent upon the size of the ground plane and the array radius, can be minimised by using directional elements.

Figure 3.3 illustrates the result of applying the beam co-phasal method to a 16-element ideal

UCA with positive cosine elements. In this case ϕ_0 is set to the array's boresight and the array radius set to $R = R_{opt}$ and $R = \frac{N\lambda}{4\pi}$, for comparison purposes. It can be seen that the pattern produced with radius $R = R_{opt}$ yield SLL that is $\approx$ 3dB lower than that of $R = \frac{N\lambda}{4\pi}$.

It is also evident in Figure 3.3 that by using directional elements, the system has lost its $J_o(x)$ -shaped distribution. Further, it is apparent that this method is only capable of achieving a sidelobe level of ≈ -8dB below the main beam peak, thus may not be sufficient for use in multipath environments where unwanted signals arrive from a number of different directions. An improvement to this technique can be achieved by taking into account the amplitudes of each individual element radiation patterns at ϕ_0. Thus, the improved weights are given by:

$$\omega_n = |A_n(\varphi_0)|\, e^{-jkR\ cos(\phi_0 - \varphi_n)} \tag{3.7}$$

where $|A_n(\varphi_0)|$ is the amplitude of the n^{th} element pattern in the direction of φ_0. This method is often termed the *optimum SNR excitation.* It effectively accounts for the amplitude variations in the individual elements. Hence the Optimum SNR method is not applicable to UCAs with linear amplitude element patterns. As can be seen in Figure 3.3, the sidelobe level (SLL) is now suppressed to -22dB relative to the main beam peak, giving a 14dB improvement to the previous method. Experimental results of the Beam Cophasal and optimum SNR methods are discussed in Section 4.2. However, it should be noted that this method does not allow for SLL or beamwidth control.

3.1.2 Phase Mode Excitation

For certain applications which require low sidelobe levels, the use of co-phasal excitation may not yield satisfactory sidelobe performance, even with the improved method. Furthermore, the sidelobe levels produced by the Beam Co-phasal and Optimum SNR methods are dependent upon the array manifold and the type of elements used. Beyond these criterias, the two methods do not allow for control over the sidelobe levels. Another available method for circular array pattern synthesis is the phase mode excitation method, as described in [2]. In this method, the circular array is transformed into a virtual array in order to make it possible to manipulate the radiation pattern in the same manner as with linear arrays. In order for the circular array to behave similar to linear arrays (and therefore amendable for spatial smoothing and the vast array of ULA spatial processing techniques), the steering vector of the virtual array, $\tilde{\mathbf{A}}(\phi)$, needs to possess a *Vandermonde*[3] structure

$$\tilde{\mathbf{A}}(\phi) = \left[e^{qv(\phi)}, e^{(q+1)v(\phi)}, \ldots, e^{(q+N)v(\phi)}\right]^T \tag{3.8}$$

[3]A Vandermonde matrix is defined by $\mathbf{V}_{i,j} = \alpha_i^{j-1}$, for all indices i and j, where α is a complex number.

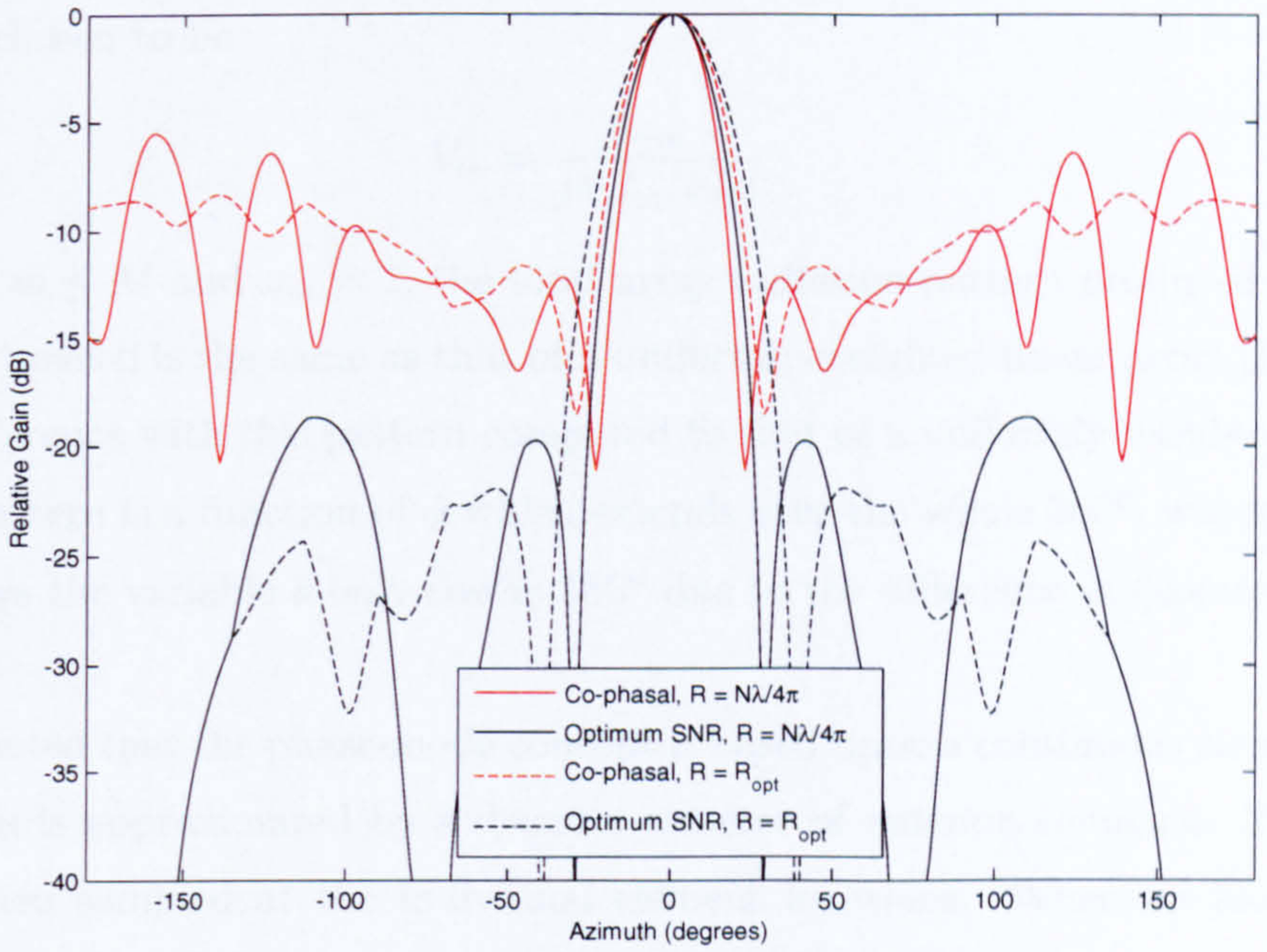

Figure 3.3: *Cophasal and Optimum SNR excitation for 16-element UCA with* $R = R_{opt}$ *and* $R = \frac{N\lambda}{4\pi}$*, and element patterns* $E_{elec}(\varphi)$ *as described in (3.1).*

where q is an integer and $v(\phi)$ is an arbitrary one-to-one function of ϕ in the field of view [3].

The phase mode method was initially developed for a continuous circular aperture. The actual array is transformed into a *virtual* array by applying a spatial Fast Fourier Transform (FFT). The excitation of the aperture $F(\varphi)$ is described as a Fourier series equation

$$F(\varphi) = \sum_{m=-M}^{M} V_m e^{jm\varphi} \tag{3.9}$$

These are the phase mode excitations of the array. V_m denotes the phase mode coefficient. The far-field radiation pattern due to the m^{th} mode is given by

$$\begin{aligned} \tilde{A}_m(\phi) &= \frac{1}{2\pi}\int_0^{2\pi} V_m e^{jm\varphi} e^{j[kR-cos(\varphi-\phi)]} d\varphi \\ &= V_m j^m J_m(kR) e^{jm\phi} \end{aligned} \tag{3.10}$$

$J_m(\cdot)$ represents the m^{th} Bessel function of the first kind. The far-field radiation pattern can therefore be described as a sum of $2N + 1$ spatial Fourier harmonics each excited to the same level, yielding a far-field radiation pattern

$$\tilde{A}(\phi) = \sum_{m=-M}^{M} V_m j^m J_m(kR) e^{jm\phi} \tag{3.11}$$

When V_m is chosen to be

$$V_m = \frac{\omega_m}{j^m J_m(kR)} \tag{3.12}$$

where $-M \leq m \leq M$ and $\omega_m = 1$, the total array radiation pattern produced is in the form of $\sin N\phi / \sin\phi$ which is the same as that of a uniformly-weighted linear array (Equation 2.5). The main difference with this pattern compared to that of a uniformly-weighted linear array is that this pattern is a function of ϕ which extends over the whole 360^o, whereas in the case of linear arrays the variable θ only covers 180^o due to the difference in geometry.

It should be noted that the phase-mode concept is based upon a continuous circular aperture. In reality, this is approximated by a discrete number of antenna elements. The excitation function is then sampled at the individual element locations. When an ideal UCA with omni-directional elements is considered while ignoring the effects inter-element interactions, Equation (3.10) becomes

$$\tilde{A}_m(\phi) = \frac{1}{\sqrt{N}} \sum_{i=n-1}^{N-1} V_m e^{j2\pi mi/N} e^{jkr\cos(\phi - \frac{2\pi i}{N})} \tag{3.13}$$

When elements each possessing a directional pattern $E_{elem}(\psi)$ are used to form the uniform circular array, they are generally pointing radially outwards from the array so that each directional pattern is pointing at a different direction to another. In terms of its Fourier components,

$$E_{elem}(\psi) = \sum_{n=-p}^{p} B_n e^{jn\psi} \tag{3.14}$$

where p denotes the maximum spatial harmonic of the element pattern and B_n is the n^{th} Fourier harmonic coefficient for the element. [15] shows that the resultant far-field radiation pattern is

$$\tilde{A}(\phi) = \sum_{m=-M}^{M} V_m \left|P_m\right| e^{j(m\phi + \psi_m)} \tag{3.15}$$

where

$$\left|P_m\right| e^{j\psi_m} = \sum_{n=-p}^{p} B_n j^{m-n} J_{m-n}(kR) \tag{3.16}$$

When $V_m = w_m / \left|P_m\right| e^{j\psi_m}$ is chosen, linear array weights can be applied to the phase mode excitation.

Discussions presented in the remaining of this chapter correspond to phase mode UCA pattern synthesis method. Experimental results obtained through the use of phase-mode excitation method and a couple of practical arrays are discussed in Section 4.3.

3.2 Array Geometry

3.2.1 Choice of radius

Davies [2] suggests that for small radii, only a few modes can be excited since the values of $J_m(kR)$ are very small for large values of m. Higher-order modes cause very large phase shifts around the array, which effectively cancel radiated signals in all directions. The highest-order mode which can be excited is $m \approx \pm(kR)$, as excitation of modes much higher than kR corresponds to superdirective conditions. It therefore follows that there should be $N \geq 2kR$ elements in the array, thus

$$R \leq \frac{N\lambda}{4\pi} \tag{3.17}$$

or

$$R_{max} = \frac{N\lambda}{4\pi} \tag{3.18}$$

Now, for lower order modes where $m \leq kR$, the asymptotic expansion of the Bessel function is

$$J_m(kR) \approx \frac{cos\left(kR\frac{\pi}{4} - \frac{m\pi}{2}\right)}{\sqrt{\frac{\pi kR}{2}}} \tag{3.19}$$

therefore in order to avoid any zero coefficient, kR should be a multiple of $\pi/2$, that is

$$kR = x\frac{\pi}{2}$$

or

$$R = x\frac{\lambda}{4}. \tag{3.20}$$

where x is an integer. Combining equations 3.17 and 3.20, $x < \frac{N}{\pi}$ therefore the maximum value for x is $N/4$. Thus,

$$R_{opt} = \frac{N \times \lambda}{16} < R_{max} \tag{3.21}$$

where R_{opt} is the optimum radius of a discrete UCA, which agrees with the criteria for optimum radius for Space Alternating Generalised Expectation (SAGE) [5] algorithm purposes described by C.M. Tan et al [6].

Figure 3.4 illustrates the pattern produced by an ideal omni-directional 16-element UCA with 0.5λ, 0.8λ, λ, 1.2λ, 1.5λ and 1.8λ radii. The figure shows that up to $R = \lambda$, the shape of the radiation pattern resembles a sinc function with decaying SLL and the highest SLL appearing directly on either side of the main beam. Beyond $R = \lambda$, the pattern no longer possess this property and eventually the SLL begins to increase. It should be noted that although the radiation pattern of $R = 0.5\lambda$ behaves similarly to that of $R = \lambda$, in practice, depending on the physical dimension of the antenna elements, the former may not be possible to manufacture due to size constraints (For this reason, radii $\leq 0.5\lambda$ are not considered in Figure 3.4). Mutual coupling will also take more effect since the elements are closer together. Further, the SLL pattern of $R = \lambda$ decays faster and therefore its front-to-back ratio is larger compared to that of $R = 0.5\lambda$ and $R = 0.8\lambda$

3.2.2 Element types

It can be seen in Equations (3.15) and (3.16) that the radiation pattern produced by phase mode excitation of directional elements does not only include a single Bessel coefficient as in Equation (3.13), it also includes a summation of coefficients corresponding to the Fourier series coefficients of each individual directional element pattern. Any shape of directional pattern, with zero spacing, yields a phase mode form which is free from any distortion terms. However, when discrete directional elements are employed, the sampling process introduces higher-order distortions to the phase mode pattern, i.e.:

$$E(\phi) = \sum_{m=-M}^{M} V_m \left|A_m\right| e^{j(m\phi+\psi_m)} + V_m \sum_{q=1}^{\infty} \left\{ \left|A_{Nq+m}\right| e^{j\left[(Nq+m)\phi+\psi_{Nq+m}\right]} + \left|A_{m-Nq}\right| e^{j\left[(m-Nq)\phi+\psi_{m-Nq}\right]} \right\} \quad (3.22)$$

where N is the total number of elements in the array. It is therefore concluded that in the case of discrete arrays, directional elements can not be used to relax the inter-element spacing.

The far-field directional patterns of two 16-element arrays with optimum radius are investigated. The first array consists of ideal omni-directional elements and the second array consists

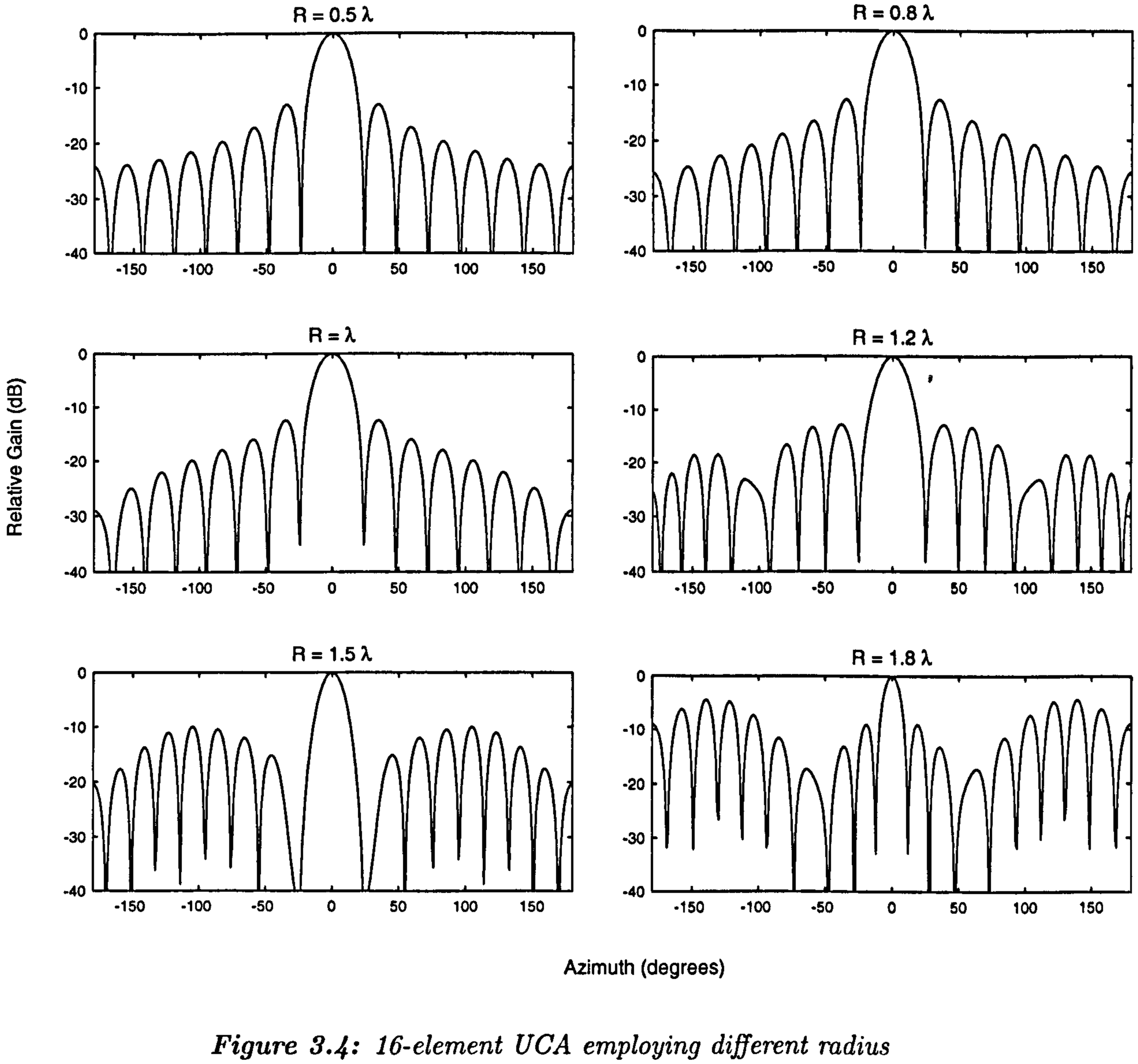

Figure 3.4: *16-element UCA employing different radius*

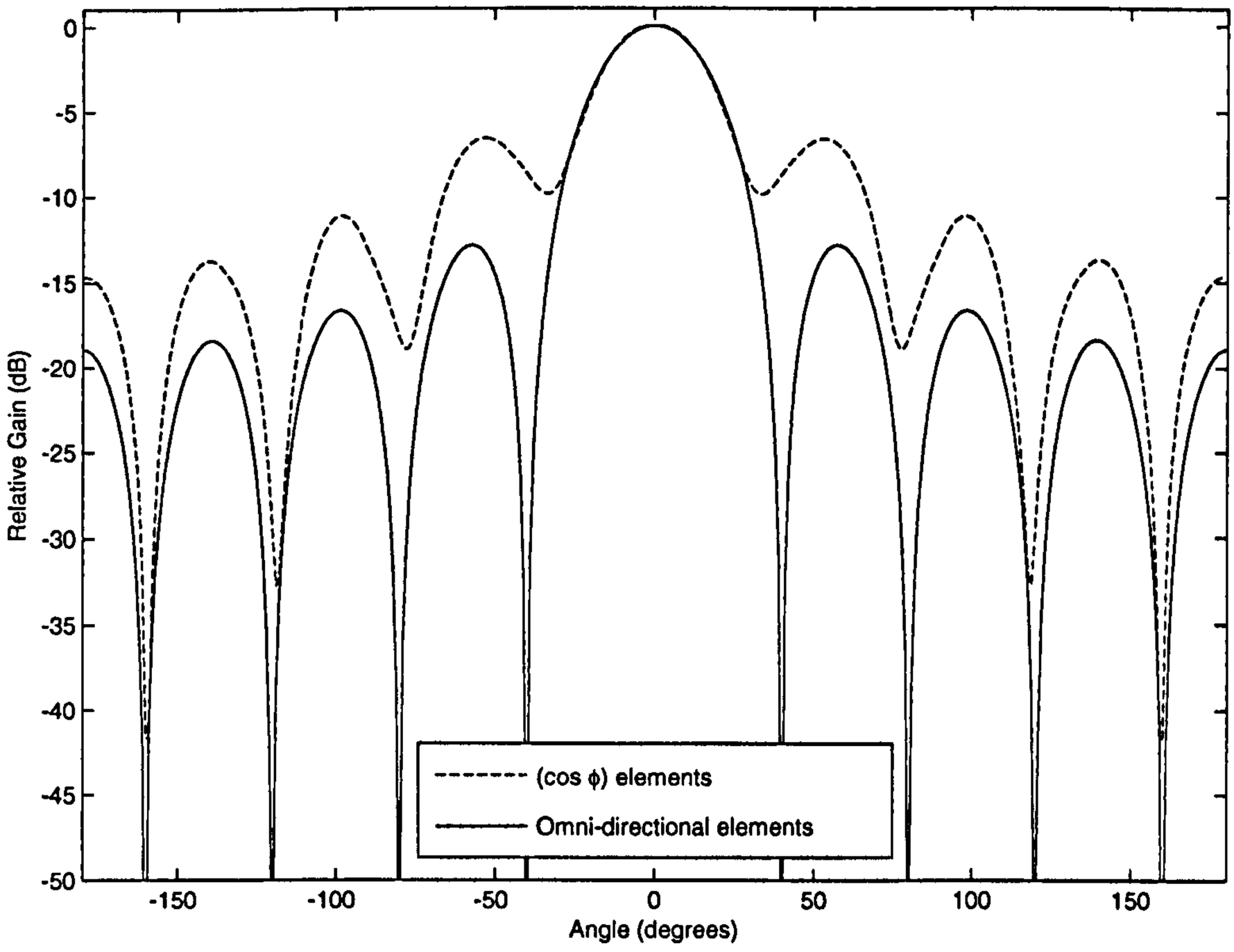

Figure 3.5: *Phase-mode excitation on 16-element arrays with* $R = R_{opt}$

of ideal directional elements with element patterns $E_{elec}(\varphi) = (cos\varphi)$. These patterns are presented in Figure 3.5. In this case, only the lower-order modes ($m = [-4, -3, ...0, ...3, 4]$) are excited as suggested in section 3.2. It can be seen that the patterns are similar in terms of the number of sidelobes and their positions on the azimuth plane, however the pattern of the array with omni-directional elements makes a better resemblance of Figure 2.6 compared to that of directional elements. Further, the omni-directional UCA produces ≈-13dB SLL and a front-to-back-ratio of ≈18dB, which is significantly lower compared to the ≈-8dB SLL and ≈14dB front-to-back ratio produced by the directional UCA. Similarly, the depth of the first null produced by the omni-directional UCA is ≈-58dB, which is ≈47dB deeper than that produced by the directional UCA at ≈-11dB.

While the effects of mutual coupling may be limited through the use of directional elements, it should also be noted that when directional elements are employed, it is necessary for the ground plane to be of cylindrical shape, such as shown in Figure 4.5(a) and 4.7. In this case, the back elements cease to contribute to the array pattern due to shadowing effect caused by the ground plane structure. This is illustrated in Figure 3.6.

Although phase-mode excitation remains a powerful tool for UCA beamforming, it may not

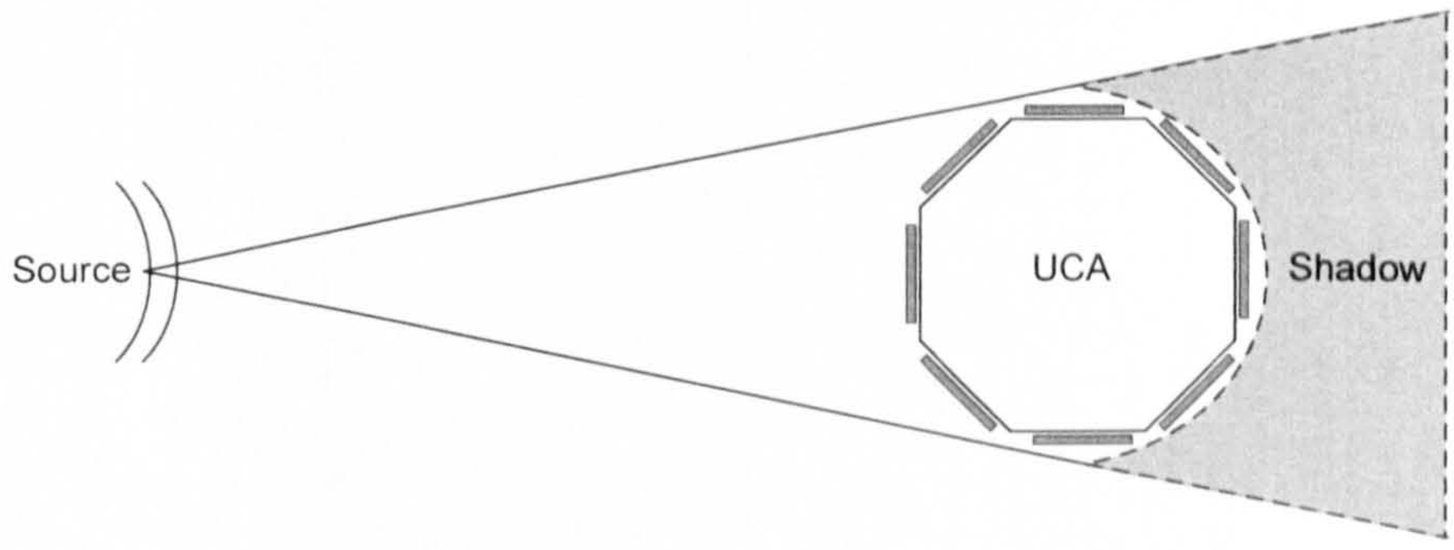

Figure 3.6: *Shadowing on back elements due to ground plane structure*

be sufficient in cases where an element spacing of $> \lambda/2$ is required due to practical reasons such as element sizes and the need to mount beamforming circuitry behind the array.

3.2.3 Number of Elements

The phase-mode excitation technique presented by Davies [2] is initially derived from a continuous circular array with zero element spacing. Figure 3.7 illustrates the array radiation patterns of eight and sixteen element linear and circular arrays employing ideal omni-directional elements. The arrays have uniform amplitude weightings, and the UCAs incorporate the phase-mode excitation technique by Davies. Here, the ULA inter-element spacing is $d = \lambda/2$ and the UCA radius is $R = R_{opt}$. It is apparent from the illustration that similar to the ULA, as the number of elements is increased, the rate of decay of the sidelobe patterns produced by the ideal UCA also increases. Additionally, the pattern of the larger array also exhibits a larger front-to-back ratio. However, it should also be noted that larger numbers of elements also in turn present higher post-processing complexity and may not be appropriate for the application. Hence, care should be taken when choosing the number of elements when designing a UCA. A geometry should be chosen that gives the right balance of array performance and system complexity that is appropriate for the intended application.

3.3 Dolph-Chebyshev Beamforming on Uniform Circular Arrays

The research presented in this thesis is based upon the problem of beamforming with UCAs. In particular, it is desirable to synthesise the array pattern in order to obtain a main beam that is as narrow as possible as well as a guaranteed maximum sidelobe level.

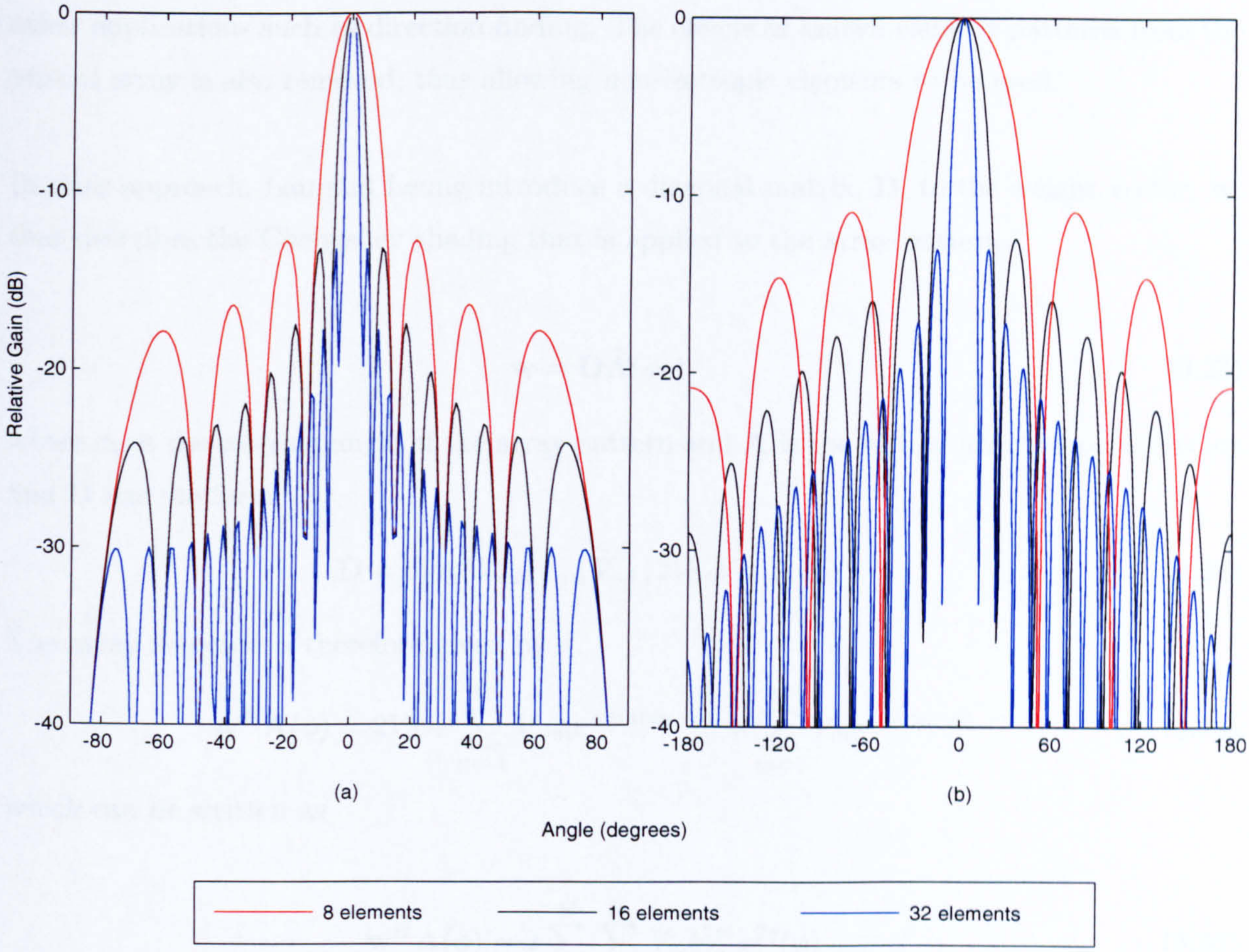

Figure 3.7: *8- and 16-element (a) ULA with $d = \lambda/2$; (b) UCA with $R = R_opt$; incorporating ideal omnidirectional elements at 5.2GHz.*

The Dolph-Chebyshev approach has been widely known as one of the standard approaches to beamforming problems. In this method, the array pattern is synthesised by defining a maximum sidelobe level. However, the method has mainly been applied only to uniform linear arrays (ULAs) and therefore needs to be adapted for use with UCAs.

Lau and Leung [7] proposes a Dolph-Chebyshev approach to synthesising UCA array patterns. In their approach to the array pattern synthesis, the transformation of the actual array to a virtual array as first proposed by Davies [2] is performed, in order to convert the spatial response of the array to a Vandermonde structure that is similar to that of a ULA and is therefore amendable to spatial smoothing. Dolph-Chebyshev array pattern synthesis can now be applied to the virtual array. Once the weights are calculated, it is no longer necessary to perform complex calculations when a different look direction is required. This in turn saves computational time savings. The transformed data can then also be used in

other applications such as direction finding. The effects of known element patterns from the virtual array is also removed, thus allowing non-isotropic elements to be used.

In their approach, Lau and Leung introduce a diagonal matrix, **D**, to the weight vector, **w**, that describes the Chebyshev shading that is applied to the array pattern.

$$\mathbf{w} = \mathbf{D}\tilde{\mathbf{A}}(\phi_0) \tag{3.23}$$

where ϕ_0 is the steering angle of the array pattern and $\tilde{\mathbf{A}}$ is the virtual array response vector and **D** has the form

$$\mathbf{D} = diag(V_{-M}, ..., V_{-1}, 2V_0, V_1, ..., V_M) \tag{3.24}$$

The array response is therefore given by

$$\mathbf{w}^H \tilde{\mathbf{A}}(\phi) = 2V_0 + \sum_{m=1}^{M} V_{-m} e^{-jm(\phi_0 - \phi)} + \sum_{m=1}^{M} V_m e^{jm(\phi_0 - \phi)} \tag{3.25}$$

which can be written as

$$\mathbf{w}^H \tilde{\mathbf{A}}(\phi) = 2 \sum_{q=0}^{M} \sum_{m=q}^{M} V_m b_{2q}^{2m} x^{2q}(\phi) \tag{3.26}$$

where

$$x(\phi) = cos[u(\phi)], \tag{3.27}$$

$$u(\phi) = \frac{(\phi_0 - \phi)}{2}, \tag{3.28}$$

and

$$b_{2q}^{2m} = (-1)^{m-q} \sum_{s=m-q}^{m} \begin{pmatrix} 1 \\ 2 \end{pmatrix} \begin{pmatrix} s \\ s-m+q \end{pmatrix}. \tag{3.29}$$

The Dolph-Chebyshev polynomials are defined by [8]

$$T_n(z) = \begin{cases} cos(n\ cos^{-1} z) & |z| < 1 \\ cosh(n\ cosh^{-1} z) & |z| \geq 1 \end{cases} \tag{3.30}$$

When applied directly to array element outputs,

$$n = \begin{cases} 2N-1 & for\ even\ N \\ 2N & for\ odd\ N \end{cases}$$

However, in this case the Chebyshev weights are applied to modal outputs which include zero mode. Therefore the value of n in this case is 2M.

The Chebyshev polynomial of degree 2M in z with roots in the range $-1 \leq z \leq 1$ can also be expressed in the form:

$$T_{2M}(z) = \sum_{q=0}^{M} b_{2q}^{2M} z^{2q} \qquad -1 \leq z \leq 1 \tag{3.31}$$

where

$$z = z_0 x(\phi), \qquad -z_0 \leq z \leq z_0 \tag{3.32}$$

Thus, substituting Equation 3.32 into 3.31 and equating the resulting polynomial with 3.26

$$2 \sum_{m=q}^{M} V_m b_{2q}^{2m} = b_{2m}^{2M} z_0^{2q}. \tag{3.33}$$

Dolph [9] reveals that equation 3.33 may be written in the form

$$V_q = \frac{1}{b_{2q}^{2q}} \left\{ b_{2q}^{2M} z_0^{2q} - \sum_{m=q+1}^{M} V_m b_{2q}^{2m} \right\}. \tag{3.34}$$

Coefficients V_q of the matrix $\mathbf{D}$ can now be solved for $q = 1, ..., M$ in terms of z_0, starting from $q = M$.

z_0 can be chosen either by specifying the sidelobe level or the position of the first null. Specifying the sidelobe level would minimise the beam width, whereas if the direction of the first null is specified, the sidelobe level is minimised.

For the first case, the main beam height β is specified as a ratio between the main beam height and the sidelobe level of the Dolph-Chebyshev pattern. The value of z_0 is chosen to satisfy the relationship

$$T_{2M}(z_0) = \beta > 1$$

and $z_0 > 0$. z_0 can then be computed using equation 3.30.

The array radiation pattern is as follows:

$$\left| \mathbf{w}^H \tilde{\mathbf{A}}(\phi) \right|^2 = \left| \tilde{\mathbf{A}}^H(\phi_0) \mathbf{D} \tilde{\mathbf{A}}(\phi) \right|^2 = \left| T_{2M}[z_0 x(\phi)] \right|^2. \tag{3.35}$$

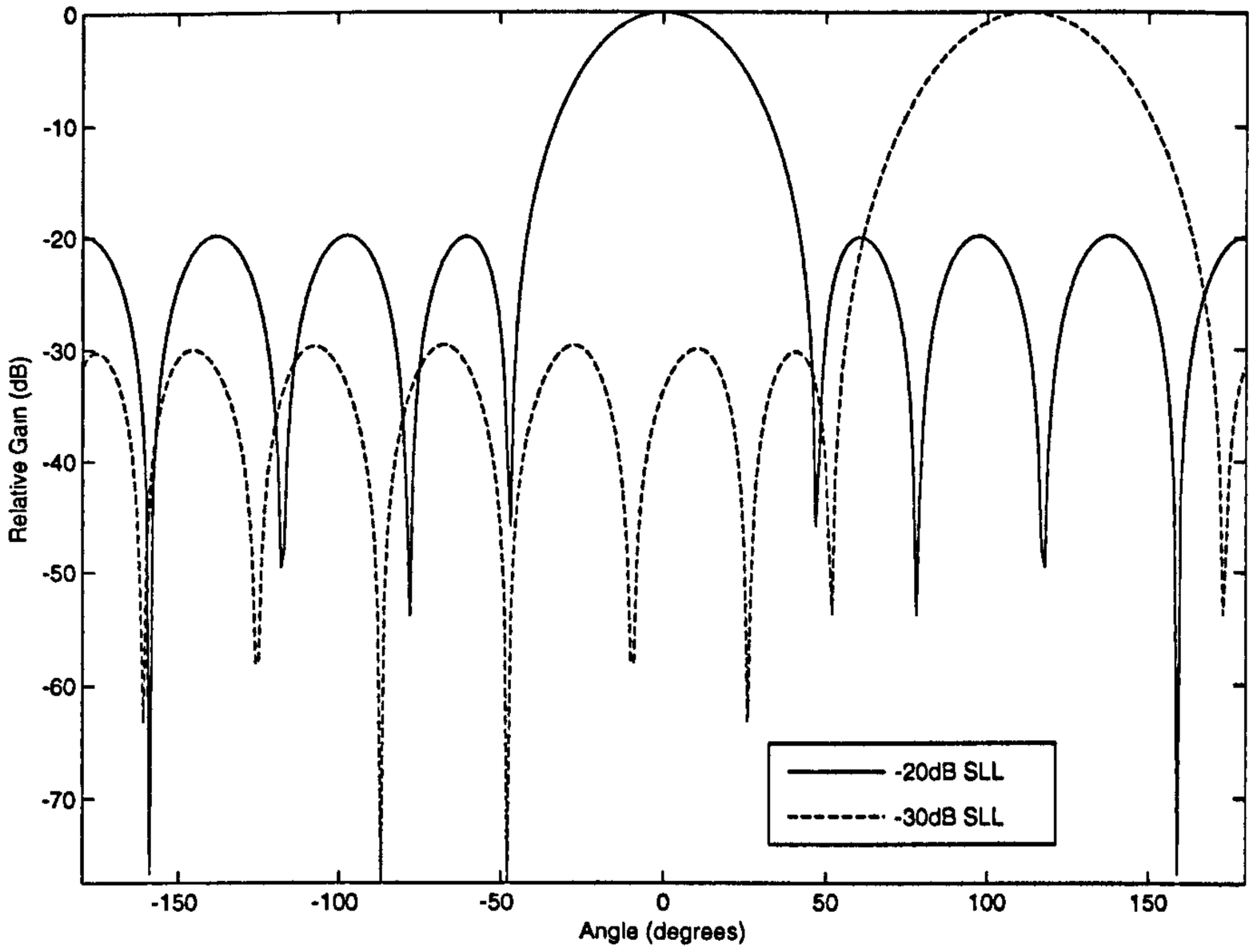

Figure 3.8: *Chebyshev weights -20dB and -30dB SLL specification applied to ideal 32-element monopole UCA with M=4. Patterns are steered towards* $\phi_0 = 0^o$ *and* $\phi_0 = 120^o$ *respectively.*

Figure 3.8 illustrates Chebyshev weights applied to an ideal omni-directional UCA with Davies' phase-mode technique. Sidelobe levels of -20dB and -30dB and steering angles of 0^o and 120^o respectively are specified.

In the second case, specifying the direction of the first null as ϕ_1, x_1^0 is defined by

$$x_1^0 = cos\ u_1^0 = cos\ \left(\frac{(\phi_0 - \phi_1)}{2}\right)$$

and z_o is chosen as

$$z_0 = \frac{1}{x_1^0}\ cos\ \frac{\pi}{4M}. \tag{3.36}$$

It follows that

$$T_{2M}(z_0 x) = T_{2M}\left[\left(cos\ \frac{\pi}{4M}\right)\frac{x}{x_1^0}\right]$$

The location of the first null, however, can only be specified for angles such that $z_0 > 1$. Smaller values are impossible to obtain. In Figure 3.9, the location of the first null is specified as 40^o and 80^o. As seen in the illustration, the sidelobe levels are no longer uniform.

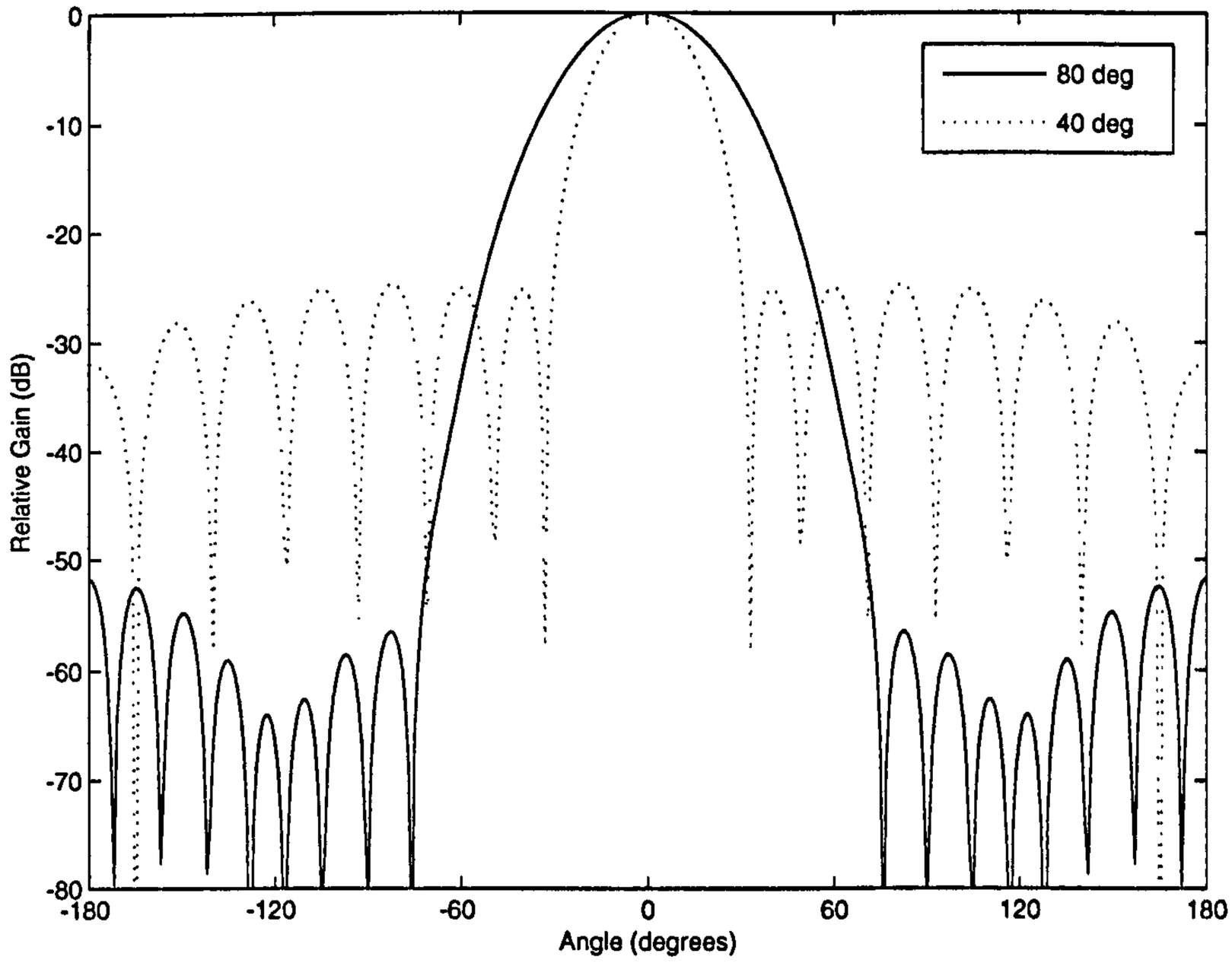

Figure 3.9: *16-element monopole UCA with M=7, with angle of first null specified at* $\pm 80^o$ *and* $\pm 40^o$

While the UCA and the ULA now behave similarly, it should be noted that the most significant difference is that UCAs are capable of serving the full 360^o of the azimuth plane. Further, in the case of UCAs, there is no end-fire broadening of the main beam as would be seen in the case of ULAs. This is illustrated in Figure 3.10, where the the radiation pattern of a 16-element ideal UCA is subjected to -20dB SLL Chebyshev weights. 16 beam peaks are formed and steered towards different positions around the azimuth plane. The diagram validates the fact that there is no broadening of the main beam at any part of the azimuth plane.

It should, however, be noted that using these methods, the weighting function (3.23) is dependent upon the beam steering angle. Hence the array tapering function would need to be computed dynamically as the beam is steered around the array.

3.4 Butler Matrix for Uniform Circular Arrays

Research has shown that a Butler matrix network [1], which is conventionally used to produce orthogonal multiple beams for linear arrays, may be used for exciting phase modes on a circular array as described in section 3.1.2.

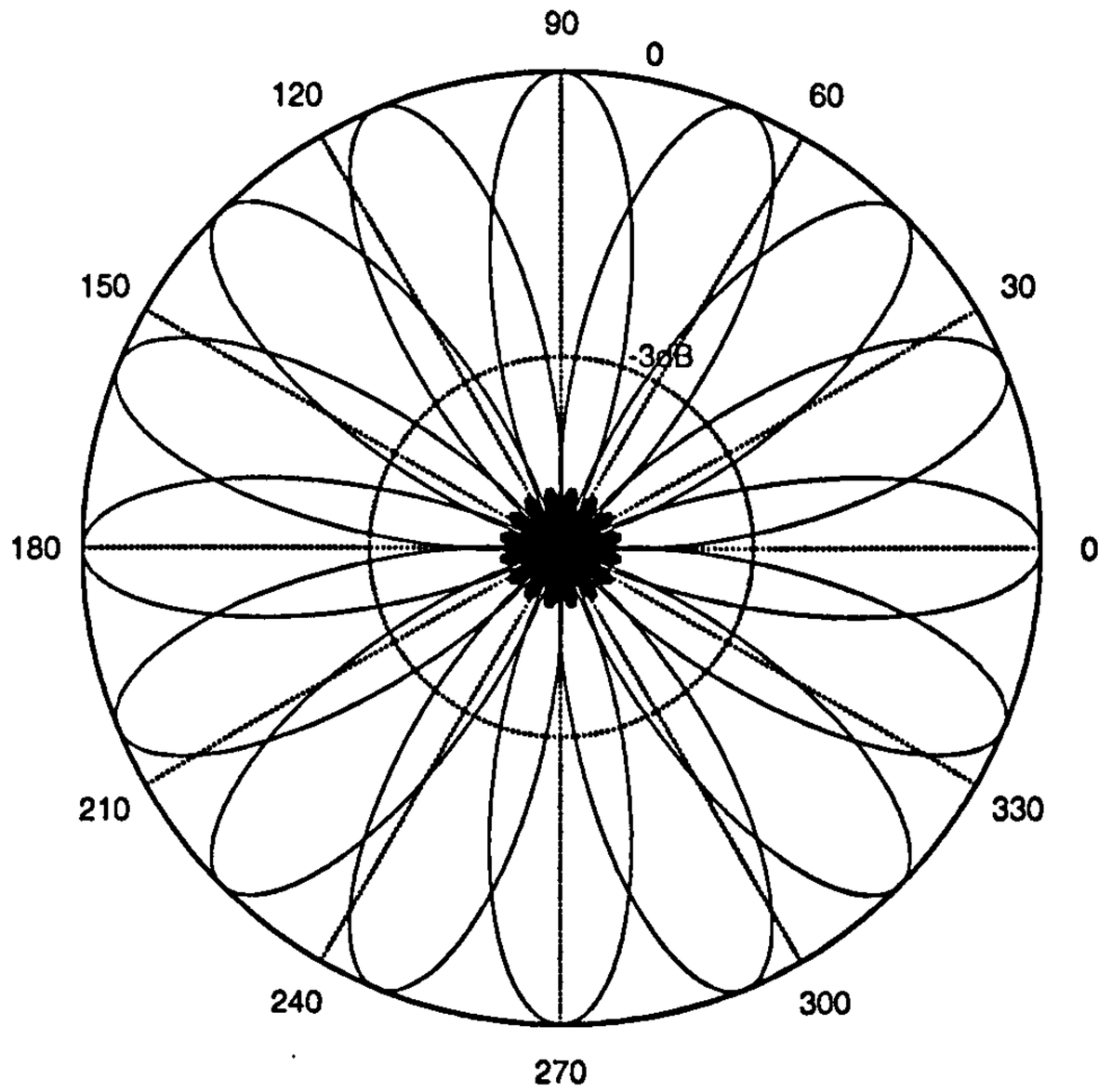

Figure 3.10: *Polar plot of 16 directional beams produced by a 16-element ideal UCA with -20dB SLL Chebyshev weights.*

The matrix shown in Figure 3.11 has X input ports and N output ports, with $N \leq X$. The output ports correspond to the array element ports and the input ports are the beam ports. A signal $\tilde{a}_m$ applied to the mth beam port produces a signal, a_{nm}, at element port, n, described by

$$a_{nm} = \frac{\tilde{a}_m}{\sqrt{N}} e^{-j2\pi m(n/N)} \tag{3.37}$$

The array excitation i_n is therefore the Fourier transform of the input signal $\tilde{a}_m$

$$a_n = \sum a_{nm} = \frac{1}{\sqrt{N}} \sum_{m=-M}^{M} \tilde{a}_m e^{-j2\pi m(n/N)} \tag{3.38}$$

where $M = (N-1)/2$. Similarly, when a Butler matrix is connected to a circular array, the X input ports correspond to mode ports. Hence a signal, a_n, arriving at the nth element port produces phase modes, $\tilde{a}_m$, at the mode ports:

$$\tilde{a}_m = \sum a_n = \frac{1}{\sqrt{N}} \sum_{N-1}^{i=n-1} a_m e^{j2\pi m(i/N)} \tag{3.39}$$

This is comparable to the first half of equation (3.13).

Davies [2] pointed out that an NxN port Butler matrix may be connected to an n-element circular array so that its n input ports produce the correct array excitation for spatially

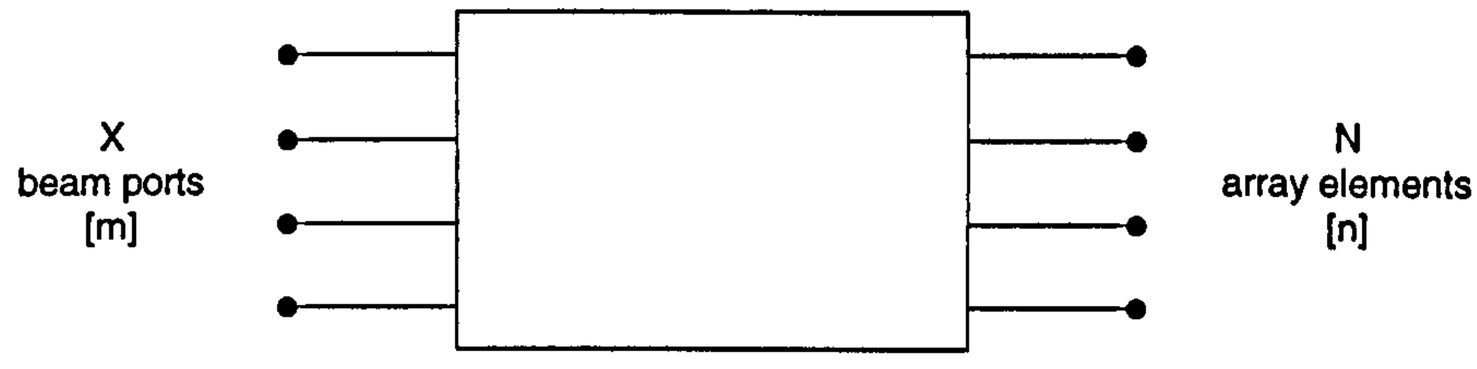

Figure 3.11: *M x N Butler Matrix*

orthogonal set of n possible phase modes as discussed in section 3.2. This is illustrated in Figure 3.12. The Butler matrix effectively performs a Discrete Fourier Transform (DFT) to the array element patterns. The excitation of the mth input yields a phase difference of $2\pi m/N$ radians between adjacent output ports. Each excitation mode corresponds to a modal pattern corresponds to $e^{jm\phi}$ and therefore can be used to synthesise a radiation pattern as described in equation (3.10). In other words, in its application to circular arrays the excitation of each input of the Butler matrix correspond to a phase mode excitation, therefore theoretically any spatially band limited radiation pattern can be excited from a uniform circular array provided correct amplitude and phase are applied to the input ports. These weights are functions of the desired radiation pattern and the individual element patterns.

Another important feature of Butler matrix feed is that in order to steer the main beam towards any direction ϕ_0, a linear progressive phase weight of $(N-1)\phi_0$ may be applied to the input ports in addition to the required amplitude and phase weights as described above, as shown in Figure 3.13. The output currents of a Butler matrix can be permuted cyclically by varying the phases of its input currents [10]. This is an attractive feature for circular array pattern synthesis, as it is no longer required for both amplitude and phase weights to be altered each time a different look direction is required.

An advantage to this system is that the Butler matrix provides a transformation between the excitation techniques of linear arrays and those of circular arrays. The system results in a beam pattern which is amendable to spatial smoothing and to which any conventional linear array excitation can be applied. Unlike the method outlined in Section 3.3, the Dolph-Chebyshev beamforming technique can now be applied to UCAs without the need for dynamic computation of the amplitude and phase weight function. The ease of which UCA beam steering can be performed through the use of a Butler matrix provides the main source of interest for the work presented in this thesis.

Since constant phase shift over the frequency band of interest is required in phase mode

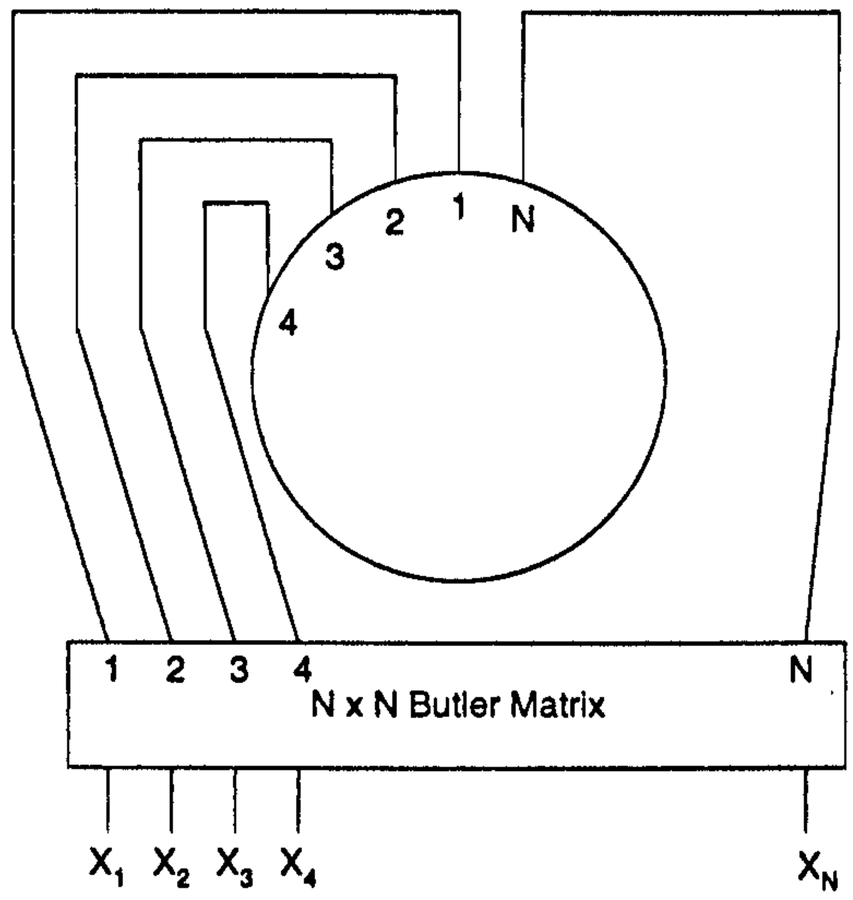

Figure 3.12: *Butler matrix applied to uniform circular array*

excitation, only the Butler matrix configuration can be used. Other networks such as the Maxson matrix and lens configurations are based upon time delay compensation. The Butler matrix would have to be suitably modified for wideband operation. Foti and MacNamara [11] presents the design of octave-bandwidth stripline Butler matrix using single section Schiffman lines and three-branch branch line couplers augmented by Schiffman lines. The use of tandem couplers and multi-section Schiffman lines are discussed for multiple-octave operations. [12] presents sectoral phase modes and superresolution techniques to circular arrays which are both usable over broad bandwidths of two octaves or more using digital filtering techniques in order to compensate the phase mode variations as a function of frequency. The application of Butler matrix on 32-element UCA is discussed in detail by Sheleg [13]. In this paper, Sheleg demonstrated how Butler matrix can be used to produce narrow beams ($10^o - 11.5^o$) with sidelobe levels of -19 to -21dB. However, it should be noted that the application presented in [13] involves 32 elements and 32×32 Butler matrix, which is complex to manufacture. Furthermore, it is also shown that the mode patterns that do not compare with the theoretical patterns due to phase and amplitude errors. These errors can also be seen in the analysis presented in the next chapter, and are tackled in Chapter 5.

3.5 Modifications to Butler Matrix

Wax [14] pointed out that a virtual array smaller than the size of the actual array is necessary if the number of elements, N, is even. Choosing $M = \frac{N}{2}$ would yield phase mode contribution corresponding to $m = -1$ that is identical to the contribution from $m = 0$,

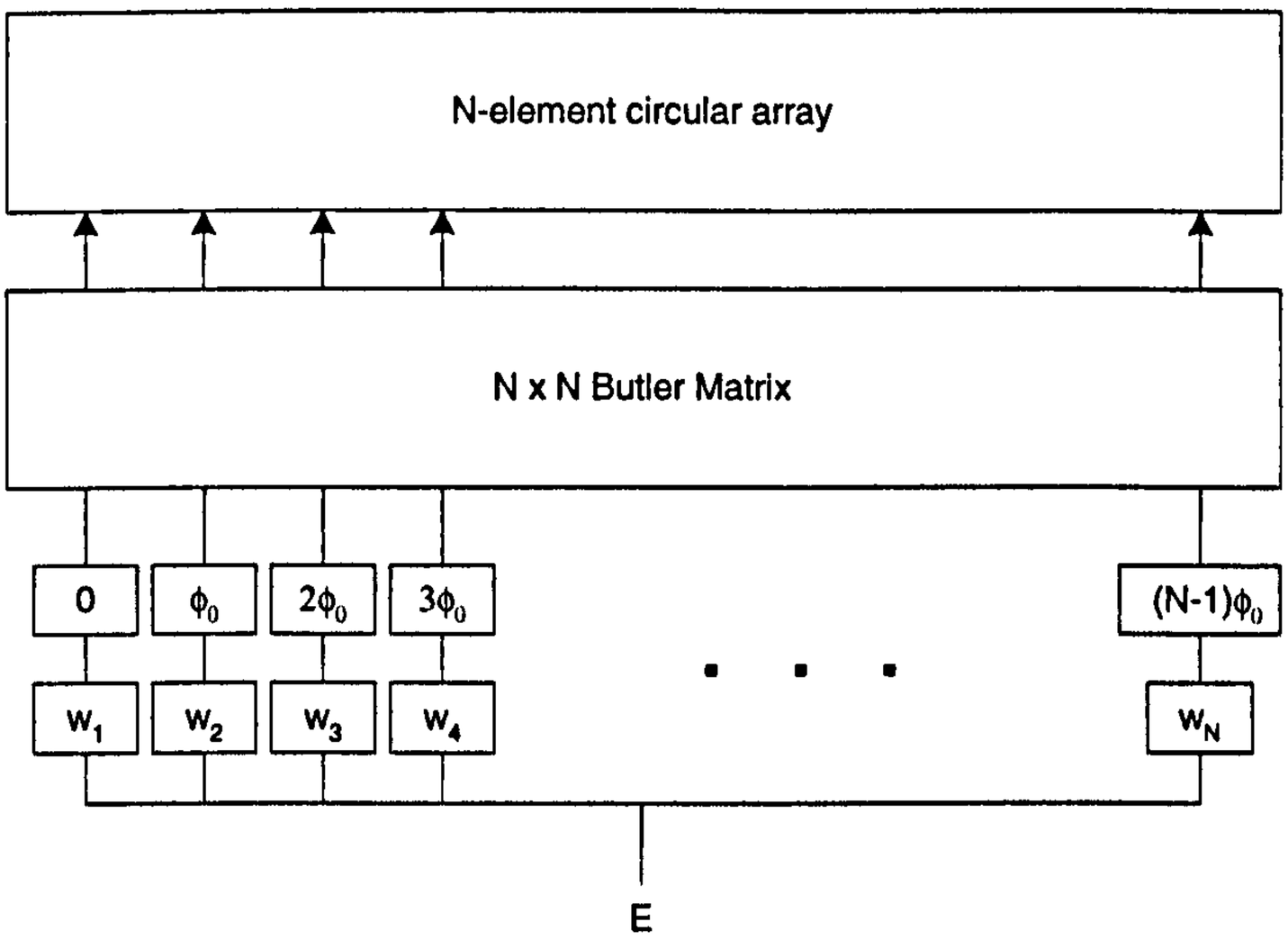

Figure 3.13: *Application of linear progressive phase weights to Butler matrix feed system*

which results in an error.

For an N element array where N is even, it is therefore necessary to employ an $N \times N$ Butler matrix, with one of the output ports terminated using a 50Ω load, as described by Sheleg [15] and illustrated in Figure 3.14. Due to the circular geometry of the array, the choice of port to be terminated does not affect the resulting patterns. However, this approach introduces deviations in the resultant radiation pattern due to the terminated port, which now creates a symmetrycal imbalance. However, it should be noted that this termination process by no means *waste* the received power of one of the UCA elements as all the received power from every single element of the UCA is distributed among the ports within the Butler Matrix.

The most common size of a Butler matrix is $2^x \times 2^x$ where x is an integer. Shelton [16] proposes the use of three input - three output as well as four input - four output junctions in order to increase the number of elements in the array that can be supported. However, as most of these still yield matrices of even number of elements, the port elimination process is more often than not inevitable. The effect of the terminated port is illustrated in Figure 3.15. In this model, an ideal 16-element uniform circular array with omnidirectional elements and radius $R = \frac{N\lambda}{16} = \lambda$ is employed with a 16×16 Butler matrix and no additional amplitude and phase weighting. The figure shows that the elimination of one of the end ports causes a ≈2dB increase in SLL, $\approx 20^o$ widening of the beamwidth at -10dB, and a ≈5dB increase in the front-to-back ratio.

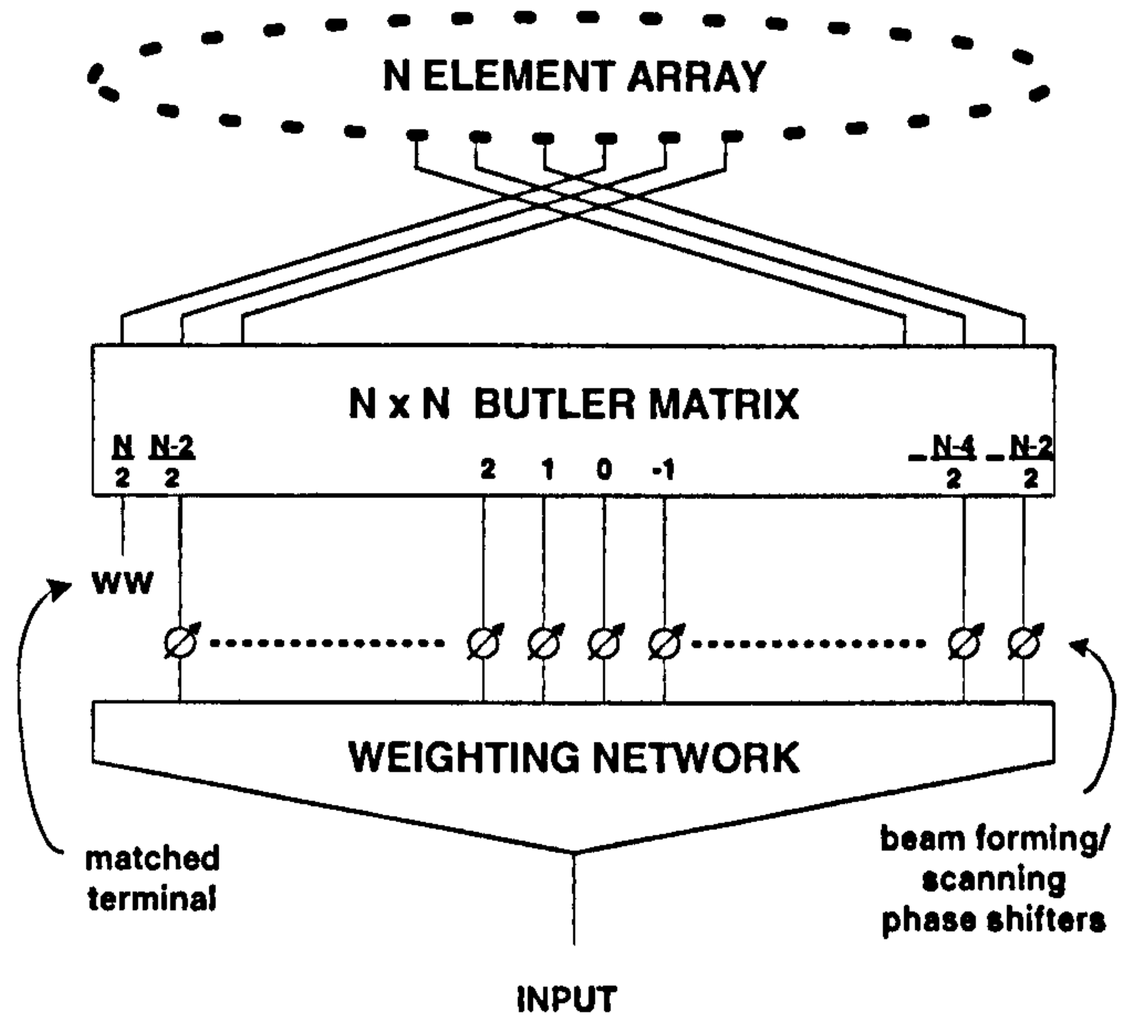

Figure 3.14: *Scanning multimode circular array with Butler matrix feed system [15]*

Large numbers of array elements impose a disadvantage to Butler matrix systems in that the matrix design becomes more complicated. Designs for 32 or more elements, or apertures greater than 5λ diameter, become more complex. This defeats the overall aim of the work, which is to find a cost-effective solution. Intermediate Frequency and digital processing can be used instead for receive-only configurations in order to overcome this complexity issue. Sheleg [15] suggests that for practical element spacings only 2/3 of the modes are usable since the patterns of the higher order excitation modes are poorly approximated by $e^{jm\phi}$. The use of more modes for narrow beam patterns will result in higher sidelobe levels. Sheleg proposes the use of a set of smaller submatrices in applications where fewer than N/2 modes are required. This method reduces complexity and is particularly useful for large N, however the complexity reduction comes at the cost of wider beamwidth. Further, the submatrices effectively eliminate a pair of phase modes. When a UCA of smaller N is considered, this may not be feasible due to the limited phase mode components available. Discarding a phase mode pair a UCA with small N would cause a more significant degradation in the beam pattern compared to a UCA with large N. This is illustrated in Figure 3.16. It is evident that although the increase in the level of the outermost sidelobes is similar for the cases of both $N = 8$ and $N = 32$, the beamwidth remains unchanged for $N = 32$ and increases by $\approx 50\%$ in the case of $N = 8$.

Reference [4] presents a different technique for feeding a UCA with Butler matrix, whereby an

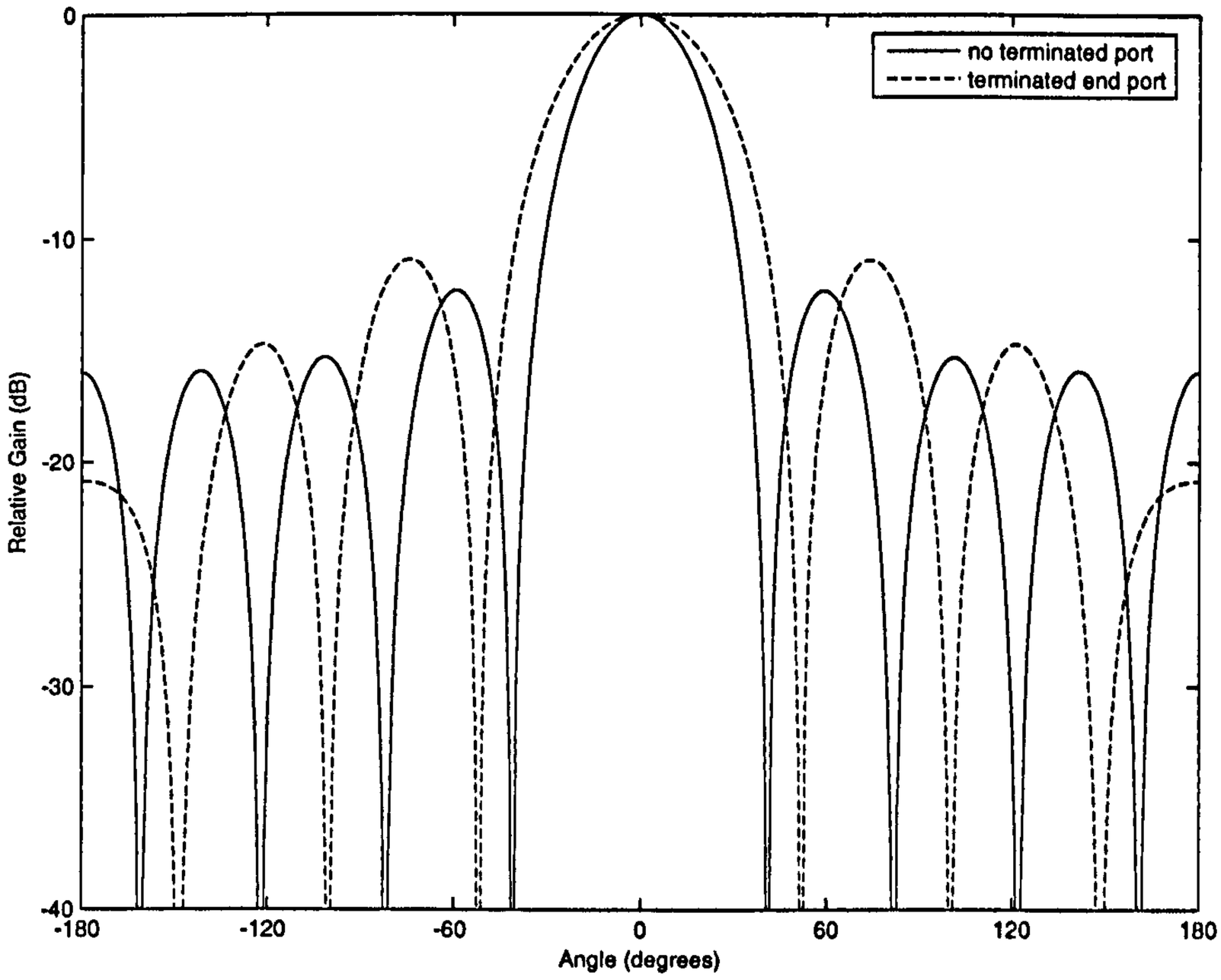

Figure 3.15: *The effects of terminating one port of the Butler matrix*

array of N elements is configured so that N/M (M = 1,2,3...) adjacent elements of the UCA serving an angular sector $2\pi/M$ are simultaneously excited to form a radiation pattern. Each of these M sub-arrays is then excited by an N/M-way power divider and an $N/M \times N/M$ Butler matrix. N/M phase shifters and 1P4T attenuator switches are used to achieve pattern selection or rotation. When a phase progression of β is applied between adjacent steering phasers, the excitations of the outputs of the Butler matrix translate, in turn rotating the pattern by β/M. In this paper, the authors described the use of a 32-element UCA fed by an 8×8 Butler matrix. This method, however, is not desirable as the element - radius ratio of each subarray would be four times larger in comparison to that of the array.

3.6 Applications of Circular Arrays

The complexity of circular array excitation and beam rotation has limited the number of circular array applications. Limited sidelobe level and beam rotation problems in the case of co-phasal beam patterns has deterred researchers from considering application of circular arrays. However, the breakthrough of phase mode excitation in the 1960s coupled with the prospect of a Butler matrix as a feed system for the modes represent a substantial development in circular array theory. The phase-mode concept has since been studied and applied in null-steering, radar and direction-finding systems.

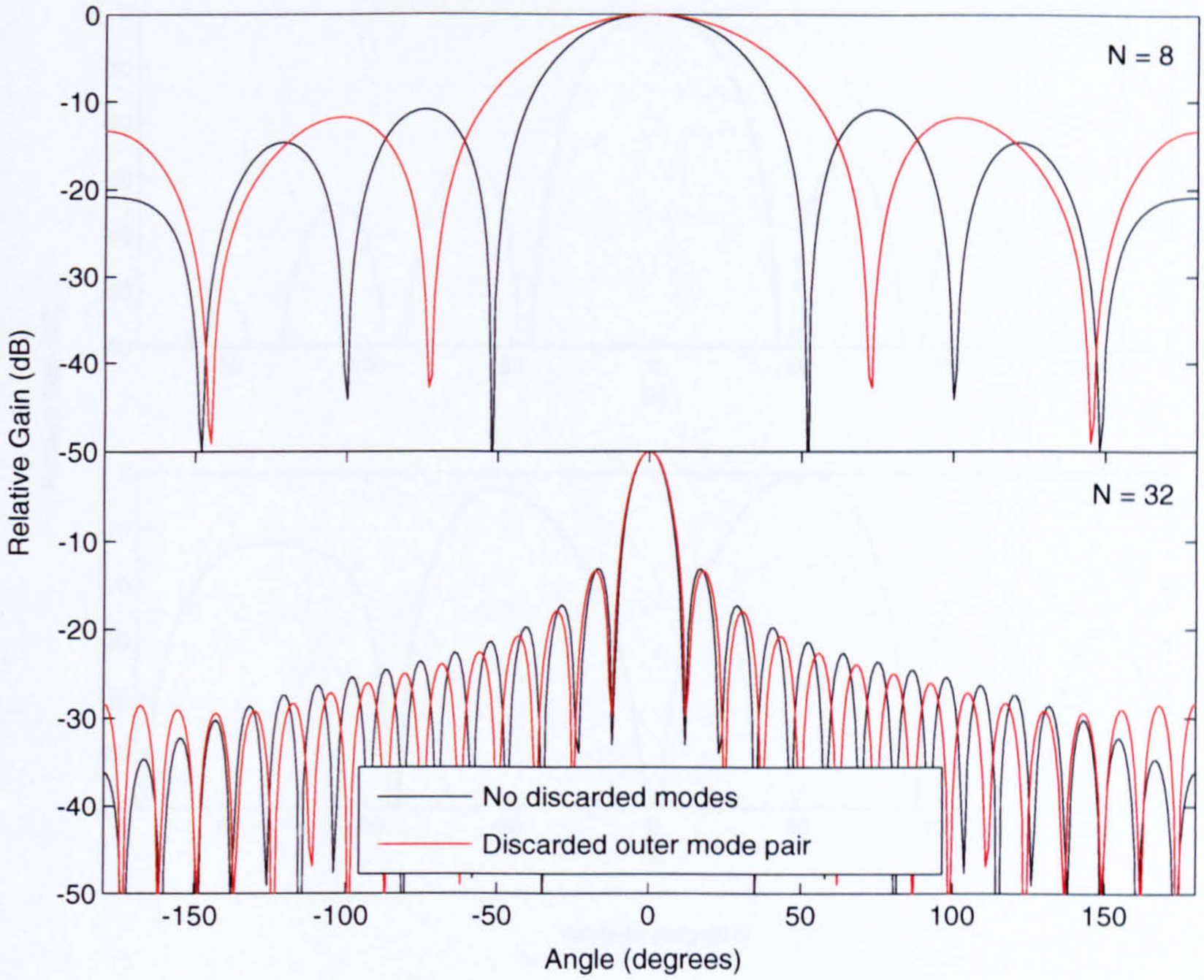

Figure 3.16: *The effects of discarding a phase mode pair on ideal omnidirectional UCA with N=8 and N=32.*

3.6.1 Null Steering

The simplest method of null steering is achieved by applying weights to the signal received at each element of the array such that

$$\sum_{n}^{N} \mathbf{w}_n(\phi_0)\mathbf{E}_n(\phi_0) = 0 \tag{3.40}$$

where ϕ_0 represents the desired null position. Up to N-1 nulls can be steered using this method. Figure 3.17(a) illustrates the array response of an eight-element ideal monopole array with nulls specified at seven different positions. The downside of this technique is that when smaller number of nulls are specified, extra nulls occur in directions that have not been specified, as shown in Figure 3.17(b).

Reference [17] presents the application of phase mode excitation for null steering. A single phase mode is used to provide omni-directional coverage, while a second adjacent mode is used to provide a single directional null. Equal amplitudes of the two phase modes yields

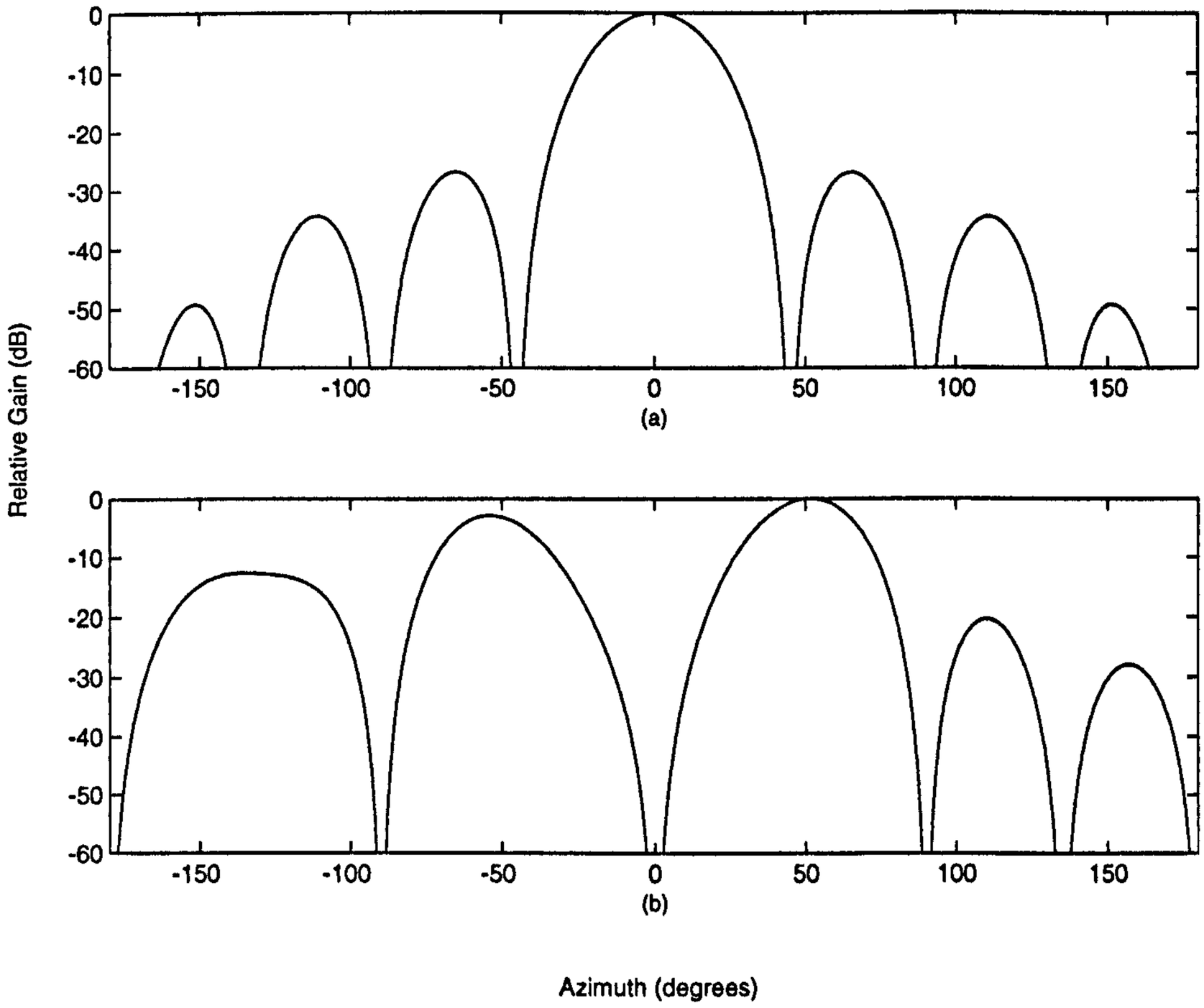

Figure 3.17: *(a) Nulls at* -135^o, -90^o, -45^o, 45^o, 90^o, 135^o *and* 180^o*;*
(b) Nulls at -90^o, 0^o, 180^o

an angle at which signals from these modes are in phase oppositions. Combination of the two signals produces a single null pattern. The angle of the null can be steered through 360^o by changing the phase shift of either of the two modes. This can be achieved by using a single phase shifter. Additional nulls or broadening of the existing null may be achieved by introducing additional phase modes [17] - [19]. This concept can be extended to include a directional beam in order to enhance gain in a required direction in addition to multiple nulls for eliminating unwanted interference signals.

Davies and Guy at the University College London provided an extension to the above concept in [20] by incorporating an automatic null steering feature based upon an open-loop control system. An experimental system consisting of a 4x4 Butler matrix network and a 4-element circular array with microcomputer in order to control null locations. The outputs from two phase modes are distributed to two receivers, each combining these modes using phase shifters in order to control a null. These signals are also used to determine the angle of arrival of the strongest signal. A phase sensitive detector is used to measure the phase difference between the received signals on the two mode patterns. The information is then used to set the appropriate value of phase shifter to control the null positions. The micro-

computer makes measurements of directions of arrival when two or more receivers are in use. The appropriate nulls are then steered for each receiver.

In [21], Griffiths and Eiges show that the null steering agility of a multi-beam null-steering system may be improved by confining the circular array phase modes to angular sectors. Each of these sectoral phase mode is a broadband directional beam characterised by a phase slope which is approximately linear.

3.6.2 Direction Finding with Circular Arrays

Reference [15] briefly reviews the properties of modally-excited circular and cylindrical arrays and their application to sonar systems. The authors present the basis of a sectoral phase mode technique, allowing direction finding with improved immunity to interference, and the application of super-resolution techniques to circular arrays which have particular benefits in operating with correlated signals. Griffiths [22] also considers the application of circular array phase modes for direction finding.

Matthews and Zoltowski [23] developed an algorithm for azimuth angle estimation for narrowband signals using a uniform circular array. Phase-mode excitation technique is utilised in order to synthesise the beam patterns in the azimuth plane. Azimuthal search at each considered elevation angle is performed using a root version of the MUSIC algorithm. As the synthesised far-field patterns are entirely real-valued, computational savings is achieved since only a single real-valued eigenvalue decomposition is required for the algorithm. The authors of [24] developed alternate array response models based on array geometry and electromagnetic characteristics of the array elements. Direction finding algorithms are calibrated using the array output generated by these models. Simulation studies showed that the method, when applied to MUSIC algorithm, provides greater estimation performance compared to the standard MUSIC algorithm.

Cvetkovic [25] described a portable receiving direction finding 4-element circular array at 2-30MHz. The system, also capable of beam and null steering, includes a processor unit and an analogue HF receiver. The system uses wideband antenna elements, adaptive signal processing techniques and microprocessor control in order to perform direction finding, null steering and simultaneous direction finding and null steering. A null is pointed at an interfering signal and direction finding process is performed on a wanted co-channel signal.

Additionally, the system is also capable of steering two independent cardioid directional patterns.

A new algorithm applicable to *filled circular arrays* (FCAs) for simultaneous estimation of azimuth and elevation angles of arrival of multiple co-channel signals is presented in [26]. The algorithm is called FCA-ESPRIT, and is applicable to any FCA geometry provided the spacing between adjacent sensors is $\leq 0.5\lambda$ on average. The algorithm solves a set of ESPRIT-like equations to produce paired azimuth and elevation angle estimates. This is achieved through a closed-form procedure and hence does not require computationally expensive search or optimisation procedures. In [27], Mathews and Zoltowski proposes a novel UCA 2D azimuth and elevation angle estimation called the unitary UCA-ESPRIT. The algorithm provides azimuth and elevation estimates of closed-form automatically-paired source. Avoiding iterative solutions, multi-dimensional optimisation and computationally intensive search procedures, UCA-ESPRIT makes a very powerful angle estimation algorithm.

3.6.3 Circular Array for Radar Applications

There has been limited applications of circular arrays in operational radar systems. However, several experimental systems have been developed for electronic rotation of circular array patterns. Skahill and White [28] at the University of Birmingham, UK, developed an electronic scanning system using a Butler matrix and a simple switching matrix for exciting a sector of a circular array. Only the sector that contributes to the formation of a desired radiation pattern is excited, which reduces complexity. With this technique, an array of N elements is configured so that N/M elements, where M=1,2,3..., in an angular sector of $2\pi/M$ are simultaneously excited. The resultant radiation pattern is selected or rotated by using $N/4$ phasers and $N/4$ 1P4T switches.

A 32-element circular dipole array with 5.1λ diameter was constructed at the Naval Research Laboratory in Washington [29]. The array, operating at 900MHz is fed from a Butler matrix. The current phase was controlled by variable phase shifters and different amplitude distributions were applied over the matrix inputs through the use of printed circuit structures. Experimental results show that the system is capable of producing a narrow radiation pattern which can be scanned through 360^o.

The authors of [13] at the Naval Electronics Laboratory, San Diego, designed a circular-array

radar antenna of 128 elements for operation over 20% bandwidth. The authors proposed the use of a lens feed system for feeding and scanning the array. A parallel-plate region with spacing of less than 0.5λ is employed. Monopole elements mounted 0.25λ in front of the ground plane were used to launch and extract energy from the lens. The system provided 128 beam positions with a -2dB beam crossover levels, 4-5 degrees -3dB beamwidths and -25dB sidelobe levels. Practical implementation of step scanning can be achieved due to step increments of one element per beam position.

A circular array of 1000 elements operating in the X-band was developed for the European AMSAR (Airborne Multifunction Solid-state active Array Radar) programme [30]. Each elements were linked to a dedicated transmit/receive (TX/RX) module which is capable of controlling amplitude and phase transmission within each channel. The produced beam is steerable over a 120^o scan angle. The radiation pattern shape can also be easily adapted to serve various radar missions.

3.6.4 Other applications

References [31] and [32] investigate the use of beam switching of circular antenna arrays intended for indoor wireless LAN terminals. In [33], Sibille et all propose the use of circular arrays of monopoles for beam steering based on electronic switching. Appreciable directivity gain is achieved, which allows implementation of angular diversity in communications systems. The authors also modeled a circular array of 6cm diameter on a large metallic ground plane, intended for operation at 5GHz [34]. Results shows that appreciable directivities achieved though the use of such array, although complications might arise in the practical implementation due to finite ground-plane effects, poor isolation on the switches needed for steering, as well as the complexity of the protocol between emitter and receiver. Experimental results [31] - [34] demonstrate the potential of reducing delay spread and Carrier-to-Interference (C/I) radio in an indoor channel.

Circular array beamforming can also be used in Multiple-Input Multiple-Output (MIMO) applications. Chakraborty [35] at the National Institute of Oceanography, Goa, India studies the use of coaxial circular array for underwater transducer application as an alternative to the usual shading methods. The use of beam patterns with suppressed sidelobe levels for this particular application is analysed at different operating wavelengths. Multiplicative array techniques produce improved beamwidths and suppressed sidelobe levels useful for

high-resolution bathymetry.

The development of an ultrasonic circular array for endoscopic application in medicine is discussed in [36]. A circular array of 100 strip elements and diameter 10mm is constructed for operations at 3.5-7.5 MHz. The paper discusses the manufacturing process of the array and shows preliminary ultrasonic pictures obtained from a simple phantom.

3.7 Discussion

The subject of circular antenna array radiation pattern synthesis is a promising area. Unlike their linear counterpart, circular arrays possess the ability to cover the entire 360^o plane of the array. However, due to the complexity of the analysis caused by their circular geometry, circular arrays have received limited attention in the wireless world. In this chapter, various methods of UCA pattern synthesis have been discussed in order to gain a better understanding of the UCA behaviour when subjected to these pattern synthesis methods.

It is revealed in Section (3.1.1) that in the case of monopole UCAs for beam co-phasal method, a maximum radius R_{max} of $\frac{N\lambda}{16}$ is needed in order to obtain beam patterns with decaying sidelobes. The beam co-phasal with optimum SNR method is found to perform best as it takes into account the amplitude variations in the element patterns. In the case of 16-element ideal directional UCA, the optimum SNR method improves the SLL by $\approx$ 22dB. However, this method may be costly as it would be necessary for each array element pattern to be known. Further, the method allows no mechanism for SLL and beamwidth control.

In Section 3.2, various array geometry variables such as the radius, number and type of elements for phase mode excitation technique is discussed. Bearing in mind that the aim of the studies in this thesis is to find an affordable solution, the author concludes that an optimum combination for the purpose would be:

- *8-element UCA* due to the added complexity in the Butler matrix implementation otherwise needed for larger number of elements.

- *Monopole elements* due to the added complexity and cost associated with directional elements as it is required that the active element patterns be known. Furthermore, the added distortion terms as described in Section 3.2.2 may degrade the performance of the UCA. This will be investigated further in the following chapter through the use of

practical arrays.

- *Radius* $R = R_{opt} = \frac{8\lambda}{16} = \frac{\lambda}{2}$

The chapter proceeds with discussions on the use of Dolph-Chebyshev [9] technique for UCA beamforming, allowing beamwidth and SLL control. The use of Butler matrix [1] for phase mode excitation is discussed in the preceding sections, revealing the need for terminating one of the output ports of the matrix and its effect on the beam patterns.

Studies presented in this chapter has provided a better understanding of the UCA behaviour through the use of ideal arrays. While the findings in this chapter present the evidence of complexities involved in UCA pattern synthesis, the chapter also shows the potential of UCA pattern synthesis, which is the basis of the work presented in this thesis. The findings in this chapter are explored further in Chapter 4 when measured data is applied.

It should be noted that unlike the objective of the work presented in this thesis, the UCA-Butler matrix systems that have been used in the past, such as those described in section 3.6.3 (References [28] - [29]), have not been based on low-complexity requirements. Both arrays proposed in the publications are of large sizes (larger than 8 elements), hence would be more costly than a smaller array. Furthermore, a large number of array elements also incurs a large physical dimension. Although complexity is suppressed by only selecting a sector of the array, the electronic scanning system presented in [28] requires an additional switching network in order to select the appropriate sector of the array. The system described in [29], involving a 32-element UCA, requires a 32×32 Butler matrix, which is complex in itself, but would be even more complex at operating frequencies of Wi-Fi applications as error margins are significantly lower compared to those at 900MHz.

References

[1] J. Butler, R. Lowe, "Beam-Forming matrix simplifies design of electronically scanned antennas", *Electronic Design*, pp.170-173, April 1961.

[2] D.E.N. Davies, "Circular Arrays", in Rudge et all. [37]

[3] C.P. Mathews, M.D. Zoltowski, "Eigen-structure techniques for 2-D angle of arrival with uniform circular arrays", *IEEE Transactions on Signal Processing*, Vol.42, pp2395-2407, September 1994.

[4] G. Skahill, W.D. White, "A new technique for feeding a cylindrical array", *IEEE Transactions of Antennas and Propagation*, Vol. 23, Issue 2, pp253-256, March 1975.

[5] J.A. Fessler, A.O. Hero, "Space-alternating generalized expectation-maximization algorithm", *IEEE Transactions on Signal Processing*, Vol. 42, Issue 10, pp.2664-2677, October 1994.

[6] C.M.Tan, M.Landmann, A.Richter, L.J.Pesik, M.A.Beach, Ch.Schneider, R.S.Thoma, A.R.Nix, "On the application of circular arrays in direction finding Part II: Experimental evaluation on SAGE with different circular arrays", COST 273, May 2002.

[7] B.K. Lau, Y.H. Leung, "A Dolph-Chebyshev approach to the synthesis of array patterns for uniform circular arrays", *The 2000 IEEE International Symposium on Circuits and Systems (ISCAS) Proceedings*, Vol. 1, pp.124-127, May 2000.

[8] G.T.Freitas de Abreu, R. Kohno, "A Modified Dolph-Chebyshev Approach for the Synthesis of Low Sidelobe Beampatterns with Adjustable Beamwidth", *IEEE Transactions on Antennas and Propagation*, Vol.51, No.10, October 2003.

[9] C.L.Dolph, "A current distribution for broadside arrays which optimizes the relationship between beam width and side-lobe level", *Proc. of the I.R.E. and Waves and Electrons*, Vol. 34, Issue 6, pp.335-348, June 1946.

[10] R. Brown, "The uniqueness of the Butler matrix as a commutating switch", *IEEE Transactions of Antennas and Propagation*, Vol. 19, Issue 5, pp694-695, September 1971.

[11] S.J. Foti, T. Macnamara, "Design of wideband Butler matrices using Schiffman lines", *IEE Colloquium on Multiple Beam Antennas and Beamformers*, pp5/1 - 5/8, November 1989.

[12] H.D. Griffiths, J.W.R. Griffiths, C.F.N. Cowan, R. Eiges, T. Rafik, "Processing techniques for circular sonar arrays", *Sixth International Conference on Electronic Engineering in Oceanography*, pp67-72, July 1994.

[13] B. Sheleg, "A matrix fed circular array for continuous scanning", *IEEE Proceedings*, Issue 56, pp2016-2027, November 1968.

[14] M. Wax, "Direction Finding of Coherent Signals via Spatial Smoothing for Uniform Circular Arrays", *IEEE Transactions on Antennas and Propagation*, Vol. 42, no. 5, pp613-620, May 1994.

[15] B. Sheleg, "Butler submatrix feed systems for antenna arrays", *IEEE Transactions on Antennas and Propagation*, Vol.21, Issue 2, pp228-229, March 1973.

[16] J. Shelton, K. Kelleher, "Multiple beams from linear arrays", *IEEE Transactions on Antennas and Propagation*, Vol. 9, Issue 2, pp.154-161, March 1961.

[17] D.E.N. Davies, M.S.A.S. Rizk, "A broadband experimental null-steering antenna system for mobile communication", *Radio Electronic Engineering*, Vol. 48, pp511-517, October 1978.

[18] D.E.N. Davies, M.S.A.S. Rizk, "Electronic steering of multiple-nulls for circular arrays", *Electronic Letters*, Vol. 13, pp669-670, October 1977.

[19] J.C. Lim, "Introduction of a sharp steerable null response in an otherwise omnidirectional pattern using a circular array", *Radio Electronic Engineering*, Vol.47, pp30-32, January/February 1977.

[20] D.E.N . Davies, J.R.F. Guy, "A UHF communication antenna employing open-loop control null steering", *Antennas and Propagation Society International Symposium*, Vol.19, pp276-279, June 1981.

[21] H.D. Griffiths, R. Eiges, "Sectoral phase modes from circular antenna arrays", *Electronic Letters*, Vol. 28, Issue 17, pp1581-1582, August 1992.

[22] H.D. Griffiths, "The use of circular arrays for direction finding applications", *IEE Colloquium on Passive Direction Finding*, pp7/1-7/4, January 1989.

[23] C.P. Mathews, M.D. Zoltowski, "Direction finding with circular arrays via phase mode excitation and Root-MUSIC", *Antennas and Propagation Society International Symposium*, Vol.2, pp1019-1022, July 1992.

[24] M. Zeytinoglu, J. Litva, J. Qian, "High-resolution direction finding using circular arrays", *International Conference on Acoustics, Speech, and Signal Processing*, Vol.5, pp3341-3344, April 1991.

[25] M. Cvetkovic, "A four element circular array direction finding and null steering system", *Sixth International Conference of Antennas and Propagation*, Vol.1, pp168-172, April 1989.

[26] J. Ramos, C.P. Mathews, M.D. Zoltowski, "FCA-ESPRIT: a closed-form 2-D angle estimation algorithm for filled circular arrays with arbitrary sampling lattices", *IEEE Transactions on Signal Processing*, Vol. 47, Issue 1, pp213-217, January 1999.

[27] C.P. Mathews, M.D. Zoltowski, "Eigen-structure Techniques for 2D Angle of Arrival with Uniform Circular Arrays," *IEEE Transaction on Signal Processing*, Vol. 42, pp.2395-2407, September 1994.

[28] G. Skahill, W. White, "A new technique for feeding a cylindrical array", *IEEE Transactions on Antennas and Propagation*, Vol.23, Issue 2, pp253-256, March 1975.

[29] J. Boyns, C. Gorham, A. Munger, J. Provencher, J. Reindel, B. Small, "Step-scanned circular-array antenna", *IEEE Transactions on Antennas and Propagation*, Vol. 18, Issue 5, pp590-595, September 1970.

[30] M. Uhlmann, J.S. Tanner, G. Albarel, "Design characteristics of the AMSAR airborne phased array antenna", *IEE Colloquium On Electronic Beam Steering*, pp 3/1 - 3/5, October 1998.

[31] A. Chelouah, A. Sibille, P. Rosson, J.P. Couvy, "Angular diversity based on beam switching of circular arrays for HIPERLAN terminals", *Electronic Letters*, Vol. 36, Issue 5, pp387-388, March 2000.

[32] L.J. Pesik, M.A. Beach, D.P. McNamara, P.N. Fletcher, "Performance analysis of smart antenna systems for indoor wireless LANs", *Third International Conference on 3G Mobile Communication Technologies*, No. 489, pp418-422, May 2002.

[33] A. Sibille, C. Roblin, G. Poncelet, "Circular switched monopole arrays for beam steering wireless communications", *Electronic Letters*, Vol. 33, Issue 7, pp551 - 552, March 1997.

[34] A. Sibille, C. Roblin, G. Poncelet, "Beam steering circular monopole arrays for wireless applications", *Tenth International Conference of Antennas and Propagation*, Vol.1, pp358-361, April 1997.

[35] B. Chakraborty, "Coaxial circular array: studies related to sidelobe suppressed beam patterns for underwater transducer application", *Proceedings of the IEEE*, Vol.76, Issue 10, pp1374-1376, October 1988.

[36] H.-P. Schwarz, H.-J. Welsch, P. Becker, M. Biebinger, R.M. Schmitt, "Development of a new ultrasonic circular array for endoscopic application in media and NDT", *IEEE Proceedings on Ultrasonics Symposium*, pp687-690, October 1989.

[37] A.W.Rudge, K. Milne, A.D. Olver, and P. Knighet, Eds., "The Handbook of Antenna Design", vol. 1 and 2, Peter Peregrinus Ltd, London, UK, 1986.

Chapter 4

UCA Evaluation by Simulation and Measurements

The review and analysis presented in the previous chapter have been based on ideal antenna elements, in an ideal environment. In reality, the manufacturing process as well as the environment in which the array operates introduces imperfections leading to deviation in performance from the ideal scenario. This chapter presents some experimental results obtained by applying the UCA excitation methods described in the previous chapter to measured active element far-field radiation patterns of practical antenna arrays. The use of directional elements in a UCA is re-evaluated using measured data to investigate the array performance despite the added complexity caused by the presence of higher order distortions in the phase mode patterns as discussed in Section 3.2.2. Several practical arrays are employed in this investigation, ranging from a simple monopole array to a state of the art circular patch array. Further, a monopole UCA model is constructed by means of FDTD method in order to provide an additional comparison for the analysis. The performance of the practical arrays as well as the FDTD model is investigated and compared with the ideal scenario in terms of the achieved beamwidth and sidelobe level (SLL).

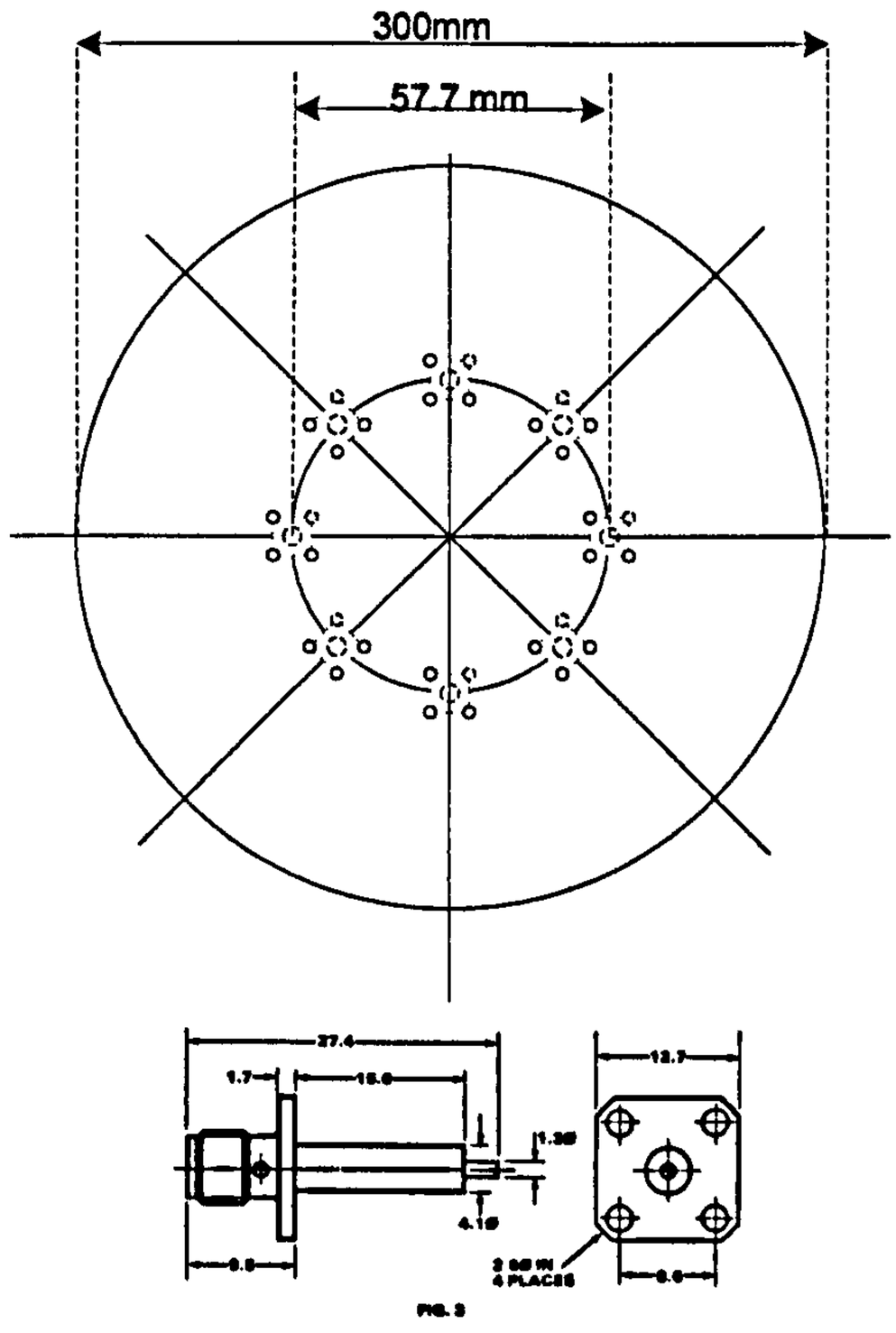

Figure 4.1: *The 8-element monopole array*

4.1 The Initial Test Arrays

An eight-monopole UCA is constructed using eight stub-contact SMA connectors mounted on a circular ground plane. The array elements are optimised for 5.2GHz operation and the radius chosen as $R = R_{opt}$. The optimum radius requirement is easily achieved using the monopole elements as oppose to patch antennas, in which case optimum radius proves impossible due to the much larger dimension of each element. Figure 4.1 illustrates the array. More detailed description of the construction and dimension of the monopole array is presented in Appendix D. The element radiation patterns are shown in Figure 4.3. The monopole array can be seen in Figure 4.2. The deployment of such array would be such that the antenna elements point vertically downwards, with the ground plane mounted to the ceiling.

In order to facilitate additional analysis to the experimental evaluations, an 8-element monopole UCA model was generated using the Finite Difference Time Domain (FDTD) method. Using this method, the element far-field radiation patterns are generated which incorporates the effects of inter-element interactions as well as the effects of ground plane edge reflections. Figure 4.4 illustrates the element radiation patterns generated by the FDTD model. Unlike

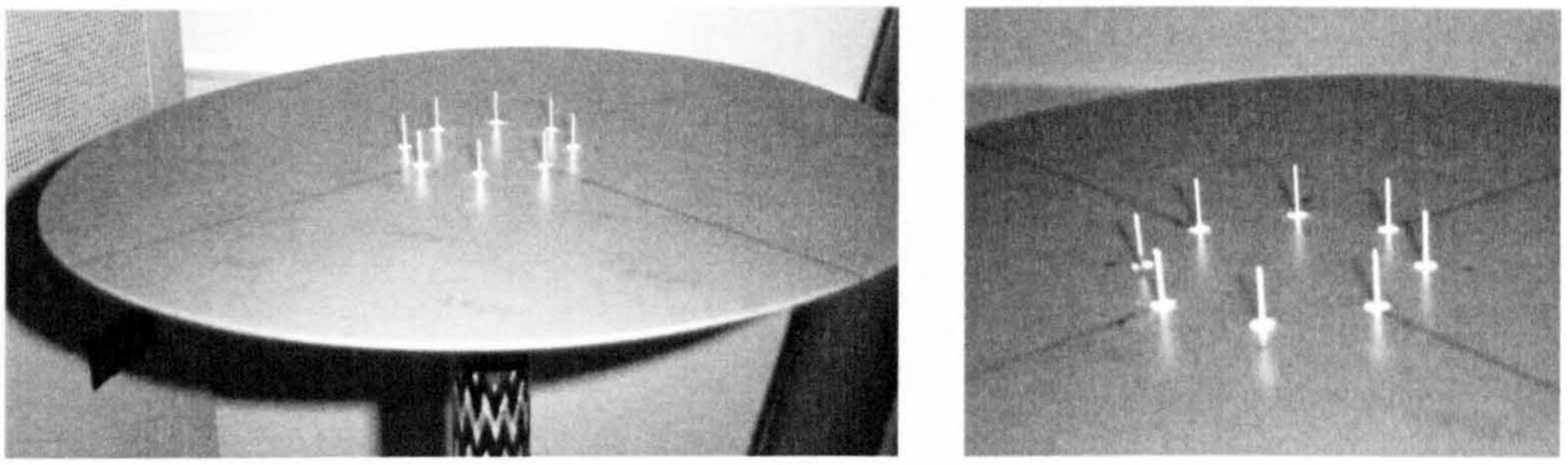

Figure 4.2: *The 8-element monopole array*

the radiation patterns produced by an ideal array produced purely by Matlab Mathematical modeling, the amplitude patterns of the FDTD model are non-uniform due to the inclusion of element interactions as well as ground plane effects. The main lobes in the individual element patterns reflect the positions of each elements in the array[1]. Further description of the FDTD modelling can be found in Appendix C.

The directional UCA used in the analysis presented in the first part of this section is a patch-elements UCA, built by Thales for the University of Bristol for the purposes of the indoor measurements presented in Appendix B. It consists of eight dual-polarised directional patch antenna elements, each of which is mounted at 45^o in order to generate $\pm 45^o$ polarisations at boresight. These elements are arranged on the sides of an octagonal metal ground plane. Each patch is optimised to operate at 5.2GHz centre frequency[2], with a 1dB bandwidth in excess of 120MHz. The array configuration is shown in Figure 4.5. The array elements are protected by a cyllindrical radome material not shown in the pictures for illustrative purposes. Figure 4.6 shows an example of one element pattern. The illustration shows an isolation of $\approx$ 12dB within the -3dB beamwidth between the two polarisations, and a $\approx$ 15dB front-to-back isolation.

The third array was built at the University of Bristol, consisting of eight dual-polarised patch elements mounted vertically on an octagonal metal ground plane, as shown in Figure 4.7. The vertical mounting on this array is chosen in order to eliminate the added complexity caused by a slanted mount given by the Thales array. Figure 4.8 illustrates the far-field radiation pattern of one of the array elements. It can be seen that an isolation of $\approx$ 17dB between the two polarisations exists within the -3dB range and there is a $\approx$ 28dB front-to-back isolation

[1]The slight difference between the null depth of the odd elements and even elements seen in the illustration is caused by the fact that the FDTD grids are rectangular as oppose to circular, thus introducing discrepancies in the near-to-far field transformation as the circular ground plane is seen as rectangular steps.

[2]This is the operating frequency of the IEEE 802.11(a) and Hiperlan/2.

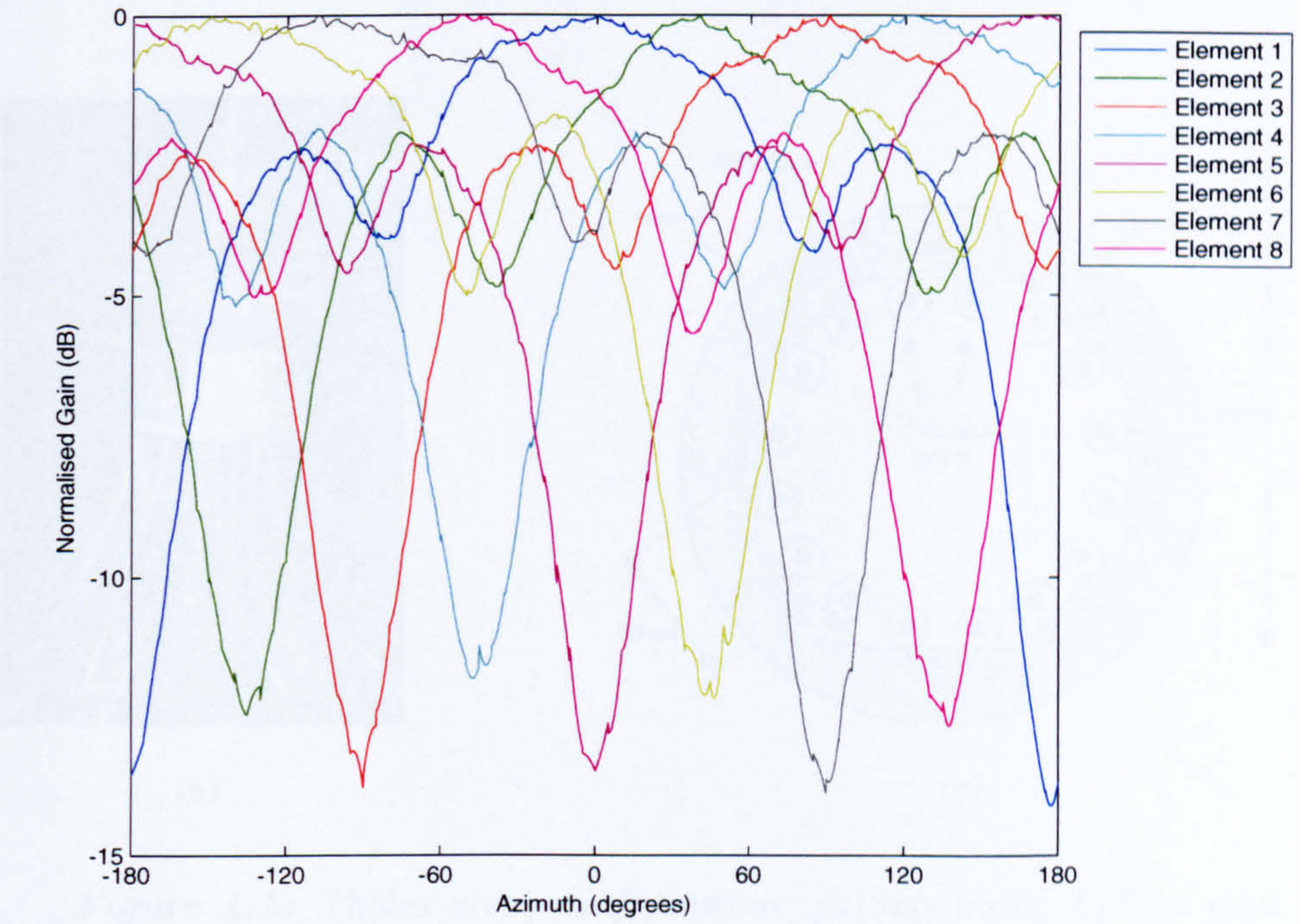

Figure 4.3: *Element far-field radiation patterns produced by the monopole UCA*

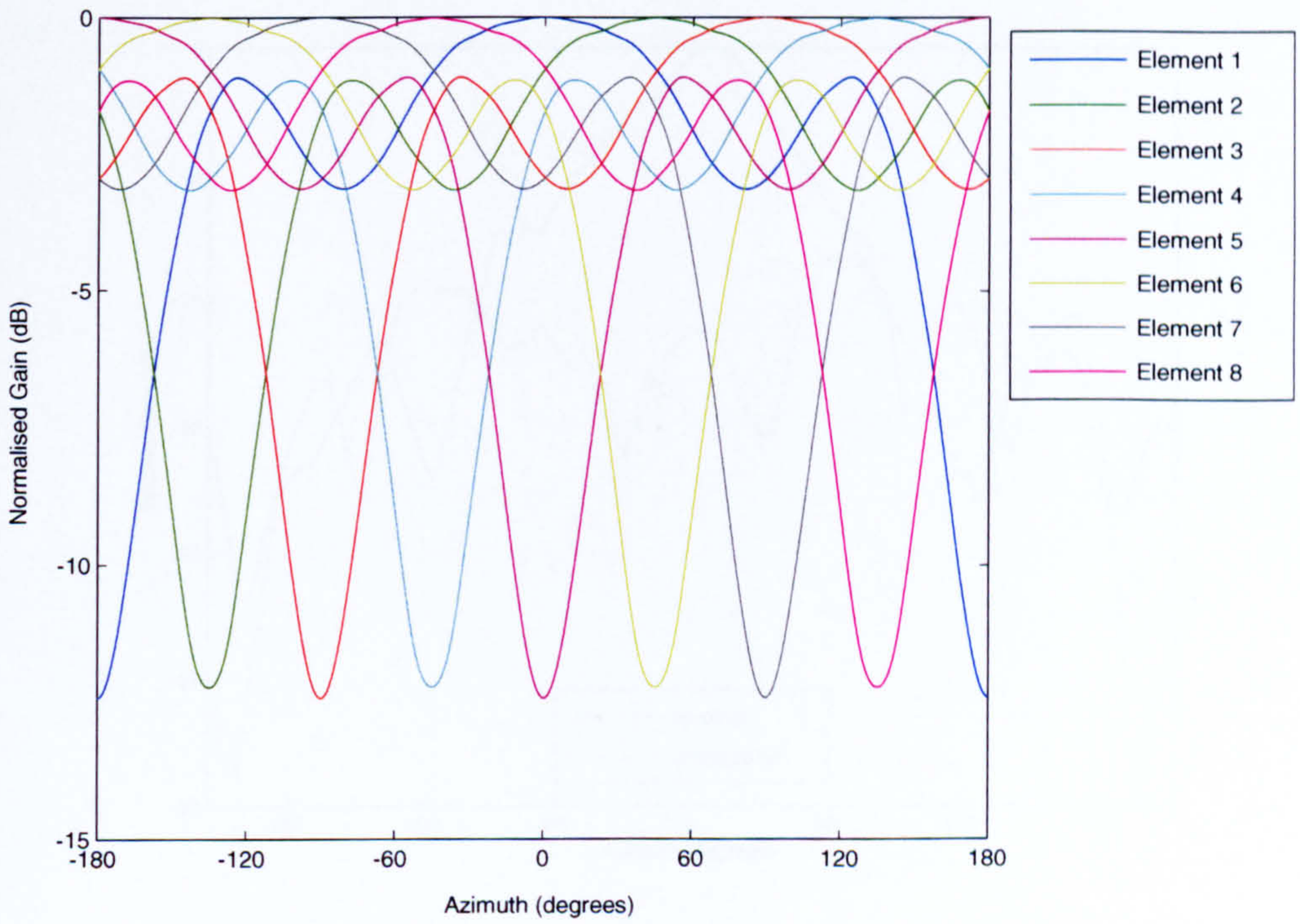

Figure 4.4: *Element far-field radiation patterns generated by FDTD method*

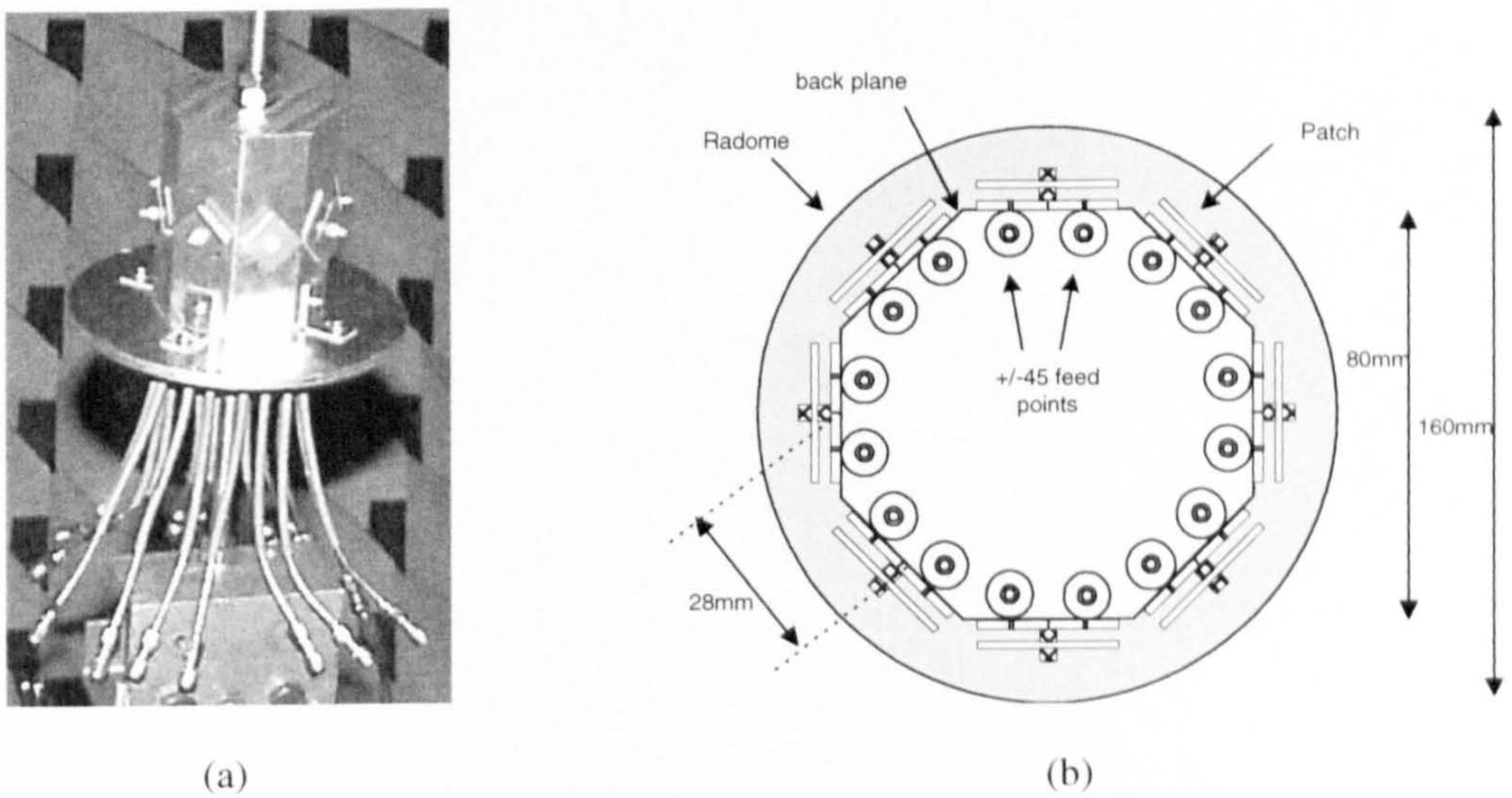

(a) (b)

Figure 4.5: *Thales array configuration: (a)Side view; (b)Plan view*

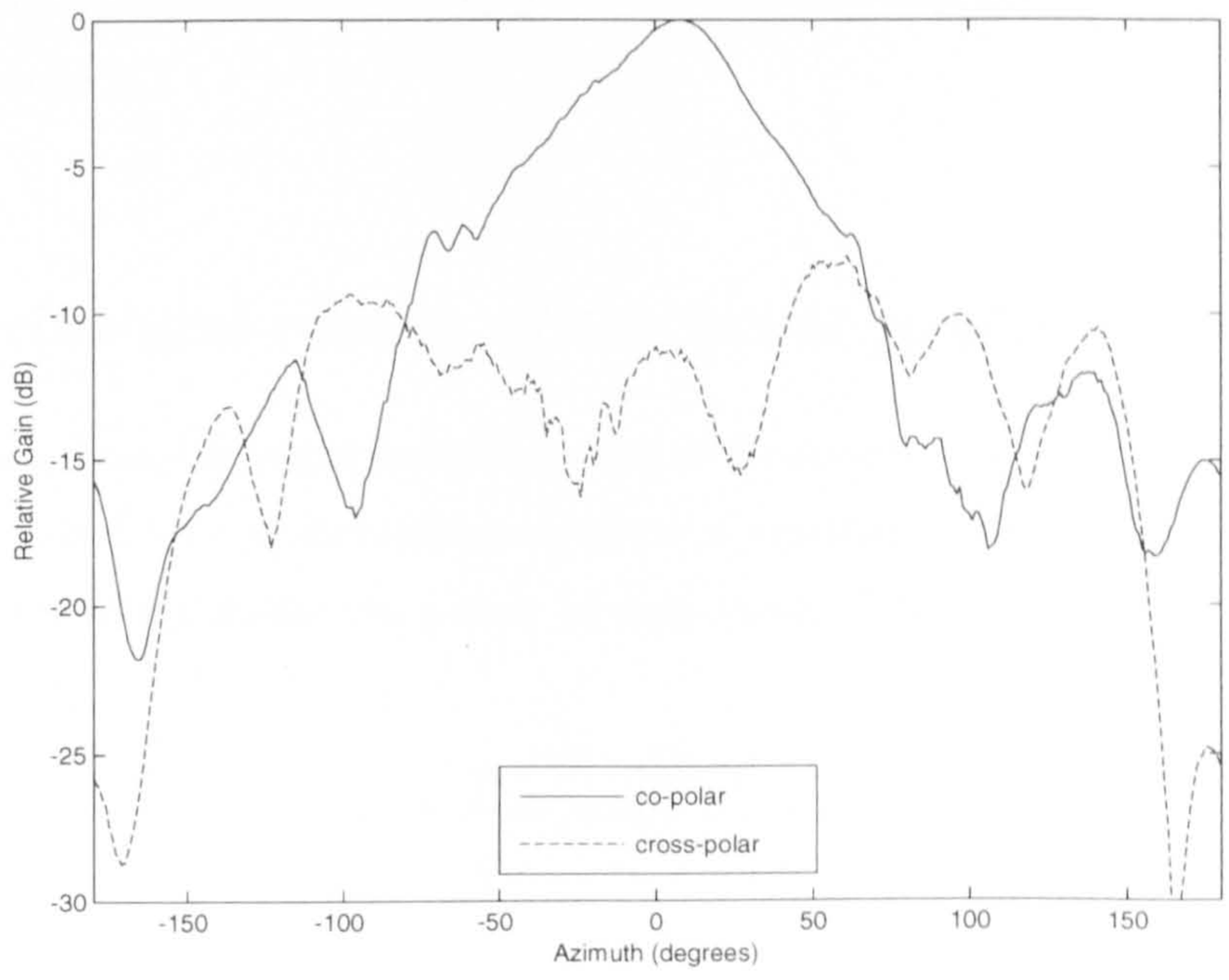

Figure 4.6: *Thales array: sample element pattern*

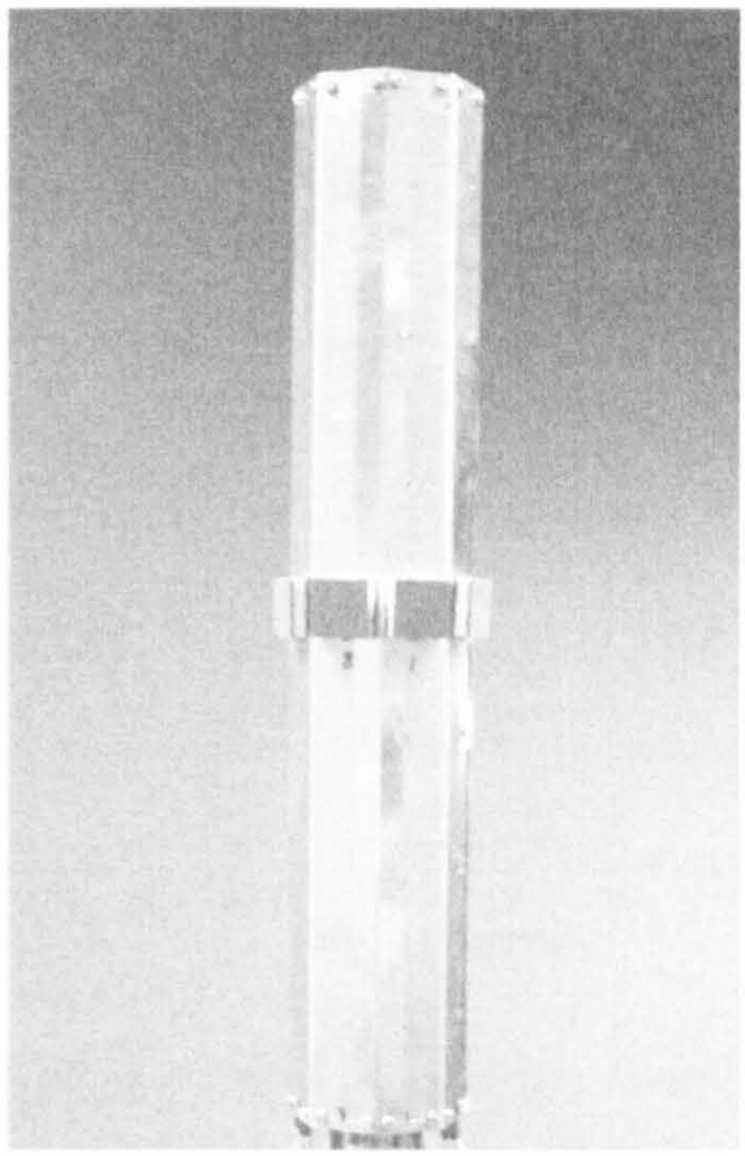

Figure 4.7: *8-element vertical patch array.*

in the E-field pattern.

Both the directional UCAs are built with $R = R_{max}$[3] or $\lambda/2$ adjacent elements spacing. Due to the dimensions of the patch elements it is impossible to build the array with $R = R_{opt}$ as suggested in Section 3.2.1.

4.2 Experimental results of the beam co-phasal method

This section elaborates the experimental results of the beam co-phasal excitation technique presented in section 3.1.1. A normalisation factor is employed in addition to equations (3.5) and (3.7), in order to normalise the power of each beam. These become:

$$\omega_n = \frac{e^{-jkR\ cos(\phi_0 - \varphi_n)}}{\sqrt{\sum_{n=1}^{N} |I_n(\phi_0)|^2}} \tag{4.1}$$

and

$$\omega_n = \frac{|E_n(\varphi_0)|\, e^{-jkR\ cos(\phi_0 - \varphi_n)}}{\sqrt{\sum_{n=1}^{N} |I_n(\phi_0)|^2}} \tag{4.2}$$

[3]See Section 3.2.1

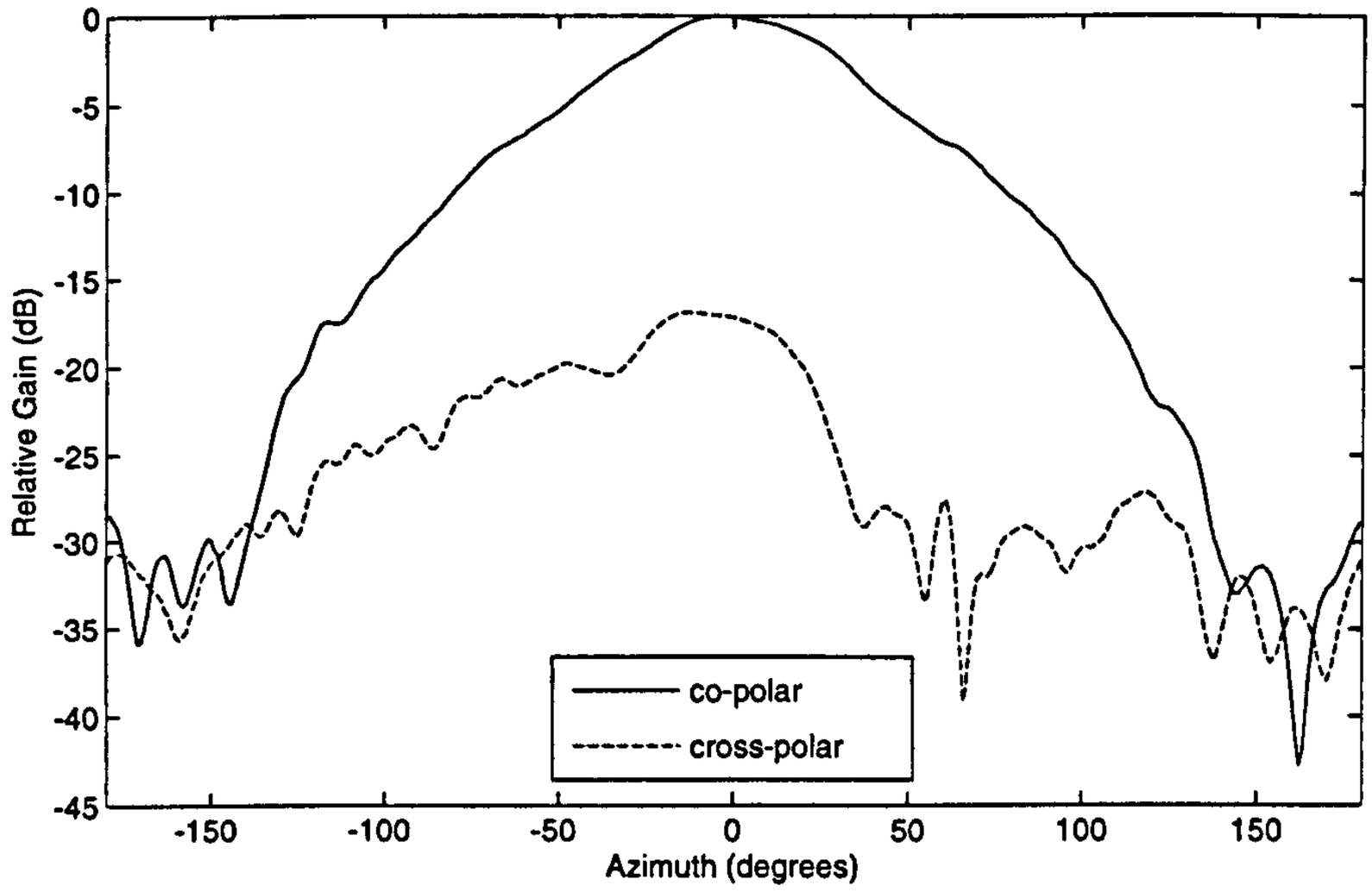

Figure 4.8: 8-element vertical patch array sample element pattern.

Due to limitations in practical construction, measurement tolerances[4], mutual coupling and other array imperfections, distortions may appear in the individual element amplitude and phase patterns[5]. Since the complex far-field radiation patterns are known, this problem can be overcome by applying conjugate element weights such that

$$w_n(\phi_0) = \frac{I_n(\phi_0)^*}{\sqrt{\sum_{n=1}^{N} |I_n(\phi_0)|^2}} \tag{4.3}$$

where (*) indicates complex conjugate.

In Figure 4.9, the performance of the ideal, FDTD-generated, and practical monopole UCAs are compared when the ideal phase weights and conjugate weights are applied. It can be seen that, while the ideal case remains unchanged when conjugate weights are employed, in the case of the real and FDTD-generated arrays, a $\approx 2dB$ improvement is seen. The arrays produce SLLs of $\approx -10dB$ while the ideal phase weights produce SLLs of $\approx -8dB$. While the -3dB beamwidth of the ideal UCA remains the same for both ideal phase excitation and conjugate weights excitation, there is a 2-3dB reduction in beamwidth in the case of the practical and FDTD model of monopole UCAs when conjugate weights are used. Note that

[4]Possible error sources associated to the array measurements are presented in Appendix A

[5]The issue of practical construction tolerances as well as other array imperfections are discussed further in Chapter 5.

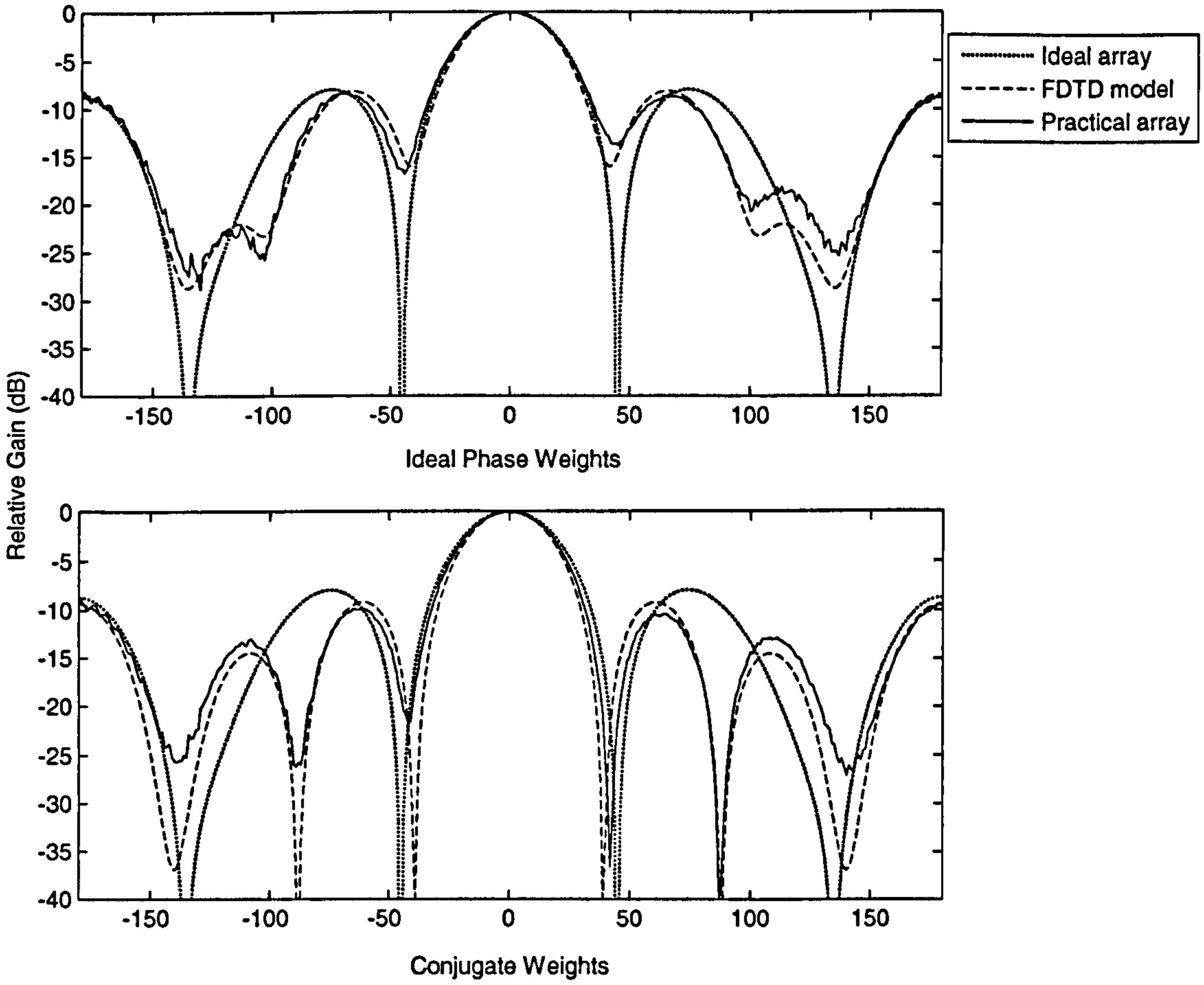

Figure 4.9: *Beam patterns obtained through the application of ideal phase weights and conjugate weights on 8-element ideal omni-directional, FDTD model, and practical monopole UCA.*

the beamwidth as well as first SLL level reductions occur at the cost of 5-7dB increase in the second SLL levels. Furthermore, it should be noted that the nulls seen in the FDTD model and the practical array are not as deep compared to those of the ideal array. This is the case for both ideal phase as well as conjugate weight systems.

It should also be noted that, despite the ideal array having tapered sidelobe patterns as described in Section 3.1.1, it can be seen that the practical and FDTD-generated arrays do not demonstrate the same behaviour. Figure 4.10 illustrates eight beam patterns produced by the monopole test UCA, using the two weighting methods. The beam peaks are specified at -180^o, -135^o, -90^o, -45^o, 0^o, 45^o, 90^o and 135^o. It is evident that the conjugate weights produce much deeper nulls, however it is only capable of suppressing the sidelobe level (SLL) to $\approx -10dB$, which is a 2dB improvement from the results obtained by the Beam Cophasal method, which produces $\approx -8dB$ SLL.

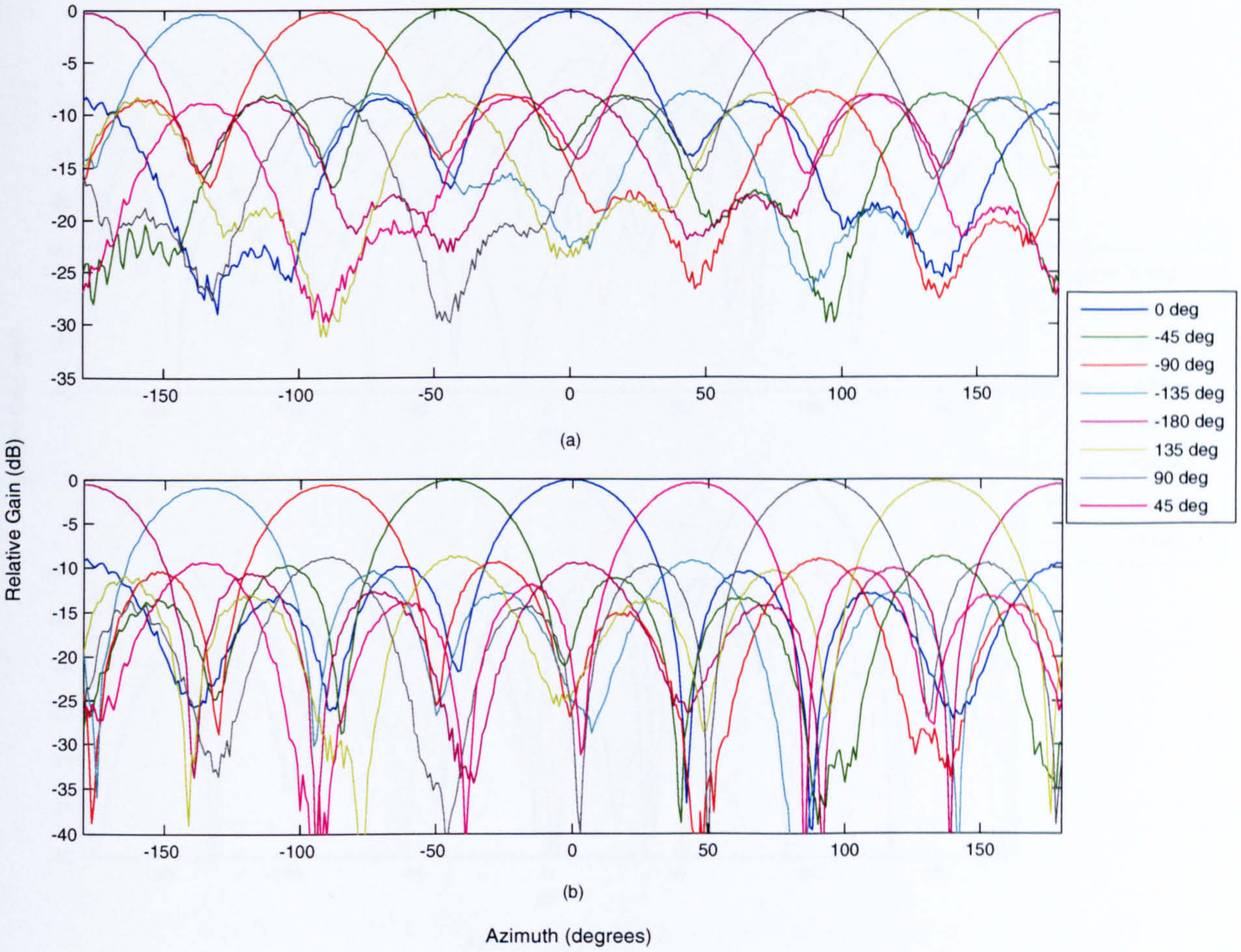

Figure 4.10: *Beam patterns obtained through the application of (a) ideal phase weights (b) conjugate weights on 8-element experimental monopole array.*

In Figure 4.11, eight main beams are formed and steered towards the directions -180^o, -135^o, -90^o, -45^o, 0^o, 45^o, 90^o and 135^o using ideal and conjugate weights on the Thales patch-element UCA. As can be observed in Figure 4.11(a), the beamwidths are non-uniform and sidelobe levels rise to -5dB.

Figure 4.11(b) shows that the resulting beam patterns are more uniform in terms of beamwidths as well as cusping loss when conjugate weights are utilised. The sidelobe levels are reduced to $\approx -12dB$. This method is able to provide front-to-back isolations of up to 30dB. However, it is evident that the use of directional elements does not aid in suppressing the SLL further than that of the monopole UCA. It is also clear that the conjugate weights yield better performance. Appendix B describes a performance analysis on the application of conjugate

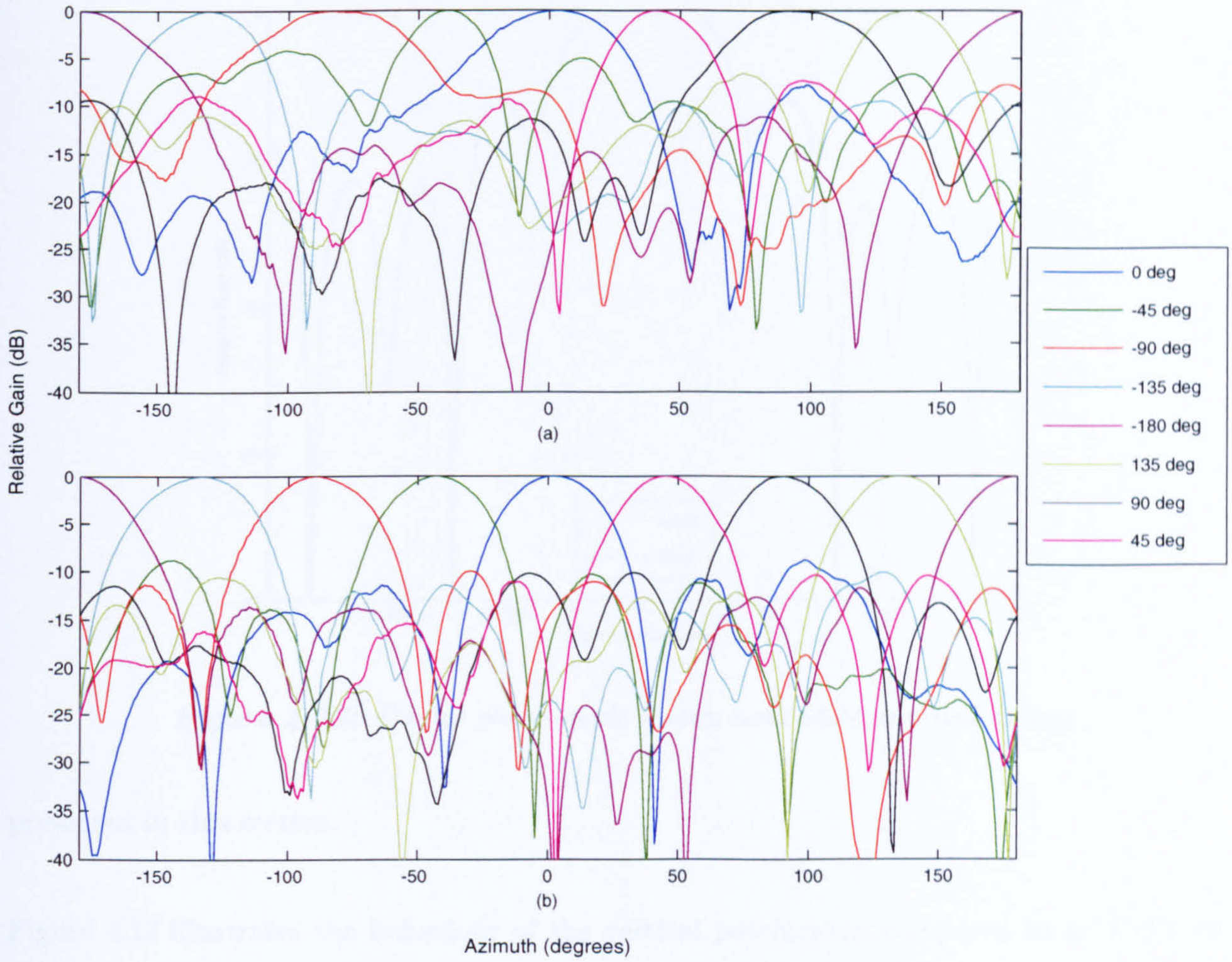

Figure 4.11: *Beam patterns obtained through the application of amplitude and (a) ideal phase weights (b) conjugate weights on 8-element experimental patch array.*

weights on the Thales array within an indoor office environment[6]. However, it should be noted that it is impossible to control sidelobe level and beamwidth by using this method of beamforming. The conjugate method also requires that each element pattern be known in order to find the correct excitation functions. This process can be costly and therefore undesirable.

4.3 Experimental results of the phase-mode excitation method

Having analysed the behaviour of a real array employing the simplest method of beamforming, the performance of phase-mode excitation theory [2] is evaluated with the use of real arrays. The vertical patch, FDTD-generated and monopole UCAs are used in the analysis

[6]Due to the performance, the conjugate weights are used in further analysis presented Appendix B.

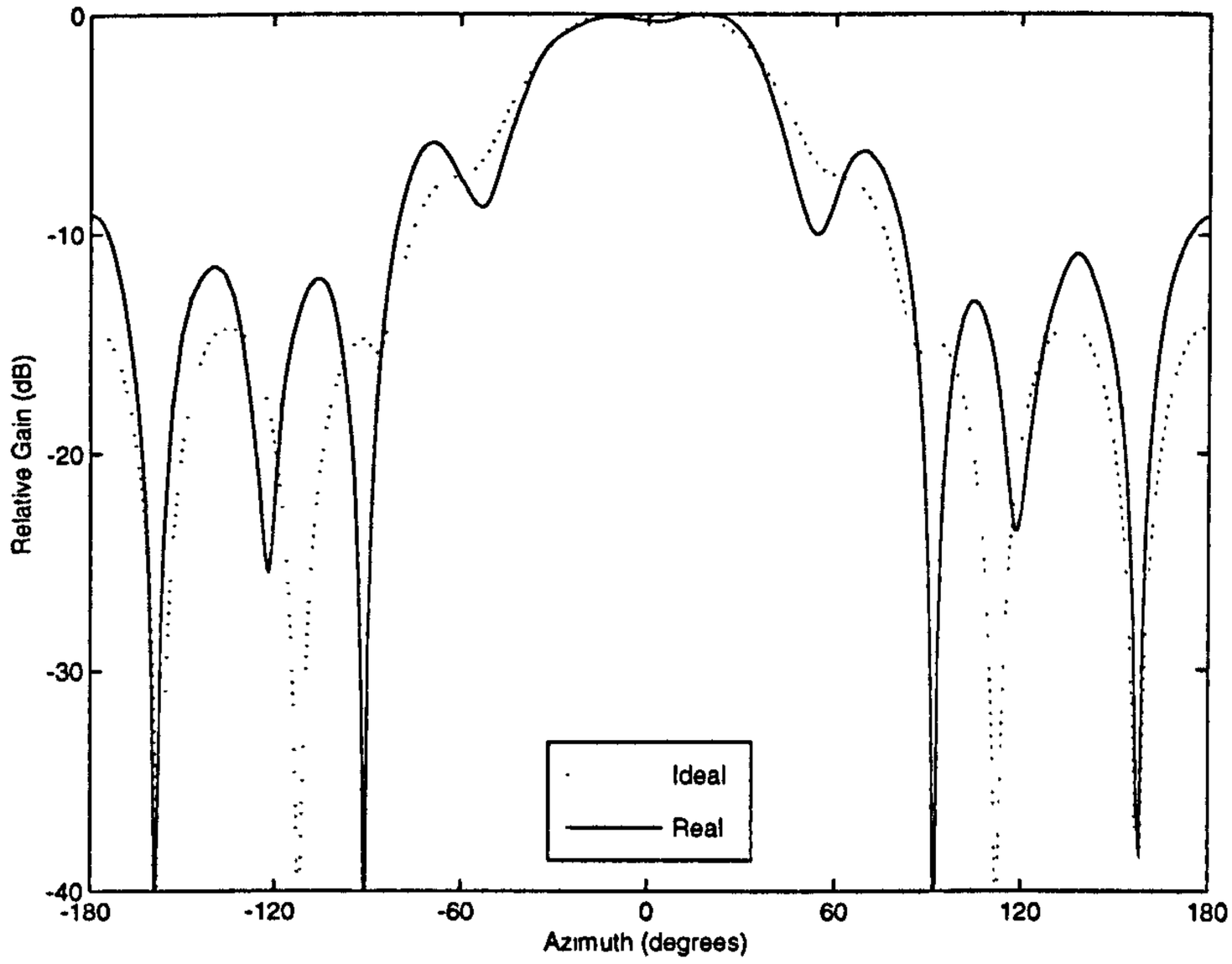

Figure 4.12: *Davies phase-mode theory with ideal and real arrays*

presented in this section.

Figure 4.12 illustrates the behaviour of the vertical patch array compared to an 8-element ideal UCA with positive cosine elements, both employing Davies' [2] phase-mode excitation method. The figure shows similar behaviours from both arrays, however the real array shows effects of element interactions in the added peaks and troughs as well as the rise in the front-to-back ratio. Figure 4.13 illustrates the performance of the vertical patch array when Chebyshev weights are added to Davies' method. It can be seen that the resultant pattern is approximately 5dB above the specified levels. The sidelobe levels continue to decrease as the specified SLL is decreased up to a specified level of -25dB, which yields an actual pattern with approximately -15dB SLL. Beyond this level, the pattern fails to produce any lower SLL. It can also be seen that the -3dB beamwidth remain at $\approx 80^o$ when the SLL requirement is lowered. It should be noted that the array patterns possess *flat* magnitude within $\pm 30^o$ of the steering angle. In practical applications, this presents a limitation to the ability of the system to locate the mobile user accurately.

As discussed earlier in Section 3.2.2, the use of directional elements introduces distortion to the phase mode sampling. This is due to the fact that where the element is facing away from the required beam position, contribution of that element is lost due to the front-to-back isolation of the element pattern. Furthermore, it is also apparent from (3.14) - (3.16) that finding the correct excitation function for directional UCAs is more complicated since the

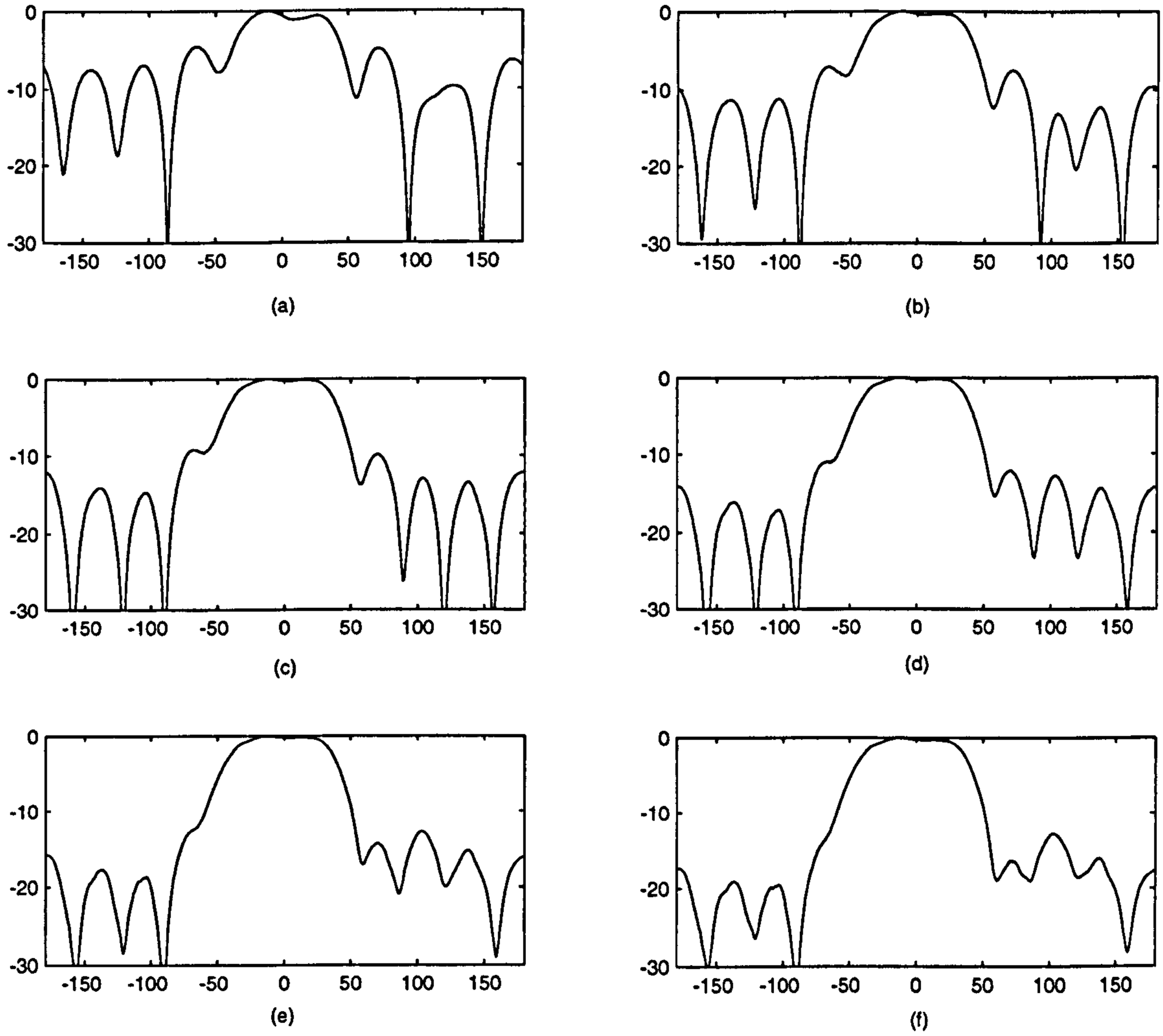

Figure 4.13: *Vertical patch array with Chebyshev weights: (a)-10dB; (b)-15dB; (c)-20dB; (d)-25dB; (e)-30dB; (f)-35dB.*

individual element patterns have to be known.

Figure 4.14 illustrates the application of phase-mode excitation method on ideal, real and FDTD-generated monopole arrays. As can be seen in Figure 4.15, when Chebyshev weights are applied to the real monopole array, the SLL decreases only up to approximately -12dB as the SLL requirement is lowered. Beyond this point, decreasing the SLL requirement results in widening of the beamwidth and decreased null depths. It should also be noted that the FDTD array behaves similarly to the real array, indicating a reliable model. Figure 4.16 also illustrates the fact that the beam pattern holds its shape when rotated to any angle in the Azimuth plane.

The limited performance of the practical and FDTD-generated arrays compared to that of

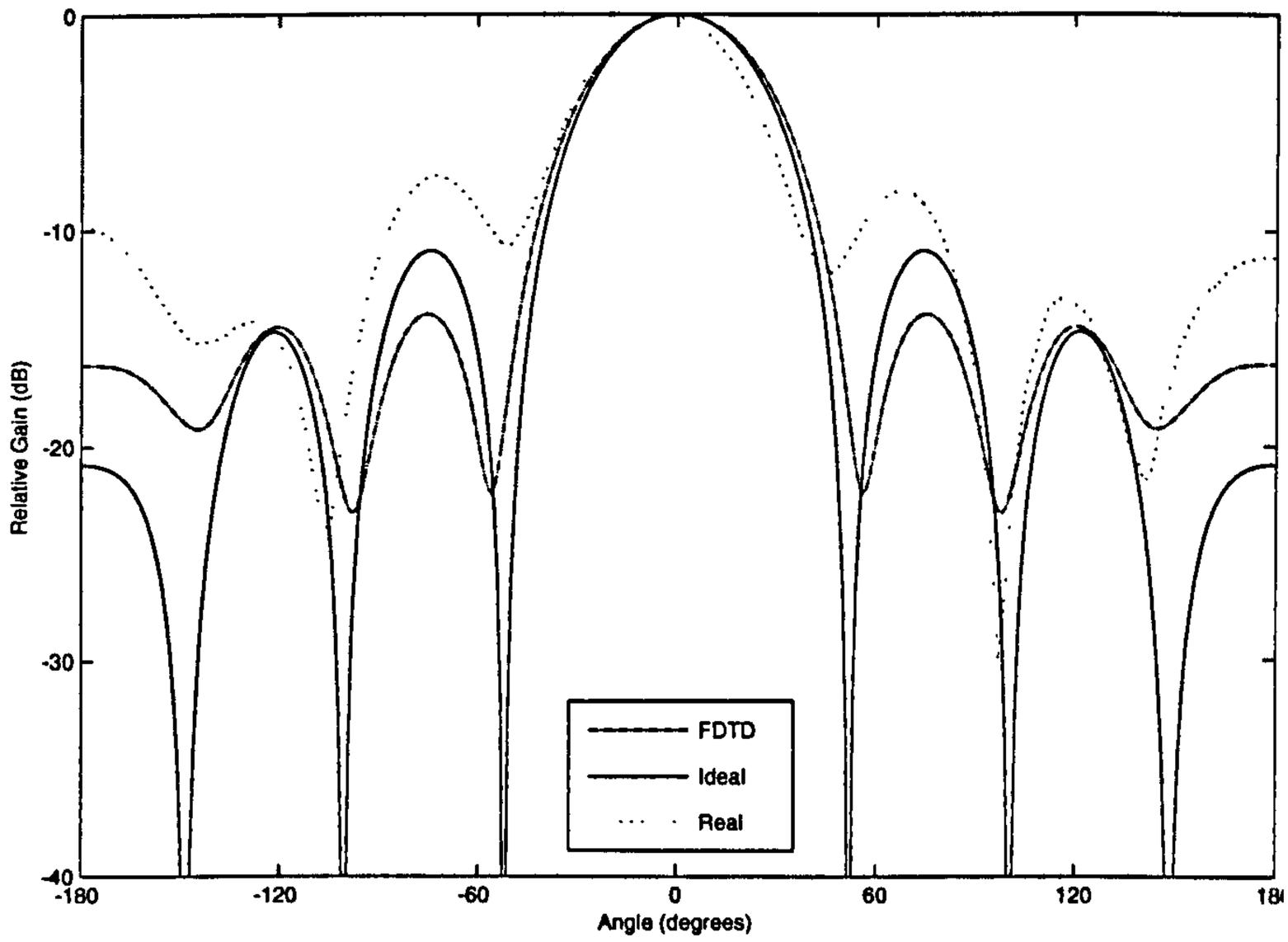

Figure 4.14: *Phase-mode excitation on UCAs with omni-directional elements*

an ideal array is caused by the fact that Davies' [2] theory for monopole arrays assumes that the element radiation patterns are uniform and perfectly identical to each other. However, in real life scenario, element interactions and other array imperfections make it impossible for this to be true.

Although the monopole array performs 2dB worse in terms of the maximum achievable SLL compared to the vertical patch array, the added complexity involved with the use of directional elements should be taken into consideration when choosing the type of elements to be used for such a system.

4.4 Discussion

In this chapter, the UCA pattern synthesis techniques presented in the previous chapter are put to the test. The Beam Cophasal and Phase-Mode excitation methods are applied to a number of experimental arrays in order to observe their performances in a practical environment. Two practical 8-element directional patch UCAs as well as 8-element practical and FDTD-generated monopole UCAs are utilised in the experimental evaluations. Due to their physical dimensions, it is impossible to construct the patch arrays with radius smaller than $R = R_{max}$.

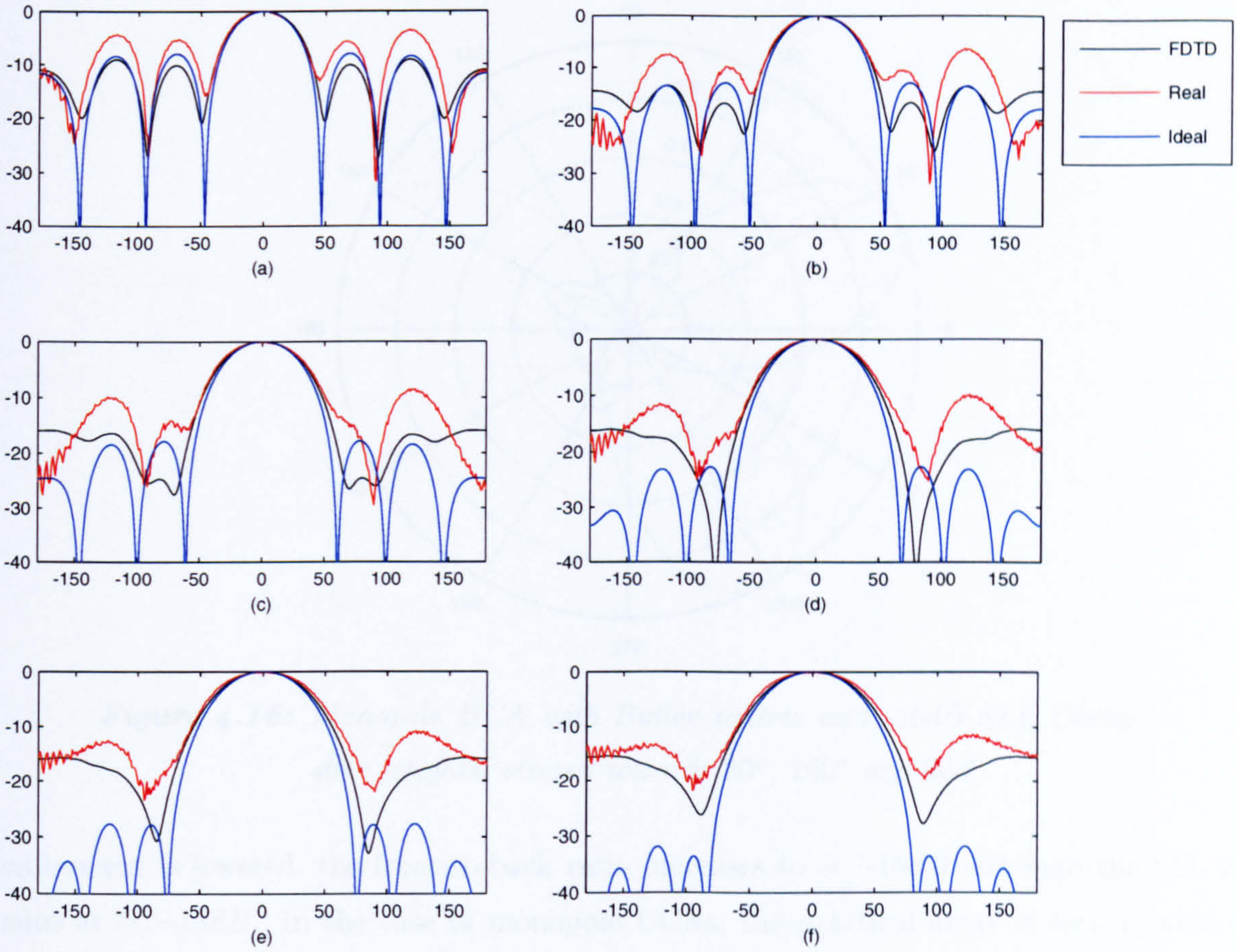

Figure 4.15: *Omnidirectional FDTD, real and ideal arrays with Chebyshev weights: (a)-10dB; (b)-15dB; (c)-20dB; (d)-25dB; (e)-30dB; (f)-35dB.*

In the first part of the chapter, it is shown that both the practical monopole UCA and the FDTD model produce the same level of SLL compared to the ideal case when subjected to ideal phase weights. When conjugate weights are employed, an improvement of $\approx 2dB$ is seen in both the practical and FDTD-generated UCAs. When directional elements are employed, the use of conjugate weights causes the beam patterns to take a similar shape and width. An improvement in the magnitude of 7dB is also seen compared to the case when ideal phase weights are used. Further, a front-to-back isolation level of up to $\approx 30dB$ is achieved through the application of conjugate weights.

Further on in the chapter, Phase-Mode excitation method is applied to the practical arrays as well as the FDTD model. The system is subjected to additional Chebyshev weighting function and the result is analysed in terms of the achievable SLL. It is shown that the directional patch UCA is capable of producing SLL of up to $\approx -15dB$. As the Chebyshev

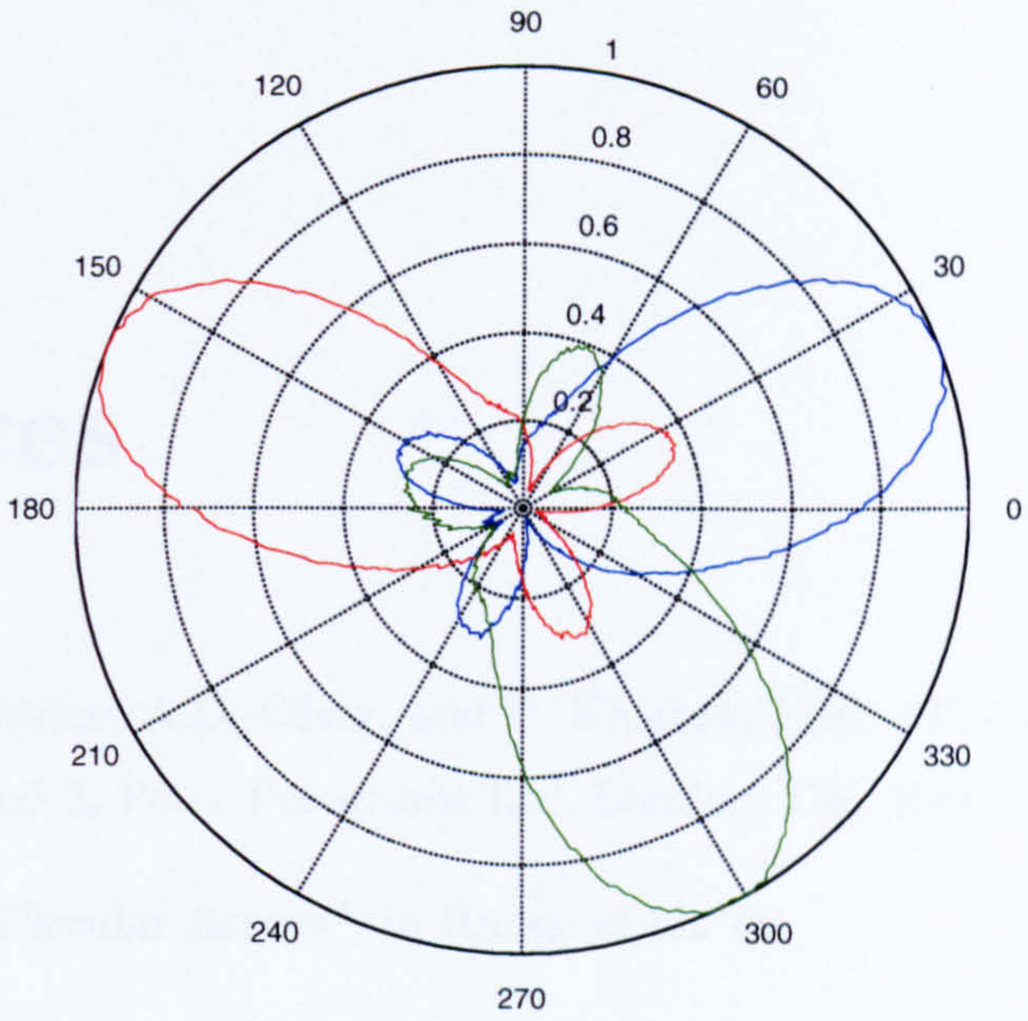

Figure 4.16: *Monopole UCA with Butler matrix and -20dB SLL Chebyshev weights, steered towards* 20^o, 160^o *and* 300^o.

requirement is lowered, the front-to-back ratio increases to $\approx -18dB$ although the SLL remains at $\approx -15dB$. In the case of monopole UCAs, the practical array is seen to able to produce a limited SLL of $\approx -12dB$ and a front-to-back ratio of up to $\approx -22dB$.

The limited performance of the practical arrays compared to the ideal case, particularly in the Phase-Mode applications, is caused by the fact that Davies' [2] theory assumes the perfect scenario where the element radiation patterns are perfectly identical to each other. In real life scenarios, this is never the case. Element interactions and scattering effects also play an important role in the shape of element radiation patterns in the practical case, which is also not included in Davies' theory.

The following chapter presents a discussion on element interactions and other array imperfections associated with practical arrays. A method for including these effects in the array pattern synthesis is revealed and error analysis presented.

References

[1] A.W.Rudge, K. Milne, A.D. Olver, and P. Knighet, Eds., "The Handbook of Antenna Design", vol. 1 and 2, Peter Peregrinus Ltd, London, UK, 1986.

[2] D.E.N. Davies, "Circular Arrays", in Rudge et all. R1

Chapter 5

Compensation for Element Interactions and Array Imperfections

In the previous chapter, only ideal uniform circular arrays have been considered. The effects of interactions between the antenna elements have been ignored. Uniform circular array theory suggests that for the case of these arrays there is no need for coupling compensation since the mutual coupling between the elements cancel each other out due to the nature of the array geometry. In practice, however, some degree of mutual coupling exists due to the fact that a practical array is often not perfectly symmetrical. Further, the active element radiation patterns are generally not identical. These imperfections affect the radiation patterns and therefore cannot be ignored.

In addition to mutual coupling, the element patterns of a practical array is also affected by *scattering effects* as well as other imperfections such as manufacturing tolerance and losses. These in turn yield results that deviate from the ideal scenario. Although the array elements are intended to be identical to each other, in practice this is rarely the case. Array elements may also deviate from their nominal locations due to limited manufacturing precision. The presence of interactions between the array elements as well as imperfections in the array affect the element radiation patterns in such a way that they are no longer omni-directional. Limited size of the ground plane also impose a deviation from the ideal scenario.

In order to achieve the desired radiation pattern performance in terms of beamwidth and sidelobe levels, array calibration is often essential. In this chapter, a compensation method

for embedded pattern and mutual coupling as well as other array imperfections is discussed and some experimental results are presented. The resulting beam patterns are compared between ideal, measured and FDTD model UCAs. Due to findings in Chapters 3 and 4, only 8-element monopole UCAs are considered in this chapter.

Results show that a maximum SLL of $\approx -30dB$ is achievable through the use of this method, which is far superior compared to the SLL achieved in Chapter 4 when no compensation is present, which is $\approx -12dB$. FDTD modeling and matrix manipulation is utilised in order to simplify the correction matrix and practical values presented. The final part of this chapter addresses the manufacturing accuracy needed in the production of the correction matrix in order to achieve the optimum results.

5.1 Mutual Coupling Compensation

Mutual coupling exists when radiating or receiving elements are placed within close proximity of each other. In this case, there will be interactions between the elements as the electromagnetic environment of the element is altered. In the case of two or more array elements, the current distribution and thus radiation pattern is altered for all elements involved. This change in the current distribution is also reflected on the impedances at each element, which in turn leads to matching problems and reduction in radiation efficiency. As can be expected, mutual coupling is stronger when the field polarisation of the elements are parallel. The mutual coupling also decreases as the element separation is increased. When mutual coupling is included in the design of an antenna array, the complexity of the analysis increases as the element patterns deviate from the ideal scenario. However, in the real world, mutual coupling is a critical design aspect as it is virtually unavoidable in any practical array design. Further, it is shown in [17] that antenna array steering vectors differ significantly when mutual coupling is taken into account.

Mutual coupling may arise due to radiative coupling between elements as well as internal coupling between channels of a beamforming network. However, internal coupling can be minimised through the use of seperate receiver chains in a digital beamforming network, thus providing a good degree of channel isolation. In the past years several methods have been developed to address the mutual coupling effects. These include methods involving numerical techniques as well as those employing active element patterns.

5.1.1 Free and forced excitation

The most common method is often called the *pattern multiplication* approach. This approach considers arrays of elements with similar magnitude and phase distribution. Mutual coupling on this type of arrays is evident in the variation of the elements' active input impedance instead of their current distribution shapes. The relative element patterns can thus be assumed identical and be factored out of the array factor.

The first pattern multiplication approach, often called the *free-excitation method* [2], the array excitation is modeled as a set of Thevenin-equivalent voltage sources with non-zero source impedances. This is illustrated in Figure 5.1(a) [3]. If the generator impedances Z_{gq} are zero, the method becomes *forced-excitation method.* The equivalent generator impedances generally differ when a feed network is used due to impedance mismatches and reflections

in the network. However, when identical independent sources are used, the generator impedances can be considered identical. The generator impedances are generally assumed to be identical regardless of the array feeding technique. The active element input impedance can be represented as an equivalent lumped impedance as shown in Figure 5.1(b) [3]. The resulting feed currents are therefore given by

$$I_q = \frac{V_q}{Z_{aq} + Z_{gq}} \tag{5.1}$$

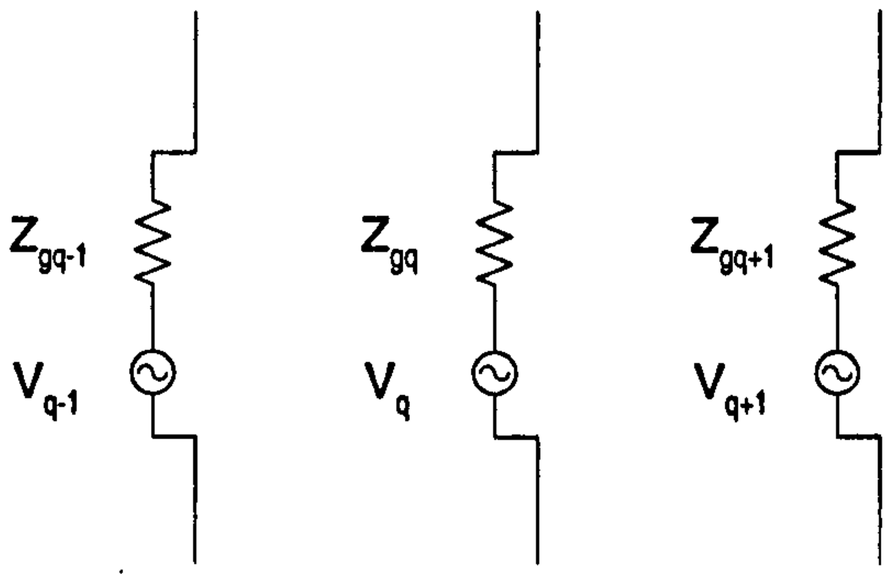

Figure 5.1: *Free excitation model*

Z_{aq} represents the active input impedance of the qth element and $q = 1, 2, ..., N_s$ where N_s is the number of voltage sources.

When the array elements are assumed to have identical element patterns which are frequently the same as the free-space element pattern, the array pattern becomes

$$E(\theta, \phi) = g_{iso}(\theta, \phi) \sum_{q=1}^{N_s} I_q e^{jk\hat{\mathbf{r}} \cdot \mathbf{r}_q} \tag{5.2}$$

where g_{iso} is the radiation pattern of an isolated element and $\mathbf{r}_q$ is the position vector from

origin to the qth element.

Clearly, the assumption of identical element patterns is valid for many applications such as arrays of parallel half-wave dipole elements which are not too closely spaced. On the other hand, it should also be noted that the assumption limits the scope of application of this method. Furthermore, there is no direct way of calculating the coupling coefficients using the free excitation approach [4].

In cases where individual element patterns are not identical, numerical techniques such as the method of moments (MoM) [17] may be used. In this method, each antenna element is represented by a wire which is divided into several smaller segments. A system impedance matrix Z_{QQ} which represents the coupling between each segment in the array is then calculated where $Q = sN$, N is the number of elements in the array and s is the number of segments in each antenna element. Generally, MoM is more accurate for larger values of Q [18], therefore although MoM offers accuracy, it involves large matrices and therefore complex computations. [19] provides the comparison between the FDTD method (Appendix C) and the MoM method for antenna modeling. The authors of this paper suggests that the run time t_{MoM} for MoM varies such that $t_{MoM} \propto xD^6$ whereas the FDTD run time is such that $t_{FDTD} \propto xD^4$ where x is an arbitrary constant and D is the linear electrical dimension of the structure.

5.1.2 Active element patterns

When neither computational nor numerical methods can be applied, the *active element pattern method* may be used. The active element pattern is defined as the radiation pattern of a single excited element in an array when all the other elements are terminated with matched loads [5], [6]. The active element pattern thus includes all the effects of mutual coupling. Hence the array radiation pattern becomes the vector summation of the individual active element patterns and their respective weights.

Two forms of active element pattern methods, namely the *unit-excitation active element pattern method* and the *phase-adjusted unit-excitation active element pattern method* are described in [3]. The *hybrid active element pattern method* is often used to accurately predict the radiation pattern of small to medium-sized uniform arrays. The method separates the individual patterns of array elements into two categories, the edge element patterns and

interior element patterns. The array radiation pattern is therefore

$$E(\theta,\phi) \approx g_e(\theta,\phi)\sum_{n=1}^{Q} w_n e^{jk\hat{\mathbf{r}}\cdot\mathbf{r}_q} + \sum_{n=1}^{N-Q} w_n g_a^n(\theta,\phi) \tag{5.3}$$

where $g_e(\theta,\phi)$is the interior active element pattern or the embedded element pattern, $g_a^n(\theta,\phi)$ is the n^{th} active element pattern, and Q is the number of interior elements [3]. Evidently, the contributions of active and embedded element patterns depend on the size of the array. In the case of large arrays, the number of edge elements is relatively few compared to the number of interior elements, thus it can be assumed that $Q = N$ and the second term of equation 5.3 disappears. On the other hand, in the case of small arrays it is safe to assume that all the active element patterns can be measured and stored and all the array elements are considered as edge elements, thus the first term of Equation 5.3 may be eliminated.

In his experimental evaluation involving a medium-sized uniform linear array of dipoles, Kelley [3] compares the array radiation patterns computed using the method outlined above with those computed using method-of-moment. It is revealed that pattern degradations are largely caused by the edge element effects. In the case of a UCA, there are no edge elements, hence such effects are eliminated.

5.1.3 Mutual coupling in uniform circular arrays

All arrays, including circular arrays, suffer from mutual coupling between their elements. Circular arrays face an additional problem since significant coupling can occur between elements located directly opposite each other in the circumference as well as coupling from adjacent elements. Due to its symmetrical property, the electrical environment of all elements in a circular array is identical, hence all the elements possess an identical radiation impedance. In practice, however, this value is still affected by mutual coupling especially since the aperture is required to be small in comparison with the wavelength, as described in the previous chapter.

Mutual coupling between array elements affects the ideal array steering vector $\mathbf{a}_I(\theta)$, given by

$$\mathbf{a}_I(\theta) = \left[e^{jkR\cos\phi}, e^{jkR\cos\left(\phi-\frac{2\pi}{N}\right)}, \ldots, e^{jkR\cos\left(\phi-\frac{2\pi(N-1)}{N}\right)}\right]^T \tag{5.4}$$

to a different steering vector $\mathbf{a}(\theta)$ in such a way that

$$\mathbf{a}(\theta) = \mathbf{C}\mathbf{a}_I(\theta) \tag{5.5}$$

where $\mathbf{C}$ is the mutual coupling matrix and has a *circulant* property since the array is circular and follows a rotational symmetry. Thus,

$$\mathbf{C} = \begin{pmatrix} c_0 & c_1 & c_2 & \cdots & c_{N-1} \\ c_{N-1} & c_0 & c_1 & \cdots & c_{N-2} \\ \vdots & \vdots & \vdots & \cdots & \vdots \\ c_1 & c_2 & c_3 & \cdots & c_0 \end{pmatrix} \tag{5.6}$$

Wax [7] presents an approach to tackling with coupling coefficients such that:

$$E(\phi) = \frac{1}{\sqrt{N}} \sum_{m=-M}^{M} \frac{1}{\check{c}_m} V_m j^m J_m(kR) e^{jm\phi} \tag{5.7}$$

where $\check{c}_m$ $(m = 0, \pm 1, \pm 2, ..., \pm M)$ denotes the mth DFT bin of $\{c_0, c_1, c_2, \cdots, c_{N-1}\}$, and M is the highest possible mode to be excited, $M = \frac{N-1}{2}$.

$$\check{c}_m = \sum_{N-1}^{i=0} c_i e^{j\frac{2\pi mi}{N}} \tag{5.8}$$

However, this process requires that the coupling coefficients $\{c_i\}$ be known.

Davies [8] suggested that in the case of single-phase mode excitation, the electrical environment of all the elements is identical due to the array symmetry, hence the array elements possess an identical radiation impedance, or *phase-sequence impedance*, for that mode. The same applies to all other phase modes, therefore the effects of mutual coupling is a modification to the various sequence impedances. When a Butler matrix network is used for phase-mode excitation, it is therefore possible to completely compensate for the mutual coupling effects simply by compensating for this impedance mismatch at each input port. This can be done through the use of a set of fixed impedance compensations at each input port. These compensations are independant up on the excitation of the array or the beam position. It should be noted that due to various other array imperfections as described in the next section, the values of these compensations may vary between each element.

Alternatively, the phase-sequence impedance can be obtained experimentally by exciting each phase mode one at a time. The far field strength and phase can be measured and the excitation of the appropriate port modified in order to achieve the desired field strength value for

each mode. This approach is a powerful method for mutual coupling compensation in applications where mutual coupling significantly degrades the performance of the array. However, when it is necessary for arrays to be mass-produced, as is the case for indoor wireless applications, the method may prove to be inefficient since a significant amount of time would be needed to individually measure and compensate each array element.

In wide-bandwidth applications, each mode impedance has to be matched over the whole operating band. Each mode excitation also has to be produced in such a way that they vary with frequency in order to maintain the correct pattern.

5.2 Scattering Effects

Scattering effect is another phenomenon which affects the shape of embedded element patterns. Although it plays a significant part in element interactions, scattering effect is often overlooked when the non-ideal case is considered, since it is often misunderstood as mutual coupling. Figure 5.2 illustrates the scattering effect phenomenon for the case of 8-element monopole UCA.

When a signal transmitted by a source antenna impinges on each of the array elements, part of the signal travels into the element and are re-radiated[1]. However, most of the signal is reflected as it bounces off the elements. These reflected signals are then absorbed by the element of interest (in this case, element 1), and affect the active element radiation pattern. As expected, the largest contribution is made by the neighbouring elements (in this case, elements 2 and 8).

In addition to scattering due to nearby antenna elements, in practice the antenna performance is also affected by scattering from local objects in the vicinity of the array, such as tables, chairs, walls, etc. However, these effects are not included in the measured radiation patterns discussed in Chapters 4 and 5, since the patterns have been measured in an anechoic chamber environment[2].

[1]This is, in effect, mutual coupling

[2]see Appendix A

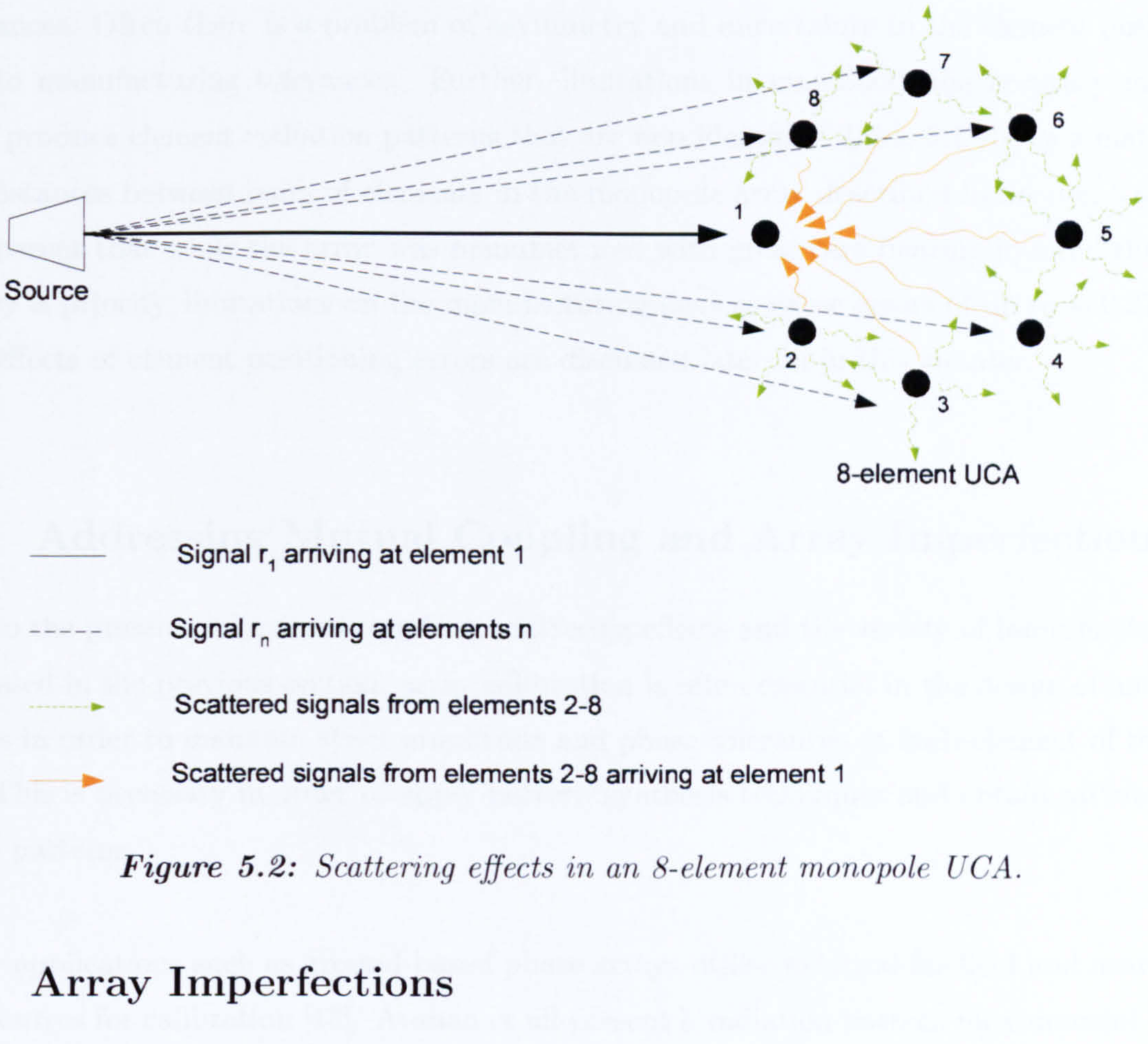

Figure 5.2: *Scattering effects in an 8-element monopole UCA.*

5.3 Array Imperfections

In addition to mutual coupling and scattering effects, several other array imperfections may cause the measured array radiation pattern to deviate from the identical case. These include effects such as those produced by delay and attenuation in the RF cables, connector and power dividers. Failure of one or more elements in an array may impose significant effects on the performance small arrays. However, in the case of large arrays the array performance can often be restored through the use of specific algorithms. The effects of element failure and the remedial methods are discussed in [10]- [13]. Ground plane effects caused by diffraction electromagnetic currents travelling along a finite ground plane are also a major cause of the deviation of measured array radiation pattern compared to the ideal case. The effects of a finite ground plane on the input impedance of a monopole antenna is investigated in [14].

Currents induced along transmission lines could also present a significant contribution to the far-field radiation pattern. Further, coupling between the transmission line and the antenna, as well as unbalanced currents on the outside surfaces of coaxial lines may contribute to further distortion in the array pattern.

Perhaps one of the primary examples of array imperfection is that caused by manufacturing

tolerances. Often there is a problem of asymmetry and uncertainty in the element positions due to manufacturing tolerances. Further, limitations in manufacturing accuracy may in itself produce element radiation patterns that are non identical. Table 5.1 shows a matrix of the distances between pairs of elements in the monopole array described in Section 3.6.2. It is apparent that while the array was manufactured with great care bearing in mind that accuracy is priority, limitations on the manufacturing devices cause errors of up to $\approx 0.27mm$. The effects of element positioning errors are discussed later on in this chapter.

5.4 Addressing Mutual Coupling and Array Imperfections

Due to the presence of mutual coupling, scattering effects and the variety of imperfections as discussed in the previous section, array calibration is often essential in the design of antenna arrays in order to maintain strict amplitude and phase tolerances at each element of the array. This is necessary in order to apply pattern synthesis techniques and obtain satisfactory beam patterns.

Many applications such as ground-based phase arrays utilise external far-field and near-field test sources for calibration [15]. Auman et all present a radiation pattern measurement technique for array calibration which utilises the inherent mutual coupling in the array in [16].

Wax [7] has developed a processing technique in order to compensate for these errors. In order to simplify the maths, matrix notations are used to represent each stage in the system. Assigning $\mathbf{C}$ to denote an arbitrary correction matrix which includes mutual coupling as well as other array imperfections, it follows that

$$\mathbf{JFC}^{-1}\mathbf{A}(\phi) \approx \tilde{\mathbf{A}}(\phi) \tag{5.9}$$

where $\mathbf{A}(\phi)$ is the element radiation pattern vector, $\tilde{\mathbf{A}}(\phi)$ is the desired steering vector of the virtual array with Vandermonde structure:

$$\tilde{\mathbf{A}}(\phi) = \left[e^{kv(\phi)}, e^{(k+1)v(\phi)}, \ldots, e^{(k+p)v(\phi)}\right]^T \tag{5.10}$$

k is an integer and $v(\phi)$ is an arbitrary one-to-one function of ϕ in the field of view. $\mathbf{F}$ is a $(2M+1) \times N$ matrix which represents the spatial DFT operation, i.e. the Butler matrix. The system is described in Figure 5.3.

	1	2	3	4	5	6	7	8
1	0.0000	22.0604	41.0604	53.3619	57.7840	53.2970	40.9525	22.1802
2	22.0604	0.0000	22.3118	40.7579	53.2849	57.5795	53.3811	40.8201
3	41.0604	22.3118	0.0000	21.8930	40.7370	53.2690	57.9387	53.5453
4	53.3619	40.7579	21.8930	0.0000	22.1320	40.8108	53.4618	57.7612
5	57.7840	53.2849	40.7370	22.1320	0.0000	22.0878	40.9070	53.3485
6	53.2970	57.5795	53.2690	40.8108	22.0878	0.0000	22.0773	40.7277
7	40.9524	53.3811	57.9387	53.4618	40.9070	22.0773	0.0000	22.1071
8	22.1802	40.8201	53.5453	57.7612	53.3485	40.7277	22.1071	0.0000

(a) Actual array dimension

22.0779	40.7946	53.3008	57.6923

(b) Accurate array dimensions

	1	2	3	4	5	6	7	8
1	0.0000	-0.0175	0.2658	0.0611	0.0917	-0.0038	0.1579	0.1023
2	-0.0175	0.0000	0.2339	-0.0367	-0.0159	-0.1128	0.0803	0.0255
3	0.2658	0.2339	0.0000	-0.1849	-0.0576	-0.0318	0.2464	0.2445
4	0.0611	-0.0367	-0.1849	0.0000	0.0541	0.0162	0.1610	0.0689
5	0.0917	-0.0159	-0.0576	0.0541	0.0000	0.0099	0.1124	0.0477
6	-0.0038	-0.1128	-0.0318	0.0162	0.0099	0.0000	-0.0006	-0.0669
7	0.1578	0.0803	0.2464	0.1610	0.1124	-0.0006	0.0000	0.0292
8	0.1023	0.0255	0.2445	0.0689	0.0477	-0.0669	0.0292	0.0000

(c) Error

Nearest neighbour elements
Nearest but one elements
Nearest but two elements
Adjacent elements

Table 5.1: *Monopole array (Array 1) dimensions in mm.*

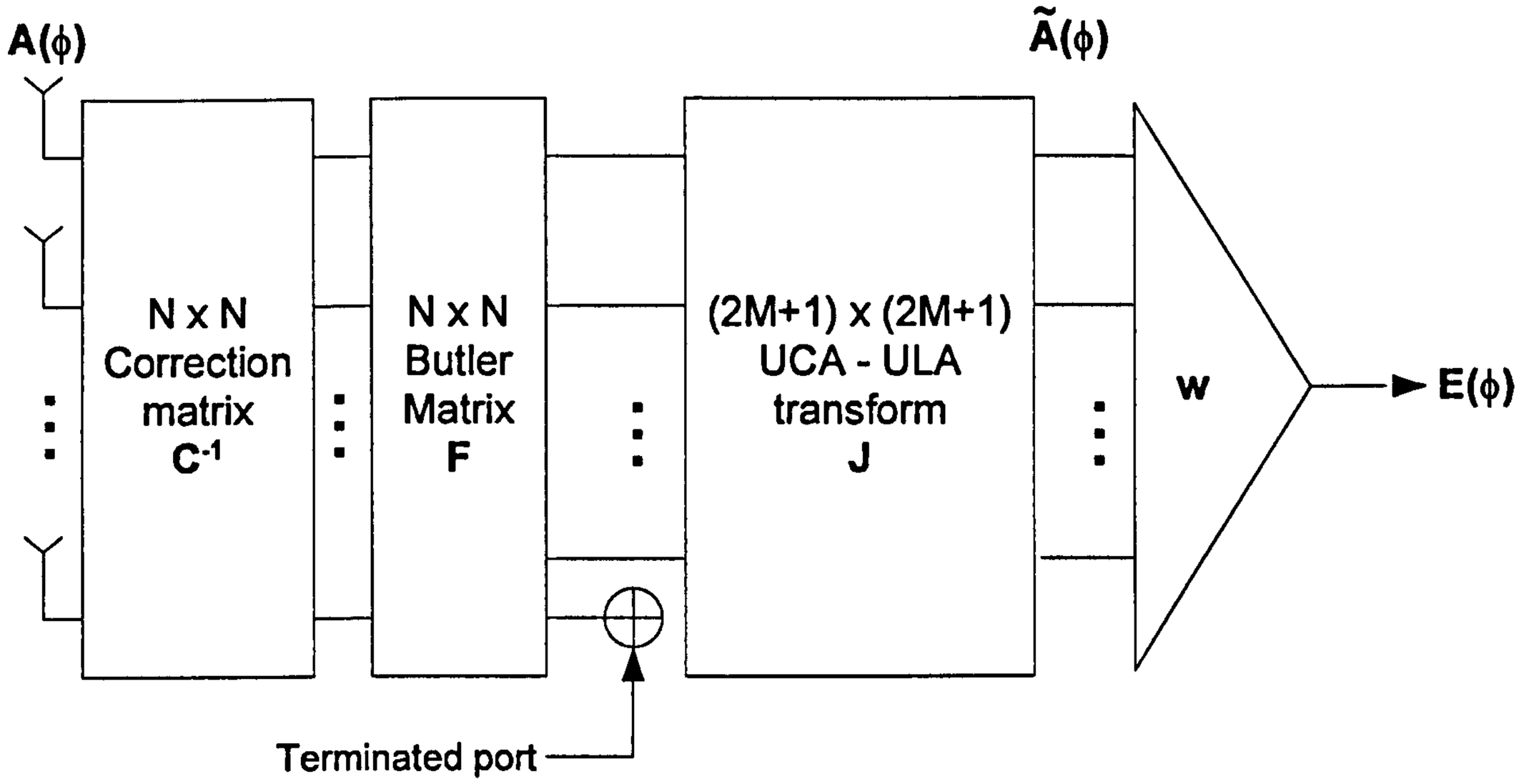

Figure 5.3: *Block diagram of Wax [7] correction matrix theory*

$$\mathbf{F} = \frac{1}{\sqrt{N}} \begin{pmatrix} 1 & \omega^{-M} & \omega^{-2M} & \dots & \omega^{-(N-1)M} \\ \vdots & \vdots & \vdots & \dots & \vdots \\ 1 & \omega^{-1} & \omega^{-2} & \dots & \omega^{-(N-1)} \\ 1 & 1 & 1 & 1 & 1 \\ 1 & \omega^{1} & \omega^{2} & \dots & \omega^{(N-1)} \\ \vdots & \vdots & \vdots & \dots & \vdots \\ 1 & \omega^{M} & \omega^{2M} & \dots & \omega^{(N-1)M} \end{pmatrix} \tag{5.11}$$

where $\omega = e^{j2\pi/N}$. $\mathbf{J}$ is a $(2M+1) \times (2M+1)$ diagonal matrix

$$\mathbf{J} = diag\left\{ \frac{1}{\sqrt{N} j^m J_m(kR)} \right\} \quad m = -M, \dots, 0, \dots, M. \tag{5.12}$$

$J_m(.)$ represents the m^{th} Bessel function of the first kind, and R denotes the array radius.

Equation 5.9 implies that there is a linear transformation between the virtual and the actual array. It follows that the equation can be written as

$$\mathbf{BA}(\phi) \approx \tilde{\mathbf{A}}(\phi) \tag{5.13}$$

where $\mathbf{B}$ is a $(2M+1) \times N$ matrix. Although it is possible to compute $\mathbf{B}$ by estimating $\mathbf{C}$

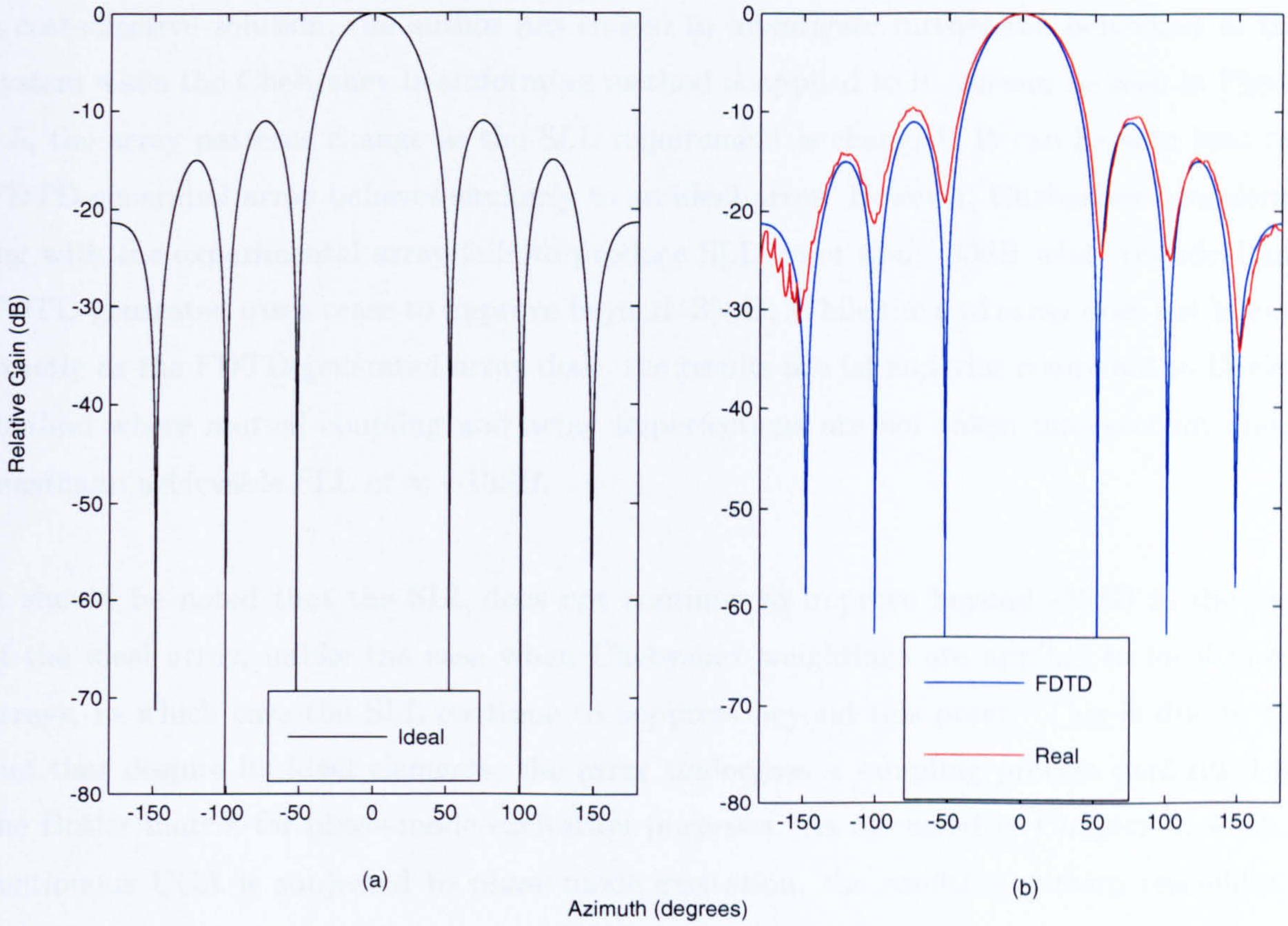

Figure 5.4: *Wax [7] theory applied to 8-element monopole (a)Ideal UCA; (b) FDTD-generated UCA and experimental UCA; with* $R = R_{opt}$

from the measured actual array patterns $\mathbf{A}(\phi)$, Wax found that a more powerful approach is to estimate $\mathbf{B}$ directly. By process of minimisation, the matrix $\mathbf{B}^H$ can be approximated as

$$\hat{\mathbf{B}}^H = (\mathbf{A}\mathbf{A}^H)^{-1}\mathbf{A}\tilde{\mathbf{A}}^H \tag{5.14}$$

The resultant virtual array is now amendable to spatial smoothing, and includes the various array imperfections that may arise in a real-life environment. Any ULA beamforming weights $\mathbf{w}$ can now be applied to the virtual array. Figure 5.4 illustrates the radiation pattern produced by ideal, real and FDTD-generated arrays using this method. It can be seen that the FDTD-generated array behaves almost identically to the ideal array. The radiation pattern produced by the real array does not possess the same null depth as that of the FDTD-generated array, however the general shape and null positions agree.

As the patterns are now amendable to spatial smoothing, any linear array pattern synthesis method may be applied to the system output. In keeping with the attempt of finding

a cost-effective solution, the author has chosen to investigate further the behaviour of this system when the Chebyshev beamforming method is applied to it. As can be seen in Figure 5.5, the array patterns change as the SLL requirement is changed. It can be seen that the FDTD-generated array behaves similarly to an ideal array. However, Chebyshev beamforming with the experimental array fails to produce SLL lower than -30dB while the ideal and FDTD-generated cases cease to improve beyond -35dB. While the real array does not behave exactly as the FDTD-generated array does, the results are far superior compared to Davies' method where mutual coupling and array imperfections are not taken into account and a maximum achievable SLL of $\approx -13dB$.

It should be noted that the SLL does not continue to improve beyond -35dB in the case of the ideal array, unlike the case when Chebyshev weightings are applied to ideal linear arrays, in which case the SLL continue to suppress beyond this point. This is due to the fact that despite its ideal elements, the array undergoes a sampling process performed by the Butler matrix for phase-mode excitation purposes. As discussed in Chapter 3, when a continuous UCA is subjected to phase-mode excitation, the resulting pattern resembles a sinc function as produced by a ULA with uniform weights. However, when the UCA possess a finite number of elements, the sampling process limits the transformation process. Hence the resulting pattern differs from a sinc function as the number of sampling points is reduced and Chebyshev weights fail to produce the required SLL beyond a certain point.

5.5 Simplification of Parameters

Theoretically, the contents of the correction matrix $\mathbf{C}^{-1}$ should only consist of $N/2$ different values due to the symmetrical properties of the circular array. However, a closer look into the results when the experimental array is used confirms that by attempting to eliminate mutual coupling and array imperfection effects, each element of the correction matrix $\mathbf{C}^{-1}$ takes a different value. Table 5.2 shows the correction matrix for the practical monopole array described in Section 4.1, which is labeled as Array 1 throughout this chapter. The matrix is obtained through the numerical procedures in the previous section. This means that while the results presented in the previous section is an improvement to the results obtained purely by phase-mode excitation as shown in the previous chapter, in attempt to improve the array response the RF circuitry has become much more complex. NxN amplitude and phase controls are now needed in order to produce the desired radiation pattern. This in turn would make the system much less cost-effective.

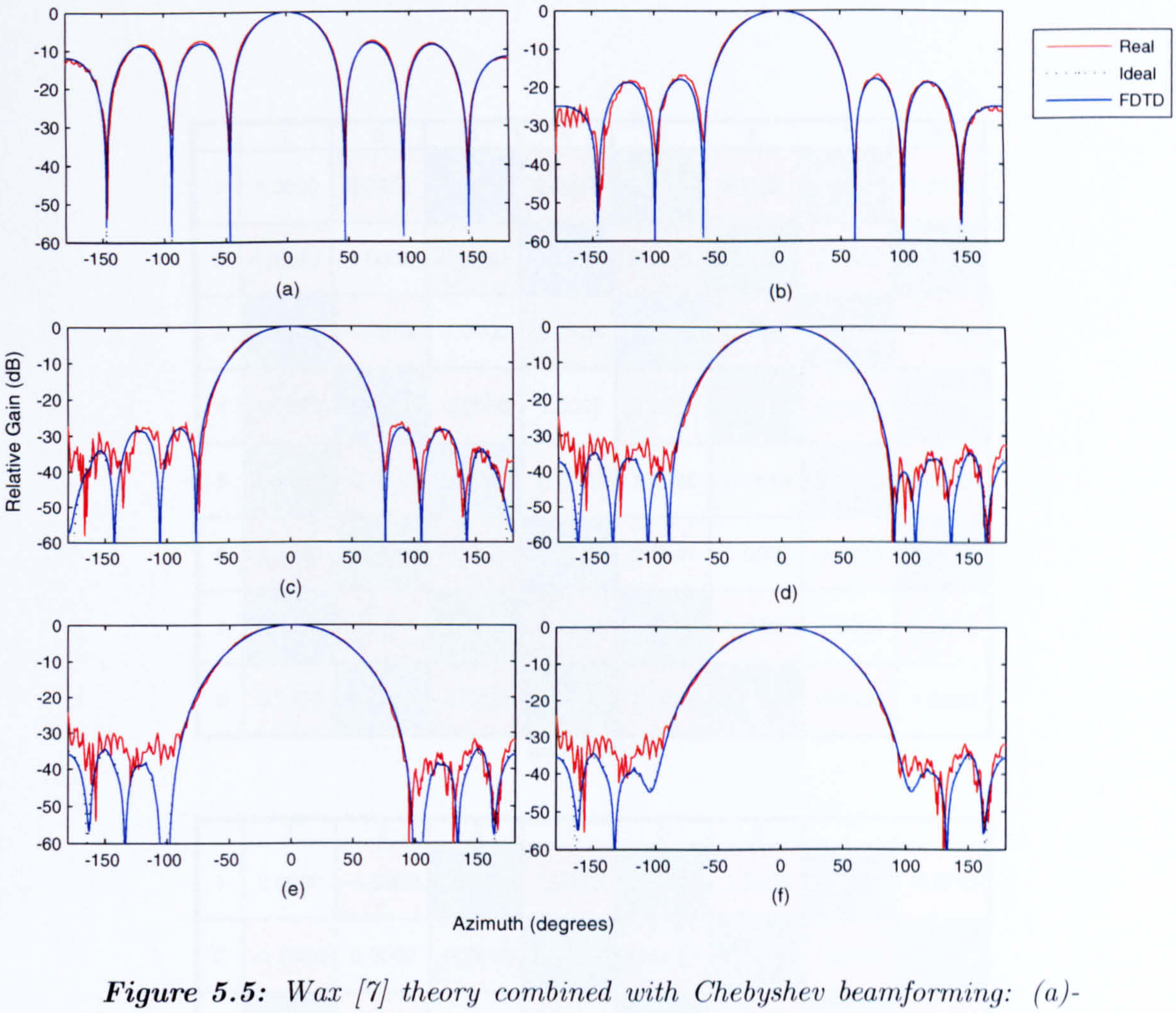

Figure 5.5: *Wax [7] theory combined with Chebyshev beamforming: (a)-10dB SLL; (b)-20dB SLL; (c)-30dB SLL; (d)-40dB SLL; (e)-45dB SLL; (f)-50dB SLL*

A closer look into Equation (5.14) reveals that the correction matrix $\mathbf{C}^{-1}$ is highly dependent upon the correlation matrix of the array pattern $\mathbf{E}$. This explains the behaviour of the correction matrix $\mathbf{C}^{-1}$ when non-identical element patterns are in place. It is therefore important to take a more detailed investigation into the correlation matrix behaviour. Table 5.3 and 5.4 show the correlation and correction matrices of the FDTD-generated array[3].

In order to further investigate the behaviour of the correlation as well as correction matrix when exposed to errors in each antenna element's position, more FDTD models are constructed which include displacements of each element in the array. Models are constructed

[3]The slight variations in the values within each diagonal is a result of the rectangular grid of the FDTD model. While the array as well as the ground plane is circular, this results in a slight variation between the generated radiation pattern of element numbers 1,3,...(N/2)-1 and element numbers 2,4...(N/2).

	1	2	3	4	5	6	7	8
1	1.0000	0.2404	0.1876	0.1322	0.1143	0.1236	0.1849	0.2418
2	0.2240	1.0000	0.2030	0.1824	0.1529	0.1300	0.1477	0.1859
3	0.2153	0.2656	1.0000	0.2524	0.2127	0.1690	0.1404	0.1333
4	0.1573	0.2295	0.2650	1.0000	0.2553	0.2327	0.1576	0.1466
5	0.1495	0.1498	0.2216	0.2682	1.0000	0.2819	0.2218	0.1797
6	0.1852	0.1541	0.1626	0.2289	0.2241	1.0000	0.2466	0.2252
7	0.2575	0.1674	0.1432	0.1483	0.1925	0.2355	1.0000	0.2674
8	0.2709	0.2339	0.1333	0.1296	0.1445	0.1918	0.2239	1.0000

(a) Amplitude

	1	2	3	4	5	6	7	8
1	0.0000	-0.9822	3.1335	1.5983	1.8507	1.8110	-3.0041	-0.9743
2	-1.0880	0.0000	-1.0890	3.1317	1.5417	1.4658	1.6171	-2.8923
3	-3.0572	-0.8823	0.0000	-1.0323	-3.0973	1.6591	1.7830	1.7703
4	1.5143	-3.0167	-0.9686	0.0000	-1.0464	-3.0369	1.6755	1.7772
5	1.6315	1.6963	-3.0082	-0.9897	0.0000	-0.8196	-3.1012	1.7031
6	1.3784	1.4380	1.5162	-2.9408	-1.1146	0.0000	-0.8553	-3.0639
7	-3.0802	1.5286	1.6102	1.3889	-3.0657	-1.0311	0.0000	-0.9034
8	-1.1447	-3.0004	1.3543	1.4133	1.4857	-3.1062	-1.1958	0.0000

(b) Phase

Nearest neighbour element pairs
Nearest neighbour but 1 element pairs
Nearest neighbour but 2 element pairs
Nearest neighbour but 3 or adjacent element pairs

Table 5.2: NxN *Correction matrix for the practical monopole array (Array 1) described in Section 4.1.*

	1	2	3	4	5	6	7	8
1	1.0000	0.1198	0.0538	0.2026	0.1221	0.2026	0.0538	0.1198
2	0.1198	1.0000	0.1200	0.0552	0.2028	0.1223	0.2024	0.0549
3	0.0538	0.1200	1.0000	0.1201	0.0540	0.2023	0.1223	0.2024
4	0.2026	0.0552	0.1201	1.0000	0.1197	0.0548	0.2023	0.1223
5	0.1221	0.2028	0.0540	0.1197	1.0000	0.1197	0.0540	0.2028
6	0.2026	0.1223	0.2023	0.0548	0.1197	1.0000	0.1201	0.0552
7	0.0538	0.2024	0.1223	0.2023	0.0540	0.1201	1.0000	0.1200
8	0.1198	0.0549	0.2024	0.1223	0.2028	0.0552	0.1200	1.0000

(a) Magnitude

	1	2	3	4	5	6	7	8
1	0	3.138	-3.1414	-0.0018	-0.0004	-0.0018	-3.1416	3.1382
2	-3.138	0	-3.1357	3.1355	0.0027	0.0027	0.001	3.1414
3	3.1414	3.1357	0	3.1387	3.1379	-0.0028	0	-0.001
4	0.0018	-3.1355	-3.1387	0	-3.1344	3.1414	0.0028	-0.0027
5	0.0004	-0.0027	-3.1379	3.1344	0	3.1345	-3.1379	-0.0027
6	0.0018	-0.0027	0.0028	-3.1414	-3.1345	0	-3.1387	-3.1353
7	3.1416	-0.001	0	-0.0028	3.1379	3.1387	0	3.1356
8	-3.1382	-3.1414	0.001	0.0027	0.0027	3.1353	-3.1356	0

(b) Phase

Table 5.3: NxN *normalised correlation matrix for the FDTD-generated array*

	1	2	3	4	5	6	7	8
1	1	0.2417	0.1921	0.13	0.1001	0.13	0.1921	0.2416
2	0.2417	1	0.2417	0.1916	0.1292	0.0994	0.1291	0.1916
3	0.1921	0.2417	1	0.2416	0.1921	0.13	0.1002	0.13
4	0.1292	0.1916	0.2417	1	0.2418	0.1916	0.1292	0.0994
5	0.1002	0.13	0.1921	0.2416	1	0.2416	0.1921	0.13
6	0.1292	0.0994	0.1292	0.1916	0.2418	1	0.2417	0.1916
7	0.1921	0.13	0.1002	0.13	0.1921	0.2417	1	0.2417
8	0.2418	0.1916	0.1291	0.0995	0.1292	0.1916	0.2417	1

(a) Amplitude

	1	2	3	4	5	6	7	8
1	0	-0.9344	-2.9338	1.6495	1.8461	1.6495	-2.9338	-0.9345
2	-0.9332	0	-0.9334	-2.9454	1.6469	1.8501	1.6469	-2.9453
3	-2.9336	-0.9341	0	-0.9342	-2.9336	1.6501	1.8467	1.6498
4	1.6476	-2.9452	-0.9331	0	-0.9334	-2.945	1.6473	1.8504
5	1.847	1.6502	-2.9335	-0.9341	0	-0.9342	-2.9336	1.6502
6	1.6475	1.8504	1.6473	-2.9451	-0.9333	0	-0.9332	-2.9452
7	-2.9336	1.65	1.8468	1.6501	-2.9337	-0.9341	0	-0.9341
8	-0.9332	-2.9453	1.647	1.8502	1.6469	-2.9454	-0.9333	0

(b) Phase

Table 5.4: NxN *normalised correction matrix for the FDTD-generated array*

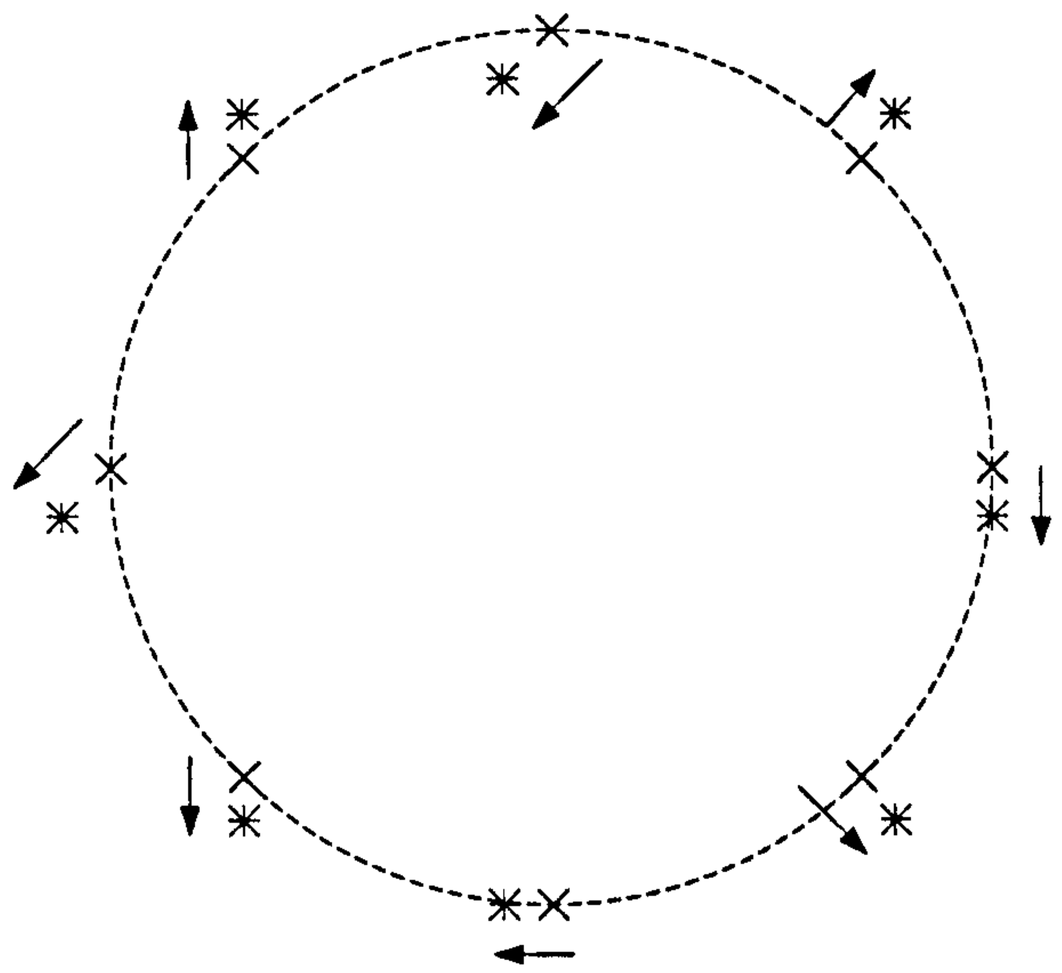

Figure 5.6: *Arbitrary displacements imposed on FDTD array model.*

with the elements displaced by 0.1, 0.2, 0.5 and 1mm each in arbitrary[4] directions as shown in Figure 5.6. As expected, the presence of these displacements on the models result in the change in the element amplitude and phase patterns which are no longer uniform due to the change in mutual coupling effects. The radiation patterns of the four new models are shown in Figure 5.7. The changes are also reflected in the correlation matrix as the values deviate further away from those where the elements are perfectly placed. Figure 5.8 shows how the correlation and correction values deviate from those shown in Equations (5.3) and (5.4). It is shown that the standard deviations of the correction factor are approximately linearly dependent upon the amount of displacements in the element position.

In order to validate the function of the correction matrix $\mathbf{C}^{-1}$, two scenarios are compared. That is, the first of the FDTD-generated UCA against the FDTD-generated UCA with 1mm displacements on its elements. It can be seen in Figure 5.9 that the correction matrix attempts to correct the dimension errors in the array, as it is evident in the cases where -10 and -20dB Chebyshev SLL are specified, the resulting patterns produced by the array with displaced elements overlap those produced by the array with correctly-placed elements. However, as the Chebyshev SLL requirement is pushed to lower levels, it can be seen that the beam patterns start to deviate from each other. Figure 5.10 confirms the fact that despite the -40dB SLL requirement, the correction matrices are still capable of performing their functions in the cases of 0.1 and 0.2mm element displacements. It therefore follows that

[4]Direction of displacements had to be chosen arbitrarily since they are limited by grid positions and size in the case of 0.1 and 0.2mm displacements. However, an FDTD model of the array with 0.5mm displacements in *random* directions shows similar results to those of the arbitrary 0.5mm displacements.

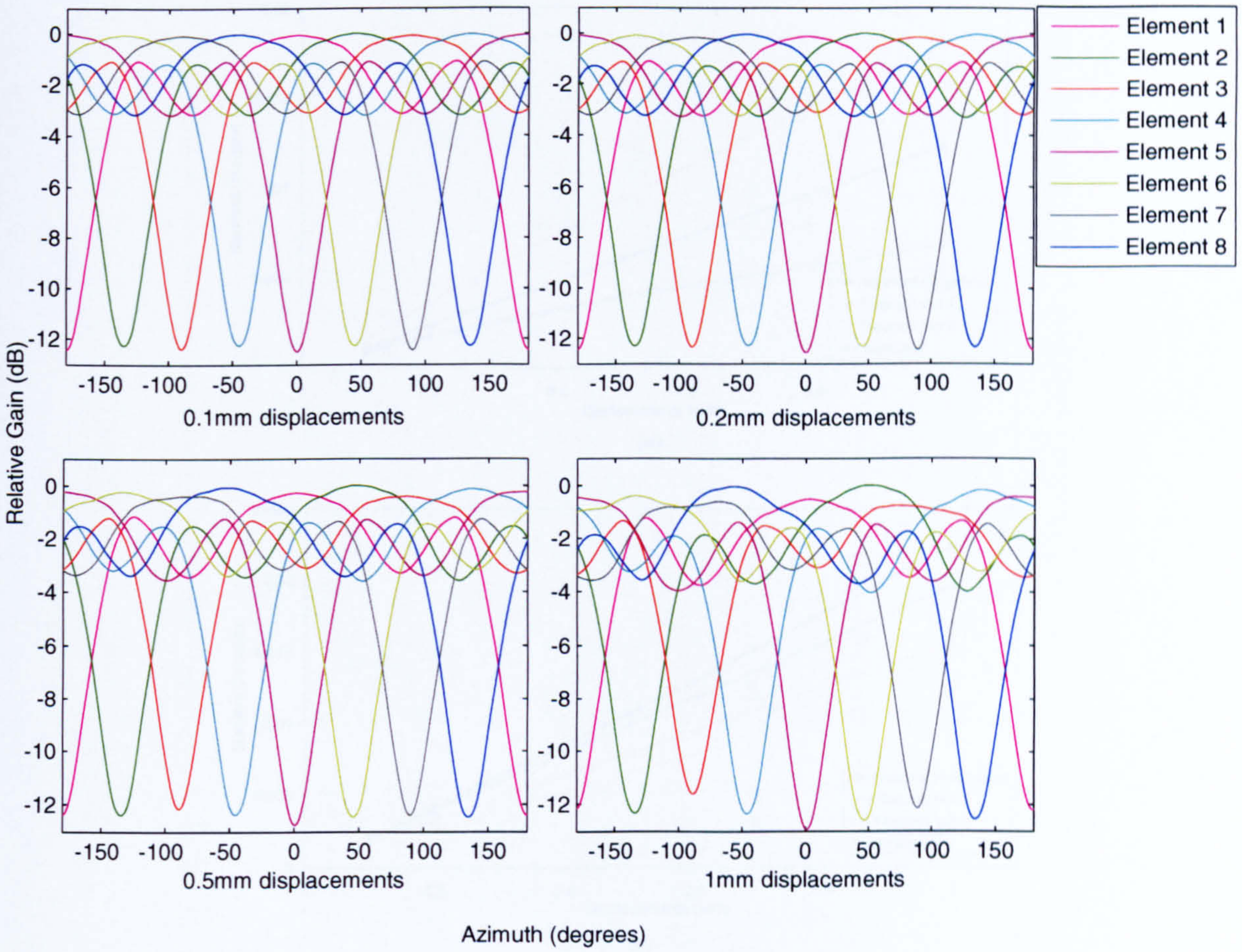

Figure 5.7: *Element radiation patterns produced by the FDTD-generated arrays with arbitrary displacements.*

although the correction matrix does attempt to correct for manufacturing errors, there is a limit to the amount of error it is capable of correcting. In this case, the limit lies at $\pm 0.2mm$.

It is proposed that an average correction matrix $\mathbf{C}_{av}^{-1}$ constructed from the normalised average of the correction values obtained from the original FDTD-generated array should be used (Table 5.5)[5]. Figure 5.11 illustrates the effects on the array magnitude patterns by applying the $\mathbf{C}_{av}^{-1}$ onto the different FDTD-generated arrays with uniform weights. It is shown that the magnitude of error in the element position affects the sidelobe levels, where there is a discrepancy of a magnitude $\approx$ 3dB between the array with perfectly placed elements and the array with 1mm displacement. This effect is also reflected in Figure 5.12 where a set of Chebyshev weights with -10, -20, -30, -35 and -40dB SLL requirements are applied. The figure shows that for higher SLL requirements, there is little difference between the patterns of

[5]Values averaged across the colour-coded diagonals such that every matrix element of the same colour inherit an identical value that is an average across values in this particular colour. Averaged values are normalised with respect to the diagonal.

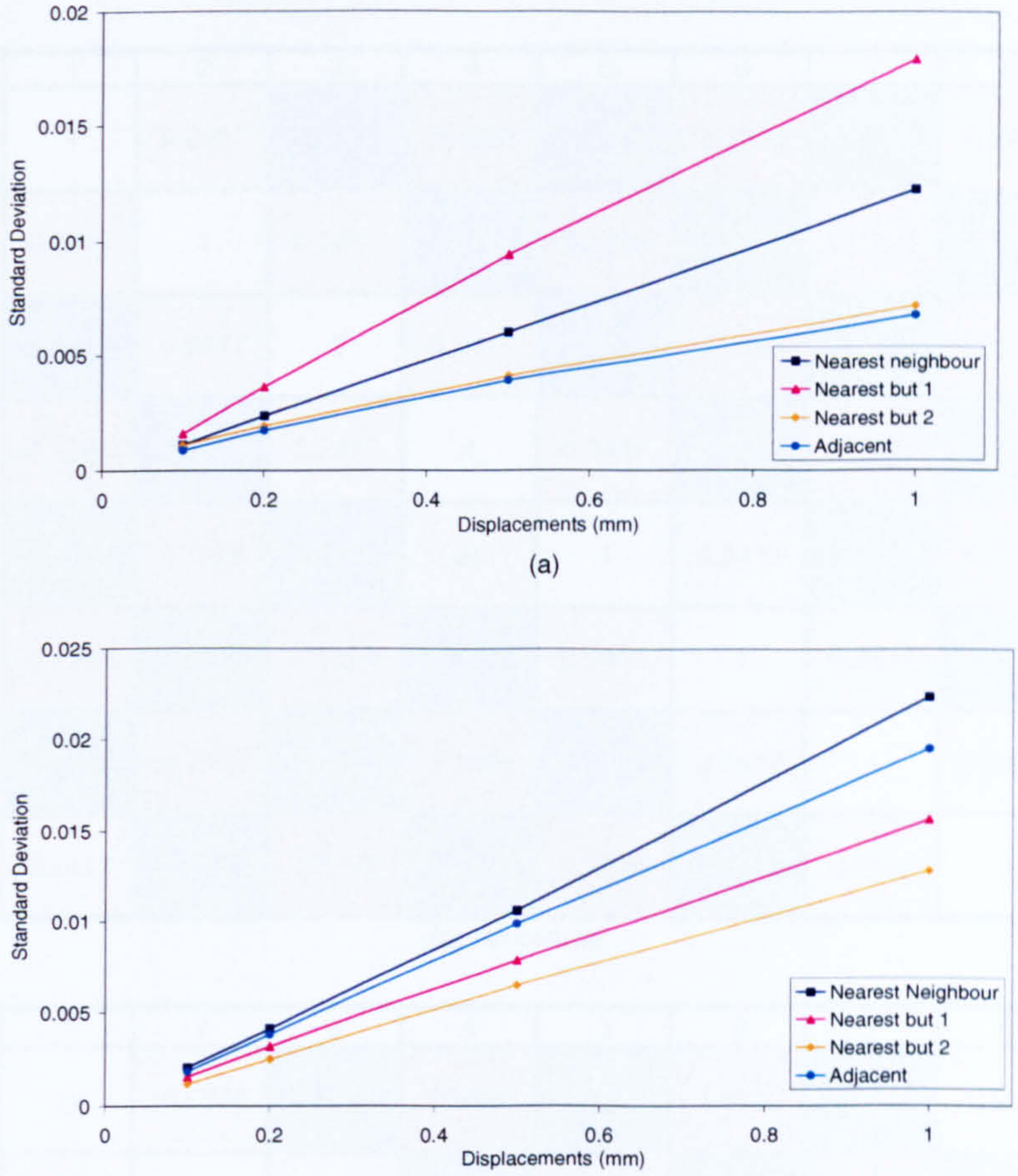

Figure 5.8: *Standard deviations in: (a)Correlation matrix (b)Correction matrix, produced by the FDTD-generated arrays with different displacements.*

the array without any displacement errors and those with displacement errors. However, as the SLL requirement is increased, the patterns begin to separate. It is shown that the maximum sidelobe suppression level that can be achieved is limited to a level that is dependent upon the amount of element displacements. It is seen that with 0.5mm displacements, the maximum suppression that can be achieved is $\approx -26dB$. In the case of 1mm displacements, SLL suppression reaches its error floor at $\approx -21dB$. Beyond these levels, SLL siezes to go any lower. Further increasing the Chebyshev SLL requirement results in the widening of the main beam. The same phenomenon is also seen in the behaviour of the real array in Figure 5.5.

For further comparison, another monopole UCA is built with a slightly relaxed accuracy. As can be seen in Table 5.6, this array, labeled Array 2 throughout this chapter, has up to $\approx$ 0.88mm errors in its dimensions. Figure 5.13 compares the performance of Array 2 with

	1	2	3	4	5	6	7	8
1	1	0.2417	0.1918	0.1296	0.0998	0.1296	0.1918	0.2417
2	0.2417	1	0.2417	0.1918	0.1296	0.0998	0.1296	0.1918
3	0.1918	0.2417	1	0.2417	0.1918	0.1296	0.0998	0.1296
4	0.1296	0.1918	0.2417	1	0.2417	0.1918	0.1296	0.0998
5	0.0998	0.1296	0.1918	0.2417	1	0.2417	0.1918	0.1296
6	0.1296	0.0998	0.1296	0.1918	0.2417	1	0.2417	0.1918
7	0.1918	0.1296	0.0998	0.1296	0.1918	0.2417	1	0.2417
8	0.2417	0.1918	0.1296	0.0998	0.1296	0.1918	0.2417	1

(a) Amplitude

	1	2	3	4	5	6	7	8
1	0	-0.9337	-2.9394	1.6486	1.8485	1.6486	-2.9394	-0.9337
2	-0.9337	0	-0.9337	-2.9394	1.6486	1.8485	1.6486	-2.9394
3	-2.9394	-0.9337	0	-0.9337	-2.9394	1.6486	1.8485	1.6486
4	1.6486	-2.9394	-0.9337	0	-0.9337	-2.9394	1.6486	1.8485
5	1.8485	1.6486	-2.9394	-0.9337	0	-0.9337	-2.9394	1.6486
6	1.6486	1.8485	1.6486	-2.9394	-0.9337	0	-0.9337	-2.9394
7	-2.9394	1.6486	1.8485	1.6486	-2.9394	-0.9337	0	-0.9337
8	-0.9337	-2.9394	1.6486	1.8485	1.6486	-2.9394	-0.9337	0

(b) Phase

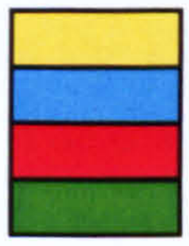

Table 5.5: NxN *Average normalised correction matrix* $\boldsymbol{C}_{av}^{-1}$ *for the FDTD-generated array with no displacements. Values are averaged across the colour-coded diagonals.*

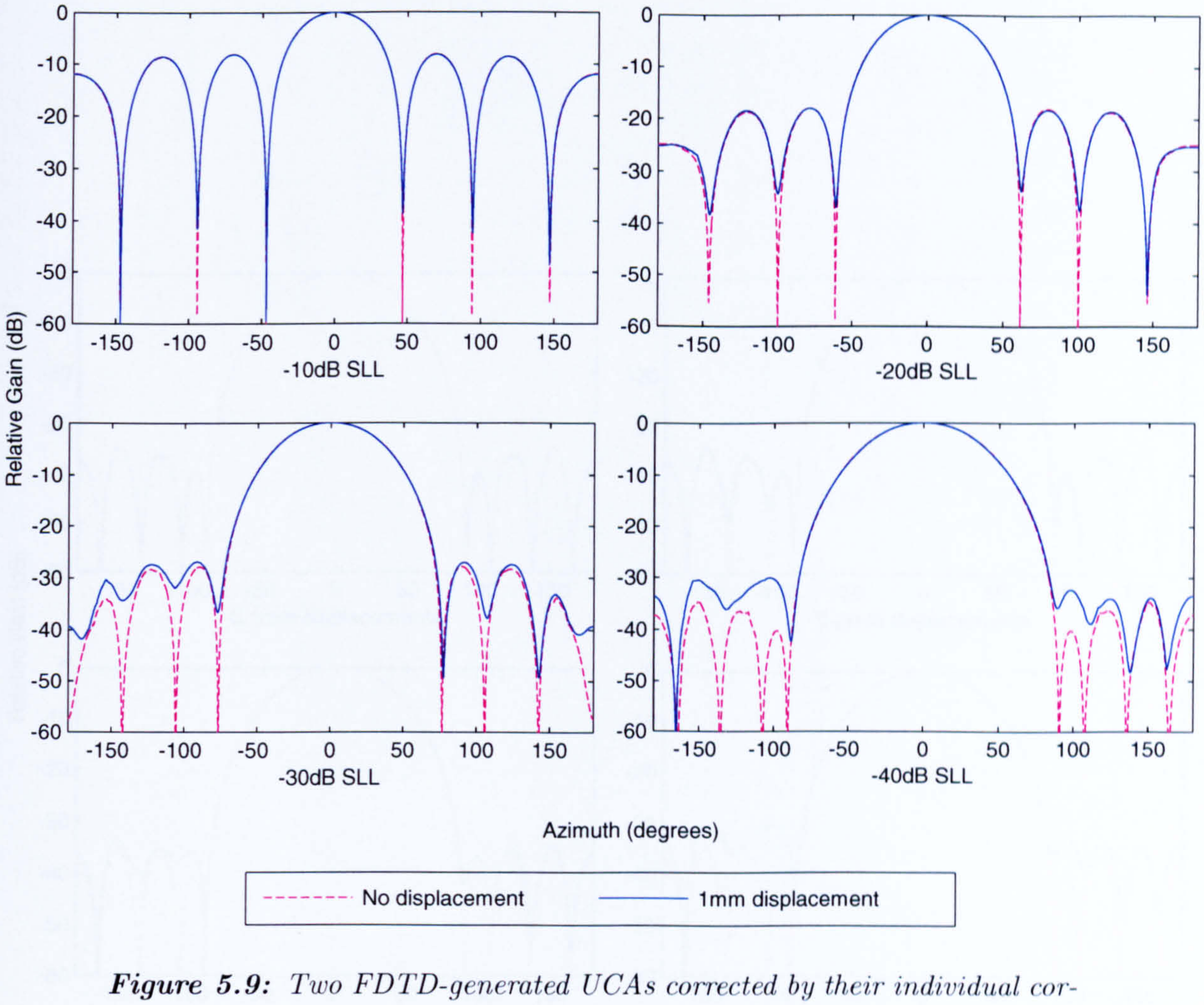

Figure 5.9: *Two FDTD-generated UCAs corrected by their individual correction matrix C^{-1} obtained through Equations (4.9), (4.13) and (4.14). Chebyshev weights with different SLL requirements are then applied to the corrected patterns.*

that of the original array. $\mathbf{C}_{av}^{-1}$ is used in this case, and Chebyshev weights with different SLL requirements are applied. It can be seen that as the SLL requirements are lowered, Array 1 is capable of producing sidelobes up to $\approx -25dB$ whereas SLL fails to reduce beyond $\approx -20dB$ in the case of Array 2.

The achievable SLL from the FDTD-generated arrays as well as the practical arrays is summarised in Figure 5.14. The diagram illustrates that as the dimensions error is increased, the maximum achievable SLL decreases accordingly. Further, it can be seen from Figure 5.14 as well as comparison between Figure 5.12 and Figure 5.13 that in terms of the achievable SLL, Array 1's performance is similar to that of the FDTD array with 0.5mm displacement, while Array 2 performs more similarly to the FDTD array with 1mm displacement.

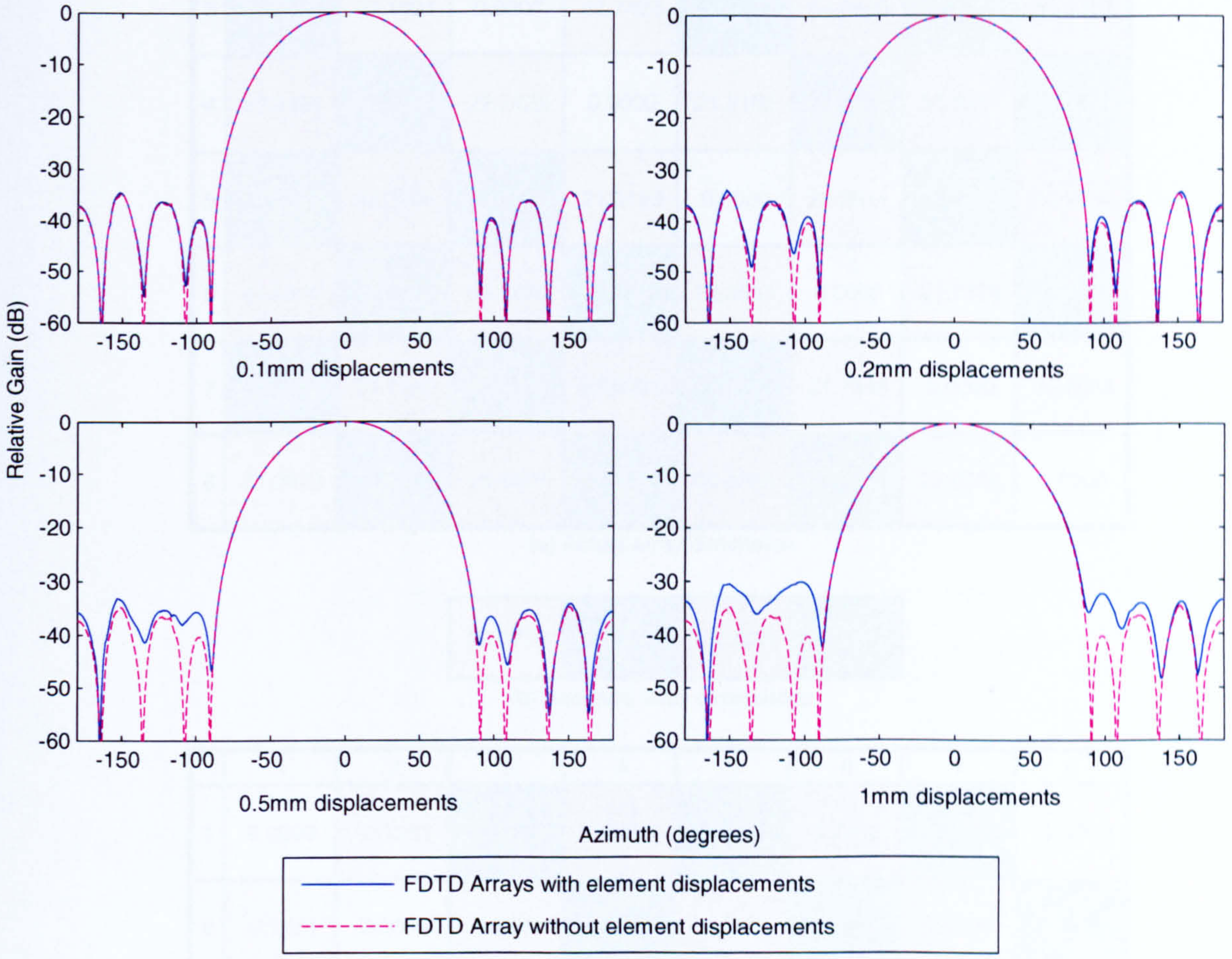

Figure 5.10: *FDTD-generated UCAs corrected by their individual correction matrix* $\boldsymbol{C}^{-1}$ *obtained through Equations (4.9), (4.13) and (4.14). Chebyshev weights with -40dB SLL requirement are then applied to the corrected patterns. Patterns produced by the original FDTD model with no element displacements are compared to those of the FDTD models with element displacements.*

	1	2	3	4	5	6	7	8
1	0.0000	21.9498	40.9806	53.9429	58.0171	54.0310	41.6775	21.3873
2	21.9498	0.0000	22.1631	41.3527	53.3906	58.1782	53.7146	40.8922
3	40.9806	22.1631	0.0000	22.7423	41.1085	54.0690	58.2100	53.6407
4	53.9429	41.3527	22.7423	0.0000	21.9160	41.1865	53.4931	58.1249
5	58.0171	53.3906	41.1085	21.9160	0.0000	22.3511	40.6021	53.3764
6	54.0310	58.1782	54.0690	41.1865	22.3511	0.0000	21.7598	41.0470
7	41.6775	53.7146	58.2100	53.4931	40.6021	21.7598	0.0000	22.6034
8	21.3873	40.8922	53.6407	58.1249	53.3764	41.0470	22.6034	0.0000

(a) Actual array dimension

22.0779	40.7946	53.3008	57.6923

(b) Accurate array dimensions

	1	2	3	4	5	6	7	8
1	0.0000	-0.1281	0.1860	0.6421	0.3248	0.7302	0.8829	-0.6906
2	-0.1281	0.0000	0.0852	0.5581	0.0898	0.4859	0.4138	0.0976
3	0.1860	0.0852	0.0000	0.6644	0.3139	0.7682	0.5177	0.3399
4	0.6421	0.5581	0.6644	0.0000	-0.1619	0.3919	0.1923	0.4326
5	0.3248	0.0898	0.3139	-0.1619	0.0000	0.2732	-0.1925	0.0756
6	0.7302	0.4859	0.7682	0.3919	0.2732	0.0000	-0.3181	0.2524
7	0.8829	0.4138	0.5177	0.1923	-0.1925	-0.3181	0.0000	0.5255
8	-0.6906	0.0976	0.3399	0.4326	0.0756	0.2524	0.5255	0.0000

(c) Error

Nearest neighbour elements
Nearest but one elements
Nearest but two elements
Adjacent elements

Table 5.6: *Array 2 dimensions in mm.*

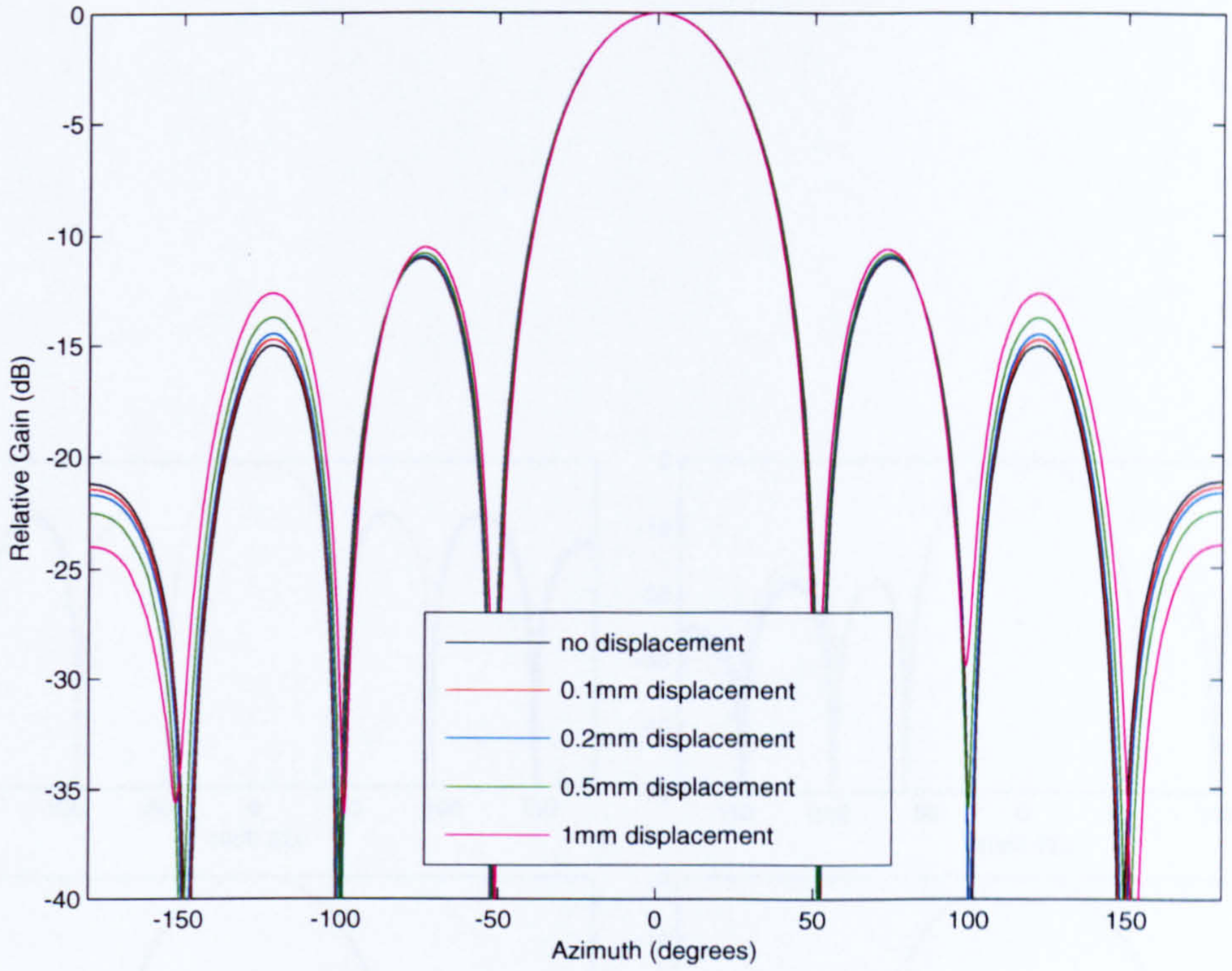

Figure 5.11: *Normalised Average correction matrix* $\boldsymbol{C}_{av}^{-1}$ *(Table 5.5) applied to FDTD-generated arrays with various displacements. No linear array weights are applied to the corrected patterns.*

The proposed design of $\mathbf{C}_{av}^{-1}$ is shown in Figure 5.15. The matrix involves eight 5-way splitters, 24 2-way splitters, and eight identical copies of weight functions A, B, C and D. Bearing in mind that the original correction matrix would have involved 64 unique amplitude and phase weights, the new method has cut the number of required amplitude and phase weights by 94%. Although the number of components needed in the matrix is still 64 (i.e. $N \times N$), in the new proposed design many of the elements are identical copies and therefore allowing for mass manufacture, cutting costs even further.

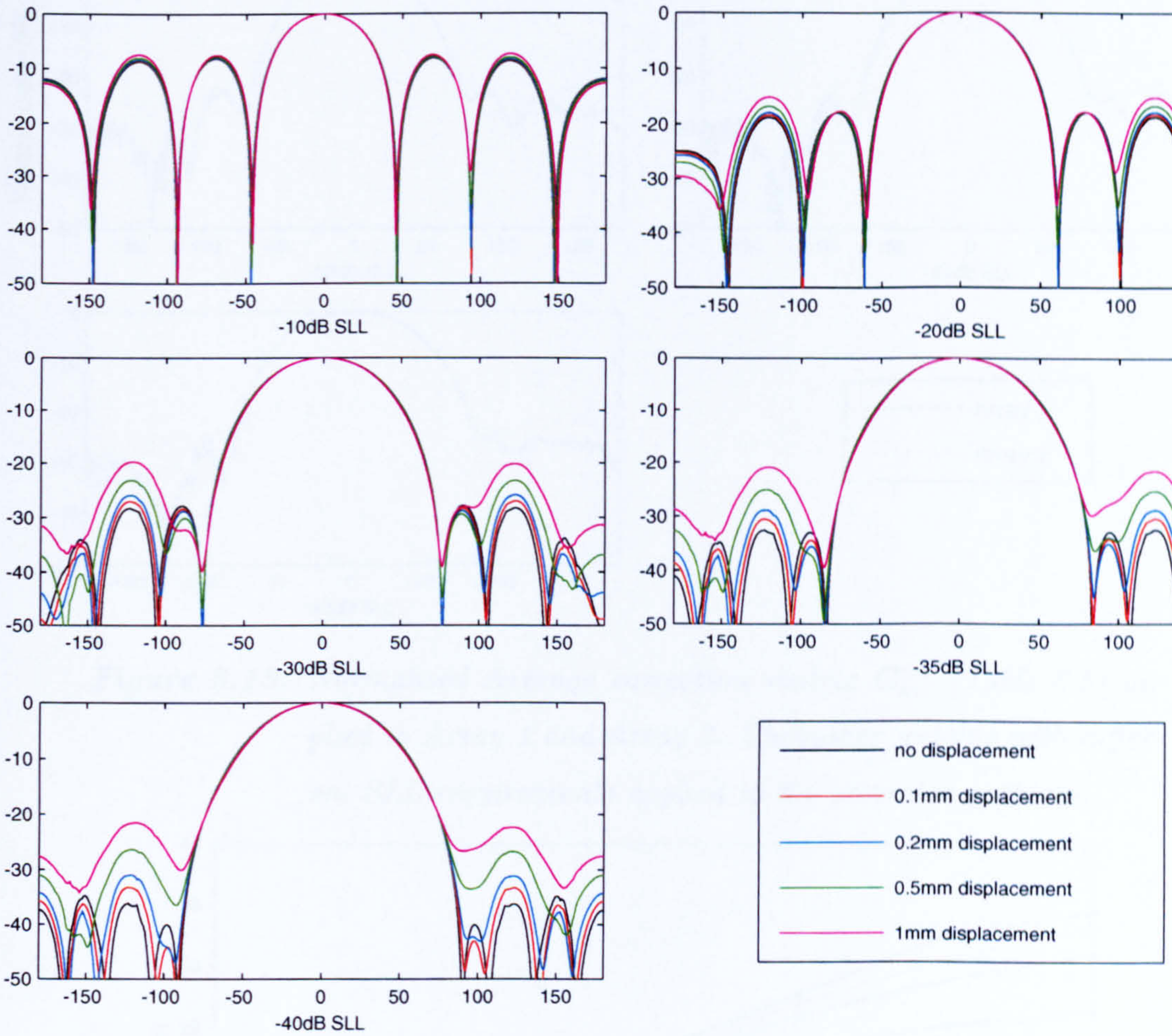

Figure 5.12: *Normalised Average correction matrix* $\boldsymbol{C}_{av}^{-1}$ *(Table 5.5) applied to FDTD-generated arrays with various displacements. Chebyshev weights with different SLL requirements applied to the corrected patterns.*

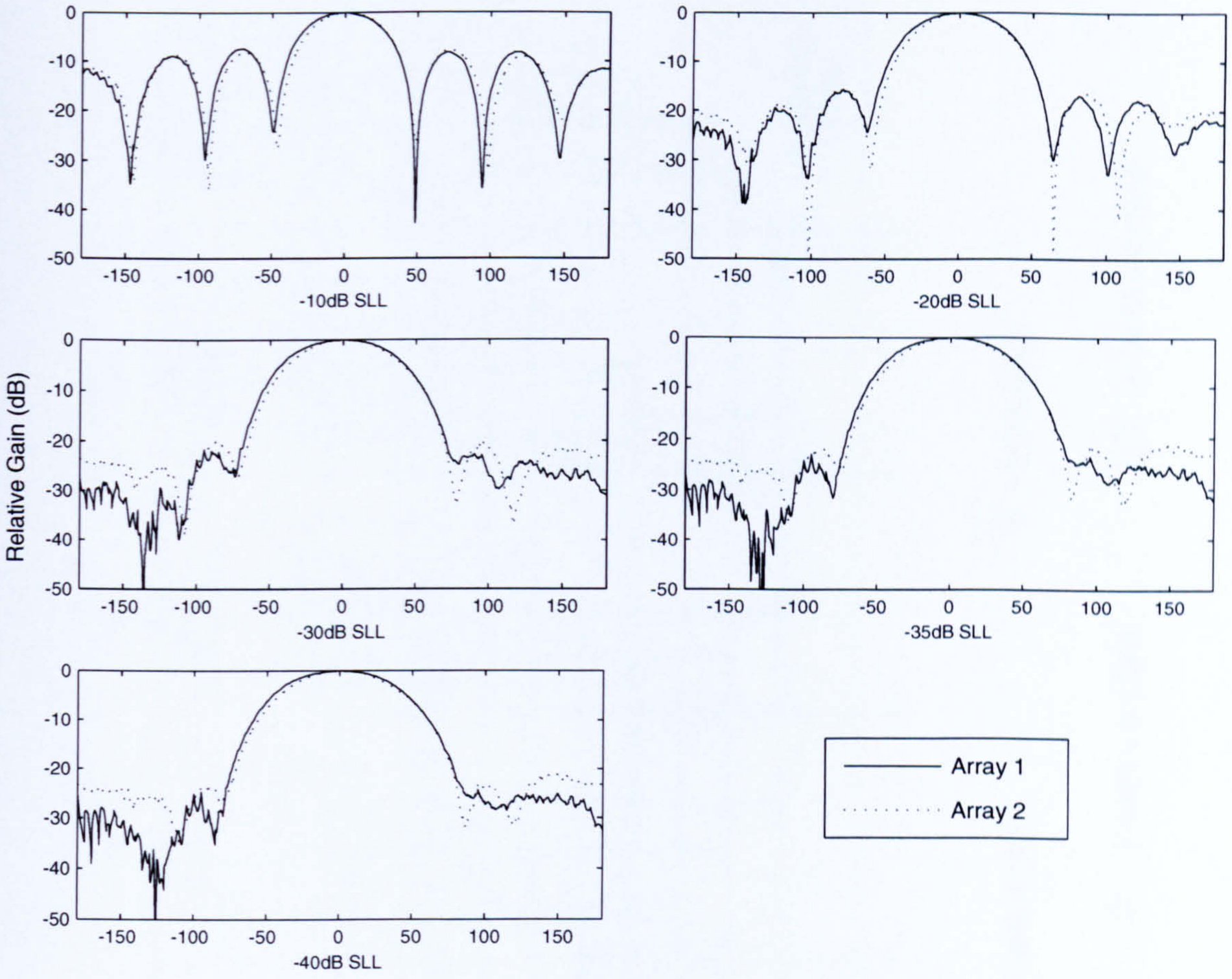

Figure 5.13: *Normalised Average correction matrix* $\boldsymbol{C}_{av}^{-1}$ *(Table 5.5) applied to Array 1 and Array 2. Chebyshev weights with different SLL requirements applied to the corrected patterns.*

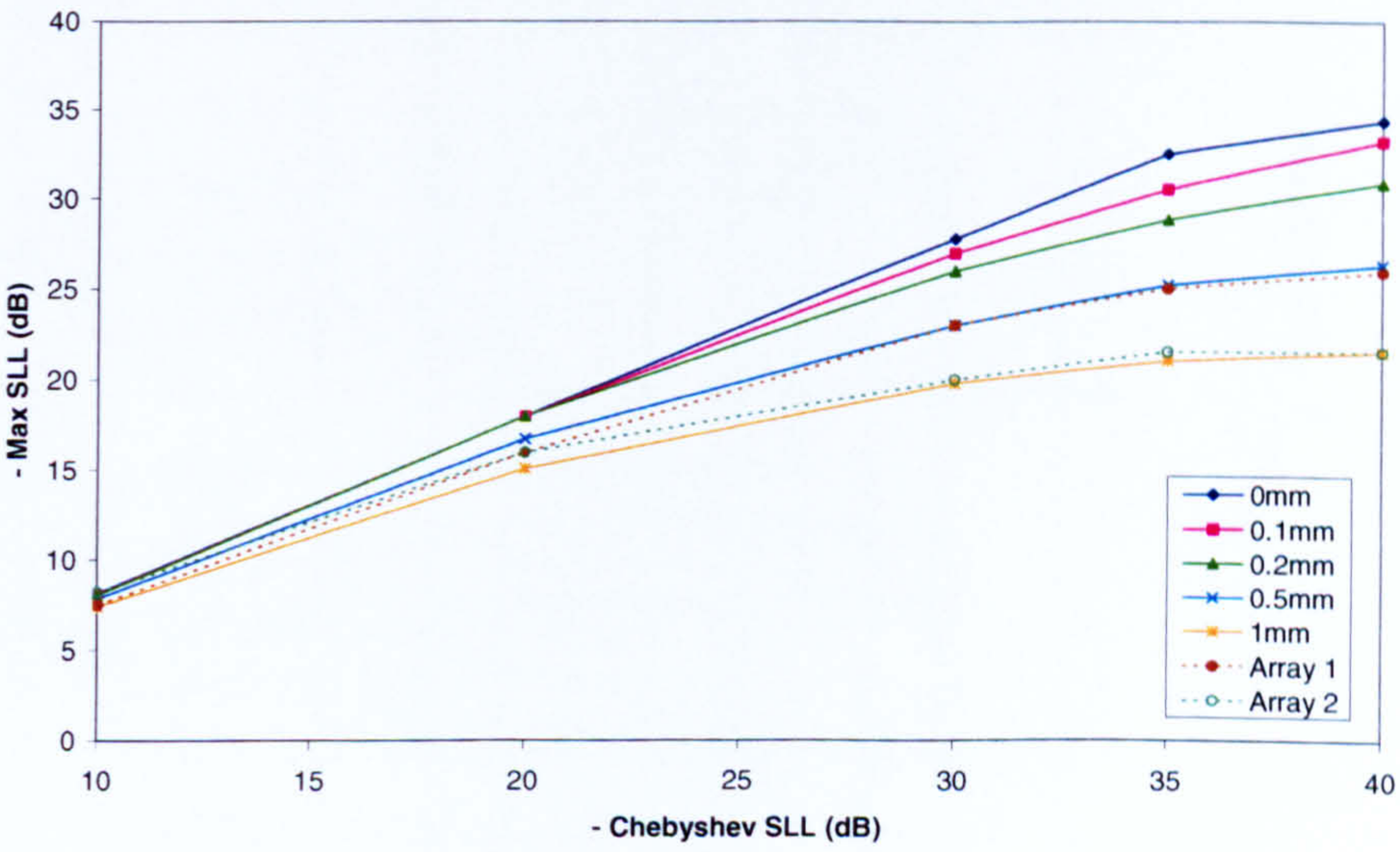

Figure 5.14: *SLL achieved by Array 1, Array 2 and the various FDTD-generated arrays when Chebyshev weights are applied, with the normalised average correction matrix resolution of between 0.01 and 0.0001.*

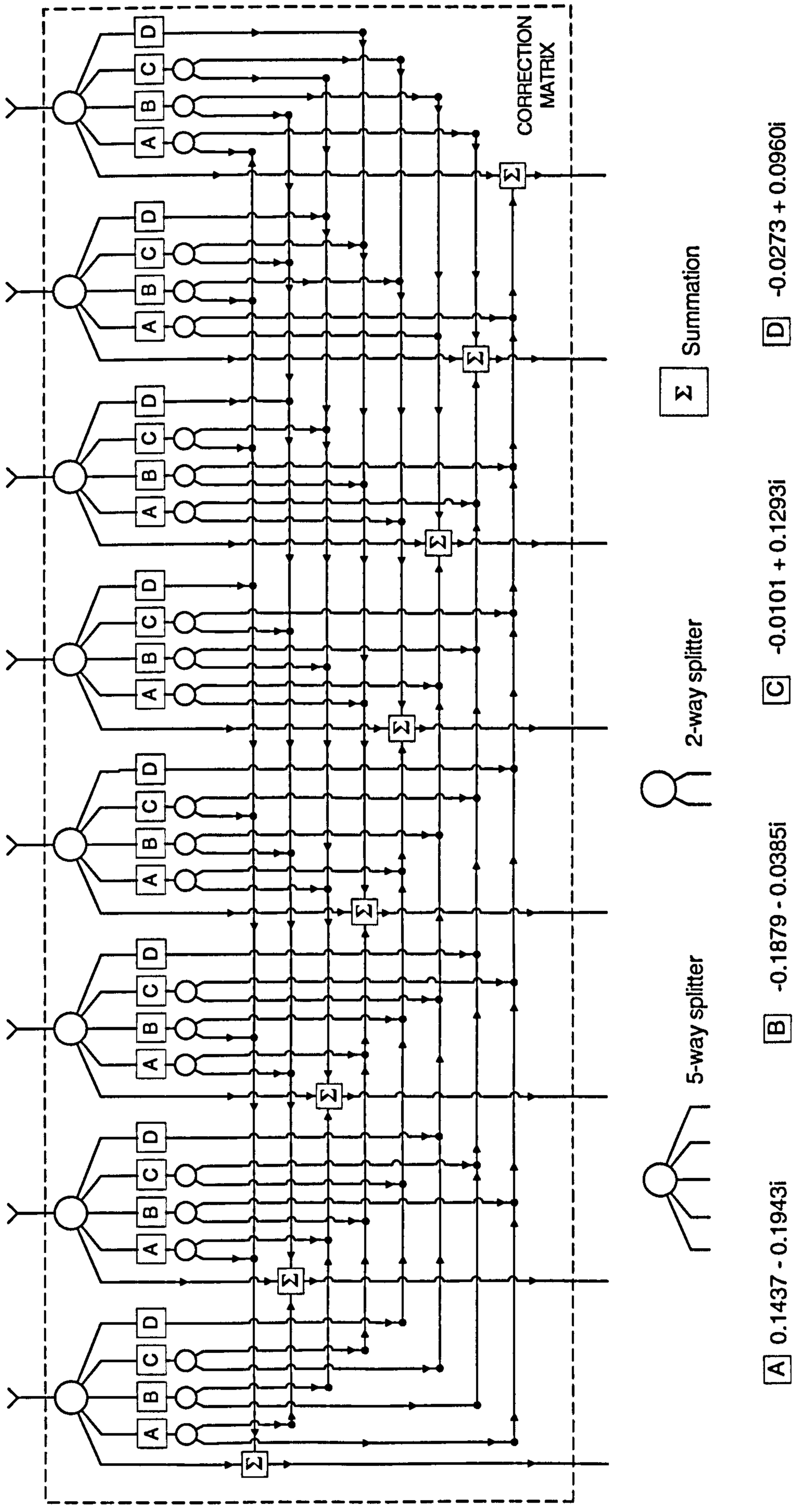

Figure 5.15: *Proposed correction matrix for 8-element UCA with $\lambda/2$ radius at 5.2GHz.* 134

5.6 Manufacturing Tolerance and Measurement Resolution

Thus far, it has been assumed that a resolution of 0.0001 is applicable for the correlation and correction matrices. However, it practice it is often not possible to produce with such accuracy. In order to investigate the level of accuracy needed for production of the proposed correction matrix $\mathbf{C}_{av}^{-1}$, array patterns are analysed while the values of $\mathbf{C}_{av}^{-1}$ are truncated to 1,2 and 3 decimal places, corresponding to 0.1, 0.01 and 0.001 resolution. These patterns are compared with those of the original 0.0001 resolution. It was found that the resulting patterns are identical for resolutions down to 0.01, hence the 0.001 has been omitted from Figure 5.16. In this illustration, the patterns of Array 1 with the corrected Butler matrix system with 10, 20, 30 and 40dB SLL with various resolutions are revealed. However, changes in SLL occurs when a 0.1 resolution is employed on the matrix. It is shown that a rise in SLL of $\approx 5dB$ is seen at this resolution.

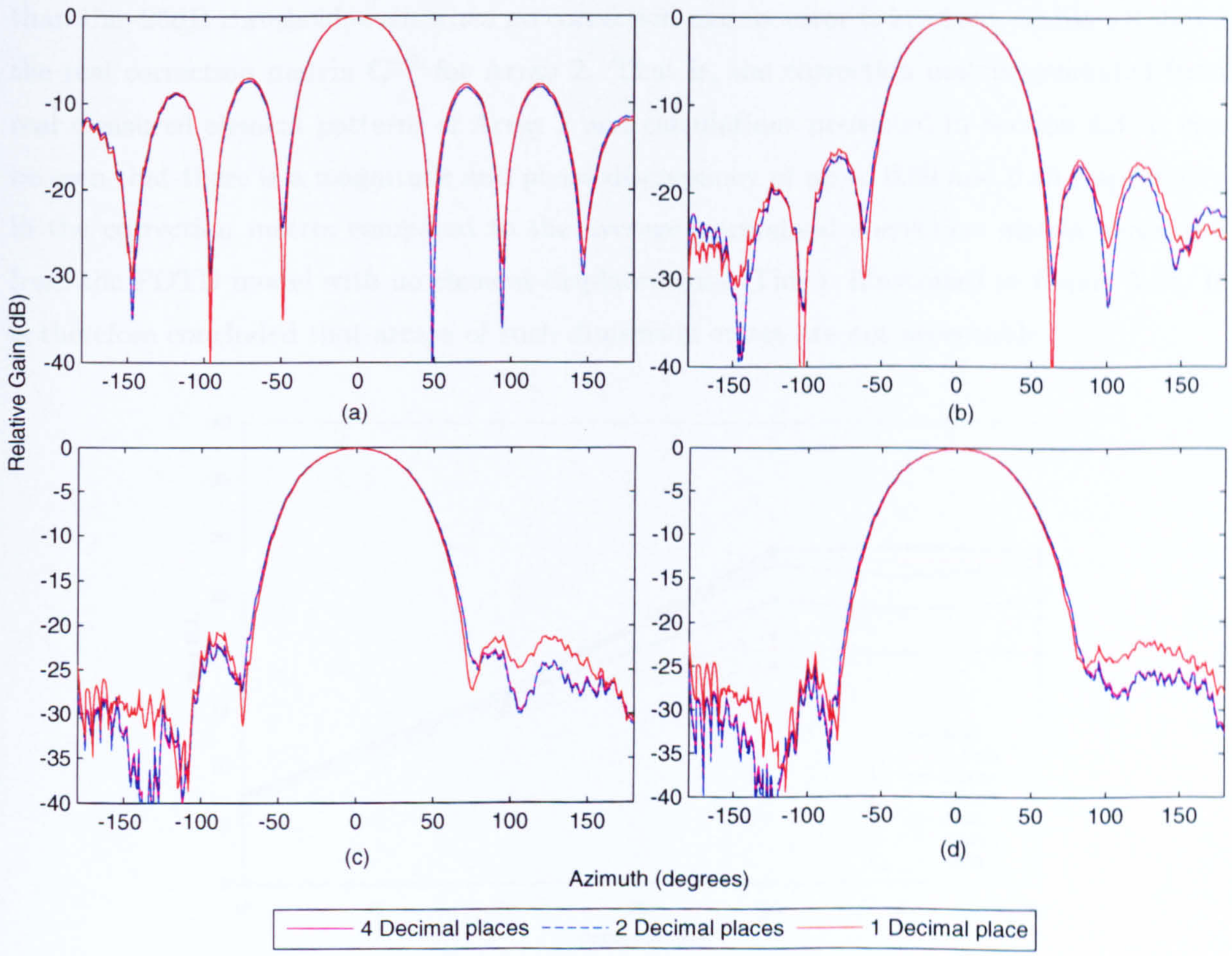

Figure 5.16: *Radiation patterns produced by Array 1 when Chebyshev weights are applied, with 0.1, 0.01 and 0.0001 resolutions of* $\boldsymbol{C}_{av}^{-1}$.

Figure 5.17 shows the SLL levels achievable by the different test arrays when different Chebyshev weights are employed. It is seen that in the case of the FDTD-generated arrays, when Chebyshev requirements beyond -30dB SLL are specified, the system fails to respond with lower SLL. In the case of the practical arrays, i.e. Array 1 and Array 2, this threshold level appears to be at -35dB SLL Chebyshev requirement.

Table 5.7 illustrates the amount of error that is acceptable in the production of the average correction matrix $\mathbf{C}_{av}^{-1}$, based on the variety of FDTD-generated arrays as well as the practical arrays, assuming an achievable SLL threshold of -25dB. The table summarises the fact that as the manufacturing error in terms of the array dimensions increases, the acceptable correction matrix error is reduced. Further, it is also shown that Array 1 performs similarly to the FDTD-generated array with 0.5mm element displacements. The worst of the FDTD models, i.e. that with 1mm element displacements, as well as Array 2 are marked *N/A* due to the fact that these arrays are not capable of producing SLL of equal or larger magnitude than the -25dB threshold, even when no correction matrix error is involved. Table 5.8 shows the real correction matrix $\mathbf{C}^{-1}$ for Array 2. That is, the correction matrix generated from real measured element patterns of Array 2 and calculations presented in Section 4.3. It can be seen that there is a magnitude and phase discrepancy of up to 0.09 and 0.43 respectively in the correction matrix compared to the average normalised correction matrix generated from the FDTD model with no element displacements. This is illustrated in Figure 5.18. It is therefore concluded that arrays of such dimension errors are not acceptable.

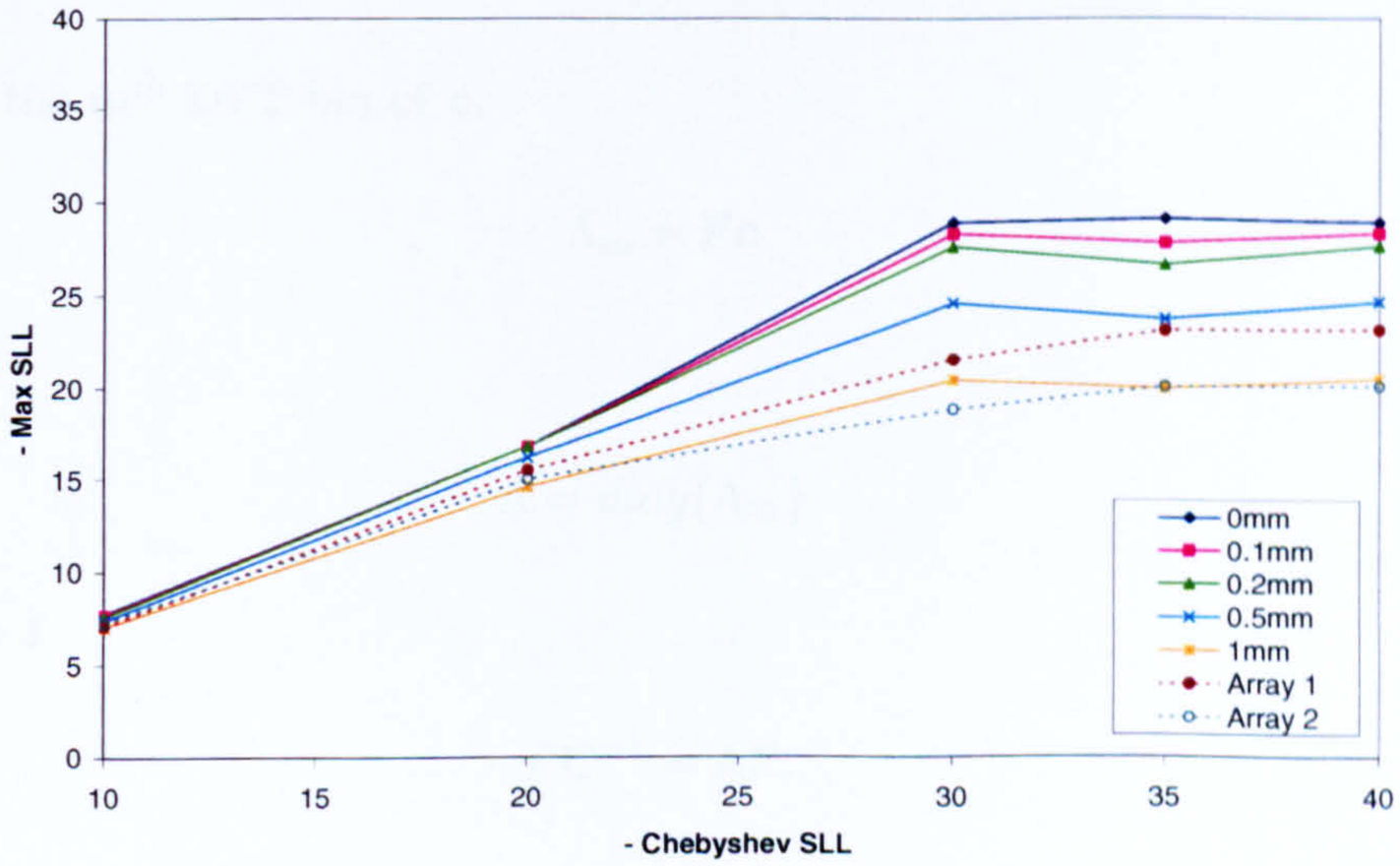

Figure 5.17: *SLL achieved when Chebyshev weights are applied to Array 1, Array 2 and the various FDTD-generated arrays, with resolution of* $\boldsymbol{C}_{av}^{-1}$ *limited to 0.1.*

		Tolerance
FDTD UCA models	No displacement	+/- 0.05
	0.1mm displacement	+/- 0.04
	0.2mm displacement	+/- 0.04
	0.5mm displacement	+/- 0.02
	1mm displacement	N/A[2]
Array 1		+/- 0.02
Array 2		N/A[2]

Table 5.7: Correction matrix tolerance for the different arrays, assuming a minimum achievable SLL of -25dB.

5.7 Correction Matrix Diagonalisation

As can be seen in Table 5.5, the proposed correction matrix $\mathbf{C}^{-1}$ is now *circulant*. That is, it is in the form of Equation(5.6) and can be defined by its first column $\mathbf{c} = [c_0, c_1, ..., c_{N-1}]^T$. It is shown in [20] that a circulant matrix can be diagonalised by pre- and post- DFT process. Hence:

$$\mathbf{C}^{-1} = \mathbf{F}^H \Lambda \mathbf{F} \tag{5.15}$$

where Λ_m is the m^{th} DFT bin of $\mathbf{c}$.

$$\Lambda_m = \mathbf{F}\mathbf{c} \tag{5.16}$$

and

$$\Lambda = diag\{\Lambda_m\}. \tag{5.17}$$

Since $\mathbf{F}\mathbf{F}^H = \mathbf{I}$,

$$\mathbf{F}\mathbf{C}^{-1} = \Lambda\mathbf{F}. \tag{5.18}$$

It can be concluded from Equations(5.15)-(5.18) that the $N \times N$ correction matrix in Table 5.5 can now be eliminated and replaced by a $(2M+1)\times(2M+1)$ diagonal matrix Λ. Therefore

[5]N/A: These arrays are not capable of producing SLL of equal or larger magnitude than the -25dB threshold, even with no correction matrix error involved.

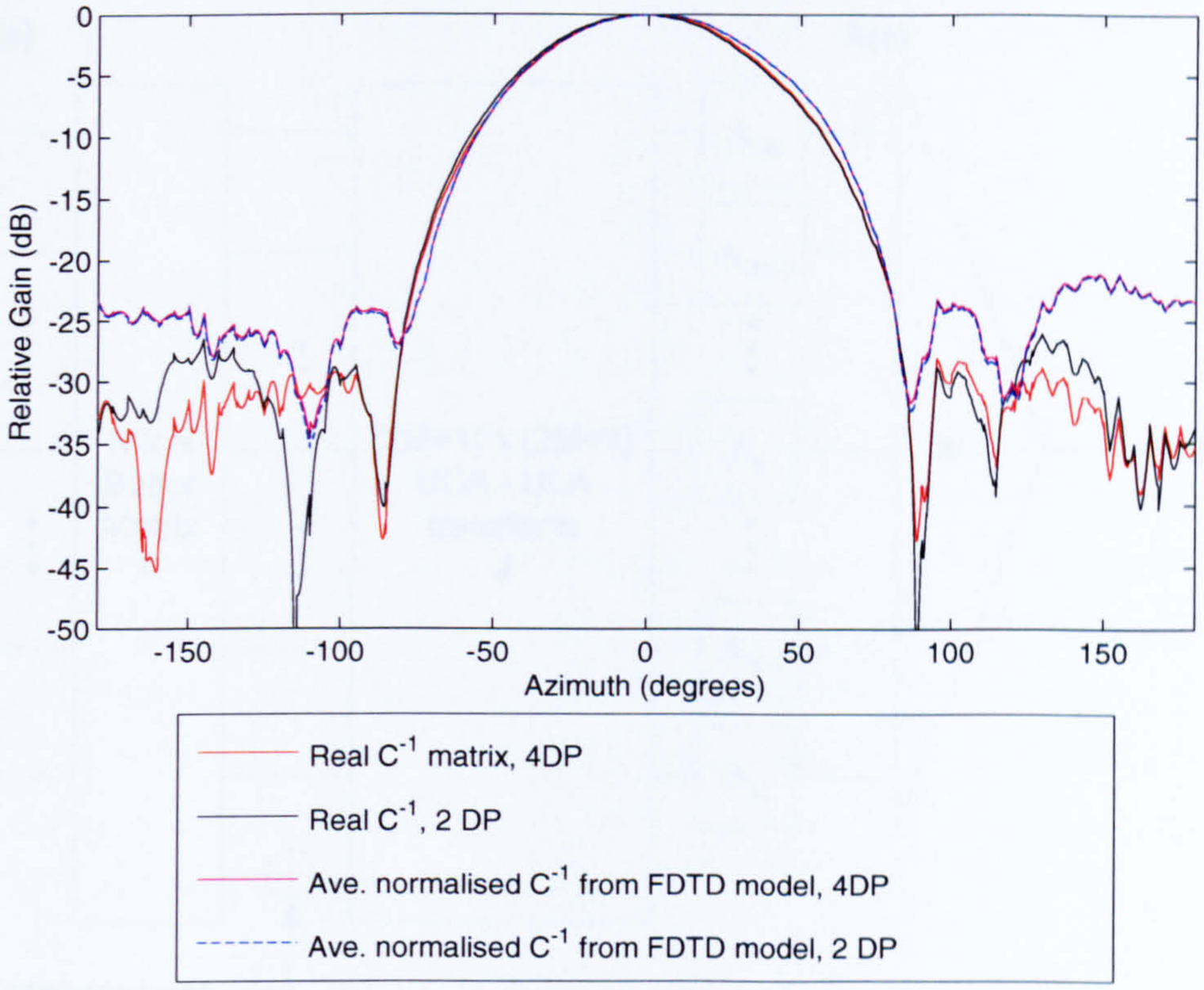

Figure 5.18: *Array 2 with specified -40dB Chebyshev SLL, with its real correction matrix shown in Table 5.8 and the average normalised correction matrix generated through the FDTD array model with no element displacements. Patterns are observed with both matrices correct to 2 and 4 decimal places.*

Equation 5.9 becomes

$$\tilde{\mathbf{A}}(\phi) \approx \mathbf{J}\Lambda\mathbf{F}\mathbf{A} \tag{5.19}$$

It should be noted that Λ is does not correspond to mutual coupling compensation. Derived from the values obtained for $\mathbf{C}^{-1}$, Λ corresponds to embedded pattern compensation. Although it does not include correction for element displacement, Λ includes compensation for the effects of scattering, ground plane effects as well as mutual coupling. When implemented, Λ corresponds to $2M+1$ amplitude and phase weights. Figure 5.19 illustrates the improved design of the corrected UCA-Butler matrix system.

Furthermore, it should also be noted that the application of Λ as oppose to the average $\mathbf{C}_{av}^{-1}$ does not affect the performance of the system in terms of the achievable SLL as well as tolerance. The proposed practical values of Λ_m for 8-element UCAs built as described in the first paragraph of Appendix D is shown in Table 5.9. These values have been normalised with respect to the centre value, hence no amplitude and phase compensation is needed at m=0.

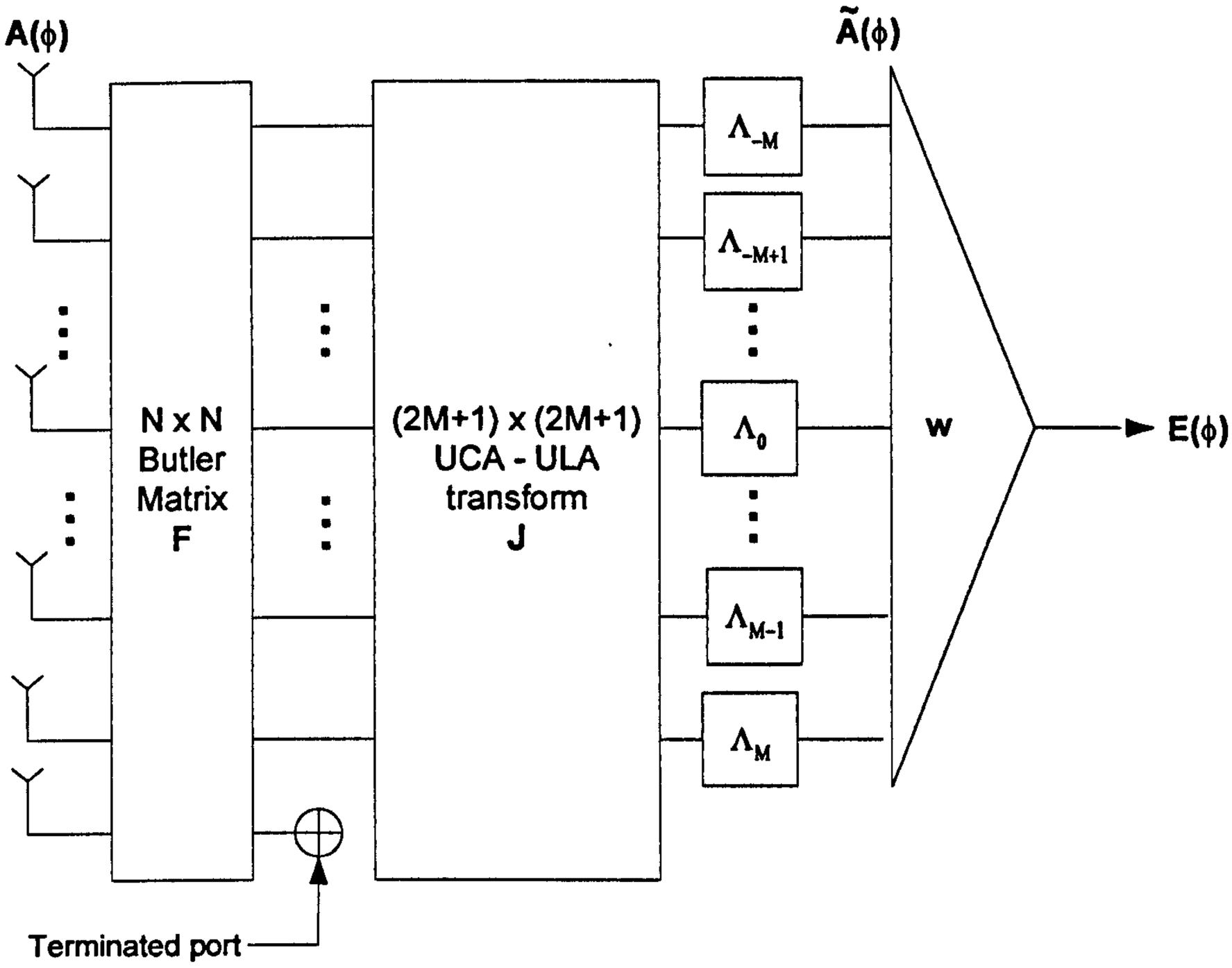

Figure 5.19: *Block diagram of the simplified UCA-Butler matrix system incorporating embedded pattern compensation.*

Further, it can be seen that there is a symmetry in the amplitude and phase compensations. Hence only M unique values are needed.

5.8 Discussion

Despite their promising abilities, circular arrays have received far less attention than their linear and planar counterparts. Limited studies and applications are available involving this array geometry. In many cases, circular array pattern synthesis requires complex signal manipulations as well as costly signal processing architecture.

This chapter takes a more detailed look at the use of Butler matrices for circular array pattern synthesis. Although the theory has been presented by Davies in [8], the amount of research and application of this method on a practical array has been limited. The subject is extended in this chapter where mutual coupling and other array imperfections are no longer assumed to be non-existent. As was revealed in the previous chapter, these effects influence and limit the performance of circular arrays, particularly at higher frequencies such as the frequency

of interest in the work presented in this thesis, which is 5.2GHz. At these frequencies, slight variations in the array antenna positioning could lead to significant variations in the array radiation patterns. This is evident in Figure 5.7.

Compensation for mutual coupling as well as other array imperfections is addressed in this chapter. A method proposed by Wax [7] includes compensation for both mutual coupling and array imperfections, unlike other mutual coupling compensations which rarely take other imperfections into account. A closer look into the results obtained by this method reveals that the array radiation patterns are greatly improved through the use of the correction matrix. Results in Figure 5.5 shows that this method, when used with the 8-element monopole test UCA and combined with Chebyshev windowing function, is capable of producing maximum SLL of $\approx -30dB$. However, it was also revealed that due to the non-identical element patterns and asymmetrical positions of the array elements, the correction matrix requires $N \times N$ individual phase and amplitude values.

In Section 5.5, four additional arrays are generated by the FDTD method and a more detailed look into the correlation and correction matrix is presented. It is shown that error in the element positions is reflected in the matrices as deviations from the initial values. This error is also visible in the element patterns as they become less identical as the error is increased. The section also illustrates how the correction matrix attempts to correct for the errors in the manufacturing accuracy of the array itself. However, it can be seen that for larger manufacturing errors, i.e. those beyond 0.2mm accuracy, the matrix struggles to perform its task, particularly when lower Chebyshev SLL is specified.

The matrices produced by the FDTD-generated models are however not directly comparable to those of the practical arrays. This is due to the fact that the practical arrays are also affected by other sources of error associated with the antenna measurements (Appendix A), which are not taken into account in the FDTD models. Nevertheless further analysis shows that the average normalised correction matrix obtained from the original FDTD model can still be used to correct the practical arrays. This yields maximum SLL levels of $\approx -25dB$ in the case of Array 1 and $\approx -20dB$ in the case of Array 2. Although this is $\approx 5 - 10dB$ lower than the non-simplified matrix, the simplified matrix for 8-element monopole UCA only consists of 8 identical copies of 4 different set of amplitude and phase weights, thus reducing the design and manufacturing cost.

Section 5.6 discusses the resolution needed in order to obtain the results presented in the

previous sections. It is revealed that assuming a minimum achievable SLL of -25dB, an accuracy of the order 0.01 ± 0.02 is needed for the correction matrix. Lower resolutions will affect the maximum SLL that can be achieved by the system.

This chapter has revealed through a variety of measurements, simulations and calculations a more in-depth view of the use of Butler matrix for UCA beamforming purposes. Practical issues are considered and error analysis presented, yielding proposed practical values for the correction matrix appropriate to use for an eight-element monopole UCA operating at 5.2GHz. Numerous findings presented in this chapter has led to the conclusion that for the particular type and operating frequency of UCA, a $\pm 0.2mm$ or $3.47 \times 10^{-3}\lambda$ limit to the amount of array manufacturing tolerance is essential in order to achieve a minimum SLL of -25dB.

Further investigations reveal that the average correction matrix C_{av}^{-1} can be reduced further due to its new circulant property. Simple matrix manipulation leads to a $(2M+1)\times(2M+1)$ diagonal matrix Λ following the Butler matrix, as a replacement of C_{av}^{-1}. Further, due to its symmetrical property, only 2 identical copies of M unique values are now needed for the compensation matrix Λ. Although the compensation matrix has lost its ability to correct for imperfections in the actual element positions[6], Λ still provides compensation for changes in the embedded element patterns due to scattering and mutual coupling effects while cutting manufacturing costs by $\approx 80\%$ and potentially cutting design costs by at least $\approx 95\%$ as the need for complex correction matrix is removed.

[6] as did C_{av}^{-1}

	1	2	3	4	5	6	7	8
1	1	0.2146	0.1889	0.1803	0.14	0.1527	0.2101	0.3342
2	0.2988	1	0.2423	0.1776	0.1415	0.171	0.1284	0.1933
3	0.2055	0.3188	1	0.2607	0.1871	0.1581	0.1468	0.1529
4	0.1455	0.2115	0.2745	1	0.2185	0.1624	0.1593	0.1352
5	0.1159	0.1195	0.1997	0.263	1	0.1983	0.1715	0.1322
6	0.1451	0.1625	0.1388	0.1817	0.3035	1	0.248	0.1706
7	0.1946	0.1473	0.1342	0.1359	0.2294	0.2926	1	0.2183
8	0.2582	0.1436	0.1548	0.1914	0.156	0.22	0.2996	1

(a) Amplitude

	1	2	3	4	5	6	7	8
1	0	-1.1162	-3.0766	1.6652	1.8742	1.5606	-2.9448	-0.6614
2	-0.7474	0	-1.2306	-3.0228	1.5014	1.8955	1.5892	-3.031
3	-3.1015	-0.7662	0	-1.0938	-3.1007	1.6807	1.9021	1.6739
4	1.4412	-2.9699	-0.9071	0	-1.2802	-3.1208	1.262	1.5651
5	1.6182	1.3329	-3.0419	-0.6685	0	-1.1024	-3.0873	1.236
6	1.2084	1.5514	1.1828	3.0594	-0.8494	0	-1.3566	-3.1201
7	3.1272	1.3257	1.856	1.5086	-3.1182	-0.7076	0	-1.1743
8	-1.3389	-3.1355	1.3165	1.6857	1.5355	3.1202	-0.9722	0

(b) Phase

Table 5.8: *Array 2 real correction matrix* $\boldsymbol{C}^{-1}$ *obtained from calculations based on Equations (4.9), (4.13), (4.14).*

	Amplitude	Phase
Λ_{-3}	1.02	0.55
Λ_{-2}	1.56	0.26
Λ_{-1}	1.56	-0.29
Λ_0	1.00	0.00
Λ_1	1.56	-0.29
Λ_2	1.56	0.26
Λ_3	1.02	0.55

Table 5.9: *Practical values for Λ_m for 8-element monopole arrays.*

References

[1] A.W.Rudge, K. Milne, A.D. Olver, and P. Knighet, Eds., "The Handbook of Antenna Design", vol. 1 and 2, Peter Peregrinus Ltd, London, UK, 1986.

[2] A.A. Oliner, R.G. Malech, "Mutual coupling in infinite scanning arrays", *Microwave Scanning Antennas*, R.C. Hansen, Ed. New York: Academic Pross, pp.195-335, 1966.

[3] D.F. Kelley, "Array antenna pattern modeling methods that include mutual coupling effects", *IEEE Transactions on Antennas and Propagation*, Vol. 41, No. 12, pp.1625-1631, December 1993.

[4] R.C. Hansen, "Planar arrays", in Rudge et al. [1].

[5] R.J. Mailloux, "Phased array theory and technology", *Proceedings of the IEEE*, Vol. 70, No. 3, pp.246-291, March 1982.

[6] D.M. Pozar, "The active element pattern", *IEEE Transactions on Antennas and Propagation*, Vol. 42, NO. 8, pp.1176-1178, August 1994.

[7] M. Wax, "Direction Finding of Coherent Signals via Spatial Smoothing for Uniform Circular Arrays", *IEEE Transactions on Antennas and Propagation*, Vol. 42, no. 5, pp613-620, May 1994.

[8] D.E.N. Davies, "Circular Arrays", in Rudge et all. [1]

[9] R.W.P. King, R.B. Mack, S.S. Sandler, "Arrays of cylindrical dipoles", Cambridge University Press, 1968.

[10] P.J. Wright, D.H. Brandwood, "Re-optimisation of linear and planar arrays with failed elements", *IEE 9th International Conference on Antennas and Propagation*, April 1995, pp.81-84.

[11] T.J. Peters, "A conjugate gradient-based algorithm to minimise the sidelobe level of planar arrays with element failures", *IEEE Transactions on Antennas and Propagation*, Vol. 39, No. 10, pp.1497-1504, October 1991.

[12] H. Steyskal, R.J. Mailloux, "Generalisation of an array-failure-correction method", *IEE Proceedings on Microwaves, Antennas and Propagation*, Vol. 145, Issue 4, pp.332 - 336, August 1998.

[13] A. Taskin, C.S. Gurel, "Antenna array pattern optimisation in the case of array element failure", *33rd European Microwave Conference*, Vol. 3, pp.1083-1085, October 2003.

[14] K. Awadalla, T. Maclean, "Input impedance of a monopole antenna at the center of a finite ground plane", *IEEE Transactions on Antennas and Propagation*, Vol. 26, Issue 2, pp.244-248, March 1978.

[15] Y. Rockah, P. Schultheiss, "Array shape calibration using sources in unknown locations-Part II: Near-field sources and estimator implementation", *IEEE Transactions on Acoustics, Speech, and Signal Processing*, Vol. 35, Issue 6, pp.724-735, June 1987.

[16] H.M. Aumann, A.J. Fenn, F.G. Willwerth, "Phased array antenna calibration and pattern prediction using mutual coupling measurements", *IEEE Transactions on Antennas and Propagation*, Vol. 37, No. 7, pp.844-850, July 1989.

[17] C. Balanis, *Antenna Theory: Analysis and Design*, 2nd edition, Wiley, 1998.

[18] K.R. Dandekar, H. Ling, G. Xu, "Experimental study of mutual coupling compensation in smart antenna applications", *IEEE Transactions on Wireless Communications*, Vol. 1, No. 3, pp.480-487, July 2002.

[19] A.D. Monk, M. Rayner, A.D. Olver, "A comparison of FD-TD and the method of moments to model electrically small antennas", *Antennas and Propagation Society International Symposium*, Vol. 1, pp.644-647, June 1995.

[20] R. Yarlagadda, B. Babu, "A note on the application of FFT to the solution of a system of Toeplitz normal equations", *IEEE Transactions on Circuits and Systems*, Vol. 27, pp.151-154, February 1980.

Chapter 6

Conclusions and Suggestions for Further Work

The wireless network has been and continues to be a growing industrial sector. As Wi-Fi and WiMAX are becoming ever more popular applications in the everyday market, today and more so future users will expect greater coverage to enable them to connect to the internet wherever they go. This, coupled with the limited bandwidth resources available, in turn presents a challenge for the industry to provide a cost-effective solution. Wi-Fi and WiMAX providers are finding increasing needs for effective AP systems that are also affordable in order for them to be able to install enough to provide the coverage in demand.

It is now a common knowledge that antenna arrays present a capacity enhancement solution. Provided that wanted and interference signals are spatially separated, pattern control achieved through the use of antenna arrays maximises wanted signal whilst reducing sensitivity to interference. Linear arrays have had their fair share of research and their applications are common feature to wireless networks. In the case of cellular networks, tri-sector base stations involving three linear arrays arranged in a triangular configuration are common place and have proven to be sufficient. However, in the case of Wi-Fi applications where centrally located access points are desirable, circular arrays present an attractive solution with their ability for 360^o azimuth coverage. For this reason, studies presented in this thesis have been based on this type of array architecture.

In order to validate theoretical results and aid with further analysis for embedded pattern compensation, two 8-element directional patch UCAs, two 8-element monopole UCAs, and five 8-element FDTD monopole UCA models have been constructed. These provided the experimental valuations that are currently very limited in circular array literature.

In this chapter, results and findings of the research described in this thesis are put together. The promise of 360° azimuth coverage earns circular arrays the attention that they have been lacking. Various UCA theories are put to the test with measured data. Pattern compensation is addressed and a proposed novel solution is presented.

6.1 Discussion

6.1.1 Beam Cophasal Excitation

The first UCA pattern synthesis technique under evaluation in this thesis was the Beam Cophasal excitation, which is perhaps the simplest form of UCA pattern synthesis.

Through rigorous simulations using ideal UCA patterns, it was found that for the case of discrete monopole UCAs, a maximum radius of $R = \frac{N\lambda}{16}$ is needed in order to produce a beam pattern that is the shape of the $J_0(x)$ distribution with decaying sidelobe pattern and maximum sidelobes occurring directly on either side of the main beam peak. This was shown in Figure 3.2. This is in contrary to Davies' theory [2] that states that the maximum radius for this Beam Cophasal excitation should be $R = \frac{N\lambda}{4\pi}$, as Davies' theory is based on the assumption that the UCA includes a large number of elements. However, when the technique was applied to real measured data in Chapter 4, it was apparent that even when a radius of $R = \frac{N\lambda}{16}$ was used in the construction of the practical array, the resulting pattern did not possess the decaying sidelobe patterns (Figure 4.9). Experimental evaluations showed that when directional elements were used in the array, there were significant differences in the shape of the resulting pattern when they were rotated around the azimuth angles (Figure 4.11(a)). The practical arrays used in the evaluation, which include manufacturing and measurement imperfections as well as element interactions, were not taken into account in the theory. In order to overcome some of these effects, conjugate weights in equation (3.5) may be used instead of the ideal phase weights described by Davies. This resulted in more even beam widths when they are rotated along the azimuth plane (Figure 4.11(b)).

Results revealed that while the Beam Cophasal technique seems low-cost at first glance due to its low complexity, when element interactions and other array imperfections are involved, conjugate weights are needed in order to account for these effects. This in turn increases costs as it becomes necessary for the individual element patterns to be measured. Figure 4.11(b) also suggested that in the case of 8-element directional UCA, a maximum sidelobe level (SLL) of $\approx -12dB$ was achieved. Furthermore, rotation of the beam pattern involves adjusting both the amplitude and phase weights. Considering the limited SLL that can be achieved, this technique does not seem to be ideal as a low-cost solution.

6.1.2 Phase Mode Excitation

The next and perhaps most popular excitation technique for UCAs is the Phase Mode Excitation, as described in Section 3.1.2. The technique is based upon the application of spatial FFT on to the array pattern in order to transform it to a *virtual array* that is amendable to spatial smoothing. The main advantage of this technique is that any ULA weighting functions can now be applied to the virtual array. Another advantage of the virtual array is that rotation of the beam pattern can be performed by simply applying progressive phase shift to the beam pattern.

6.1.2.1 Butler Matrix for UCA

Davies [2] and Wax [3] suggests that Phase Mode Excitation can be realised through the use of Butler matrix (Section 2.9). The matrix provides the correct array excitation for spatially orthogonal set of n possible phase modes. However, the size of Butler matrices are limited to BxB where $B = 2^n$ and n is an integer, whereas the total number of modes in Phase Mode excitation is $2M + 1$ where M is an integer and represents the highest mode that can be excited. Therefore one of the Butler matrix port has to be terminated as only $B - 1$ output ports are utilised. The choice of port to be terminated is irrelevant due to the symmetrical property of UCAs.

6.1.2.2 UCA Elements and Dimensions

Simulations in Section 3.2.3 illustrated that the use of larger number of elements for Phase Mode excitation produced beam patterns that were better resemblance to the *sinc* function produced by a ULA. It was shown in Section 3.2.1 that an optimum radius of $R_{opt} = \frac{N\lambda}{16}$ should be used in order to obtain patterns that resemble the $J_0(x)$ function that has decaying sidelobes with the highest sidelobe level occuring directly on either side of the main beam. Figure 3.4 showed that although radii $R < R_{opt}$ also produces $J_0(x)$-like patterns, the pattern produced by $R = R_{opt}$ exhibited lower SLL. In terms of choice for number of elements, Figure 3.7 showed that the SLL pattern produced by an 8-element UCA was $\approx 5dB$ higher than that of a 16-element UCA.

Further examinations with ideal directional and omnidirectional UCAs revealed that the SLL produced by a 16-element directional UCA without any additional ULA weights was $\approx 8dB$ higher than its omnidirectional counterpart. There was also a discrepancy of $\approx 15dB$ in

terms of the front-to-back ratio. This is in agreement to Davies' suggestion that directional elements can not be used to relax the distortions caused by inter-element spacing. It should be noted at this point that shadowing effect occurs when directional elements are in place as the ground plane used for mounting the elements would have to be cylindrical in shape. Hence contribution from the back elements is lost.

The ideal cases were put to the test when 8-element vertical patch and monopole UCAs as well as an FDTD model of an 8-element monopole UCA (Section 4.1) were used to verify the theoretical findings. Figure 4.12 showed that there was a $\approx 5dB$ difference in the pattern produced by the directional array compared to the ideal case in terms of the front-to-back ratio. There was also a rise in the SLL directly on either side of the main beam due to mutual coupling[1]. When the 8-element monopole array and its FDTD model were employed, the patterns produced front-to-back ratios that were respectively $\approx 10dB$ and $\approx 5dB$ higher than the ideal case. The levels of the first sidelobe were also $\approx 7dB$ and $\approx 3dB$ higher compared to the level produced by the ideal array.

6.1.2.3 Chebyshev weighting for UCA

Performance of the practical arrays was evaluated further by applying sets of Chebyshev weights in addition to the phase mode excitation in order to find the lowest achievable SLL. It was found that the directional array used in this evaluation was capable of producing SLL up to $\approx -15dB$. In the monopole cases, the practical array produced up to $\approx -12dB$SLL and the FDTD model produced up to $\approx -15dB$ SLL. Beyond these threshold, SLL ceases to decrease any further as the Chebyshev SLL requirement was increased.

Although a variety of ULA weighting techniques are available, only Chebyshev weights were used throughout Chapters 3, 4 and 5. It should be noted that the virtual array patterns are amendable to other ULA weights. Chebyshev weights in particular were chosen since SLL can easily be specified and Chebyshev weights produces the narrowest possible beamwidth for the required SLL. Lowering the Chebyshev requirement to a point where beam patterns cease to respond provides a measure for the maximum achievable SLL.

The previous exercise proved that ULA weighting function can be applied to UCAs with Phase Mode excitation, as it was seen in Figures 4.13 and 4.15 that increasing the Cheby-

[1]The same trend was seen in the case of practical monopole array, as shown in Figure 4.3

shev SLL requirement resulted in lowering of the resulting SLL. However, it is evident that the performance of the practical and FDTD model arrays were relatively poor compared to the ideal case where much lower SLL was achievable. This is a result of the fact that the practical arrays only employ 8 elements while the Phase Mode theory is based on the assumption of continuous UCA. Another important factor that is not taken into account in Davies' Phase Mode theory is mutual coupling, which is unavoidable in practical cases.

Theories and investigations regarding the array geometry has led to the conclusion that for low-cost antenna solution for Wi-Fi applications, an eight-element monopole UCA with radius $R = R_{opt}$ should be used. This is supported by the fact that:

- Larger numbers of elements would incur added costs as the Butler matrix needed for Phase Mode excitation becomes more complex.

- Chapter 3 revealed that the use of directional elements imposes higher-order distortion terms which causes further deviation in the resulting pattern from the intended *sinc* envelope. Furthermore, Phase Mode pattern synthesis for directional UCAs require that each individual element patterns be known, which could be costly and time consuming if multiple production is needed. The choice in element type was supported by the fact that only a 3dB improvement was seen when the practical 8-element directional UCA was employed, compared to the performance of the practical 8-element monopole UCA.

6.1.3 Element Interactions and Array Imperfections

Figures 4.3 and 4.4 summarised the fact that even when monopole elements were used in the array, element interactions as well as the element positions in the array affect the element patterns. The patterns, otherwise uniform in magnitude, now include peaks and troughs due to these effects. The effects of element interactions and other array imperfections were addressed in Chapter 5. Additional UCA FDTD models constructed with random element displacements revealed that the slightest imperfection in the UCA manufacture creates an impact to the element patterns (Figure 5.7).

The embedded pattern compensation presented in Chapter 5 is based on compensation technique proposed by Wax [3]. Promising to simultaneously compensate for mutual coupling as well as other array imperfections through the use of a simple $N \times N$ correction matrix $\mathbf{C}^{-1}$, this technique seemed very attractive. Figure 5.5 illustrated that by using this technique together with the Butler matrix excitation, maximum SLL levels of $\approx -30dB$ (produced by the 8-element monopole UCA) and $\approx -35dB$ (produced by the FDTD model) were achievable.

This is 13-18dB lower than the maximum SLL achieved without the correction matrix $\mathbf{C}^{-1}$. Figure 5.9 and 5.10 also illustrated that the matrix attempts to correct for the dimension imperfections in the array as the beam patterns of the FDTD models with displaced elements attempt to imitate the behaviour of the model with perfectly placed elements.

However, further examination into the correction matrix $\mathbf{C}^{-1}$ revealed that the matrix involves $N-1 \times N$ unique amplitude and phase values (Figure 5.2). For an 8-element array, 56 different amplitude and phase compensations are needed in order to correct the imperfections in the array. This would obviously make the matrix difficult to manufacture, not to mention the high cost. Furthermore, a unique matrix would be needed for every single array. Therefore, if this technique was to be employed the correction matrix has to be simplified. Based on this finding, further research was carried out in attempt to simplify the correction matrix.

As $\mathbf{C}^{-1}$ is highly dependent upon the correlation between elements in the array, it was revealed that ideally, the matrix should only involve eight identical sets of three different amplitude and phase elements and four identical sets of the fourth amplitude and phase element, each corresponding to interactions between the nearest neighbour, nearest but one neighbour, nearest but two neighbour, and adjacent elements. A proposed correction matrix (Table 5.4) was extracted from the initial FDTD model with no element displacement. The correcting values in this matrix were then normalised and averaged along the diagonals (according to the colour code) to obtain a matrix of the format described above(Figure 5.5). A proposed design of the average correction matrix $\mathbf{C}_{av}^{-1}$ was shown in Figure 5.15, where through the use of 5-way and 2-way splitters, the required amplitude and phase weights were cut further to only 8 identical sets of four different amplitude and phase weights.

Figures 5.11 and 5.12 illustrated the behaviour of the displaced FDTD models compared to the model with perfectly placed elements, when $\mathbf{C}_{av}^{-1}$ and uniform as well as Chebyshev weightings were applied. It is evident that as the element displacements increase in magnitude, the discrepancy of achieved SLL between the patterns produced by the models with displaced elements and those produced by the model with perfectly placed elements increased. Figure 5.14 illustrated the SLL achieved by the FDTD models as well as the practical arrays when different Chebyshev SLL requirements were imposed. It is evident that up to Chebyshev SLL requirement of -20dB the real achieved SLL are approximately linearly dependent on the Chebyshev requirement. Beyond this point, the gradients decrease at different rates according to the magnitude of element displacements.

Figure 5.16 illustrated the response of the practical 8-element monopole UCA (Array 1) when different degrees of resolution is imposed. It was concluded that a resolution of 0.01[2] is needed in $\mathbf{C}_{av}^{-1}$ in order to achieve the optimum results. Table 5.7 summarised the amount of tolerance acceptable for the different FDTD models as well as the practical arrays, assuming a maximum achievable SLL of at least -25dB. This, coupled with numerous findings throughout Chapter 5, has lead to the conclusion that a manufacturing tolerance of up to $\pm 0.2mm$ or $3.47 \times 10^{-3}\lambda$ is acceptable in the construction of 8-element monopole UCA.

The proposed design for $\mathbf{C}_{av}^{-1}$ (Figure 5.15) promised low-cost manufacture compared to the original correction matrix proposed by Wax [3]. The matrix can be constructed of identical copies of only 6 different components. However, further research revealed that due to its *circulant* property, the average correction matrix can now be diagonalised through a DFT transform of the contents of its first column. This yielded a much simpler compensation matrix Λ which is diagonal and symmetrical about the center of the diagonal, as shown in Table 5.9. Hence once normalised with respect to the symmetrical point, the matrix can be easily employed through the use of two identical sets of $\frac{N}{2}$ different amplitude and phase weights.

Perhaps the most valuable result of the matrix simplifications is the fact that provided they are manufactured within the tolerance limit in Table 5.7, the matrix are applicable to any 5.2GHz monopole UCA of similar material to Array 1, with radius $R = R_{opt}$, ground plane radius of 10λ. In other words, the new method allows for mass manufacture. It should also be noted that although experimental evaluations presented in this thesis is based on 5.2GHz operating frequency, the same technique can be applied to any other frequencies simply by obtaining the equivalent matrix through an FDTD model tailor-made for the frequency of interest.

Overall, studies presented in this thesis has brought about a deeper understanding of UCAs through a series of pattern synthesis using ideal and measured patterns. Results have shown that the UCA technology which has often been seen as a complex technology can be used for low-cost applications. FDTD modeling has aided to the formulation of practical values applicable to practical UCAs, as well as definitions for manufacturing accuracy needed in order to achieve a desirable beam pattern. SLL and beamwidth control has been made possible through the use of Butler matrix and simple amplitude and phase weighting network. The compensated UCA Butler matrix system proposed in this thesis can be deployed in Wi-Fi

[2]Bearing in mind that the correction matrix has been normalised such that the maximum value is 1.

applications either on its own at the access point as a SIMO system, or in a pair to complement a MIMO system. Furthermore, the vast range of ULA pattern synthesis methods currently available, ranging from simple to complex algorithms, can be applied to the system as desired, extending the coverage from $-90^o \geq \phi \geq 90^o$ to $-180^o \geq \phi \geq 180^o$.

6.2 Future Work

The work presented in this thesis has opened up a new door into the understanding of UCAs, extending on the limited knowledge presently available in literatures. However, there are several areas beyond the scope of this thesis that would enhance the understanding of UCA behaviour.

An obvious extension to the work presented in this thesis would be the physical realisation of the Butler matrix as well as the compensation matrix Λ. While some of the array data used for experimental evaluations are measured data, practical implementation of the beamforming system would yield further errors which may cause further complication to the design due to effects such as internal coupling and losses. The effects of these errors on the overall performance of the beamforming system would certainly be of interest. In addition, indoor channel measurements using the proposed system would be beneficial in order to analyse the system performance within a real environments. Capacity and efficiency benefits can also be evaluated. Full system tests involving the practical array and 802.11a/g modems could also be performed in order to evaluate its performance under the WLAN application.

While the behaviour of the UCA has been analysed in terms of radius and number of elements under the ideal case, experimental results obtained through the use of practical arrays would provide more valuable insights. As can be seen in Section 4.2, the optimum value found through simulations of ideal UCAs may not necessarily hold when practical arrays are utilised. Research presented in this thesis has been based on 2D azimuth pattern synthesis. However, as WLAN APs would generally be placed on ceilings and other high places, elevation and 3D synthesis would be beneficial as there is very limited literature in these areas. 3D data is easily measured as well as obtained from the FDTD model used in Chapters 4 and 5. However it should be noted that the run-time for 3D model would be far larger as near-to-far field transformation would be required for both azimuth and elevation plane, hence increasing the computational requirements. Most UCA elevation literature are based on adaptive algorithms for DoA estimation [4] - [6]. Hilton et al [7]- [8] suggest that measured

correlation values are lower than expected at smaller element separations due to distortion from the neighbouring elements on a linear array. A similar analysis involving a UCA would be beneficial. As seen in Chapter 5, the proposed method of mutual coupling compensation is dependent upon the pattern correlations between elements in the array.

Having analysed the UCA behaviour for different radius, element type and element number, another variable to be investigated would be the ground plane size. Ideal theoretical arrays assume infinite ground plane. However, this is not the case in practice. [10] suggests through a series of simulations and measurements that a reduction in the ground plane size causes an increase in the back lobe elevation radiation. It should be noted that the choice of ground plane size should take the intended mounting position into account. Given that the intended application of the work presented in this thesis is mostly as indoor wireless APs, a large ground plane size could be unattractive unless the antenna is mounted on a ceiling. When the antenna is mounted on a ceiling, the shielding provided by a large ground plane would avoid noticeable changes in the antenna radiation patterns. An antenna with a smaller ground plane would be more prone to effects caused by reflections from the mounting structure (for example, the ceiling). In turn, this would affect the element radiation pattern and hence the suggested compensation matrix would cease to be valid. The size and effects of the ground plane should be analysed in order to determine the suitable ground plane radius which takes into account the intended mounting position.

[11] presents an alternative to wire monopole for linear array elements in the form of electrically-small conformal elements of annular slot antennas operating at 'DC' mode. Designed to be resonant at 2.03GHz and 10MHz bandwidth at -10dB, the annular slot presented in this paper are fed by a stripline-feed which is screened in order to reduce unwanted coupling from the RF front-end. Results from measured pattern, input response and directivity analysis reveal that this type of array is similar in radiation pattern and directivity compared to a conventional wire monopole array. However, the significant advantage of the annular slot array is the notable decrease of $\approx 6-9dB$ in mutual coupling. Given the radiation properties of the annular slot, it should be readily applicable to the pattern synthesis method of interest in this thesis. Due to the size of the annular slot, particularly when scaled down to operate within the 5GHz frequency range, it may even be possible to deploy annular slot arrays within MTs for MIMO diversity.

References

[1] A.W. Rudge, K. Milne, A.D. Olver, and P. Knight, Eds., "The Handbook of Antenna Design", vol. 1 and 2, Peter Peregrinus Ltd, London, UK, 1986.

[2] D.E.N. Davies, "Circular Arrays", in Rudge et all. R1

[3] M. Wax, "Direction Finding of Coherent Signals via Spatial Smoothing for Uniform Circular Arrays", *IEEE Transactions on Antennas and Propagation*, Vol. 42, no. 5, pp613-620, May 1994.

[4] P. Ioannides, C.A. Balanis, "Uniform circular arrays for smart antennas", *IEEE Antennas and Propagation Society International Symposium*, Vol. 3, pp.2796-2799, June 2004.

[5] C. Li, X-C. Xiao, "Performance study of 2D DOA estimation using UCA with five sensors", *IEEE 2002 International Conference on Communications, Circuits and Systems and West Sino Expositions*, Vol. 2, pp.1012-1016, Vol. 2

[6] M. Pesavento, J.F. Bohme, "Direction of arrival estimation in uniform circular arrays composed of directional elements", *Sensor Array and Multichannel Signal Processing Workshop Proceedings*, pp. 503-507, August 2002.

[7] I.J. Craddock, G.S. Hilton, P. Urwin-Wright, "An investigation of pattern correlation and mutual coupling in MIMO arrays", *IEEE Antennas and Propagation Society International Symposium*, Vol. 2, pp.1247-1250, June 2004.

[8] G.S. Hilton, P.R. Urwin-Wright, I.J. Craddock, "Full radiation pattern measurements of antenna arrays to obtain accurate pattern correlation levels for use in MIMO system performance", *IEE Antenna Measurements and SAR*, AMS 2004, pp.83-86, May 2004.

[9] S. Collins, Y.M.M. Antar, "Antenna with a reduced ground plane size", *IEEE Antennas and Propagation Society International Symposium*, Vol. 1, pp.6-9, June 2002.

[10] C. Phongcharoenpanich, S. Suriya, T. Lertwiriyaprapa, P. Ngamjanyaporn, M. Krairiksh, "Analysis of circular array of monopole on the ground plane radiating linearly polarized conical beam for wireless LAN applications", *5th International Symposium on Antennas, Propagation and EM Theory Proceedings*, ISAPE 2000, pp.646-649, August 2000.

[11] P.R. Urwin-Wright, G.S. Hilton, I.J. Craddock, P.N. Fletcher, "Comparison of an electrically-small planar antenna array with a conventional monopole array", *IEEE 56th Vehicular Technology Conference Proceedings*, VTC 2002-Fall, Vol. 1, pp.596-600, September 2002.

Appendix A

Radiation Pattern Measurements

The various practical arrays used in practical evaluations throughout this thesis was measured by process and techniques described in this Appendix. It also lists some sources of errors associated with the antenna radiation pattern measurements.

A.1 The Measurement System

Conventionally, the antenna under test (AUT) is measured in its far-field zone, where the radiated field can be represented by the electric field components E_θ and $E\phi$, as shown in Figure A.1 [1]. Measurements for far-field radiation pattern is necessarily performed at a sufficient distance from the source antenna where the approximation of plane wave to be valid. While there is no pre-defined region for the far-field, it is generally assumed that this region, often called the Fraunhofer region, exists at distances greater than $2D^2/\lambda$, where D is the maximum dimension of the antenna [2]. The field components are combined to yield a total radiation pattern represented by

$$|E_{total}(\theta,\phi)|^2 = |E_\theta|^2 + |E_\phi|^2 \tag{A.1}$$

The antennas are measured in an anechoic chamber, which is fully lined with radar-absorbing material (RAM). Two stepper motors are used to provide two axis rotation θ and ϕ. These are connected to an antenna positioning device. The RF source and received signals at the AUT are controlled and processed by a Wiltron Network Analyser. These two devices are controlled by a computer which records the magnitude and phase information received at the AUT, as well as the antenna position. The source antenna used in the measurements used for the purposes of research presented in this thesis is a dual-polarised horn which can

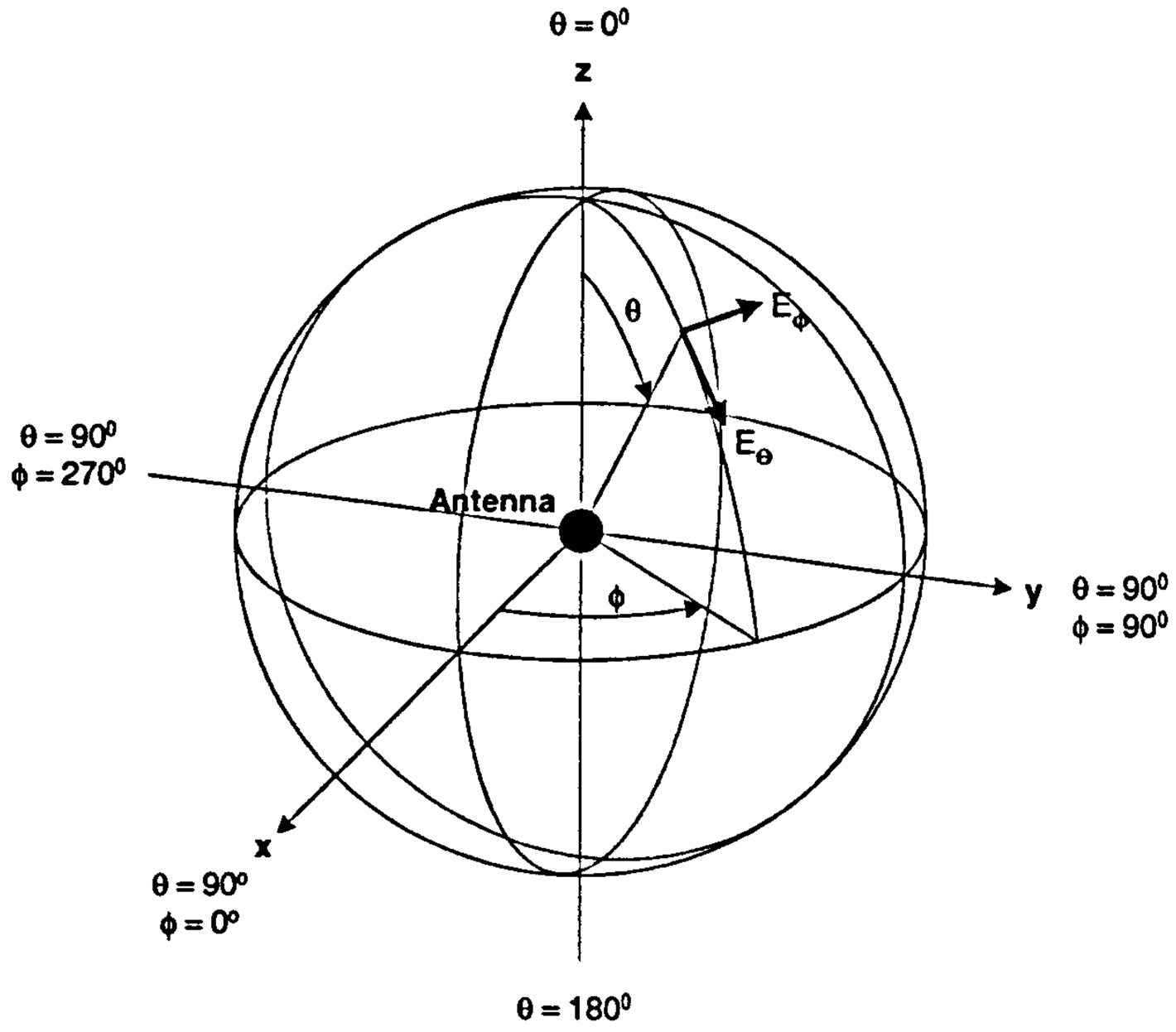

Figure A.1: *Orthogonal electric field components in the spherical co-ordinate system*

be easily switched for the two different polarisations. The antenna measurement facility is illustrated in Figure A.2 [1].

While the system is capable of measuring 3D radiation patterns, only 2D radiation patterns are performed for the work in this thesis as only the azimuth patterns are considered. Thus, the array needed only be measured around $\theta = 90^o$, $-180^o \leq \phi \leq 180^o$. For each active element, the measurement system performs two sets of measurements automatically, that is one for each polarisation. The dual-polarised horn automatically switches from co-polar to cross-polar radiation after the first set of measurements. The active element pattern of each array element is measured one by one while terminating the other elements with a 50Ω loads.

A.2 Phase Centres

While it is usually sufficient to measure only the magnitude of the radiation pattern, the phase information may also be of importance in many applications. The anechoic chamber facility described in the previous section automatically measures both magnitude and phase information of the co- and cross-polar elements.

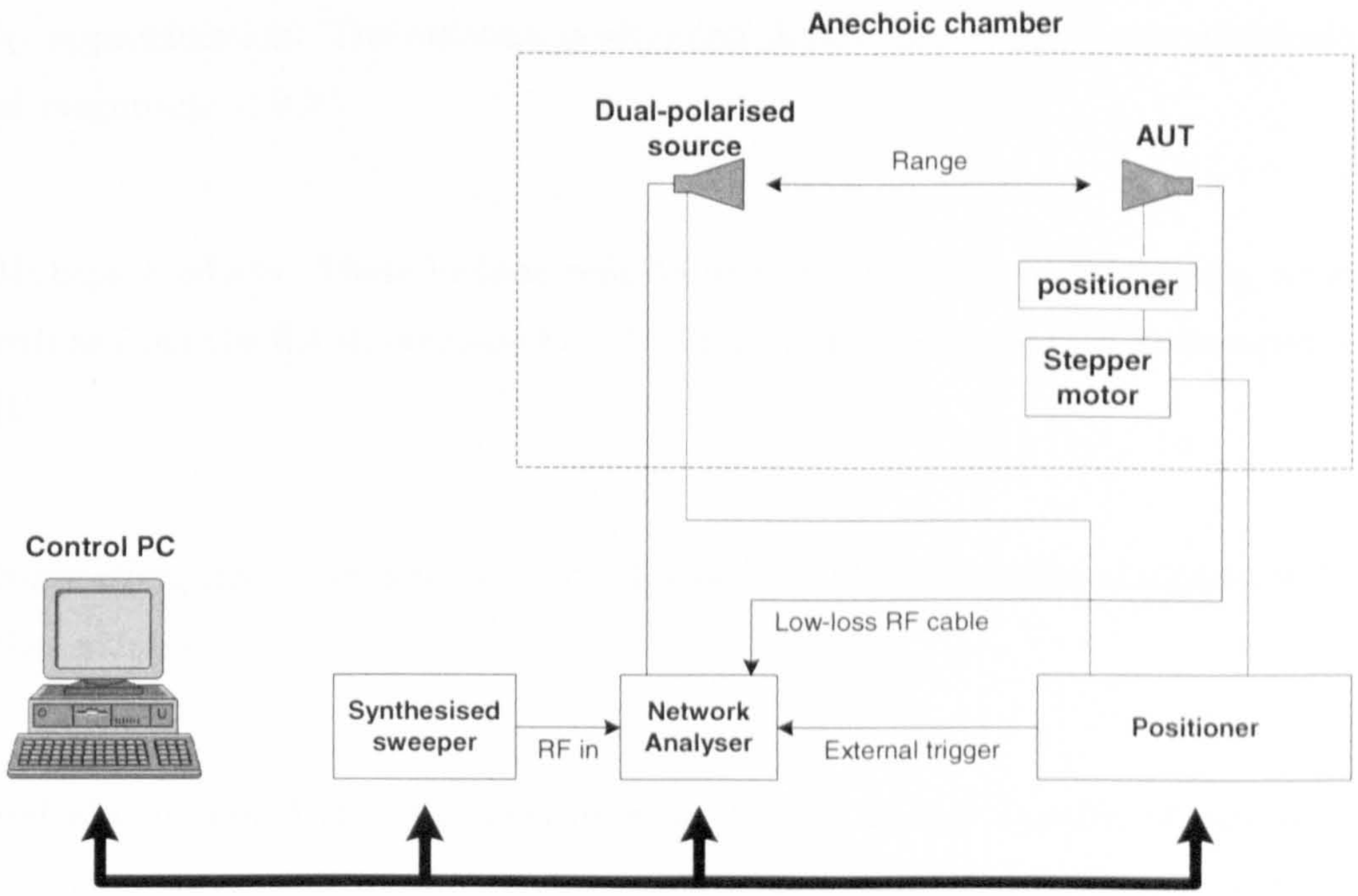

Figure A.2: *The far-field measurement facility*

For many applications the choice of the origin O, which is the centre of the coordinate system, is important in order to simplify the form of the phase pattern. In some cases it is possible to reduce the phase to a constant value by shift of origin. The pattern is then reduced to a real function. When this is achieved, O is often called the *phase centre* of the antenna.

For the case of UCAs, it is often necessary to choose the centre of the circular ground plane as the phase centre. This will yield phase patterns at the elements that are identical to each other, separated by $2\pi/N$.

A.3 Error Sources

A number of possible errors may be introduced in the radiation pattern measurements. These include:

- Cabling effects, introduced due to non-ideal cable screening or imperfect cable termination. This results in leakage from the cable, thus creating additional source of radiation.

- Antenna positioning error. While every effort is made to ensure the arrays are placed with their phase centres coinciding with the centre of rotation, this can only be done

by approximation. The antenna positioning device also introduces a positioning error of magnitude $< 0.5^o$.

- Multipath effects. These include reflections from the antenna positioning structure as well as from the RAM, estimated at -50dB at normal incidence for frequencies $> 2GHz$ [1].

- Noise effect due to preamplification, losses in cables and external signals leaking into the chamber.

It should also be noted that the measurement facility is only capable of measuring in 1^o steps. In some array post-processing cases such as that presented in chapter 4 in this thesis where the post-processing includes a correlation function, this may not be sufficient. In order to overcome this problem, the measured patterns can be passed through a curve fitting technique to increase the angular resolution, in this case 0.1^o.

References

[1] P.B. Darwood, *Pattern Synthesis for Small Phased Array Antennas*, PhD Thesis,Centre of Communications Research, University of Bristol, pp.164-170, January 1998.

[2] C.A. Balanis, *Antenna Theory Analysis and Design*, J. Wiley & Sons, New York, USA, 1982.

Appendix B

UCA as an Indoor Wireless LAN Access Point

In this appendix, the performance of the 8-element Thales UCA was investigated in a real-life office environment. Characteristics of indoor channels were obtained through a series of measurements performed within various indoor environments at the University of Bristol and the performance of the test antenna array using the switched-sector and switched-beam techniques was evaluated in terms of the average received power and Carrier-to-Interference (C/I) ratio. Results demostrate average improvements of up to 5dB in the received power and a 22% chance for multiple access.

B.1 The measurement system

The characteristics of indoor channels were obtained through a series of measurements performed within an indoor office accommodation at the University of Bristol. Figure B.1 shows the transmit and receive positions employed for use in the analysis. The Medav RUSK BRI vector channel sounder [1] was used to sample the wideband characteristics of the indoor environment at the center frequency of 5.2GHz.

The measurement parameters were set up to meet the channel time variation requirements. The maximum Doppler frequency v_D of the indoor channel at 5.2GHz is typically about 35Hz for moving speeds around 2m/s.

$$v_D = v/\lambda = 2/0.0577 = 34.7\ Hz.$$

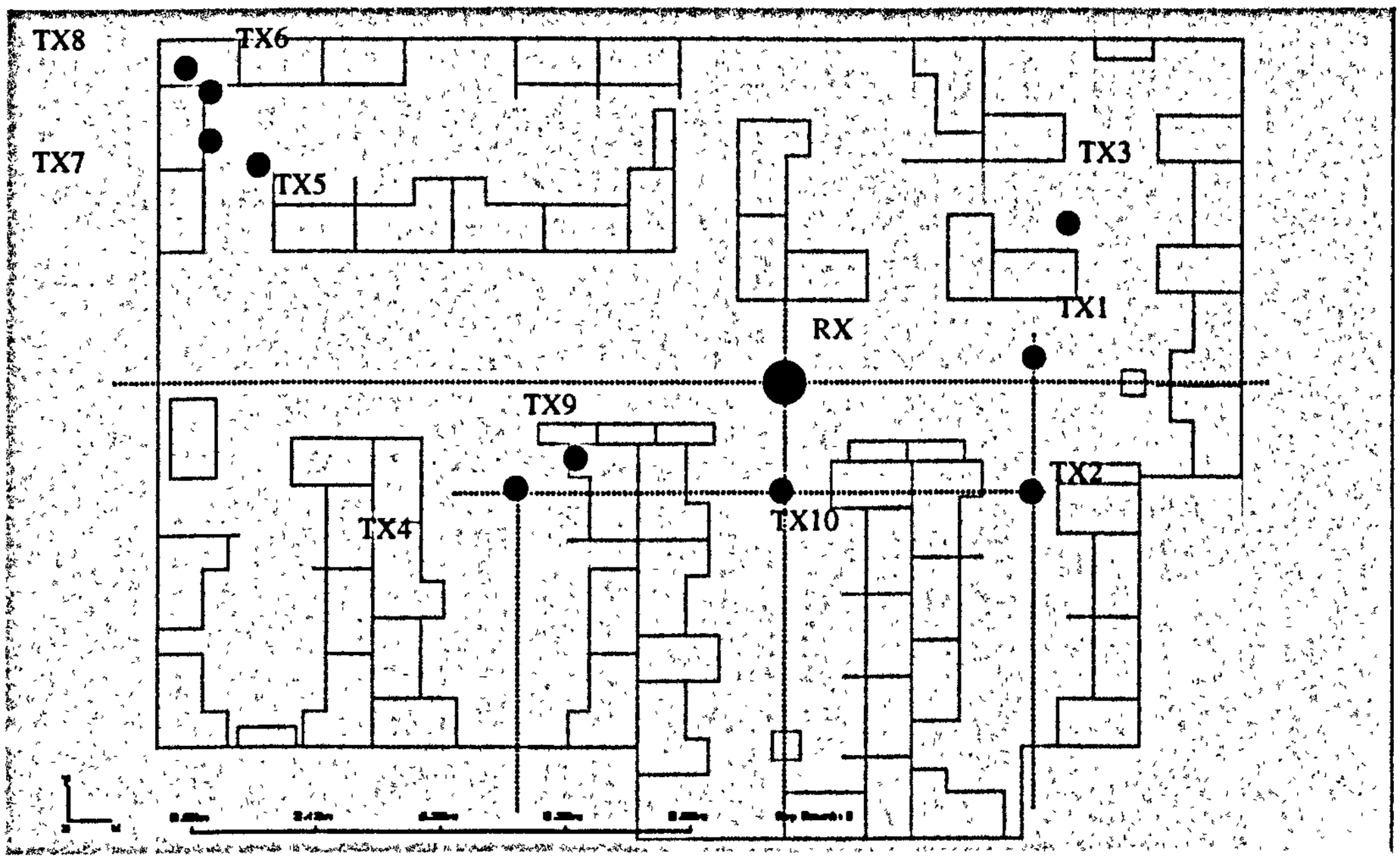

Figure B.1: *TX and RX posititon in indoor office environment*

The corresponding coherence time of the channel, Δ_t, is approximately 30ms, which has been confirmed by initial measurements made with the RUSK channel sounder. In an indoor office environment, it is estimated that the average and shortest coherence time are 800ms and 16ms respectively. However, it should be noted that the channel must be *over-sampled* in order to follow the variations of amplitude and phase of the multipath components. Furthermore, the Complex Impulse Response (CIR) snapshots made within this time frame allows an accurate system comparisons to be made. For direction of arrival (DoA) estimations [3]- [6] using ESPRIT, MUSIC or similar algorithms, 8-20 snapshots are typically required and the total measurement time for this amount of data must be shorter than the coherence time and the 2ms MAC frame.

The transmitting unit employs a vertically-polarised sleeve dipole antenna transmitting at +25dBm, with an operating frequency of 5.2GHz. At the receiving end, the Thales array was interfaced to the channel sounder through a filter and low-noise amplifier unit. A multiplexer was used to rapidly switch between each element of the array in turn. The received RF signals were down-converted to 80MHz IF signals and sampled at 320MHz. The receiver configuration is illustrated in Figure B.2.

The receiver was set to a stationary position during all measurements, thus acting as an Access Point (AP). The tranmitter was acting accordingly as a mobile terminal and can oth-

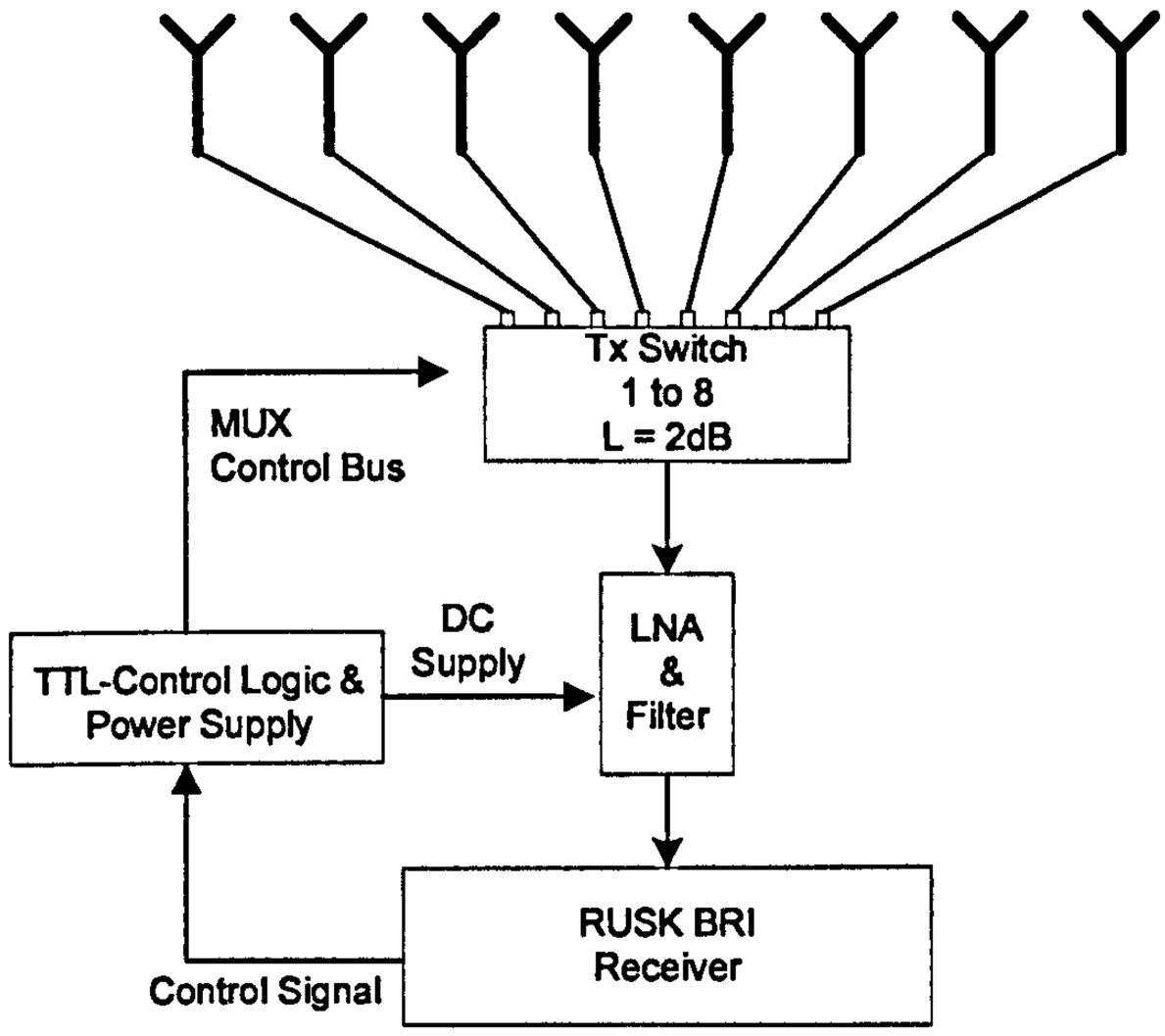

Figure B.2: *Receiver array configuration*

erwise be stationary or moved during the measurements. In this analysis, the tranmitter was set to a stationary position. Synchronisation was achieved between the transmitter (TX) and receiver (RX) by coherently aligning stable rubidium clocks in each unit. A measurement was completed in the anechoic chamber within the units synchronised by a coaxial cable for comparison.

The test- signal waveform of the RUSK BRI transmitter was set to the maximum 120MHz bandwidth and the excess delay window of $3.2\mu s$ was chosen. This gives 385 frequency fingers spread across the bandwidth. A simplified block diagram of the Single Input Multiple Output (SIMO) antenna configuration is shown in Figure B.3.

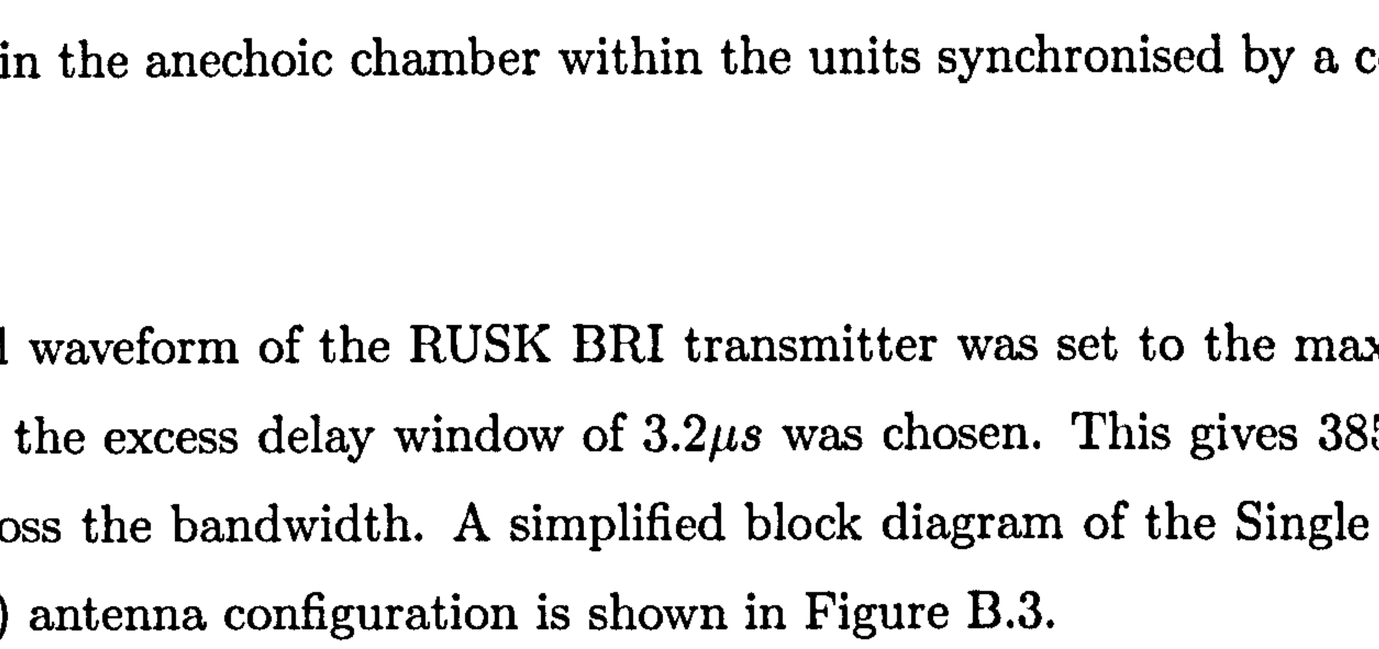

Figure B.3: *Antenna configuration for SIMO evaluation at 5.2GHz*

The measurement parameters were set to ten consecutive SIMO snapshots within each block in order to fulfil the coherence time requirements ($\approx 30ms$). Given that Hiperlan/2 and the 802.11 standards have a frequency spacing of 312kHz, a tone period of 3.2μs was used. This tone period gives 385 lines over 120MHz, which yields the 312kHz spacing. However, this gives an impact on the period of a single SIMO snapshot, the Fast Doppled Block (FDB) period and the total number of blocks that can be sampled. In this case, the maximum number of FDBs that can be taken is 763, and the measirement time for each of these blocks is 51.2μs. An extended time grid equal to 10.240ms was used in the measurement parameters so that some *short-term* variations due to moving people etc. can be followed. The total time for sampling these blocks is 7.813s, allowing long-term channel variations to be followed. Figure B.4 illustrates a block diagram of the test signal configuration that has been described.

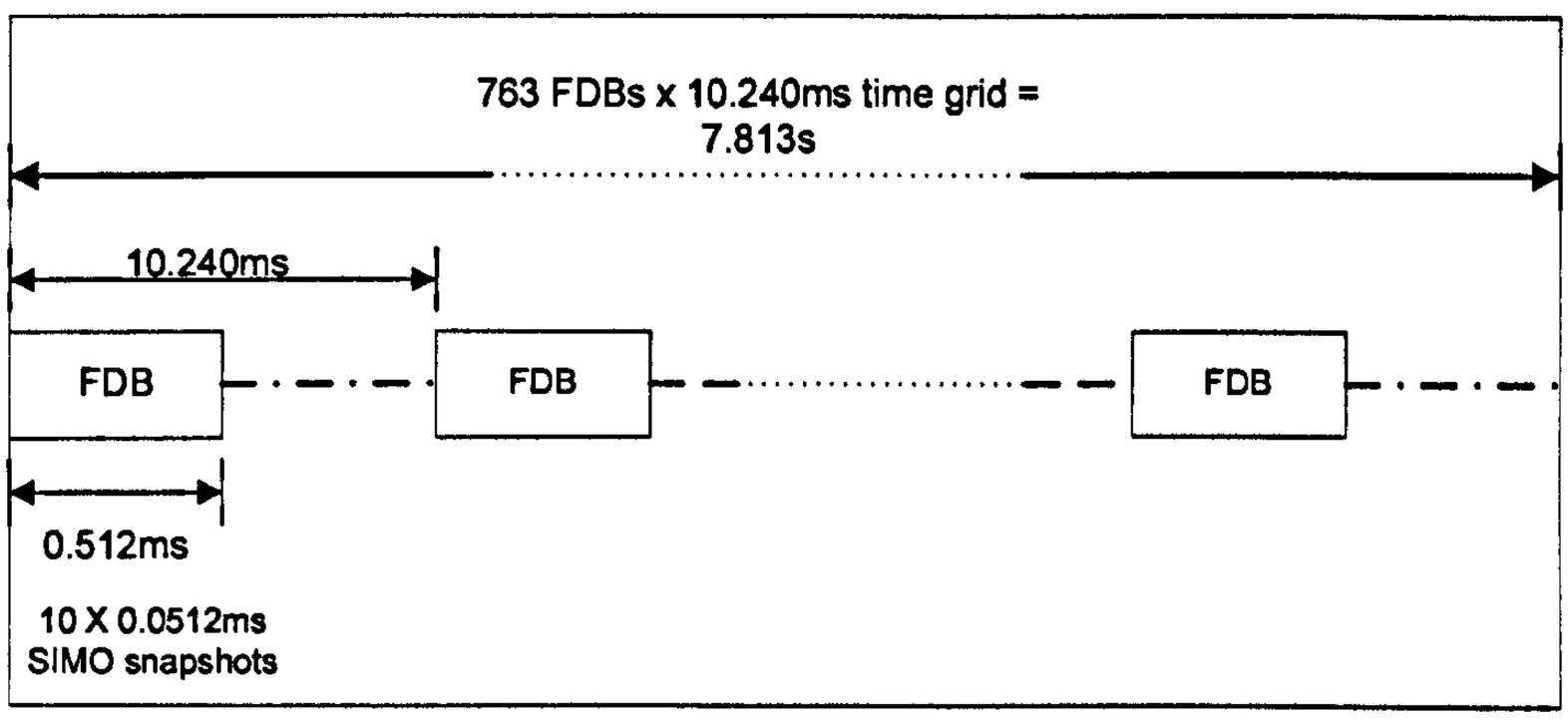

Figure B.4: *Illustration of block lengths for the general measurements*

Following calibration to remove the amplitude and phase variations in the hardware, the resulting data was stored on the hard disk in the frequency domain for further analysis.

B.2 Analysis

Results from the channel measurements were post-processed and used for further beamforming analysis. The beamforming methods used in this analysis are the switched-sector and the switched-beam method. Both methods are then compared to the performance of an omni-directional antenna. The omni-directional antenna at the base station was approximated by summation of the power received by all eight patches, and normalising the value in order to account for the number of elements in the array. Due to the performance described in section 3.6, the conjugate weights are used for the switched-beam analysis.

- **Element pattern vs. Beam pattern**

  In order to fully comprehend the behaviour of the switch-sector and switch-beam systems, it is necessary to compare the element patterns with the beam patterns. Different numbers of beams can be implemented, however for the sake of fair comparison the patterns of an eight-beam system are used and compared to the eight element patterns produced by the Thales array. The patterns shown in Figure B.5 have been normalised to the maximum gain amongst all beams. The plots reveal that in general, the element patterns are approximately 3dB lower than the beam patterns. On the other hand, it is also apparent that the elements give a smaller cusping loss compared to the beam patterns since they possess wider beams in comparison. On average, the elements have a maximum sidelobe level of approximately -13dB relative to their maximum gain, as oppose to -10dB in the case of the beams.

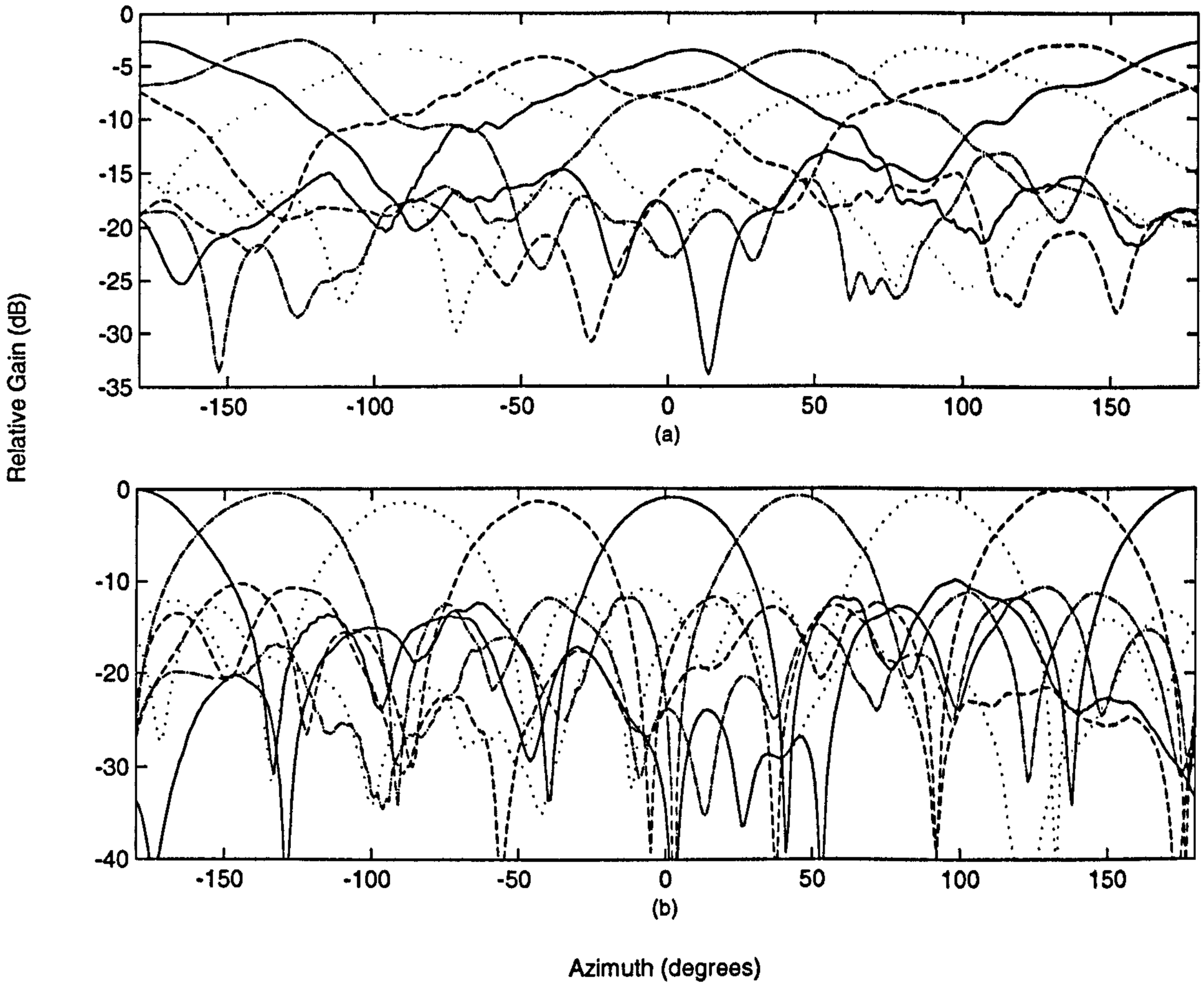

Figure B.5: *Element patterns vs. Beam patterns*

- **Single user scenario**

The first scenario is based upon the traditional TDMA scenario whereby a single user is served within a single timeslot. In this section the effect of forming a beam towards the wanted user is investigated.

Assuming an input power of 0dBm to the TX antenna, Figure B.6(a) shows the power received by the AP from the TX positions as shown in Figure B.1, when the various techniques are employed. The received power values have been averaged over time and frequency, in order to eliminate the effects of multipath fading.

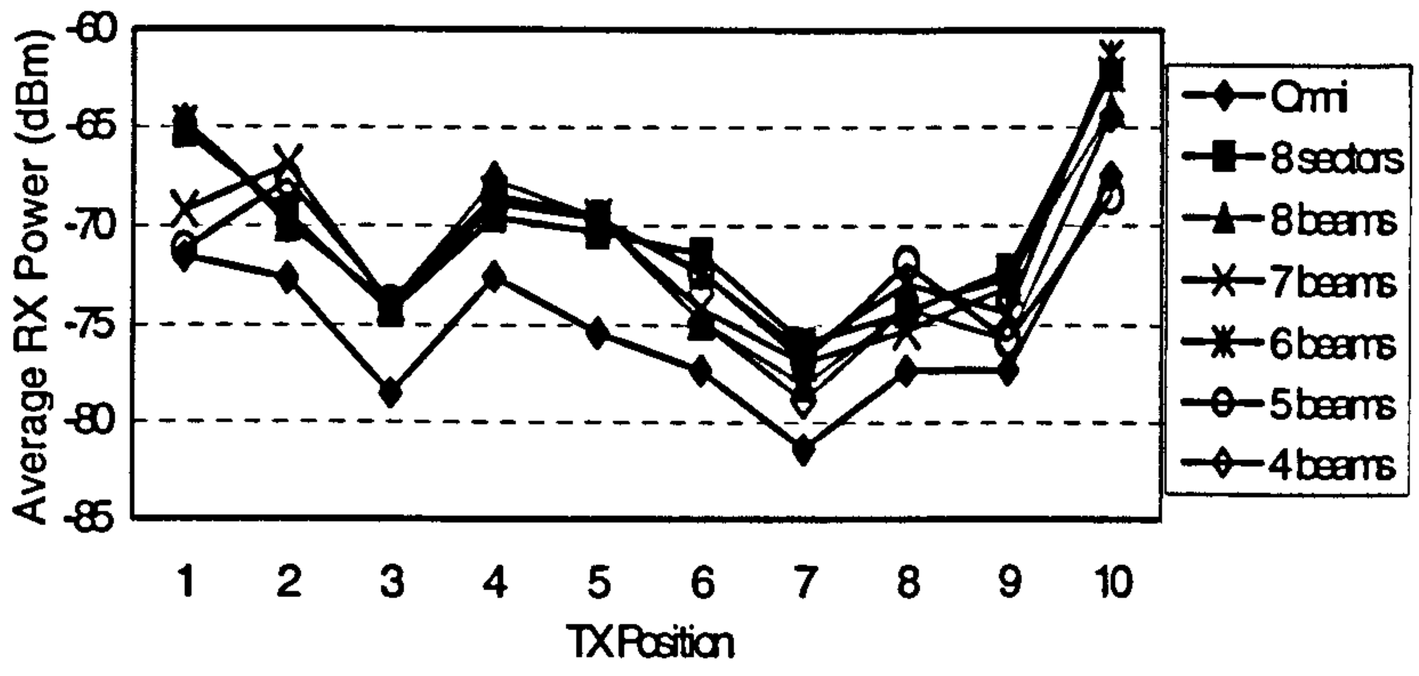

(a)

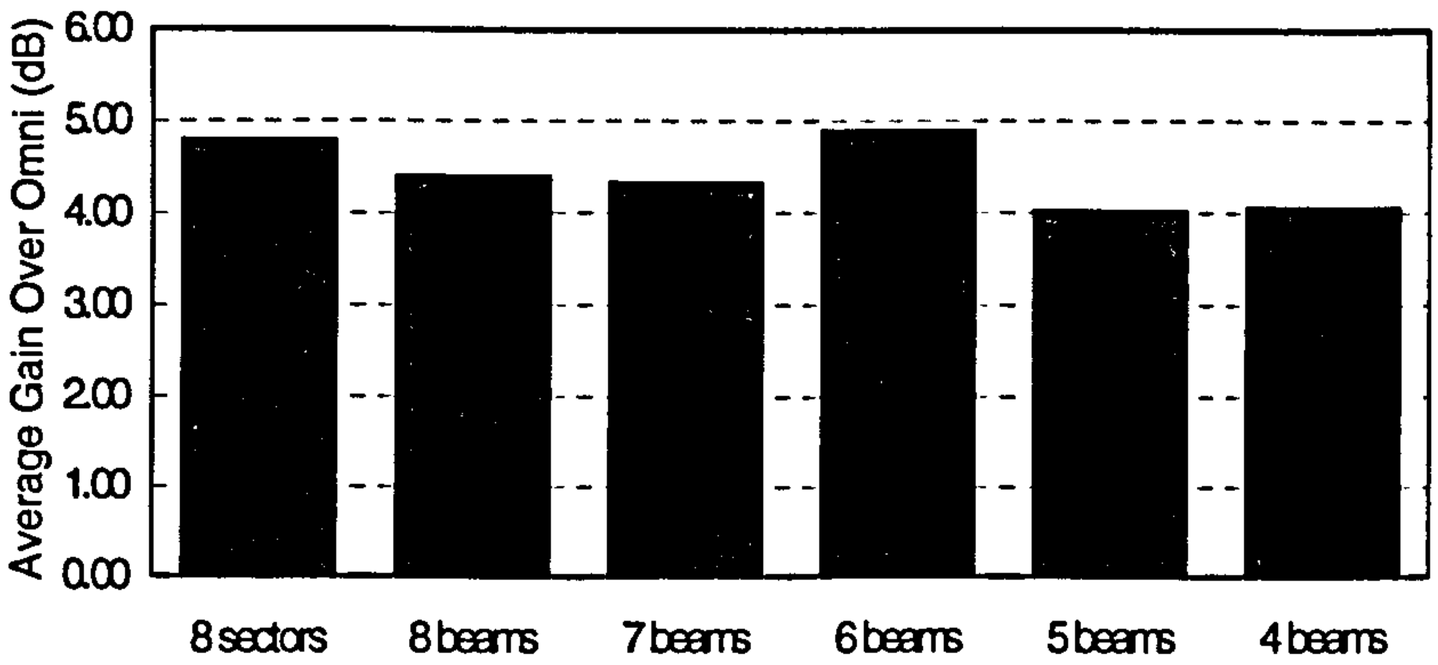

(b)

Figure B.6: *Average received power from 10 MT positions placed within a modern office environment*

The switch-sector and switch-beam systems provide similar performances in terms of the received power level, yielding average gains of between 4 and 5dB over the omni. Given the results here, the six-beam system appears to provide the best performance, with an average gain of 4.9dB over an omni-directional AP (Figure B.6(b)). It is believed that this is solely due to the limited number and spatial distribution of the MT positions, and that in general the switched-sector system offers the better performance

due to the element patterns exhibiting broader beamwidth and smaller cusping loss.

- **Two user scenario**

  For the two user scenario, one MT position in Figure B.1 is chosen as the wanted MT, and the 9 other MT positions are treated as interferers one at a time. A perfect power control mechanism is implemented in the system, which normalises the power received at the AP to the lowest received power level, thereby eliminating the near-far effect. The Carrier-to-Interference (C/I) values are computed for all different combination of wanted and unwanted MT. These values are then averaged and compared for the case of a single omnidirectional AP as well as a circular array AP employing both switch-sector and switch-beam mechanism.

  With the power control mechanism employed, the switch sector system produces a C/I of up to 24.8dB with an average value of 12.0dB, while in the cases of the switched-beam systems the highest C/I is achieved by the six-beam system, giving C/I values of up to 26.1dB and an average value of 12.9dB. It is also noted that the C/I levels of the omnidirectional AP falls to 0dB, demonstrating perfect power control.

  Simulation results presented in [2] illustrate that for a packet error rate (PER) of 1%, a C/I of 12dB is required for the simplest operation mode, BPSK. The results in Figure B.7 show that 22.2% of the time, the switch-sector system is capable of supporting two users at one point in time. In the cases of switch-beam system, the C/I levels only rise above the 12dB threshold 10 to 20% of the time, depending on the number of beams employed.

- **Multi user scenario**

  In order to investigate the behaviour of the beamforming system within a multi-user environment, a multi-user model is developed. A wanted MT is present, and 9 random MTs are added to the system one at a time, acting as interferers. C/I ratios are calculated as the interferers are added to the system. The MT positions are randomly chosen from the 10 transmit positions shown in Figure B.1. The remaining 9 MTs are then randomly and gradually added to the system. C/I ratios are calculated at each stage when an additional unwanted user is added to the system. 100 different wanted and unwanted MT combinations are used and the results are averaged for analysis purposes.

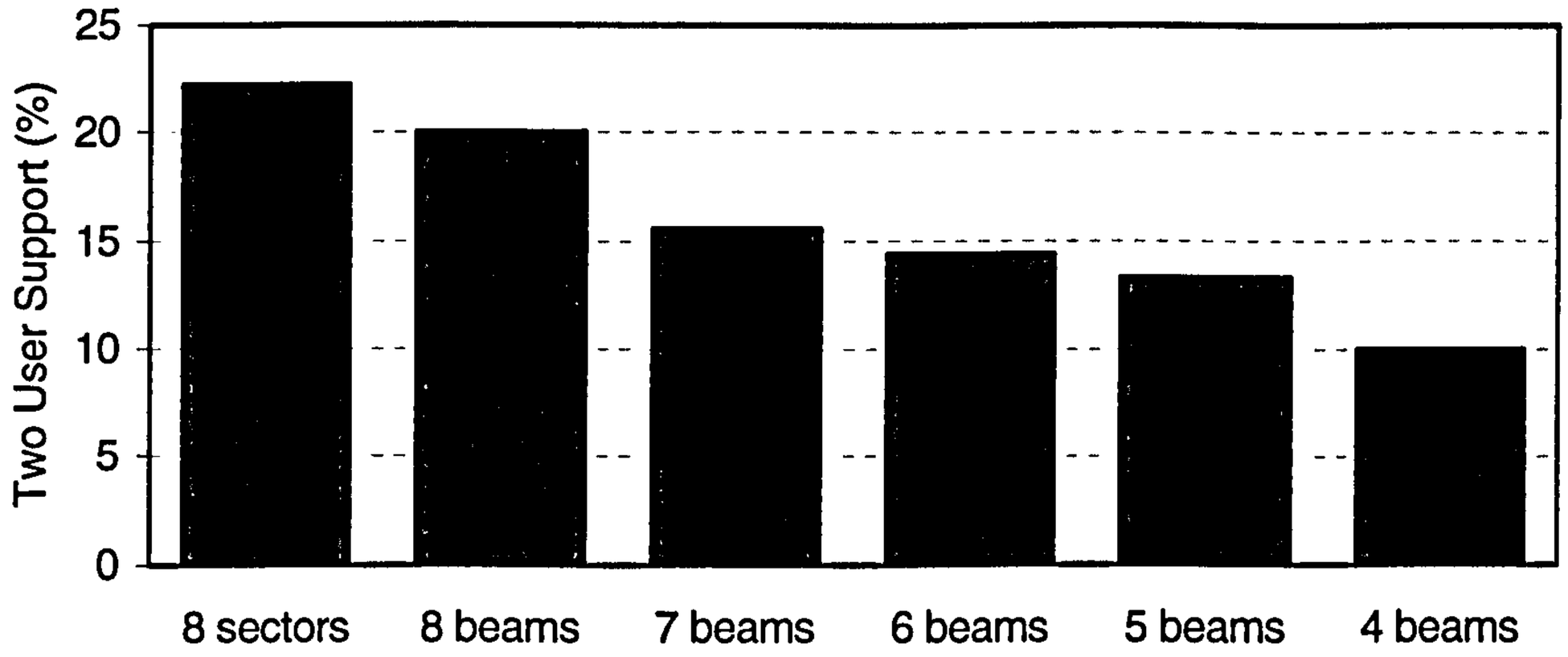

Figure B.7: *Two user support*

Figure ?? illustrates the percentage of supportable number of users for the switched-sector as well as switched beam techniques, with the assumption of 12dB minimum C/I. Once again a perfect power control has been implemented in the analysis. It is shown that both the switched-sector and the 7-beam systems are capable of serving up to 5 users within a single timeslot. It should be noted however, that the performance of the systems is highly dependant upon the order in which the interferers are added to the system. In contrary to that, an omni-directional antenna would fail completely when one or more interferer is introduced to the channel.

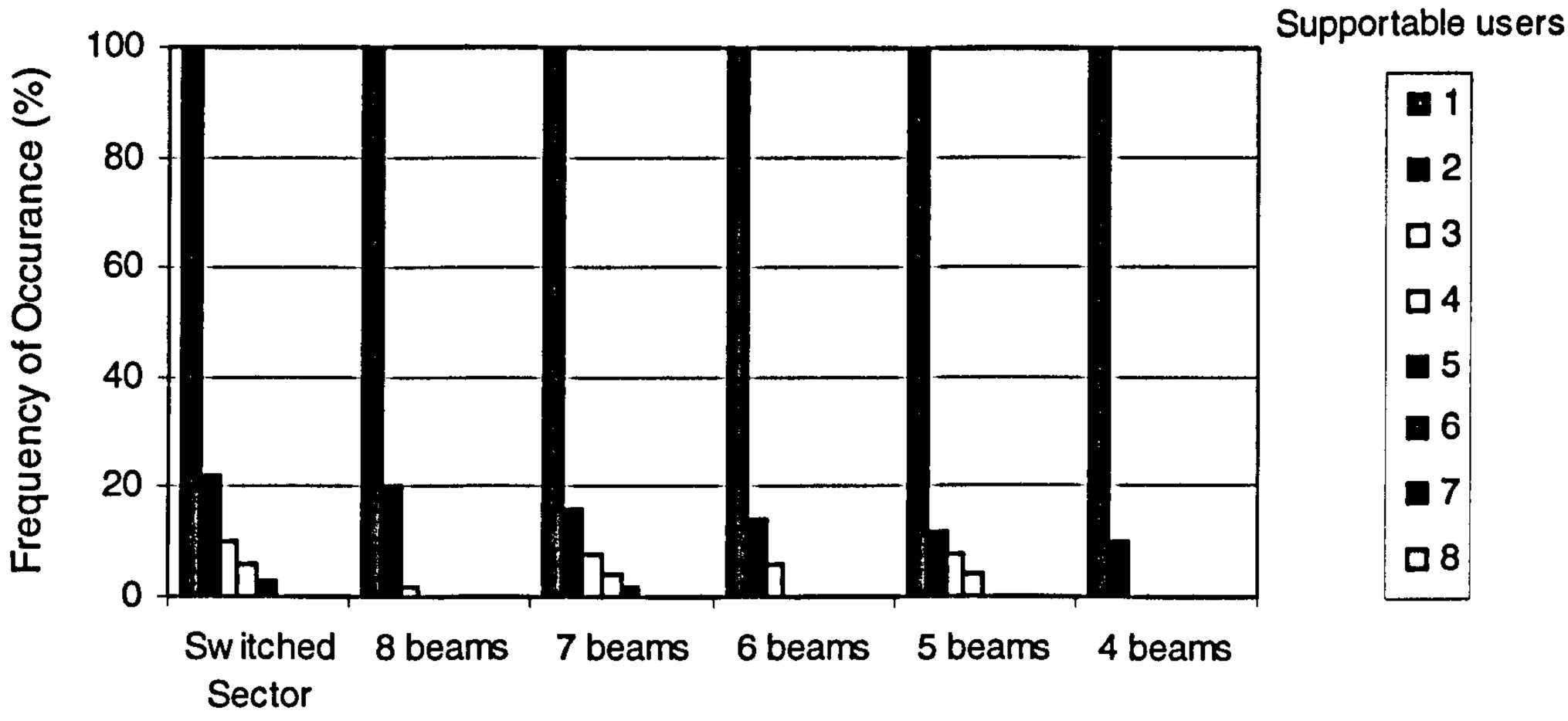

Figure B.8: *Multi user support*

B.3 Conclusion

A measurement system for measuring the space-time characteristics of indoor environments at 5.2 GHz has been presented in this Appendix. The performance of an eight- element circular array acting as an Access Point, coupled with simple smart antenna techniques, has also been presented. The received power level is evidently improved through the use of the array. The switch-sector and switch-beam systems provide similar performances in terms of the received power. In the two-user scenario, results show that with the assumption of perfect power control mechanism and a minimum C/I level of 12dB, 22.2% of the time the switch-sector system is able to support two users within a single timeslot. In the multi-user scenario, results illustrate that the particular switched-sector system as well as the 7-beam system are able to support up to 5 users within a single timeslot. However, it should be noted that performance of switch-sector systems is greatly dependent upon the array element radiation patterns. It should also be noted that any detailed conclusion can not be drawn from this analysis due to the non-uniform distribution of the TX positions. Nevertheless, the results have evidently shown that channel capacity can be increased by means of a simple smart antenna array. Clearly, these results need to be considered during implementation, weighing up the cost, complexity, and the potential improvements that can be achieved through the use of the different systems.

References

[1] http://www.medav.de

[2] J. Kuhn-Jush, G. Malmgren, P. Schramm, J. Torsner, "Overview and Performance of Hiperlan Type 2 - A Standard for Broadband Wireless Communications", *IEEE Vehicular Technology Conference*, Vol. 1, pp112-117, 2000.

[3] N. Yuen, B. Friedlander, "DOA estimation in multipath: an approach using fourth-order cumulants", *IEEE Transactions on Signal Processing*, Vol. 45 , Issue 5 , Pp1253 - 1263, May 1997.

[4] H. Weiguang, H.M. Kwon, "Effect of mixer phase distortions on the DOA tracking algorithm for an adaptive antenna array", *IEEE VTS 53rd Vehicular Technology Conference*, Vol. 1 , pp248 - 252, May 2001.

[5] F. Li, H. Liu, R.J. Vaccaro, "Performance analysis for DOA estimation algorithms: unification, simplification, and observations", *IEEE Transactions on Aerospace and Electronic Systems*, Vol.29 , Issue 4 , pp1170 - 1184, Oct. 1993.

[6] Y. Jia, H. Wu, Z. Bao, "A novel DOA estimation algorithm with uncalibrated array", *3rd International Conference on Signal Processing*, Vol.1 , pp465 - 468, Oct. 1996.

Appendix C

FDTD Method for Array Pattern Generation

A technique to solve Maxwell's curl equations using the finite-difference time-domain (FDTD) technique was proposed by Yee [1] in 1966. The method has been used to solve numerous scattering problems on microwave circuits, dielectrics, and electromagnetic absorption in biological tissue at microwave frequencies. With the advent of low cost, powerful computers and advances to the method itself, the FDTD technique has since become a well-known method for solving electromagnetic problems [2] - [7].

C.1 The Algorithm

Maxwell's curl equations for an isotropic medium are defined by

$$\nabla \times \mathbf{E} = -\mu \frac{\delta \mathbf{H}}{\delta t} \tag{C.1}$$

$$\nabla \times \mathbf{H} = \sigma \mathbf{E} + \epsilon \frac{\delta \mathbf{E}}{\delta t} \tag{C.2}$$

In cartesian co-ordinates, these become

$$\frac{\delta H_x}{\delta t} = \frac{1}{\mu}\left(\frac{\delta E_y}{\delta z} - \frac{\delta E_z}{\delta y}\right) \tag{C.3}$$

$$\frac{\delta H_y}{\delta t} = \frac{1}{\mu}\left(\frac{\delta E_z}{\delta x} - \frac{\delta E_x}{\delta z}\right) \tag{C.4}$$

$$\frac{\delta H_z}{\delta t} = \frac{1}{\mu}\left(\frac{\delta E_x}{\delta y} - \frac{\delta E_y}{\delta x}\right) \tag{C.5}$$

$$\frac{\delta E_x}{\delta t} = \frac{1}{\epsilon}\left(\frac{\delta E_z}{\delta y} - \frac{\delta E_y}{\delta z} - \sigma E_x\right) \tag{C.6}$$

$$\frac{\delta E_y}{\delta t} = \frac{1}{\epsilon}\left(\frac{\delta E_x}{\delta z} - \frac{\delta E_z}{\delta x} - \sigma E_y\right) \tag{C.7}$$

$$\frac{\delta E_z}{\delta t} = \frac{1}{\epsilon}\left(\frac{\delta E_y}{\delta x} - \frac{\delta E_x}{\delta y} - \sigma E_z\right) \tag{C.8}$$

The grid coordinates (i,j,k) are defined as

$$(i, j, k) = (i\Delta x, j\Delta y, k\Delta z)$$

where Δx, Δy and Δz are the actual grid separations. The function of space and time is written as

$$F^n(i, j, k) = (i\Delta x, j\Delta y, k\Delta z, n\Delta t)$$

where Δt is the time increment and n is the time index. The spatial and temporal derivatives is written using central finite difference approximations as

$$\frac{\delta F^n(i, j, k)}{\delta x} = \frac{F^n(i + 1/2, j, k) - F^n(i - 1/2, j, k)}{\delta} \tag{C.9}$$

$$\frac{\delta F^n(i, j, k)}{\delta t} = \frac{F^{n+1/2}(i, j, k) - F^{n-1/2}(i, j, k)}{\Delta t} \tag{C.10}$$

where $\delta = \Delta x = \Delta y = \Delta z$.

In all of the finite difference equations the components of **E** and **H** are located within a single unit cell in the three-dimensional lattice depicted in Figure C.1. **E** and **H** are evaluated at alternate half time steps, such that all field components are calculated in each time step Δt.

C.2 Grid spacing

To yield accurate results, the grid spacing δ in the finite difference simulation must be less than the wavelength, usually less than $\lambda/10$. The stability condition relating the spatial and temporal step size is defined by

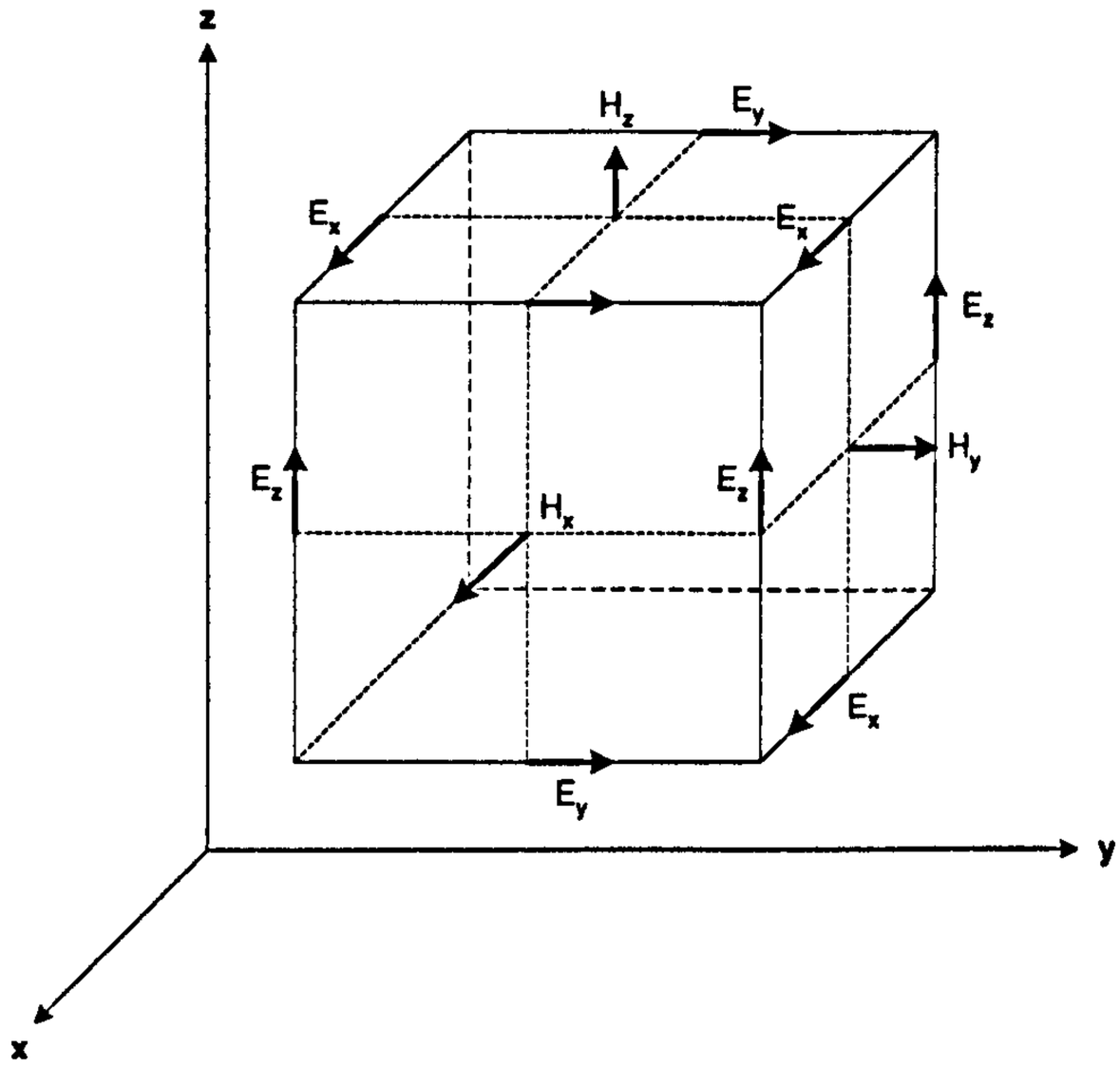

Figure C.1: *Field components arrangement within a cubical grid*

$$v_{max}\Delta t = \left[\frac{1}{\Delta x^2} + \frac{1}{\Delta y^2} + \frac{1}{\Delta z^2}\right]^{-1/2} \tag{C.11}$$

where v_{max} is the maximum velocity of the wave. When the step size δ is the same in all directions, the stability condition becomes

$$\frac{v_{max}\Delta t}{\delta} = \frac{1}{\sqrt{P}} \tag{C.12}$$

where P is the number of spatial dimensions.

In the FDTD method, the electric and magnetic fields in the region around the cell that lies in the near-field is computed in the time domain. In order to determine the far-field radiation pattern, near-field data is transformed to the far-field by converting the time domain values to frequency domain values through the use of Fourier transform. The near-field values are weighted with the free space Green's function and integrated over a surface S surrounding the cell [8].

C.3 FDTD Method for Array Modeling

The FDTD method has been known as a powerful method for modeling single antennas [9] as well as antenna arrays [10]- [12]. Far-field radiation pattern of the antennas can be generated

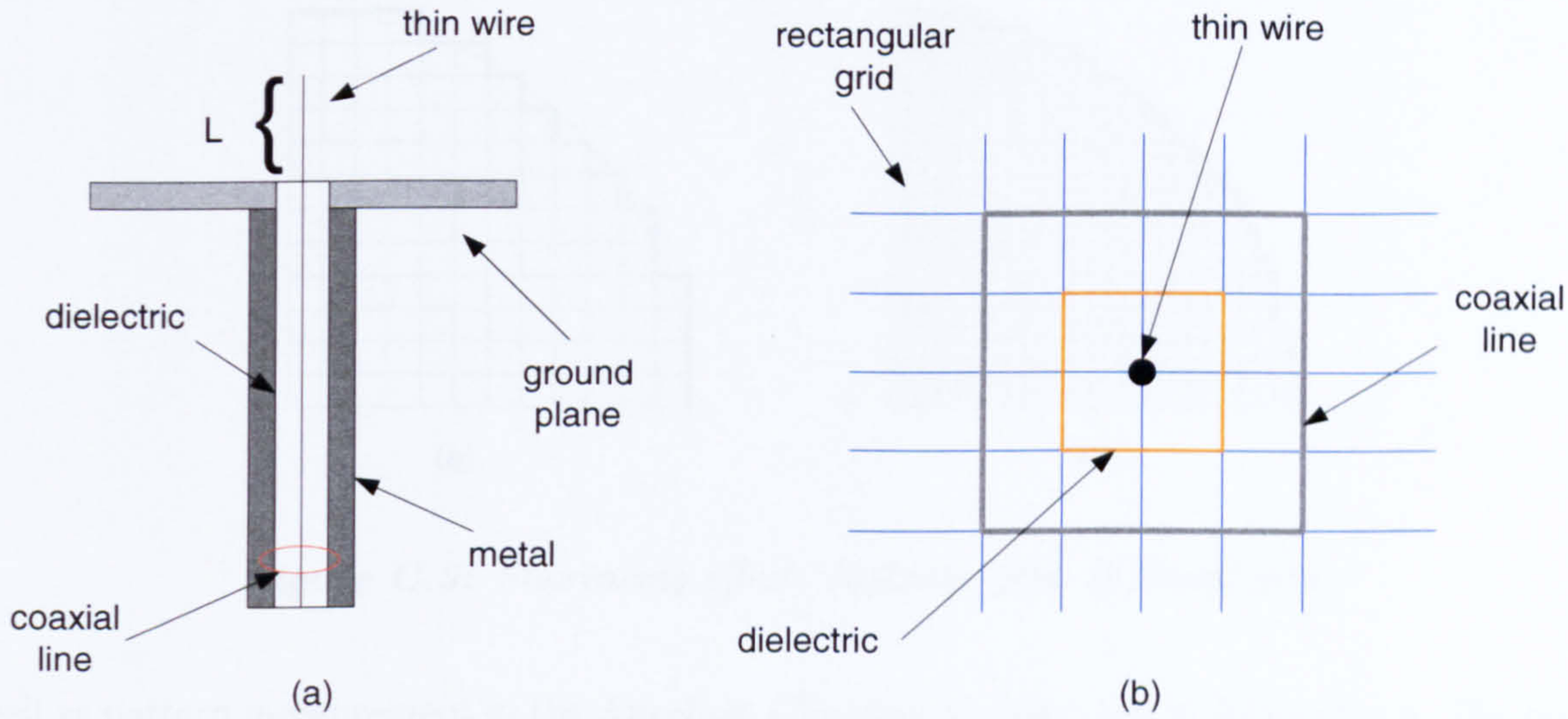

Figure C.2: *Antenna element model used on the FDTD array model: (a)Side view; (b)Cross section view.*

provided the dimensions are known. This allows the antenna characteristics to be predicted before production commences. In order to aid the work presented in this thesis, an FDTD model of the 8-element UCA was built. An FDTD-modeling tool called GEMMA, developed at the University of Bristol, aids with the visualisation of FDTD models.

The model was built with the same dimensions as the real array in terms of the ground plane size as well as the array radius R and inter-element separation d. The SMA connectors used as the antenna elements are modeled as thin-wires surrounded by dielectric material, as shown in Figure C.2(a). The FDTD grids are rectangular and cartesian, therefore the dielectric as well as the coaxial feed are modeled with rectangular cross-section as seen in Figure C.2(b). The model is surrounded by an *absorbing boundary*, preventing any signal reflections from the boundaries.

Since the grids are rectangular in shape while the array is circular, it was found that smaller grid size minimises the error caused by the staircase effects, as shown in Figure C.3. In this model, the grid sizes are non-uniform as smaller cells are required around the array elements for greater accuracy. The grid sizes in this model were set between 0.5mm and 5mm, with the smallest cell around the individual elements. Uniform grid spacing in the size of 0.5mm would incur much larger processing time. The coaxial line size is $1mm^2$. As shown in Figure C.3(a), the coaxial line is shielded by a layer of metal in order to avoid leakage of currents.

Figure C.4 shows the far-field active element pattern, obtained both through FDTD model as

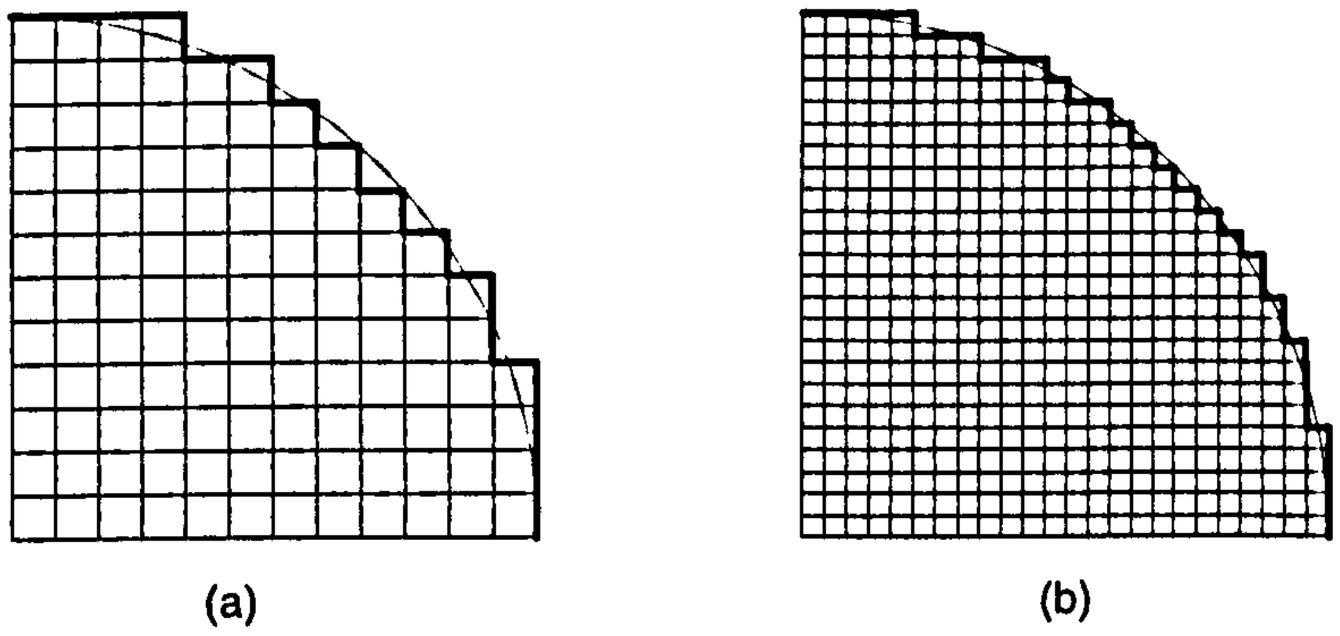

Figure C.3: Staircasing effect: (a)Large grid; (b)Small grid.

well as pattern measurement in the Anechoic Chamber as described in Appendix A. The patterns have been normalised to their maximum gains. It can be seen that the model produces a pattern that is similar in shape to the measured response, with up to $\approx 2dB$ discrepancy around the side peaks.

As can be seen in Figure 5.11, it is apparent that patterns of the even elements are slightly different from the patterns of the odd elements, by the order of $< 1dB$. This is caused by the staircasing effect outlined above. It was found that as the grid size is reduced, the discrepancy between even and odd element patterns is also reduced. However, due to the much increased computer processing time involved in reducing the grid size, it was decided that 0.5mm grid size was sufficient for the current purpose.

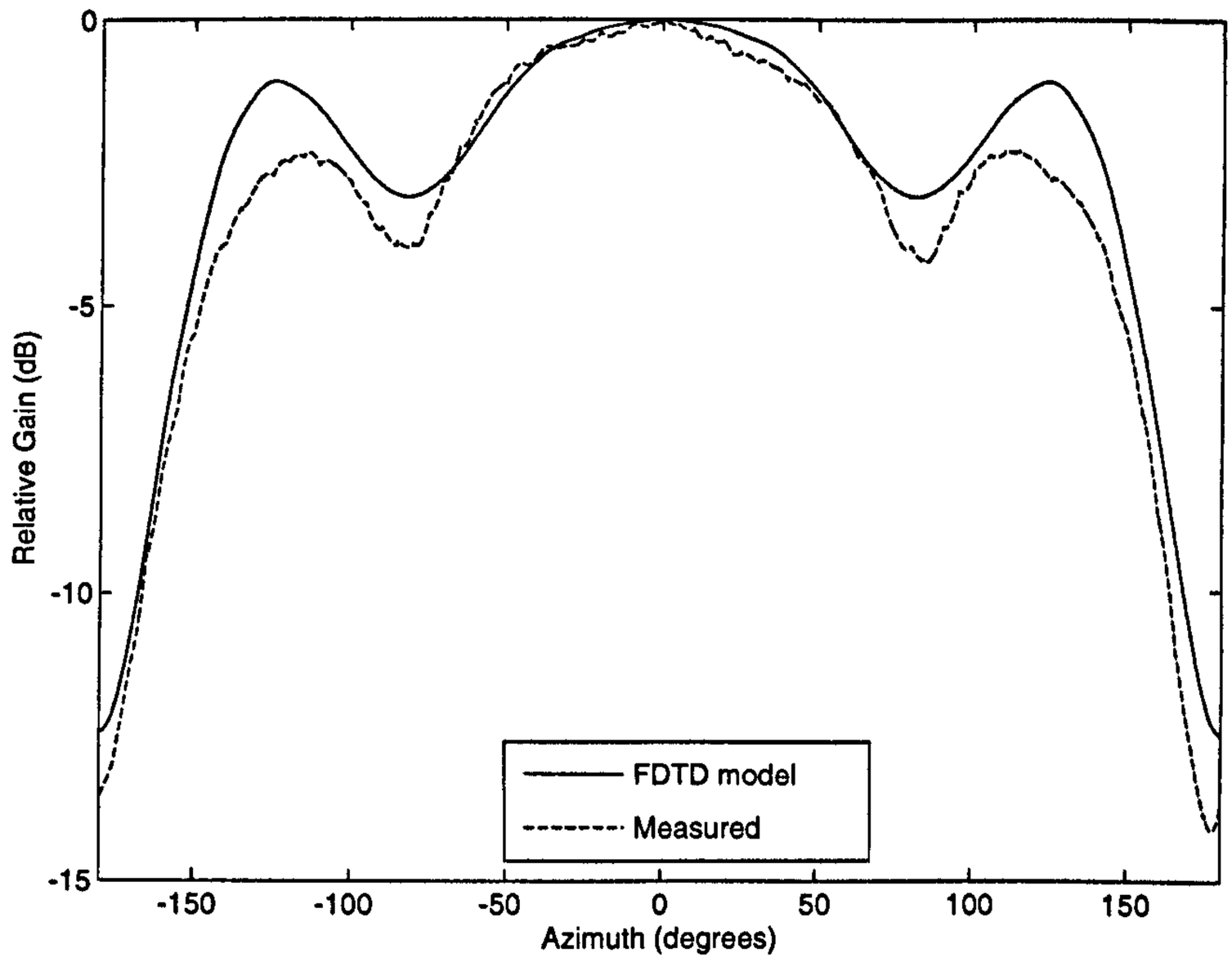

Figure C.4: *Radiation patterns obtained through FDTD model as well as real measurements of the 8-element monopole UCA.*

References

[1] K. Yee, "Numerical solutions of initial boundary value problems involving Maxwell's equations in isotropic media," *IEEE Transactions on Antennas and Propagation*, Vol. AP-14, pp302-307, 1966.

[2] J. Adhidjaja, G. Horhmann, "A Finite-Difference Algorithm for the Transient Electromagnetic Response of a Three-Dimensional Body", *Geophysics J. Int.*, Vol. 98, pp233-242, 1989.

[3] M. Piket-May, A. Taflove, "Electrodynamics of Visible-Light Interactions with the Vertebrate Retinal Rod", *Optics Letters*, Vol. 18, No. 8, pp568-570, 1993.

[4] M. Celuch-Marcysiak, W. Gwarek, "Higher order modeling of media interfaces for enhanced fdtd analysis of microwave circuits", *24th European Microwave Conference*, Vol. 24, (Cannes, France), pp1530-1535, September 1994.

[5] D. Sullivan, D. Borup, O. Gandhi, "Use of the Finite-Difference Time-Domain Method in Calculating EM Absorption in Human Tissues", *IEEE Transaction in Biomedical Engineering*, Vol. 34, No. 2, pp148-157, 1987.

[6] S. Caorsi, A. Massa, M. Pastorino, "Computation of Electromagnetic Scattering by Nonlinear Bounded Dielectric Objects: A FDTD Approach", *Microwave Opt. Technology Letter*, Vol. 7, No. 17, pp788-790, 1994.

[7] K. Shlager, J. Schneider, "A selective survey of the finite-difference time-domain literature", *IEEE Antennas and Propagation Magazine*, Vol. 37, pp39-56, 1995.

[8] R.J. Luebbers, K.S. Kunz, M. Schneider, F. Hunsberger, "A finite-difference time-domain near zone to far zone transformation [electromagnetic scattering]", *IEEE Transactions on Antennas and Propagation*, Vol. 39, Issue 4, pp.429-433, April 1991.

[9] R. Luebbers, L. Chen, T. Uno, S. Adachi, "FDTD calculation of radiation patterns, impedance, and gain for a monopole antenna on a conducting box", *IEEE Transactions on Antennas and Propagation*, Vol. 40, Issue 12, pp.1577-1583, December 1992.

[10] G.M. Turner, C. Christodoulou, "FDTD analysis of phased array antennas", *IEEE Transactions on Antennas and Propagation*, Vol. 47, Issue 4, pp.661-667, April 1999.

[11] C.J. Railton, D.L. Paul, I.J. Craddock, "Analysis of a 17 element conformal array of stacked circular patch elements using an enhanced FDTD approach", *IEE Proceedings on Microwaves, Antennas and Propagation*, Vol. 150, Issue 3, pp.153-158, June 2003.

[12] G.S. Hilton, C.J. Railton, G.J. Ball, M. Dean, A.L. Hume, "Modelling a three-element printed dipole antenna array using the FDTD technique", *IEEE Antennas and Propagation Society International Symposium*, 1997 Digest Vol. 2, pp.1062-1065, July 1997.

Appendix D

Practical Monopole UCA

The practical monopole UCAs used in analysis presented in Chapters 4 and 5 are made of eight stub-contact SMA connectors mounted on a 300mm diameter circular ground plane. The circular ground plane is made out of copper-backed FR4 material with 1.5mm thickness. The dielectric stub-contact is stripped to the ground plane level and the length of each of the SMA connectors is trimmed to a length optimised for 5.2GHz operation ($\approx 12.7mm$). The radius of the array was chosen as $R = R_{opt}$, in this case $R = \lambda/2 = 28.85mm$.

The following sections describe the measured quantities of the 8-element monopole UCAs used in the practical analysis.

D.1 Return Loss (S_{nn}) and Mutual Coupling Matrix ($S_{n(n+1)}$)

The S-parameters of Array 1 (Section 4.1) is shown in Figures D.1 and D.2. It should be noted that $S_{(n+1)n}$ is not shown in Figure D.2 as $S_{n(n+1)} = S_{(n+1)n}$.

D.2 Dimensions

Shown in Figures D.3 and D.4 are the measured actual cartesian co-ordinates of the elements in Array 1 (used in Chapters 4 and 5) and Array 2 (used in Chapter 5). The co-ordinate positions are obtained through measurements using a vertical miller with numerical x-y positioner. It should be noted that the dimensions are measured from an approximate centre of origin, and there may be a slight rotation in terms of the boresight angles. Bearing this in mind, it is felt best to compare dimensions in terms of the distances between elements in the array, as found in Chapter 5, instead of their distances from the origin.

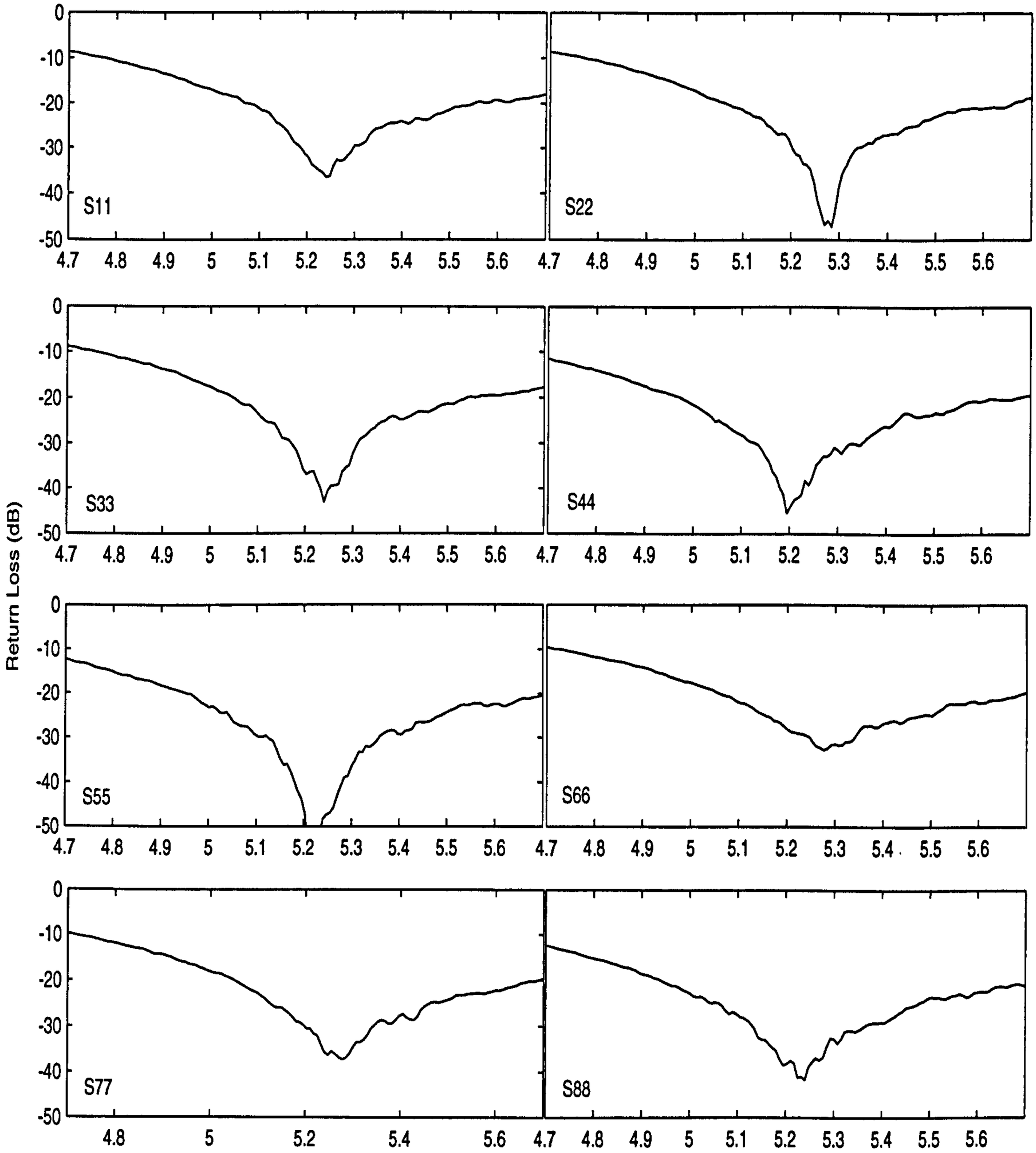

Figure D.1: *Return Loss (S_{nn}) of Array 1.*

Phase (°)

	1	2	3	4	5	6	7	8
8	107.6	-16.4	-56.4	-29.8	-59.2	-22.0	106.8	
7	-22.7	-61.8	-34.1	-57.9	-24.6	109.3		
6	-62.3	-37.7	-60.9	-26.1	107.2			
5	-38.5	-65.1	-21.4	105.2				
4	-67.0	-22.4	107.7					
3	-21.9	106.4						
2	107.6							
1								

Amplitude (dB)

	1	2	3	4	5	6	7	8
8	-11.1	-17.4	-22.9	-21.9	-23.1	-17.1	-11.2	
7	-16.7	-22.6	-21.3	-21.9	-16.7	-11.2		
6	-22.7	-21.5	-22.6	-17.2	-11.1			
5	-20.9	-22.0	-16.7	-11.0				
4	-22.7	-16.9	-11.1					
3	-16.7	-11.2						
2	-11.2							
1								
	1	2	3	4	5	6	7	

Figure D.2: *$S_{n(n+1)}$ of Array 1.*

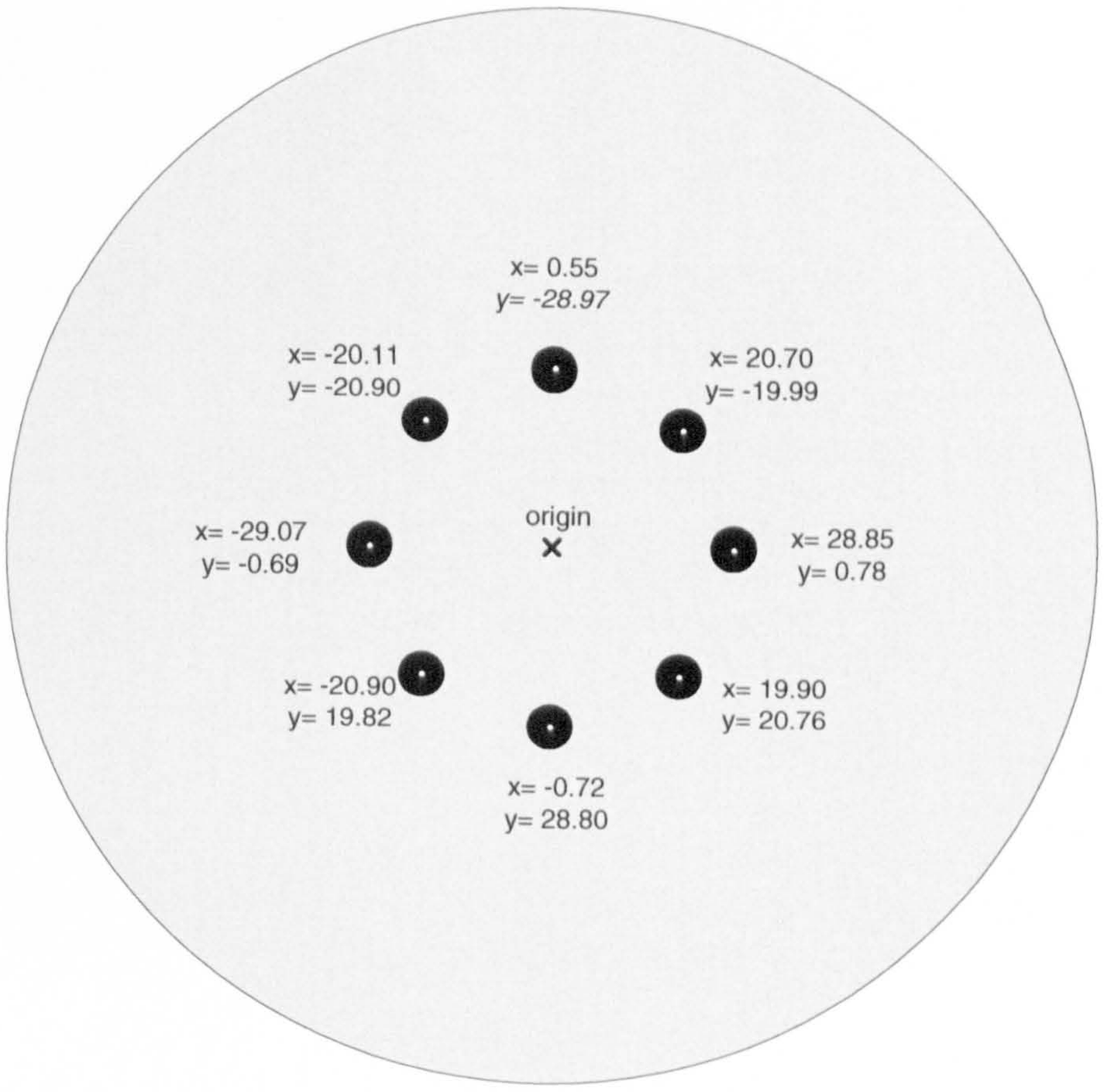

Figure D.3: *Cartesian co-ordinates for Array 1.*

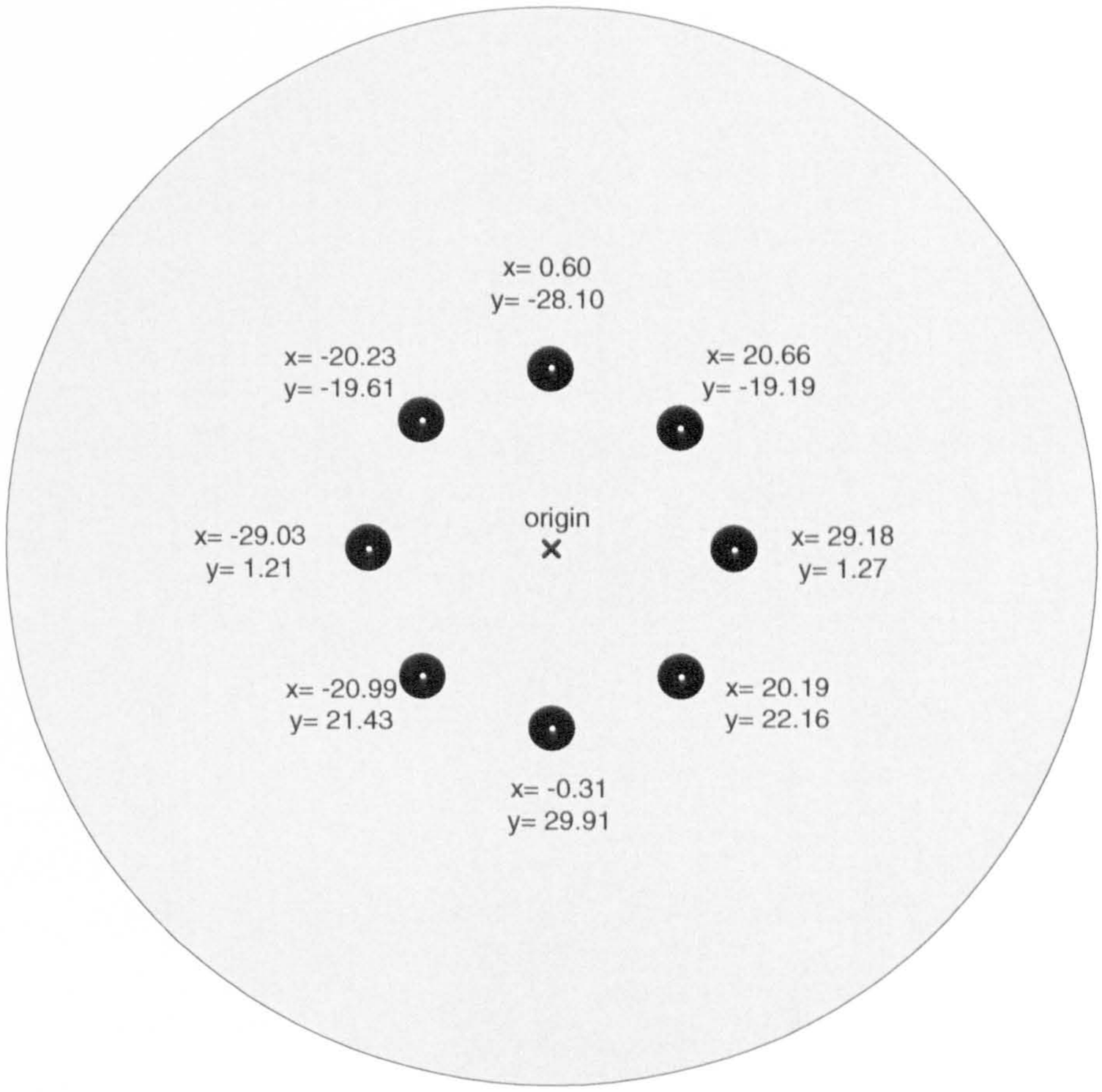

Figure D.4: *Cartesian co-ordinates for Array 2.*